



HAL
open science

Utilisation du chaos pour améliorer l'estimation du temps d'arrivée dans le cas multi-utilisateur : application à un système de télémétrie de type UWB

Hang Ma

► **To cite this version:**

Hang Ma. Utilisation du chaos pour améliorer l'estimation du temps d'arrivée dans le cas multi-utilisateur : application à un système de télémétrie de type UWB. Automatique. INSA de Toulouse, 2014. Français. NNT: . tel-01067173

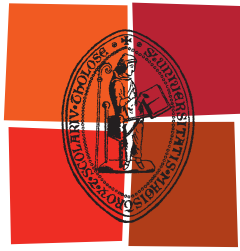
HAL Id: tel-01067173

<https://theses.hal.science/tel-01067173>

Submitted on 23 Sep 2014

HAL is a multi-disciplinary open access archive for the deposit and dissemination of scientific research documents, whether they are published or not. The documents may come from teaching and research institutions in France or abroad, or from public or private research centers.

L'archive ouverte pluridisciplinaire **HAL**, est destinée au dépôt et à la diffusion de documents scientifiques de niveau recherche, publiés ou non, émanant des établissements d'enseignement et de recherche français ou étrangers, des laboratoires publics ou privés.



Université
de Toulouse

THÈSE

En vue de l'obtention du

DOCTORAT DE L'UNIVERSITÉ DE TOULOUSE

Délivré par :

Institut National des Sciences Appliquées de Toulouse (INSA de Toulouse)

Présentée et soutenue par :

Hang MA

le mercredi 23 avril 2014

Titre :

Using chaos to enhance multiuser time-of-arrival estimation: Application to UWB ranging systems

École doctorale et discipline ou spécialité :

ED MITT : Domaine STIC : Réseaux, Télécoms, Systèmes et Architecture

Unité de recherche :

Laboratoire d'Analyse et d'Architecture des Systèmes

Directeur(s) de Thèse :

Danièle Fournier-Prunaret, Professeur Université de Toulouse, LAAS-CNRS

Marie-Laure Boucheret, Professeur Université de Toulouse, IRIT-CNRS

Pascal Acco, Maître de conférences Université de Toulouse, LAAS-CNRS

Jury :

Pascal Chargé: Rapporteur, Professeur Université de Nantes

Jean-Pierre Cances: Rapporteur, Professeur Université de Limoges

Mathieu Dervin: Examineur, Ingénieur Thales Alenia Space

Danièle Fournier-Prunaret: Directrice de Thèse, Professeur Université de Toulouse

Marie-Laure Boucheret: Directrice de Thèse, Professeur Université de Toulouse

Pascal Acco: Directeur de Thèse, Maître de conférences Université de Toulouse

Acknowledgments

I am indebted to a number of people who directly or indirectly contributed to the work which has been presented in this dissertation.

First of all, I would like to express my deepest gratitude to my supervisors Prof. Daniele Fournier-Prunaet and Prof. Marie-Laure Boucheret for their excellent supervision throughout these years, for their constructive suggestions and comments, for having allowed and encouraged me to conduct my research autonomously and independently, and for valuable suggestions of the draft of this thesis. It has been a great pleasure and privilege to work with them and to benefit from their rich knowledge and experience.

I would also like to sincerely thank my co-supervisor Dr. Pascal Acco for his professional guidance and numerous valuable discussions which helped and inspired me a lot. His optimistic and dynamic personality, his constant encouragements were of essential help when I was upset while doing my PhD. My thesis would not have completed without his help.

Thanks and deepest appreciations are extended to Prof. Pascal Charge, Prof. Jean-Pierre Cances and Mr. Mathieu Dervin for being my reviewer in their very busy schedules. It's my great pleasure that you accept to be my reviewers and to attend my PhD defense.

I gratefully acknowledge to all my former and present colleagues in the GEI department in INSA-Toulouse: Dr. Karim Braikia, Dr. Guillaume Fumat, Dr. Xinwei Zhang, Dr. Jianfei Wu, Dr. Binghong Li and He Hang for the numerous technical and non-technical discussions that have made the days of my PhD very pleasant. Special thanks to Prof. Abdel-Kaddous Taha for his kind concern, both professional and personal.

I would also like to thank to the organizers of the CSC/UT-INSA program for providing me the opportunity and financial support to come to France and to perform my PhD research. Many thanks also go to all of my friends in Toulouse, who shared my laughs and tears and gave me mentally and emotionally support during the past 3 years.

Finally, my deepest and sincere gratitude is for my parents, for their unconditional love and constant support since I was a little girl. My warmest thanks also go to Dr. Binbin Zhou for

his love and patience. Their love and trust is the driving power for my life and study.

Hang MA

23, Apr., 2014, Toulouse

Abstract

In the coming decades, highly accurate position information has the potential to create revolutionary applications in the social, medical, commercial and military areas. Ultra-Wideband (UWB) technology is considered as a potential candidate for enabling accurate localization capabilities through Time-of-Arrival (TOA) based ranging techniques. Over the past decade, chaotic signals have received significant attention due to a number of attractive features. Chaotic signals are aperiodic, deterministic, and random-like signals derived from nonlinear dynamical systems whose good autocorrelation, low cross-correlation and sensitivity to the initial conditions make them particularly suitable to ranging systems. In this thesis, two new multiuser TOA estimation algorithms are proposed with low complexity and robustness to MUI, the number of users supported by which is much larger than current multiuser TOA estimators. While, the use of classic spreading sequences and ranging pulse constrain the further improvement of ranging performance and system capacity. For breaking through the limit brought by the classic signals, the selected chaotic signals are employed as the spreading sequences or ranging pulse in our proposed algorithms. With the use of chaotic signals, our proposed algorithm not only obtains the additional improvement, but also with capability to support larger number of users comparing with its counterpart using classic signals.

Keywords: chaos, low complexity, multipath channel, multiuser interference, time of arrival (TOA) estimation, Ultra-wideband (UWB)

Résumé

Dans les décennies à venir, des informations de position très précises a le potentiel de créer des applications révolutionnaires dans les domaines sociaux, médicaux, commerciaux et militaires. Ultra-Wideband (UWB) technologie est considéré comme un candidat potentiel pour permettre des capacités de localisation précises à travers le temps d'arrivée (TOA) télémétries. Au cours de la dernière décennie, les signaux chaotiques ont reçu significative d'attention en raison d'un certain nombre de caractéristiques intéressantes. Signaux chaotiques sont des signaux non périodiques, déterministes et aléatoires provenant de système dynamique non linéaire. Leur bonne auto-corrélation, faible corrélation croisée et la sensibilité aux conditions initiales rendent particulièrement adapté à des systèmes télémétries. Dans cette thèse, deux nouveaux algorithmes d'estimation multiutilisateur de TOA sont proposés avec une faible complexité et la robustesse de MUI. Le nombre d'utilisateurs pris en charge par ces deux algorithmes sont beaucoup plus grandes que les estimateurs de TOA actuelles. Cependant, l'utilisation de séquences d'étalement classique et impulsion contraignent l'amélioration des performances et la capacité du système. Pour briser la limite apportée par les signaux classiques, les signaux chaotiques sélectionnés sont utilisés comme impulsion séquences d'étalement ou impulsion à nos algorithmes proposés. Avec l'utilisation de signaux chaotiques, notre algorithme proposé non seulement obtient l'amélioration supplémentaire, mais aussi avec la capacité de soutenir plus grand nombre d'utilisateurs de comparaison avec son homologue en utilisant des signaux classiques.

Mots-clés: chaos, faible complexité, canaux à trajets multiples, interférence multi-utilisateur, temps d'arrivée estimation, bande ultra-large

Contents

LISTING OF FIGURES	viii
1 INTRODUCTION	1
2 RANGING TECHNOLOGIES AND SYSTEM	5
2.1 Ranging Technology	5
2.2 Ultra-Wideband Ranging System	9
2.3 Conclusion	23
3 CHAOTIC SYSTEMS AND SIGNALS	25
3.1 Dynamical System and Chaos	25
3.2 Discrete-Time Chaotic System	27
3.3 Continuous-Time Chaotic System	32
3.4 Applications of Chaos	34
3.5 Conclusion	40
4 RANGING-RELATED PROPERTIES OF SOME CHAOTIC SIGNALS	41
4.1 Spectrum Property	41
4.2 Autocorrelation Property	46
4.3 Cross-correlation Property	66
4.4 Conclusion	78
5 MULTIUSER TOA ESTIMATORS	79
5.1 Decoupled Multiuser Ranging Algorithm	80
5.2 Simplified Larger Sampling Maximum Likelihood Algorithm	94
5.3 Numerical Evaluation	99
5.4 Conclusion	118

CONTENTS

6	CHAOS-BASED MULTIUSER TOA ESTIMATOR	119
6.1	Chaotic Binary Code Based DEMR algorithm	120
6.2	Chaotic Multi-valued Code Based DEMR algorithm	124
6.3	Chaotic Waveform Based DEMR algorithm	128
6.4	Conclusion	137
7	CONCLUSION AND PERSPECTIVE	139
	REFERENCES	151
	LIST OF PUBLICATIONS	153
	RÉSUMÉ	155

Listing of figures

2.2.1	The definition of UWB signals	11
2.2.2	Spectrum allocation of various wireless systems.	11
2.2.3	The FCC Emission limits for indoor UWB systems	12
2.2.4	The schematic diagram of multiuser interference	16
2.2.5	The different TOA estimator schemes (a). MF-based estimator (b). ED-based estimator (c). DAC-based estimator	17
3.1.1	Schematic diagram of the sensitivity of a chaotic system under different but very close initial conditions a_o and b_o	27
3.2.1	Trajectories of $x_{n+1} = 0.5x_n(1 - x_n)$ with the initial condition $x_o = 0.1$, $x_o = 0.2$, $x_o = 0.7$	29
3.2.2	Trajectories of $x_{n+1} = 2x_n(1 - x_n)$ with the initial condition $x_o = 0.1$, $x_o = 0.2$, $x_o = 0.7$	29
3.2.3	Trajectories of $x_{n+1} = 4x_n(1 - x_n)$ with the initial condition $x_o = 0.1$, $x_o = 0.2$, $x_o = 0.7$	30
3.2.4	Trajectories of $x_{n+1} = 4x_n(1 - x_n)$ with the initial condition $x_o = 0.1$, $x_o = 0.10001$	30
3.2.5	Bifurcation diagram of logistic map.	31
3.2.6	Bifurcation diagram of Tent map.	32
3.3.1	Lorenz system with Lorenz parameters $\sigma = 10$, $r = 28$, $b = 3/8$, and initial condition $[x(o) \ y(o) \ z(o)] = [0.3 \ 0.3 \ 0.3]$	33
4.1.1	Power spectrum density of Lorenz waveforms with the same Lorenz parameters in the length $T_c = 31ns$ and $T_c = 127ns$	44
4.1.2	Power spectrum density of the exact time scaling Lorenz waveforms in the length $T_c = 31ns$	45
4.2.1	Autocorrelation function of a typical ranging waveform.	47

LISTING OF FIGURES

4.2.2	Autocorrelation function of Lorenz pluses with length $T_s = 31ns$, $T_s = 127ns$ and $T_s = 500ns$	53
4.2.3	Cyclic Autocorrelation function of Lorenz pulses with length $T_s = 31ns$, $T_s = 127ns$ and $T_s = 500ns$	53
4.2.4	The frequency bandwidth of Lorenz pulse and Raised cosine pulse.	55
4.2.5	Autocorrelation function of selected Lorenz pulse and raised cosine pulse with Gold sequences in $T_s = 31ns$	56
4.2.6	Cyclic autocorrelation function of selected Lorenz pulse and raised cosine pulse with Gold sequences in $T_s = 31ns$	56
4.2.7	Autocorrelation function of selected Lorenz pulse and raised cosine pulse with Gold sequences in $T_s = 127ns$	57
4.2.8	Cyclic autocorrelation function of selected Lorenz pulse and raised cosine pulse with Gold sequences in $T_s = 127ns$	57
4.2.9	The procedure of the generation of Binary chaotic sequences.	59
4.2.10	Autocorrelation function of selected Chebyshev sequences and Gold sequences with length $N = 31$	60
4.2.11	Cyclic autocorrelation function of selected Chebyshev sequences and Gold sequences with length $N = 31$	61
4.2.12	Autocorrelation function of selected Tent sequences and Gold sequences with length $N = 31$	61
4.2.13	Cyclic autocorrelation function of selected Tent sequences and Gold sequences with length $N = 31$	62
4.2.14	Autocorrelation function of selected Chebyshev sequences and QCC sequences with $N_h = 13$	64
4.2.15	Cyclic autocorrelation function of selected Chebyshev sequences and QCC sequences with $N_h = 13$	64
4.2.16	Autocorrelation function of selected Tent sequences and QCC sequences with $N_h = 13$	65
4.2.17	Cyclic autocorrelation function of selected Tent sequences and QCC sequences with $N_h = 13$	65
4.3.1	Cross-correlation function of typical ranging waveform.	68
4.3.2	Cross-correlation function of selected Lorenz pulses and raised cosine pulse with Gold sequences in $T_s = 31ns$	72
4.3.3	Cyclic cross-correlation function of selected Lorenz pulses and raised cosine pulse with Gold sequences in $T_s = 31ns$	72

4.3.4 Cross-correlation function of selected Lorenz pulses and raised cosine pulse with Gold sequences in $T_s = 127ns$	73
4.3.5 Cyclic cross-correlation function of selected Lorenz pulses and raised cosine pulse with Gold sequences in $T_s = 127ns$	73
4.3.6 Cross-correlation function of selected Chebyshev sequences and Gold sequences with $N = 31$	75
4.3.7 Cross-correlation function of selected Tent sequences and Gold sequences with $N = 31$	75
4.3.8 Cross-correlation function of selected Chebyshev sequences and QCC sequences with $N_h = 13$	76
4.3.9 Cyclic cross-correlation function of selected Chebyshev sequences and QCC sequences with $N_h = 13$	77
4.3.10 Cross-correlation function of selected Tent sequences and QCC sequences with $N_h = 13$	77
4.3.11 Cyclic cross-correlation function of selected Tent sequences and QCC sequences with $N_h = 13$	78
5.1.1 The output of matched filter (MF) and integrate-and-dump filter (IDF) of raised cosine pulse	88
5.3.1 RMSE of DEMR algorithm in DS-UWB system as a function of SNR in an AWGN channel with $T_a = 100ns$	102
5.3.2 RMSE versus near-far ratio for different estimators with $M = 100, N = 31, SNR = 20dB, K = 10$ in DS-UWB system in AWGN channel.	103
5.3.3 RMSE versus K for different estimators with $M = 100, N = 31, SNR = 20dB$ and near-far ratio is 10 dB DS-UWB system in AWGN channel.	103
5.3.4 RMSE versus near-far ratio for different SNR values with $M = 100, N = 31,$ and $K = 10$ in DS-UWB system CM1 channel.	104
5.3.5 RMSE versus K for different SNR values with $M = 100, N = 31,$ and near-far ratio is 10 dB in DS-UWB system CM1 channel.	104
5.3.6 RMSE of DEMR algorithm in TH-UWB system as a function of SNR in an AWGN channel with $T_a = 100ns$	107
5.3.7 RMSE versus near-far ratio for different estimators with $M = 100, N_h = 13, SNR = 20dB, K = 10$ in TH-UWB system in AWGN channel.	107
5.3.8 RMSE versus K for different estimators with $M = 100, N - h = 13, SNR = 20dB$ and near-far ratio is 10 dB in TH-UWB system in AWGN channel. . .	108

LISTING OF FIGURES

5.3.9 RMSE versus near-far ratio for different SNR values with $M = 100, N_h = 13$, and $K = 10$ in TH-UWB system in CM1 channel. 108

5.3.10 RMSE versus K for different SNR values with $M = 100, N_h = 13$, and near-far ratio is 10 dB in TH-UWB system in CM1 channel. 109

5.3.11 RMSE of SLSML algorithm as a function of SNR in an AWGN channel with $T_a = 30ns$ 111

5.3.12 RMSE versus near-far ratio for different SNR values with $M = 600, N = 31$, and $K = 10$ in DS-UWB system in AWGN channel. 112

5.3.13 RMSE versus K for different SNR values with $M = 600, N = 31$, and near-far ratio is 10 dB in DS-UWB system in AWGN channel. 112

5.3.14 RMSE versus near-far ratio for different SNR values with $M = 600, N = 31$, and $K = 10$ in DS-UWB system in CM1 channel. 113

5.3.15 RMSE versus K for different SNR values with $M = 600, N = 31$, and near-far ratio is 10 dB in DS-UWB system in CM1 channel. 113

5.3.16 RMSE of DEMR algorithm in TH-UWB system as a function of SNR in an AWGN channel with $T_a = 30ns$ 115

5.3.17 RMSE versus near-far ratio for different estimators with $M = 200, N_h = 13$, $K = 10$ in TH-UWB system in AWGN channel. 115

5.3.18 RMSE versus K for different estimators with $M = 200, N - h = 13$, near-far ratio is 10 dB in TH-UWB system in AWGN channel. 116

5.3.19 RMSE versus near-far ratio for different SNR values with $M = 200, N_h = 13$, and $K = 10$ in TH-UWB system in CM1 channel. 116

5.3.20 RMSE versus K for different SNR values with $M = 200, N_h = 13$, and near-far ratio is 10 dB in TH-UWB system in CM1 channel. 117

6.1.1 RMSE versus near-far ratio for different SNR values with $M = 100, N = 31$, and $K = 10$ in CM1 channel. 123

6.1.2 RMSE versus K for different SNR values with $M = 100, N = 31$, and near-far ratio is 10 dB in CM1 channel. 123

6.2.1 RMSE versus near-far ratio for different SNR values with $M = 100, N_h = 13$, and $K = 10$ in CM1 channel. 127

6.2.2 RMSE versus K for different SNR values with $M = 100, N_h = 13$, and near-far ratio is 10 dB in CM1 channel. 127

6.3.1 RMSE versus near-far ratio for different SNR values with $M = 100, T_s = 127ns$, and $K = 10$ in AWGN channel. 135

6.3.2	RMSE versus K for different SNR values with $M = 100$, $T_s = 127ns$, and near-far ratio is 10 dB in AWGN channel.	135
6.3.3	RMSE versus near-far ratio for different SNR values with $M = 100$, $T_s = 127ns$, and $K = 10$ in CM1 channel.	136
6.3.4	RMSE versus K for different SNR values with $M = 100$, $T_s = 127ns$, and near-far ratio is 10 dB in CM1 channel.	136
R.1	La définition des signaux UWB	157
R.2	The schematic diagram of multiuser interference.	158
R.3	Les différents régimes de l'estimateur de TOA.	159
R.4	Schéma de la sensibilité d'un système chaotique sous différents mais très proches des conditions initiales a_0 et B_0	160
R.5	Densité spectrale de puissance de Lorenz formes d'onde avec les mêmes paramètres de Lorenz dans la longueur $T_c = 31ns$ et $T_c = 127ns$	162
R.6	Densité spectrale de puissance de l'heure exacte échelle des formes d'onde de Lorenz dans la longueur $T_c = 31ns$	163
R.7	Fonction d'autocorrélation de l'impulsion Lorenz sélectionné et élevé impulsion de cosinus avec des séquences Gold en $T_s = 31ns$	164
R.8	Fonction d'autocorrélation de l'impulsion Lorenz sélectionné et élevé impulsion de cosinus avec des séquences Gold en $T_s = 127ns$	165
R.9	The procedure of the generation of Binary chaotic sequences.	166
R.10	Fonction d'autocorrélation des séquences de Chebyshev sélectionnés et séquences Gold avec la longueur $N = 31$	166
R.11	Fonction d'autocorrélation des séquences de Tent sélectionnés et séquences Gold avec la longueur $N = 31$	167
R.12	La sortie du filtre adapté (MF) et intégrer-et-dump filtre (IDF) de l'impulsion de cosinus.	169
R.13	RMSE en fonction du rapport proche-lointain pour différentes valeurs de SNR avec $M = 100$, $N = 31$, et $K = 10$ dans le canal CM1.	170
R.14	RMSE en fonction du K pour différentes valeurs de SNR avec $M = 100$, $N = 31$, and near-far ratio is 10 dB dans le canal CM1.	171
R.15	RMSE en fonction du rapport proche-lointain pour différentes valeurs de SNR avec $M = 100$, $N = 31$, et $K = 10$ dans le canal CM1.	172
R.16	RMSE en fonction du K pour différentes valeurs de SNR avec $M = 100$, $N = 31$, and near-far ratio is 10 dB dans le canal CM1.	172

LISTING OF FIGURES

"Knowledge is power."

Sir Francis Bacon

1

Introduction

Centuries ago, Sir Francis Bacon gave the world a great statement that "Knowledge is power". The development of science and technologies in the past centuries is a great interpretation of this statement. Since knowledge, in some aspects, has the same meaning as information in communication theory, "Knowledge is power" may be easily understood as "Information is power" in communication and localization systems to some extent.

In cellular networks, the knowledge of location information can be used for emergency services, location-sensitive billing, fraud detection, resource management, and intelligent transportation systems. In the emergency situation such as natural disaster, fire scene, the location of victims is the vital information for the search and rescue operations. In the medical services, knowing where patients and doctors are could enhance the efficiency of whole systems. In the high security area, tracking the localization of authorized persons is an example how location information can be used to military and security fields. While knowing your position in the office environment or supermarket could help you find the items you looking for. Location of aging people in their home could help the medical services agency being aware what happened when they alone [1].

With the awareness of the importance of location information, various systems have been developed to provide the accurate position information. The well-known and widely used system must be the Global Positioning Systems (GPS). GPS is an outdoor localization system,

which employs the time difference of arrival (TDOA) information from 4 or more from 24 satellites around the earth to estimate target's position with an accuracy between 1m and 10 m. Following the achievements of GPS systems in outdoor applications, the challenge has shifted to the provision of such services for the indoor environment. However, the ability to locate in indoor environment remains a substantial challenge, which forms the major bottleneck preventing seamless positioning in all environments. In fact, most positioning systems can – at least theoretically – be used indoors as well as outdoors. However system performances differ greatly, because the environments have a number of substantial differences. Indoor environments are particularly challenging for positioning, for the following reasons [2]:

- severe multipath from walls and furniture reflection
- Non-Line-of-Sight (NLoS) conditions
- high attenuation due to great density of obstacles
- high demand for precision and accuracy

Impulse Radio Ultra-wideband (IR-UWB) is a promising solution to indoor positioning which become more popular after the Federal Communications Commission (FCC) in the USA allowed the unlicensed use of UWB devices in February 2002 subject to emission constraints. Due to its unlicensed operation and low-power transmission, UWB can coexist with other wireless devices, and its low-cost, low-power transceiver circuitry makes it a good candidate for short to medium range wireless systems.

In the IR-UWB technology, the most attractive feature is the potential for high precision localization. Due to large bandwidths, individual multipath components can be resolved in the receiver of UWB localization. Hence, the arrival time of the first path could be estimated accurately, which implies the distance between a wireless transmitter and a receiver can be accurately determined, yielding high localization accuracy. This high precision localization capability of UWB technology make it quite attractive to indoor positioning systems, which is also recognized by the IEEE. In 2007, IEEE adopted UWB signal as a candidate in the IEEE 802.15.4a WPAN standard for the creation of a physical layer for short-range and low data rate communications and for precise localization. Hence, UWB technology has increasingly become a focus of research for positioning in indoor environments.

Due to the extremely large bandwidth of UWB signals, ranging methods whose accuracy could be improved with the increase of bandwidth may be the most suitable approaches for UWB ranging systems. By analyzing the Cramer-Rao Low Bound (CRLB) of ranging techniques, Time of arrival (TOA) and Angle of arrival (AOA) measurements could be benefited

from the large bandwidth of UWB signals. Since the requirement of antenna array of AOA receiver, TOA based UWB ranging systems are more suitable to the low-cost, low-complexity ranging application.

Various TOA based algorithms and estimators have been proposed in the literature. Commonly, they can be classified into three types, matched filter (MF) based coherent algorithms, energy detection (ED) based non-coherent algorithms and delay-and-correlation based algorithms. MF based algorithms obtain accurate TOA estimate with high sampling rate and relatively complex transceiver. The requirement of Nyquist sampling rate or higher could be impractical due to the large bandwidth of UWB signals. As an alternative, ED based algorithms estimates TOA by measuring the energy of small blocks in time domain. Hence, the requirement of sampling rate could be quite lower than Nyquist rate, resulting in low complexity receiver as well. The third delay-and-correlation based algorithm is a modification of MF based algorithm, the template of correlation is the delay version of received signal instead of local template in MF estimator. The two latter kinds of algorithms have the low complexity at the expense of relatively low ranging accuracy compared to MF based estimators.

Meanwhile, current TOA estimators still have problems needed to be solved. The first is how to enhance the ranging accuracy in severe multipath environment. As mentioned before, a significant difference of indoor positioning and outdoor positioning is the severe multipath channel condition. Although UWB signal has high resolution of multipath, how to choose the first path exactly is still a problem not solved properly, particularly when accompanied with multiuser interference (MUI) and other effects. MUI is the second potential problems of current estimators. It is well known that MF estimator coincides with the optimal maximum likelihood (ML) method for a single user in the presence of white Gaussian noise but its performance degrades drastically in the multiuser environment. In addition, not accounting for MUI with ED estimator can greatly degrade performance further [3].

In general, UWB ranging systems assign each user a unique spreading sequences to enhance the ability of resistance the effect of multipath and MUI. Specially, the more narrow, peaky and low side-lobe autocorrelation of spreading sequence is, the better it will resist the multipath effect. Similarly, the low cross-correlation property of spreading sequences results in mitigating the MUI problem.

Over the past decade, chaotic spreading sequences have received significant attention due to a number of attractive features. Chaotic sequences are aperiodic, deterministic, and random-like sequences derived from nonlinear dynamical systems. Chaotic sequences' good autocorrelation and low cross-correlation properties make them particularly resistant against multipath fading and capable of mitigating the MUI [4]. Due to the high sensitivity to the initial conditions, a larger number of chaotic spreading sequences can be easily generated for increas-

ing the system's overall capacity. Several papers have shown that chaotic sequences can be used as an alternative to the classic spreading sequences [5–7]. Using chaotic waveforms in UWB communication systems has also been proposed in the literature [8].

The motivation of this thesis is to develop new TOA estimators which are more robust to severe multipath and MUI effect and to exploit the property of chaotic systems in order to enhance the capability of resistance the interferences and to enlarge the system capacity of UWB ranging systems. As working on a cross domain research, the organization of this thesis is given as follows:

Chapter 2 first presents a brief introduction of ranging technologies. The principle of common ranging technologies will be explained with their advantages and disadvantages. Following the ranging technologies, the overview of current UWB ranging systems are introduced. The main error sources, typical type of estimators, existing multiuser ranging algorithms and UWB channel condition are expressed consecutively.

In chapter 3, the definition of chaotic systems and their generation are explained in the beginning of this chapter, followed by the introduction of two different chaotic signals, the continuous-time chaotic signals and discrete-time chaotic signals. The final part of this chapter is devoted to the application of chaotic signals in various fields such as wireless communication, radar and sonar.

The ranging related properties of chaotic signals are shown in the chapter 4. The main focuses are the autocorrelation, cross-correlation and frequency spectrum properties of both continuous-time chaotic signals and discrete-time chaotic signals. Chebyshev and Tent maps are the examples of discrete-time chaotic signals, and the Lorenz waveform is chosen as the representative of continuous-time chaotic signals. By comparison with classic spreading sequences and waveforms, it is shown that chaotic signals can obtain identical even better autocorrelation and cross-correlation property. Moreover, frequency spectrum of Lorenz waveform can be easily adjusted to certain bandwidth by changing Lorenz parameters.

After the introduction of the state of art of UWB ranging algorithms, two new multiuser TOA estimators are proposed in chapter 5, which are suitable to multiuser environment and allow the ranging system to be fully-loaded. After giving the details of the two algorithms, the complexity and numerical evaluations are presented. In the numerical evaluation part, comparison with current multiuser algorithms can be addressed.

In chapter 6, in order to enhance the ranging performance, the chaotic sequences and waveforms are selected according to the requirements of the proposed TOA estimator. After the introduction of selection criteria, the proposed algorithm with chaotic signals are compared with their counterparts in the numerical evaluation part.

In the final part, the conclusion and perspective of the thesis are given.

"Knowledge precedes victory, confusion precedes defeat."

Sun Tzu, Chinese General

2

Ranging Technologies and System

2.1 RANGING TECHNOLOGY

Nowadays, the integration of Global Positioning System (GPS) into cellular phones, accompanying with WiFi localizations, is lighting a new era of ubiquitous localization-awareness. In the coming future, we will see the explosive emergence of high accurate position applications in the commercial, medical, and military industries. Such applications require localization systems with sub-meter accuracy, which make the position technologies as a key point of a diverse set of applications.

The purpose of position estimation is to find the unknown position of a target node, which involves signal exchanges between target node and a number of reference nodes. Node here refers to as any device involved in the position estimation process. If the position of target node is estimated by the target nodes itself, it is called *self-positioning*. When a central unit that gathers position information from reference nodes takes in charge of position estimation, it is a *remote-positioning* [1]. Moreover, how to estimate the position divides estimation schemes into two different groups generally, the *Direct positioning* and *two-step positioning*. The former estimates the position directly by the use of signals traveling between nodes [9]. On the other hand, a *two-step positioning* firstly estimates certain signal parameters related to position estimation, such as time, angle or power. Then, the second step is to estimate the position of

target node based on these parameters. Although the two-step positioning scheme is considered to be suboptimal in general, its low complexity makes it more attractive than its counterpart [1]. [9,10] show that the performance of the two approaches are quite close in the case of wide signal bandwidths or high SNR values. Therefore, two-step positioning scheme is used as a common technique in most positioning systems.

For the two-step positioning system, the first step is to estimate a signal parameter containing the position information such as *time of arrival (TOA)*, *angle of arrival (AOA)* and *received signal strength (RSS)* and so on. TOA and RSS are usually related to the distance information between target node and reference node. The direction information of nodes can be extracted from the AOA parameter. Hence, the two-step positioning systems can be further classified as range-based (based on distance estimates), angle-based and proximity-based localization systems by different measurements between nodes [11]. Since in the second step, the target nodes position is estimated based on these signal parameters obtained from the first step, the accuracy of signal parameter estimation has a significant effect on the position accuracy. In this thesis, our main focus is the estimation of position related parameter, the first step of positioning systems. Although estimation of AOA exists in the angle-based system, we still consider the AOA estimation as ranging techniques for convenience. Hence, in the following of this section, RSS, AOA and TOA, the three different ranging techniques, will be presented detailedly.

2.1.1 RECEIVED SIGNAL STRENGTH BASED RANGING

As well known that signal strength (power) varies depending on the distance, the greater the distance between two nodes, the weaker received signal between each other. Received Signal Strength (RSS) Ranging is exactly based on this principle. However, before taking advantage of RSS technique into ranging applications, how to retrieve the distance from RSS information is an important problem faced to us. In the past decades, various models have been proposed and analyzed in theoretical or experimental ways. A widely used model to characterize this relationship is given by [12] as

$$P(d) = P_o - 10\gamma\log_{10}(d/d_o) + S \quad (2.1)$$

where $P(d)$ is the received signal power in decibels at a distance d , P_o is the received power in decibels at a distance d_o . The parameter γ is known as the path-loss exponent, which typically assumes values between 2 and 6 [12]. S represents the large-scale fading which is also known as shadowing effect. S is commonly modeled as a Gaussian random variable with zero mean and variance σ_{sh}^2 . With the Eq.(2.1), relatively accurate distance estimation can be obtained from

RSS information, the accuracy of which can be enhanced further if more precise knowledge of γ and σ_{sh}^2 is available.

From Eq.(2.1), We know how the distance between nodes is estimated with RSS information. Meanwhile, another question is how accurate this estimation could be. In the signal detection and estimation theory, the accuracy of estimation can be specified by a lower bound, called the Cramer-Rao lower bound (CRLB), on the variance of an unbiased range estimation [13]. The CRLB for RSS based ranging is represented as

$$\sqrt{\text{Var}(\hat{d})} \geq \frac{\ln_{10} \sigma_{sh} d}{\gamma} \quad (2.2)$$

where \hat{d} denotes an unbiased estimate for the distance d . It is shown from the CRLB that the range accuracy increases as the standard deviation of shadowing decreases, which makes the RSS vary less around the average power. And the RSS method gets more precise with a large path loss exponent since the average power become more sensitive with a large γ . Finally, the \hat{d} has more precision with the decrease of distance d .

RSS technique is commonly used in low-cost systems since the hardware requirements and costs can be more favorable compared with other techniques. However, the primary disadvantage of RSS technique is that in cluttered environments the propagation phenomena cause the attenuation of the signal to be poorly related with distance, resulting in inaccurate distance estimates [14].

2.1.2 ANGLE OF ARRIVAL BASED RANGING

Angle of arrival (AOA) technology estimates the target node through the measurement of angle between the target node and reference nodes. In the AOA estimation, antenna arrays are commonly employed at a node in order to estimate the AOA of the signal arriving at that node. Time difference in arrival time of each antenna elements contains the angle information for a known antenna arrangement [2]. For instance, if a uniform linear array (ULA) is employed in the reference node, the differences of arriving time in each elements of antenna array are the times of $l \sin a / c$, where l is the inter-element space, a is the AOA and c denotes the speed of light [2]. Obviously, if the arriving times are known, AOA can be obtained through an inverse operation.

Following the introduction of main idea of AOA ranging technique, the lower bound of ranging accuracy is investigated, which is also described by the CRLB. For the case of ULA, the CRLB for the variance of unbiased AOA estimate \hat{a} with N_a elements can be expressed

as [15]

$$\sqrt{\text{Var}(\hat{a})} \geq \frac{\sqrt{3}c}{\sqrt{2\pi}\sqrt{\text{SNR}}\beta\sqrt{N_a(N_a - 1)}l\cos a} \quad (2.3)$$

where a is the AOA, c denotes the speed of light, SNR is the signal to noise ratio for each element, l is the inter-element spacing and β is the effective bandwidth defined as

$$\beta^2 = \frac{\int_{-\infty}^{\infty} f^2 |P(f)|^2 df}{\int_{-\infty}^{\infty} |P(f)|^2 df} \quad (2.4)$$

where $P(f)$ is the frequency spectrum of transmitted signal $p(t)$.

From the investigation of CRLB, theoretically, the accuracy of AOA estimation is improved as the increase of SNR, effective bandwidth, the number of antenna elements and inter-element space. What's different from RSS technique is that the accuracy of AOA estimation depends on the bandwidth of ranging signals, which implies that large bandwidth ranging signals could achieve high accuracy AOA estimation.

2.1.3 TIME OF ARRIVAL BASED RANGING

In AOA estimation, nodes position is estimated through the angle of incoming signals retrieved from the time difference information at the elements of antenna array. In TOA estimation, distance between nodes can be measured from the the signal propagation delay, or time of flight $\tau_f = d/c$, where d is the actual distance between two nodes and c is the speed of light. This approach can be accomplished by using one-way time of arrival (TOA), two-way TOA or time difference of arrival (TDOA) ranging techniques [16].

One-Way TOA Ranging: In one-way ranging system, one way flight time between target node and reference node is measured. Assuming that target node transmits the ranging signal at time t_1 and reference node receives signals at time t_2 , the time of flight is equal to $\tau_f = t_2 - t_1$ which yields to distance estimation. Note that an important requirement of one-way TOA ranging is the perfect synchronization between nodes. Unless, the ranging accuracy must be effected, even causes a large ranging error.

Two-Way TOA Ranging: In order to improve the ranging accuracy under the imperfect synchronization condition, the two-way ranging technique is proposed. In two-way ranging system, the signal round trip time (RTT) instead of one-way flight time is estimated. Therefore, the requirement of common time reference is no longer needed. Reference node transmits ranging signal to target node with one-way time of flight τ_f , after a processing time delay τ_d , ranging signals are sent back to reference node. Hence the RTT at reference node consists of $\tau_{RTT} = 2\tau_f + \tau_d$. If τ_d is known, τ_f is obtained consequently. Although two-way ranging

eliminates the ranging error caused by imperfect synchronization between the nodes, the response delay τ_d may become another error source. For example, in the indoor environment, the propagation delay is typically in the order of nanosecond, but the response delay can be of a few microseconds due to bit synchronization and channel estimation delay [17].

Time Difference of Arrival Ranging: Another method to avoid the imperfect synchronization problem between target node and reference node is the TDOA ranging technique. TDOA system is based on the difference between the arrival time of two signals traveling between the target node and two reference nodes. Generally, TDOA ranging can be implemented by following two schemes [16]. In the first one, multiple signals are broadcast from synchronized fixed reference nodes which are located at the known position. The target nodes measure the TDOA and estimate the position themselves. In the second scheme, signals are transmitted from target node and are received by several reference nodes. The reference nodes share their estimated TOA and compute the TDOA. Although the synchronization between target node and reference node is not needed, the reference nodes must be synchronized in TDOA approach. To estimate the position of target node, at least three reference nodes with known position and two TDOA measurements are required.

Accurate limits of TOA estimation can be also quantified by the CRLB, which is given in the following [18]

$$\sqrt{\text{Var}(\hat{\tau})} \geq \frac{1}{2\sqrt{2\pi}\sqrt{\text{SNR}\beta}} \quad (2.5)$$

where $\hat{\tau}$ represents an unbiased TOA estimate, SNR is the signal-to-noise ratio and β is also the effective bandwidth of transmitted signal. It is observed that the accuracy of TOA estimation varies in an inverse relationship with SNR and effective bandwidth β . The larger SNR or effective bandwidth β is, the more precise the TOA estimation will be.

Besides employing the above ranging techniques separately, a combination of these approaches can be found in some localization systems, including TOA/AOA [19], TOA/RSS [20], TDOA/AOA [19] and TOA/TDOA [21] localization systems. The exploitation of more information from received signals results in higher ranging accuracy.

2.2 ULTRA-WIDEBAND RANGING SYSTEM

Over the coming decades, highly accurate position information has the potential to create revolutionary applications in the social, scientific commercial and military areas. Ultra-Wideband (UWB) technology is considered as a potential candidate for enabling accurate localization capabilities through TOA based ranging techniques. In the following of this section, the history, current regulation, property and current ranging algorithm will be presented in order to have

a comprehensive view of UWB ranging systems.

2.2.1 ULTRA-WIDEBAND SIGNALS AND PROPERTY

In 1901, Guglielmo Marconi, an Italian scientist, transmitted his spark gap radio across the Atlantic Ocean, which is not only the first step of his idea of a wireless connected world, but also considered as the first use of Ultra-Wideband (UWB) systems. After more than half of a century, the rigorous investigation of UWB systems has started with an UWB communications patent issued in 1973 on transmission and reception of baseband pulse signals [2]. Early names for UWB technology include baseband, carrier-free, non-sinusoidal and impulse. The term UWB was coined by the US Department of Defense in the late 1980s.

On February 14, 2002, the United States Federal Communications Commission (FCC) announced its "First Report and Order", which allowed the frequency band between 3.1-10.6 GHz available for unlicensed operation of UWB devices, subject to certain restrictions on the spectral mask [22]. This rule triggered exponential increase of interest in this area due to the promise of unprecedented wireless data rates and precise positioning in a low-cost radio [23, 24].

A UWB signal is characterized by its very large bandwidth compared to the conventional narrowband systems. According to FCC, UWB signals are characterized by an absolute 10dB bandwidth of at least 500MHz, or a fractional 10dB bandwidth of larger than 20% [22]. As shown in Fig.2.2.1 [1], the absolute 10dB bandwidth is calculated as the difference between the upper frequency f_H of the 10dB emission point and the lower frequency f_L of the 10dB emission point [1]; i.e.

$$B = f_H - f_L \quad (2.6)$$

On the other hand, the fractional bandwidth is defined as

$$B_{frac} = \frac{B}{f_c} \quad (2.7)$$

where f_c is the center frequency and is given by

$$f_c = \frac{f_H + f_L}{2} \quad (2.8)$$

With such a large frequency bandwidth, UWB signal should exist without or with little interference to the others wireless systems in the same bandwidth. For example, frequency allocation of some wireless systems is shown in Fig.2.2.2 [2]. The bandwidth A is assigned to Global positioning system (GPS) (1.56–1.61 GHz); B is used for Personal communication

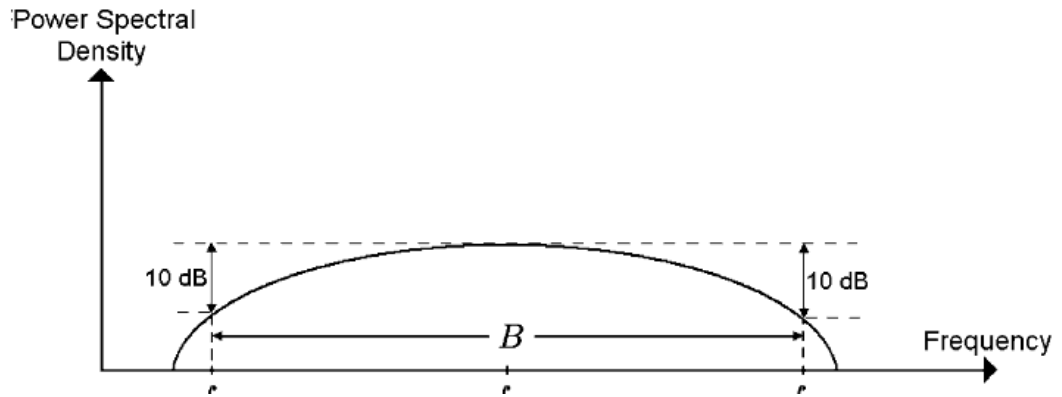


Figure 2.2.1: The definition of UWB signals

system (PCS) (1.85–1.99 GHz); C is allocated to Microwave ovens, cordless phones, blue-tooth, IEEE 802.11b (2.4–2.48 GHz); D and E are for IEEE 802.11a (5.725–5.825 GHz) and UWB (3.1–10.6 GHz), respectively. Note that the bandwidths and power levels of various systems are not drawn to scale. The FCC Part 15 limit is also shown in the figure [22]. UWB systems are required to operate below the Part 15 limit (-41.3 dBm/MHz), which is the limit for unintentional radiators, such as televisions and computer monitors [2].

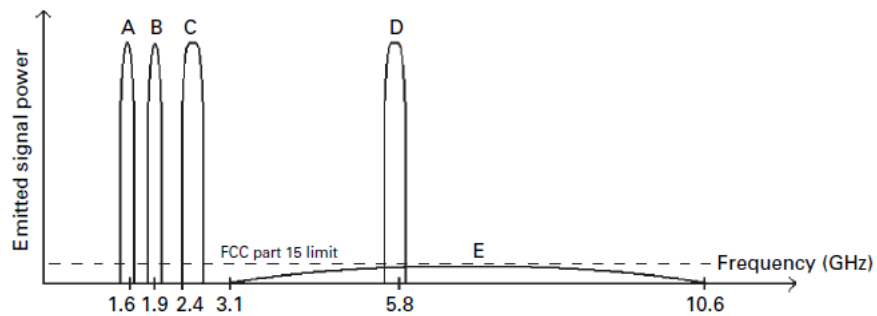


Figure 2.2.2: Spectrum allocation of various wireless systems.

Actually, FCC requires more rigorous power emission restrictions than Part 15 limit to UWB systems to avoid potential interference to other existing systems. Especially, GPS, which is used not only for commercial but also for military and homeland security purposes, should not experience performance degradation due to UWB emission. Fig.2.2.3 illustrates the FCC limits for indoor communication systems. According to this regulation, the power spectral density (PSD) must not larger than -41.3 dBm/MHz for frequency ranges from 3.1 to 10.6 GHz. In the outside bandwidth, the PSD is even lower [22]. When meeting this regulation, the interference from UWB systems can not have a significant effect to the current wireless

systems. Inspired by the FCC regulation, UWB systems became a new promising research area in the past decade. With this trend, Japan and Europe recently allowed the use of UWB systems under certain regulations [25,26].

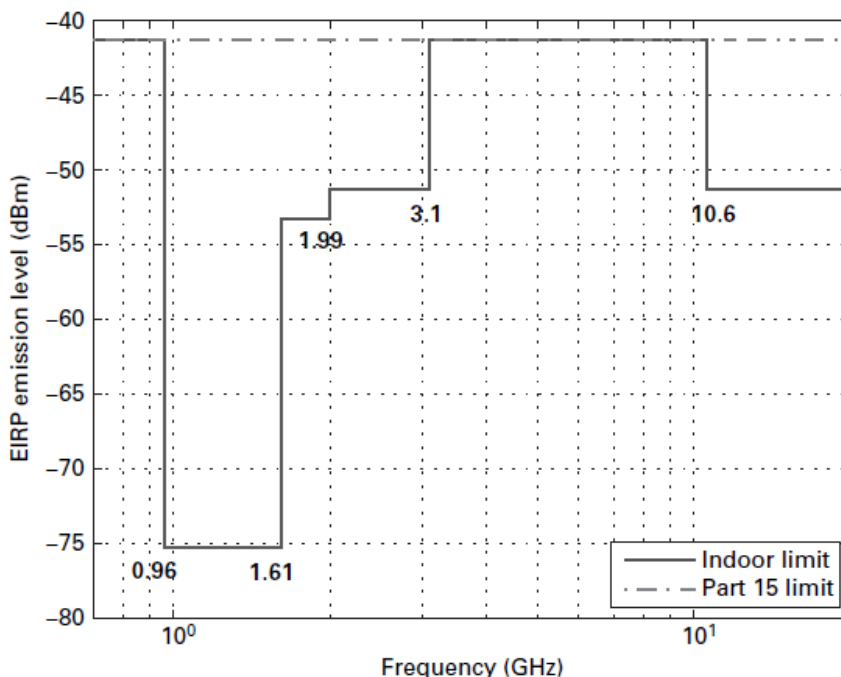


Figure 2.2.3: The FCC Emission limits for indoor UWB systems

Due to their large occupied bandwidth, UWB systems are characterized by very short duration pulses in the time domain. Since the pulse duration is usually in the order of nanosecond and is transmitted in a low duty cycle, this kind of UWB systems is named as the impulse radio (IR) UWB systems [27]. Due to the use of extremely short duration pulse and long repetition time transmission, IR-UWB systems have a possibility to have low power consumption and low complexity transceiver structure, which can be used for the wireless communication and ranging systems with such requirements.

Occupying large frequency bandwidth not only brings the simplification in signal processing procedure and transceiver structure, but it also gives rise to other attractive properties, particularly for ranging and radar applications. [1] summarized as followed:

- penetration through obstacles
- high ranging, hence positioning, accuracy
- high-speed data communications

- low cost and low power implementation

The penetration capability of a UWB signal is a result of its large frequency spectrum that includes low frequencies as well as high frequencies. If employing UWB signals in ranging systems, the large bandwidth can enhance the ranging accuracy significantly with TOA or AOA ranging techniques. Meanwhile, the extremely short pulse duration results in high resolution of multipath. Hence, using UWB signals in ranging systems has potential to achieve a high accurate positioning. For the high-speed data transmission feature, we can analyze it from the Shannon capacity formula. For an additive white Gaussian noise (AWGN) channel with bandwidth of B Hz, Shannon capacity formula gives the maximum data rate that can be acquired in communication systems, which is expressed as

$$C = B \log_2(1 + \text{SNR}) (\text{bits/second}) \quad (2.9)$$

where SNR is the signal-to-noise ratio of the system. It is observed that the channel capacity could be increased with the growth of bandwidth B . Therefore, UWB signals which has extremely large bandwidth B have the capacity to provide a high-speed data transmission. Finally, as mentioned previously, the IR-UWB systems are quite suitable for low cost and low power consuming applications due to the signal characterizations. In addition, IR-UWB signal is a carrier-free signal without requirement of RF processing part, which simplified the cost further [2].

Inspired by the attractive features of UWB systems, a larger number of applications of UWB systems have been proposed, particularly for the positioning systems. We classifies them into the following 5 aspects [1]:

- Medical Service: Monitoring of patients in a hospital
- Security and Military: Locating authorized people in high-security areas and tracking the position of military personnel
- Search and Rescue Operation: Location and communications with fire fighters or natural disaster victims
- Inventory Control: Tracking of shipments and valuable items in manufacturing plants and locating medical equipment in a hospital
- Smart Home: Controlling of home appliances, and locating inhabitants

In 2004, the IEEE 802.15 low-rate alternative PHY task group (TG4a) was formed to design an alternate PHY specification for the already existing IEEE 802.15.4 standard for WPANs. The

main purpose of the TG4a was to provide communications and high precision ranging with low-power and low-cost devices. The TG4a's efforts resulted in the IEEE 802.15.4a standard in 2007 [28]. With additional features provided by the 15.4a amendment, the IEEE 802.15.4 standard now facilitates new applications and market opportunities. The IEEE 802.15.4a specifies two optional signaling formats based on IR-UWB and chirp spread spectrum (CSS). For the IR-UWB there is an optional ranging capability, whereas the CSS signals can only be used for communications purposes.

2.2.2 ULTRA-WIDEBAND RANGING SYSTEMS

As discussed in the previous section, the position of target node can be estimated based on AOA, RSS and TOA ranging approaches. Due to the extremely large bandwidth, AOA and TOA ranging techniques are quite suitable to UWB ranging systems since the accuracy of these two approaches increases with the growth of bandwidth. Meanwhile, as AOA-based implementations requires high complexity due to the presence of antenna array, positioning based on TOA estimation is commonly chosen in UWB-based positioning systems. Therefore, the emphasis of this section is the TOA-based UWB ranging techniques. First, main sources of errors in TOA estimation are investigated, then the current TOA estimators are reviewed.

A. ERROR SOURCES IN TIME-BASED RANGING

There are a number of error sources that may seriously degrade the accuracy of the range estimation. Before getting into different ranging algorithms, some of those error sources will be reviewed briefly.

Multipath Interference In time-based ranging systems, the propagation delay of the direct path is the desired parameter. In practical environments, especially indoor environments, transmitted signals usually arrive at the receiver via different paths due to the complicated propagation mechanisms such as reflection, scattering and diffraction. Hence, how to choose the first arriving path among dense multipath is a challenge for UWB ranging systems.

In narrow band systems, the absence of a sufficient time delay between any two consecutive multipath components may cause the multipath components to be unresolvable. Consequently, pulses through multipath may overlap with each other, which brings great difficulty to estimate the propagation delay of the first path. Although UWB ranging signals have a significant resolution of multipath components due to the large bandwidth, the dense multipath plus high noise effect may also make the first path detection quite difficult.

In the single path environment, estimation of time delay is accomplished by correlator or

matched filter easily. It operates the correlation between received signal and local template which is the same as the transmitted signals. The time delay corresponding to the peak of the correlation output is considered as the TOA. When employing this simple estimation in multipath environments, the correlation output may be corrupted by the received multipath signals. Since the delay spread and attenuation of different path vary greatly, the correlation output could be quite different from that in single path condition. Consequently, the time delay corresponding to the peaky point may be much later than the true TOA. If still estimating TOA as the previous way, large ranging error occurs.

Another error source related to multipath propagation is associated with the autocorrelation properties of the spreading sequences employed in ranging systems [2]. Commonly, in the UWB ranging systems, each user (node) is assigned an unique spreading sequence to distinguish one user from others. Hence, at the receiver side, the correlation is first operated to de-spread the desired signal from received signals. It then locks onto the correlation peak, and tries to identify the first arriving multipath delay which may be early than peaky point. If the ranging signals have an perfect autocorrelation property which consists a obvious peak and low side-lobe values, the multipath propagation can be mitigated greatly. Unless, the high side-lobe values with the presence of multipath give rise to a large probability of false TOA detection. In order to prevent such inference, the autocorrelation function of ranging signals should have a sufficiently low side-lobe values. One of the main focuses of this thesis is to find new ranging signals with better autocorrelation function than current signals. The detailed analysis and comparison of autocorrelation function from different ranging signals will be given in the Chapter 4.

Multuser Interference Multuser interference (MUI) describes the interference from other users (nodes). For ranging systems, it is common to work in an environment with several users, here in each receiver, received signal not only contains the signal from desired user but also from other interfering users. As shown in the Fig.2.2.4, the Node A is the target node, the distance of which is about to be estimated by the reference node. If considering the one-way TOA approach, When the signals of Node A arrive at the reference node, they has been deteriorated due to the presence of interfering Node B and Node C. In this case, if ignoring MUI, the accuracy of the TOA-based ranging may be significantly degraded. Hence, how to mitigate the MUI is another challenging issue for UWB ranging systems.

Commonly, MUI can be mitigated theoretically by assigning orthogonal channels to different users, either in time, frequency, code, or space domains. In practice, the imperfect orthogonality of channels brings MUI in ranging system inevitably. For instance, if spreading

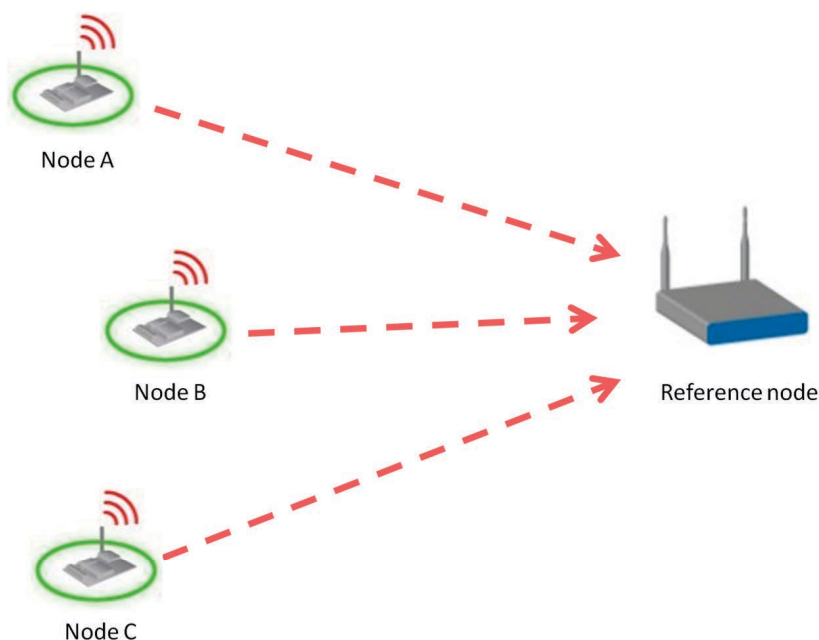


Figure 2.2.4: The schematic diagram of multiuser interference

sequences are assigned to users, the correlator output of TOA estimation includes the auto-correlation of desired user and the cross-correlation between user of interest and interfering users. If the cross-correlation is quite small compared to autocorrelation function, the MUI can be kept to a low level and even ignored. Oppositely, the peak of autocorrelation function may be masked by this interference which yields to large ranging error. Hence, the search of new ranging signal with good cross-correlation is also one of the goals of this thesis. And the results will also be represented in the Chapter 4.

When the number of users is large and systems have not perfect power control, the interfering users may be much stronger than desired user, which yield to ranging performance of correlator deteriorating significantly. Under this condition, except to make users more orthogonal, MUI mitigation algorithms should also be investigated. For example in [29], a non-linear filtering technique is proposed to improve the ranging accuracy for non-coherent receivers in the presence of MUI.

Other Sources Except multipath and multiuser interference, Non-Line-of-Sight (NLOS) propagation which means that the direct line-of-sight (LOS) signal between nodes is obstructed gives rise to excess delay of the TOA estimation. This is because the direct signal component is attenuated significantly or even cannot be detected by the receiver. The timing imperfections among reference devices and clock drifting between transmitter and receiver devices in the round-trip TOA measurements induce additional errors on range estimates. Due to their

large signal bandwidth, UWB receivers are more sensitive to timing jitter and clock drifting effects [16]. Since UWB ranging systems are seen as the candidate of low-cost and low-power ranging systems, it is desirable that accurate ranging could be achieved with low sampling rates. However, sampling UWB signals at sub-Nyquist rates usually introduces an additional ranging error then degrades the accuracy of UWB ranging systems.

B. TOA ESTIMATORS

After introducing the UWB signal and error source of time-based ranging, the current TOA estimators and their performance are presented in this section to give a comprehensive knowledge of UWB ranging systems.

Various TOA estimators have been proposed in the literature. In general, they can be classified into three common receiver architectures, which are matched filter (MF), energy detection (ED), and delay-and-correlate (DAC) based receivers. As shown in Fig.2.2.5 [30], for all receiver types, it is assumed that the signal is first passed through a band-pass filter of bandwidth B to remove out-of-band noise, and through a low-noise amplifier (LNA) to improve the signal quality. The samples may further be averaged over a number of ranging symbols to improve the ranging accuracy [30].

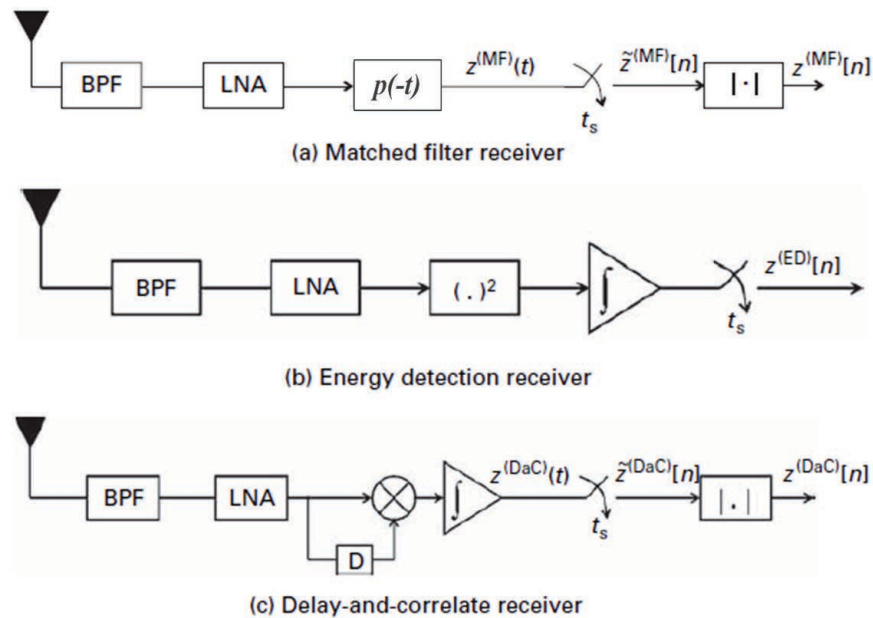


Figure 2.2.5: The different TOA estimator schemes (a). MF-based estimator (b). ED-based estimator (c). DAC-based estimator

In the following, we investigate the unmodulated UWB ranging systems with the transmit-

ted signal $s(t)$ as

$$s(t) = \sqrt{P} \sum_{m=0}^{M-1} p(t - mT_s) \quad (2.10)$$

where P is user's transmitted power per symbol which is assumed to be normalized to 1, $p(t)$ is the pulse shape with pulse duration T_p , T_s is the symbol duration, $T_s \geq T_p$. After passing through the multipath channel, the received signal $r(t)$ is expressed as

$$r(t) = \sum_{l=1}^L a_l s(t - \tau_l) + n(t) \quad (2.11)$$

L is the number of multipath components, a_l and τ_l are the channel coefficient and the delay of the l th path, respectively, and $n(t)$ is zero-mean additive white Gaussian noise (AWGN) with double-sided power spectral density $N_o/2$.

It is assumed that the TOA is uniformly distributed in $[0, T_a]$ and that the received signal is observed within an interval $[0, T_{obs}]$ where $T_{obs} \geq T_a$.

Matched Filter Based Estimator As discussed previously, matched filter (MF) operates the correlation between the received signal $r(t)$ and the local template of $s(t)$. Passing the received signal in (2.11) through an MF yields

$$z^{(MF)}(t) = \sum_{m=0}^{M-1} \sum_{l=1}^L a_l R_p(t - \tau_l - mT_s) + n_p(t) \quad (2.12)$$

where M is the number of ranging symbols in the observation interval. According to the communication theory, the impulse response of MF is given by $p(t)$, $R_p(\tau)$ is the autocorrelation function of $p(t)$,

$$R_p(t) = \int_{-\infty}^{\infty} p(\tau)p(\tau - t)d\tau \quad (2.13)$$

$n_p(t)$ is colored Gaussian noise with autocorrelation function given by $N_o R_p(\tau)/2$.

If $z^{(MF)}(t)$ is sampled with t_s interval, the average MF output can be obtained as

$$\bar{z}^{(MF)}[n] = \frac{1}{M} \sum_{m=0}^{M-1} z^{(MF)}(t)|_{t=nt_s+mT_s} \quad (2.14)$$

Note that averaging the MF outputs over M ranging symbols provides processing gain and improves the SNR. In many TOA estimation algorithms, the absolute values of the MF outputs

are compared to a threshold. The absolute value of $\bar{z}^{(MF)}[n]$ is represented by

$$z^{(MF)}[n] = |\bar{z}^{(MF)}[n]| \quad (2.15)$$

Various techniques have been proposed to detect the first path from $z^{(MF)}[n]$, including *Max* criterion [31] which takes the strongest sample in $z^{(MF)}[n]$ as first path, *P-Max* criterion [32] which is based on the selection of the earliest sample among the P largest in the $z^{(MF)}[n]$, *Simple threshold* [33], *Jump Back and Search Forward* criterion proposed in [34] based on the detection of the strongest sample and a forward search procedure. The simple threshold criterion is chosen as an example to show how to detect the first path. If we choose the threshold to be ε , the first event $z^{(MF)}[k]$ crossing ε gives the estimated TOA,

$$\hat{\tau}_1 = t_s * k + \frac{t_s}{2} \quad (2.16)$$

Energy Detected Based Estimator The MF based receiver requires the knowledge of the transmitted signal which may not be available in practice. Another key disadvantage of the MF solution is that for accurate ranging, it may require Nyquist rate sampling which yields to complex complex analog-to-digital converters. A low complexity alternative to the MF-based receiver is the energy detection (ED) receiver, which does not assume the knowledge of the transmitted pulse [33].

The integrator output samples for an ED receiver can be expressed as follows

$$z^{(ED)}[n] = \frac{1}{M} \sum_{m=0}^{M-1} \int_{mT_s+(n-1)t_s}^{mT_s+nt_s} |r(t)|^2 dt \quad (2.17)$$

where t_s here is the integration time of the ED, n denotes the block index, and the samples are averaged over M ranging symbols to increase the SNR as for the MF receiver. With the threshold ε , the first $z^{(ED)}[k]$ above the threshold is considered as the TOA estimation. Hence,

$$\hat{\tau}_1 = t_s * k + \frac{t_s}{2} \quad (2.18)$$

A drawback of an ED receiver is the sensitivity to noisy environment due to the noise-squared and signal-cross-noise terms appearing at the output of the square-law device. Therefore, a large M is needed to mitigate noise effect. In addition, the ranging accuracy also depends on the energy block width. A longer t_s requires lower sampling rate and makes the estimation time efficiency, but also with lower ranging accuracy. On the other hand, shorter t_s leads to high accuracy at the expense of high sampling rate and time consuming.

Delay-and-Correlate Based Estimator Another kind of receiver that does not require the knowledge of the received pulse is the delay-and-correlate (DaC)-based receiver. DaC-based receivers works on the principle that besides the transmitted signal, a reference signal is also sent with certain delay D . Hence, at the receiver side, a local template of transmitted signals is no longer needed. In the literature, two possible schemes of DaC based receiver are proposed [35,36]. In the first way which is also known as transmitted-reference (TR) receiver [35], at the transmitter side, pairs of pulse with a known time delay D between each pulse are transmitted. Then, the first arriving pulse is delayed the time D to correlated with the its reference pulse. The output is passed through the first arriving path detector to estimate the TOA. In the other way, the dirty-template scheme [36], the difference is that the reference signal is a transmitted symbol instead of a pulse.

The samples after correlating the received signal with the delayed version of itself can be written as

$$\bar{z}^{(DaC)}[n] = \frac{1}{M} \sum_{m=0}^{M-1} \int_{mT_s+(n-1)t_s}^{mT_s+nt_s} r(t)r(t-D)dt \quad (2.19)$$

where D represents the delay between transmitted signal and reference signal. Note that for a dirty-template receiver, $D = T_s$. For a TR receiver, delay D is pre-determined between the pulses in a pair. Following the $\bar{z}^{(DaC)}[n]$, the $z^{(DaC)}[n]$ as the absolute value of $\bar{z}^{(DaC)}[n]$ is obtained to detect the first path.

$$z^{(DaC)}[n] = |\bar{z}^{(DaC)}[n]| \quad (2.20)$$

Then, the $z^{(DaC)}[n]$ is also compared with threshold ϵ . The earliest $z^{(DaC)}[k]$ beyond ϵ is considered as the TOA estimation, which is

$$\hat{\tau}_1 = t_s * k + \frac{t_s}{2} \quad (2.21)$$

At the DaC-based receiver, received ranging signals are correlated with its delayed reference replica. Since $r(t)$ and $r(t-D)$ are noisy signals, the noise terms even signal-cross-noise terms are brought after the correlation operation. Therefore, DaC based receivers are also sensitive to the noisy environments.

C. MULTIUSER TOA ESTIMATORS

In the previous section, we give a brief overview of current different kinds of TOA estimators. In this section, we will discuss about their performance in multiuser environment. One of the main focuses of this thesis is to develop new accurate multiuser ranging algorithms. As

mentioned before, multiuser interference is one of the main error sources in TOA estimation. Hence, various algorithms have been proposed for mitigate the MUI in UWB ranging systems. For simplicity, we still classify the multiuser TOA estimators into the three types, MF-based, ED-based and DAC-based multiuser TOA estimators.

In multiuser environment, UWB ranging systems commonly assign an unique spreading sequence to each user. Depending on the different spreading sequences, UWB systems is divided into Direct Spreading (DS)-UWB systems and Time Hopping (TH)-UWB systems. For the DS-UWB systems, the transmitted signal of user k is

$$s_k^{DS}(t) = \sum_{m=-\infty}^{+\infty} \sum_{n=0}^{N-1} c_k^{DS}(n) p(t - nT_f - mT_s) \quad (2.22)$$

where $c_k^{DS}(n)$ is the direct spreading sequence of the k th user, N is the length of sequences, $p(t)$ is the transmitting pulse with duration T_p . T_f is the frame duration which is also the pulse repetition time, $T_f \geq T_p$. T_s is the symbol duration with $T_s = NT_f$. For the TH-UWB systems, the transmitted signal of the k th user is expressed as

$$s_k^{TH}(t) = \sum_{m=-\infty}^{+\infty} \sum_{n=0}^{N-1} p(t - c_k^{TH}(n)T_c - nT_f - mT_s) \quad (2.23)$$

where T_f is a frame duration which is segmented into N_h equally spaced intervals T_c . $p(t)$ is also the transmitting pulse with duration $T_p \leq T_c$. $c_k^{TH}(n)$ is the time hopping sequence of the k th user. T_s is the symbol duration with $T_s = NT_f$.

Although the use of spreading sequences improves the orthogonality of signals of different users, the imperfect orthogonality of spreading sequences and the existence of dense multipath which spoils the orthogonality further result in the MUI. This problem is worsened when the number of users is large or the interferers are sufficiently powerful, which is known as the *near-far* problem.

It is well known that MF-based estimator coincides with the optimal maximum likelihood (ML) method for a single user in the presence of white Gaussian noise but its performance degrades drastically in multiuser environment. To alleviate the effects of MUI, [37] proposed chip-level blind and data-aided synchronization algorithms by using a posterior probability of each chip to suppress MUI. Although coherent algorithms can mitigate MUI, the high sampling rate is still required.

As an alternative, subsampling TOA estimators based on energy detection have received significant attention [32,33,38]. These ED based estimators have low complexity at the expense of relatively low ranging accuracy. Meanwhile, not accounting for MUI with ED estima-

tor can greatly degrade performance further [3]. [29] proposed a nonlinear filtering technology on received signals energy to mitigate MUI for ED estimator. [39] proposed a TOA estimation scheme to mitigate both narrowband and multiuser interferences in multipath channel for ED estimator.

For the DAC-based estimator, [36] designed a specific training sequence for synchronization with dirty templates, which could mitigate the MUI effect. [35] proposed to mitigate MUI by assigning different delay D for different users.

Note that the above multiuser TOA algorithms are proposed for a small number of users. In the case of heavy or fully loaded system, especially without the perfect power control, these algorithms cannot achieve acceptable performance. How to support more users and resist to the near-far effect is the main focus of this thesis. We will propose our multiuser TOA estimators in the Chapter. 5 and Chapter. 6.

2.2.3 ULTRA-WIDEBAND CHANNEL

Wireless channel models carry significant importance for gaining insight into designing physical layer systems and selecting certain system parameters. For instance, in an IR-UWB system, a design engineer might need to know how much apart to transmit two sequential pulses in order to avoid inter-frame interference at the receiver, or how likely the first arriving signal component contains the highest energy among all signal components for accurate ranging. Answers to such questions can be obtained either directly from channel measurements conducted in an environment of interest, or from statistical models derived from channel measurements.

Large bandwidths of UWB systems result in significant differences in channel characterization compared to that for narrowband systems. For narrowband systems, the properties of the objects in a given environment, such as their reflection and scattering properties, can be considered as constant with respect to frequency due to the small frequency band of interest. However, for UWB systems, the frequency dependence of material properties as well as that of transmit and receive antennas become significant.

After being extensively discussed, the IEEE.802.15.4a has proposed UWB multipath channels based on the Saleh-Valenzuela Model (SV model) [40]. They are classified into 9 models:

- CM₁ Residential LOS 7m-20m
- CM₂ Residential NLOS 7m-20m
- CM₃ Office LOS 3m-28m
- CM₄ Office NLOS 3m-28m

- CM5 Outdoor LOS 5m-17m
- CM6 Outdoor NLOS 5m-17m
- CM7 Industrial LOS 2m-8m
- CM8 Industrial NLOS 2m-8m
- CM9 Open outdoor environment NLOS (e.g. farm, snow-covered area)

2.3 CONCLUSION

In this chapter, we presented an overview on the ranging techniques and systems, particularly on the TOA based ranging approaches and UWB ranging systems. For UWB ranging systems, following the brief introduction of its history and expected applications, the current ranging algorithms and the main challenges are introduced. The final part of this chapter is the overview of UWB channel condition, which is also our simulation environments in the following chapters.

"When the present determines the future, but the approximate present does not approximately determine the future," said Edward Lorenz, "this is chaos."

Edward Lorenz, Meteorologist

3

Chaotic Systems and Signals

In the Chapter 2, following the introduction of various ranging technologies and UWB ranging systems, the problems faced to current UWB ranging systems are also presented. In this thesis, pointing to those problems, we propose our new ranging algorithms for TOA based UWB ranging systems, whose ranging accuracy and system capacity can be enhanced further by using chaotic signal. Before we present our estimators, a brief introduction of chaotic systems and signals is addressed in this chapter. The definition and history of chaos is first be given, followed by the introduction of two kinds of chaotic systems, the discrete-time and the continuous-time chaotic systems. In the final part, the applications of chaotic signals in various field are shown.

3.1 DYNAMICAL SYSTEM AND CHAOS

"When the present determines the future, but the approximate present does not approximately determine the future," said Edward Lorenz, "this is chaos" [41]. Differently from constant state and either periodic or quasi-periodic motion of systems, Chaos describes a random behavior occurring in the deterministic systems. Chaotic systems are deterministic with no random elements involved, however, their deterministic nature does not make them predictable. This kind of behavior exists in many natural systems, such as changes in weather, the dynamics

of satellites in the solar system, and the population growth in ecology.

An early proponent of chaos theory was Henri Poincare. In the 1880s, when trying to solving the three-body problem, Henri Poincare found that there can be orbits which are aperiodic, and yet not forever increasing nor approaching a fixed point [42,43]. Much of the earlier theory was developed almost entirely by mathematicians since then, under the name of ergodic theory. The lack of an efficient method for calculating a large amount of repeated iteration was the main difficulty of developing the chaos theory and limited chaos theory only in the mathematics field.

In 1960s, due to the emergence of electronic computers, calculating a large amount of repeated iteration was not an impractical problem anymore. Chaos theory had an opportunity to develop further. In this phase, an early pioneer was Edward Lorenz, an American meteorologist. In the 1961, while working on weather prediction, he accidentally discovered a tiny difference of initial condition produced large changes in the long-term outcome, which was given the name “Lorenz attractor” [44].

From 1960s to the present, with the explosive development of computer science, a large number of mathematical model of chaos has been derived and investigated. Currently, the application of chaos theory has been spread from only mathematics field to several disciplines including meteorology, physics, engineering, economics and biology. In meteorology, Lorenz attractor shows that even detailed atmospheric modeling cannot in general make long-term weather predictions [44]. In a chemical reaction, chaos can be very useful to minimize the energy required in mixing two fluids thoroughly [45]. Several research show that chaos theory is also attractive in audio compression, video compression, public key cryptography systems [46–48]. Besides of all above, the use of chaos theory in cardiac arrhythmias can not only restore a periodic rhythm, but also is a less intrusion into the patient’s body system [49]. Similar efforts are applied to control epilepsy brain seizures which exhibit chaotic behavior [50]. Introducing the chaos theory into the study of socio-political phenomenon allows the researcher to better understand public policies and international relations problems, whose behavior seem to be, at first sight random and unpredictable [51]. Since the widely existence of chaos in natural systems, more and more new applications of chaos theory will be developed in the future.

Chaos plays such an important role in understanding our world, what’s its exact definition? Although there is no universally agreed definition of chaos, most people would accept the following working definition:

Chaos is aperiodic behavior in a deterministic system which exhibits sensitive dependence on initial conditions.

This definition reveals three distinguish features contained by chaotic systems,

1. *Aperiodic behavior* implies chaotic system is erratic, not simply quasi-periodic with a large number of periods.

2. *Deterministic system* means the chaotic system has no random variables, the aperiodic behavior arises from non-linear dynamics but not from noisy driving forces.

3. *Sensitive dependence on initial conditions* must be the most important characteristic of chaotic systems, which is popularly referred to as the *butterfly effect*. Small differences in initial conditions (such as those due to rounding errors in numerical computing) yield widely diverging outcomes for such dynamical systems, rendering long-term prediction impossible in general [52]. Fig. 3.1.1 uses a schematic diagram to show the sensitivity of initial condition in chaotic systems, where a_0 and b_0 are two different initial condition with a very close Euclidean distance.

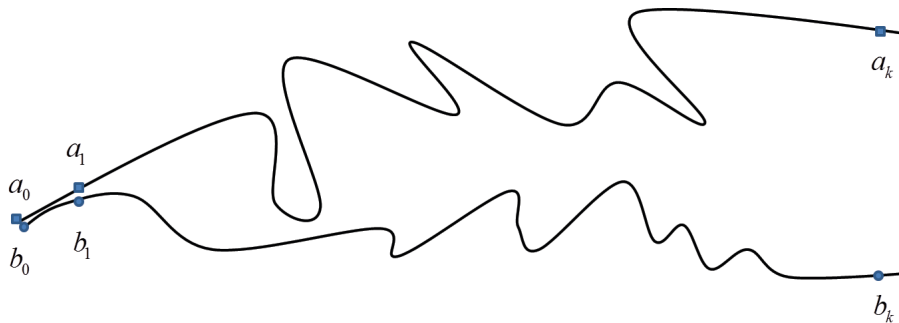


Figure 3.1.1: Schematic diagram of the sensitivity of a chaotic system under different but very close initial conditions a_0 and b_0 .

In general, chaotic systems can be classified into discrete-time chaotic system and continuous-time chaotic system. A **discrete-time chaotic system** takes the current state as the input and updates the situation by producing a new state as output. By the state of the system, we mean whatever information is needed so that the next state can be produced. These systems are known variously as difference equations, recursion relations or iterative maps. The other important type of chaotic systems is **continuous-time chaotic system** which not only can be obtained by direct modeling but also can be got by the limit of discrete systems with smaller and smaller updating times. This kind of chaotic systems are always modeled as a set of differential equations [53].

3.2 DISCRETE-TIME CHAOTIC SYSTEM

In 1976, Robert May emphasized that even simple nonlinear maps could have very complicated dynamics [54]. These “iterative maps” bring great convenience on the research of chaotic

behavior. *Logistic map* is the instance May illustrated in [54], which is given by:

$$x_{n+1} = ax_n(1 - x_n) \quad (3.1)$$

where $x_n \geq 0$, and the parameter $a > 0$. For illustrating the generation of chaotic behavior clearly and simply, we restrict the parameter a into the range of $(0, 4]$ so that the interval $0 \leq x_n \leq 1$ can be mapped by Eq.(3.1) into itself. Supposing we fix the parameter r and choosing some initial conditions, what's the relationship between r and chaotic behavior?

For the small value $a = 0.5$, as shown in Fig. 3.2.1 the sequence x_n approaches 0 with the increase of iterative number n , though it starts with the 3 different initial conditions.

When increasing $a = 2$, the corresponding difference equation is $x_{n+1} = 2x_n(1 - x_n)$. The 3 different initial conditions lead the x_n to the same nonzero steady state eventually, which is given in Fig. 3.2.2.

However, the trajectory of x_n exhibits a totally different behavior when $a = 4$. As shown in Fig. 3.2.3, x_n does not converge to a steady state any more even with a larger number of iteration. And a very slight differences in initial condition make the trajectories of x_n far from each other as shown in Fig. 3.2.4. This difference becomes larger with the increase of n , iteration number, which illustrates the feature of sensitive dependence of initial condition. Hence, according to the definition of *chaos*, logistic map with a parameter $a = 4$ is a chaotic systems.

A type of plot compresses the state space information so that variation as a function of the parameter can be viewed. This type of graph is called a **bifurcation diagram**, which shows the possible long-term values of dynamical systems. Fig.3.2.5 is the bifurcation diagram of the logistic map, which illustrates x_n converges to the unique steady state or fixed point when $0 < a < 3$, while the number of steady states is double when $a = 3$ until $a \approx 3.45$ yields to doubling the steady states again. Then, steady states double again and again with the increase of value of a . When a approaches to 4, logistic map finally gives rise to the chaos.

Although Logistic map is quite simple, it is a good example to show what are discrete-time chaotic systems and how they work. There are, nevertheless, a lot of other chaotic maps that have been well studied and applied. Such chaotic maps are listed but not limited below: *Bernoulli map*, *Tent map* and *Chebyshev map*.

Bernoulli map

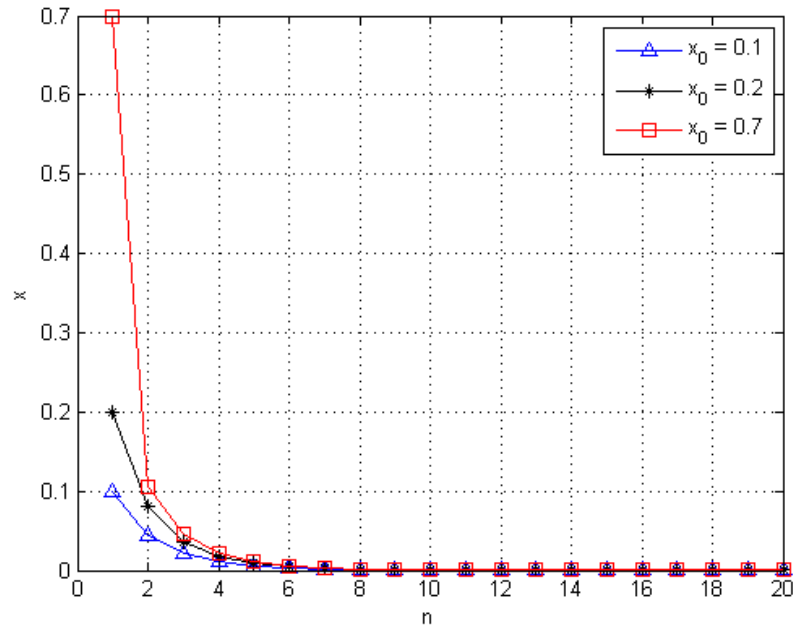


Figure 3.2.1: Trajectories of $x_{n+1} = 0.5x_n(1 - x_n)$ with the initial condition $x_0 = 0.1$, $x_0 = 0.2$, $x_0 = 0.7$.

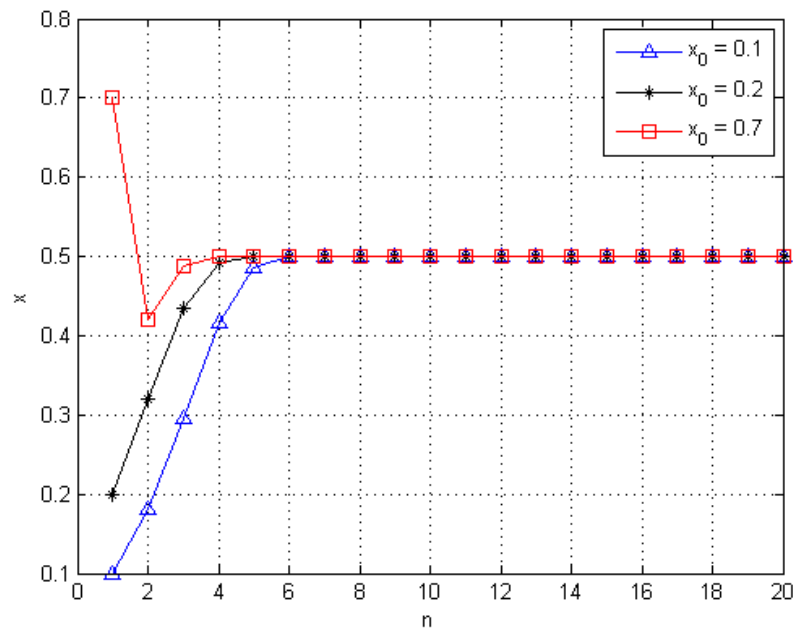


Figure 3.2.2: Trajectories of $x_{n+1} = 2x_n(1 - x_n)$ with the initial condition $x_0 = 0.1$, $x_0 = 0.2$, $x_0 = 0.7$.

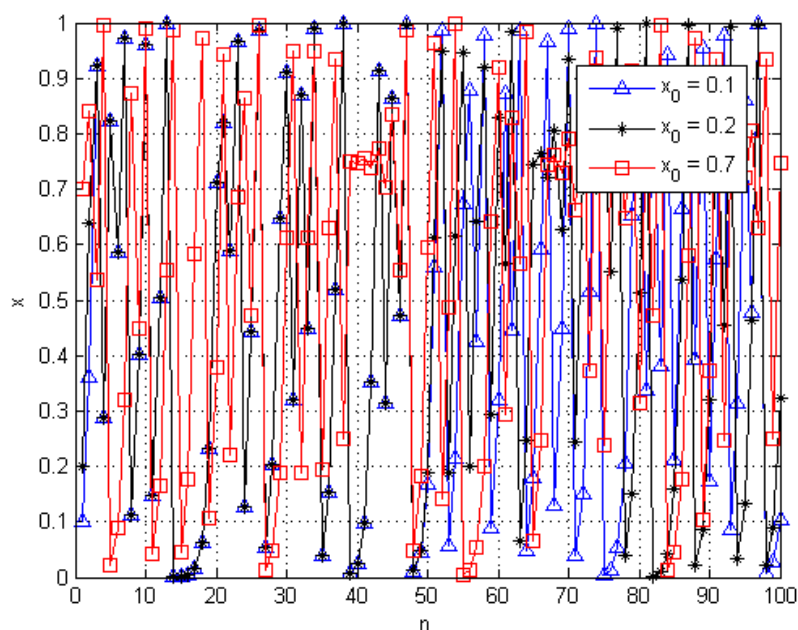


Figure 3.2.3: Trajectories of $x_{n+1} = 4x_n(1-x_n)$ with the initial condition $x_0 = 0.1$, $x_0 = 0.2$, $x_0 = 0.7$.

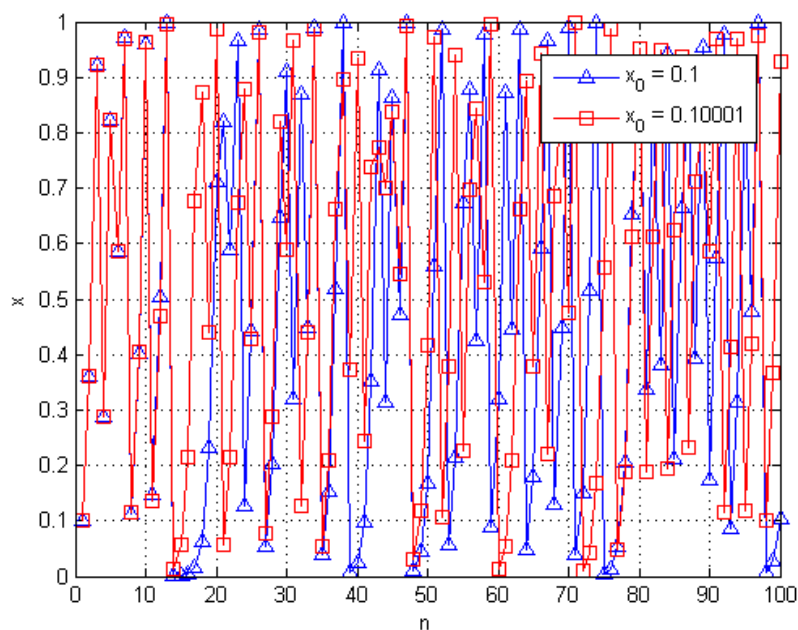


Figure 3.2.4: Trajectories of $x_{n+1} = 4x_n(1-x_n)$ with the initial condition $x_0 = 0.1$, $x_0 = 0.10001$.

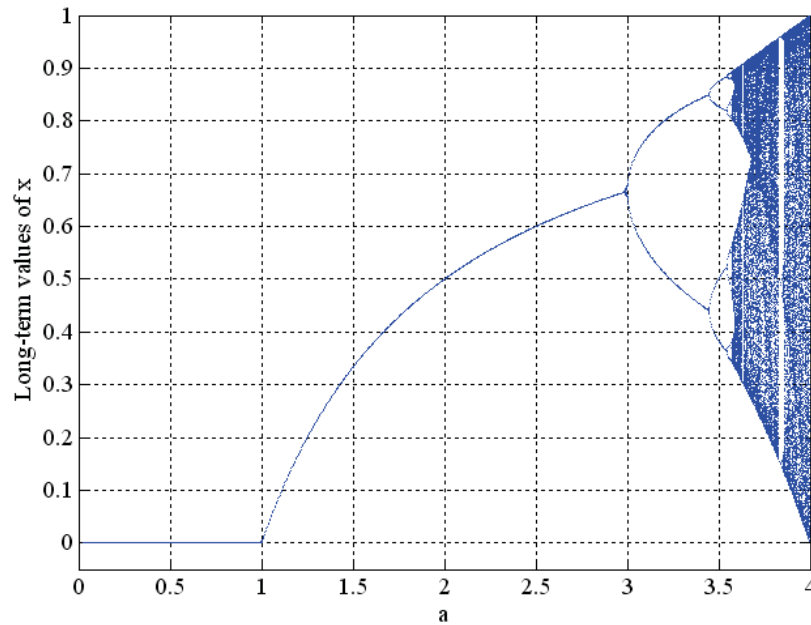


Figure 3.2.5: Bifurcation diagram of logistic map.

Bernoulli map, also known as dyadic map, is represented as

$$x_{n+1} = 2x_n \pmod{1} \quad (3.2)$$

where $x_0 \in [0, 1)$.

Tent map

Tent map with the parameter μ is the real-valued function defined by

$$x_{n+1} = \mu \min(x_n, 1 - x_n) \quad (3.3)$$

where $x_0 \in [0, 1)$. The bifurcation diagram of Tent map is illustrated in Fig. 3.2.6

Chebyshev map

Chebyshev map is the second-order Chebyshev polynomials expressed as

$$x_{n+1} = 1 - 2x_n^2 \quad (3.4)$$

where $x_0 \in (-1, 1)$. Chebyshev map can be considered as a special case of Logistic map.

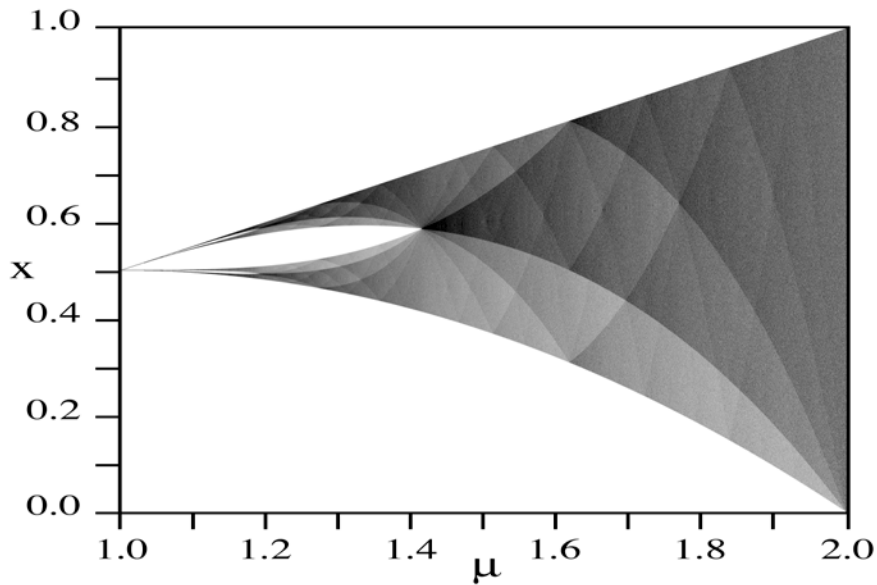


Figure 3.2.6: Bifurcation diagram of Tent map.

3.3 CONTINUOUS-TIME CHAOTIC SYSTEM

Many natural systems such as weather system exhibit the chaotic behavior. Since the time of Newton, the scientists consider that nature has arranged itself to be most easily modeled by differential equations. A differential equation, instead of expressing the current state as the function of previous state, expresses the rate of change of the current state as a function of current state. After introducing the chaotic maps thoroughly, we now turn to the continuous-time chaotic systems.

A well-studied continuous-time chaotic system is Lorenz system named after Edward Lorenz. Lorenz system is a three-dimensional chaotic system defined by

$$\begin{aligned}
 \dot{x} &= \sigma(y - x) \\
 \dot{y} &= rx - y - xz \\
 \dot{z} &= xy - bz
 \end{aligned} \tag{3.5}$$

where σ , r and b are referred to as the Lorenz parameters and all are greater than zero. If the following constraints are satisfied, Lorenz system has no steady state, and may lead to chaotic behavior [55].

$$b > 0 \tag{3.6}$$

$$\sigma > b + 1 \quad (3.7)$$

$$r > \frac{\sigma(\sigma + b + 3)}{(\sigma - b - 1)} \quad (3.8)$$

As a three-dimensional dynamical system with three parameters, Lorenz system exhibits a complicated behavior with the the different values of Lorenz parameter. Fig.3.3.1 illustrates that Lorenz system shows the well known “butterfly” shape in the x-z plane when Lorenz parameters value are $\sigma = 10, r = 28, b = 3/8$.

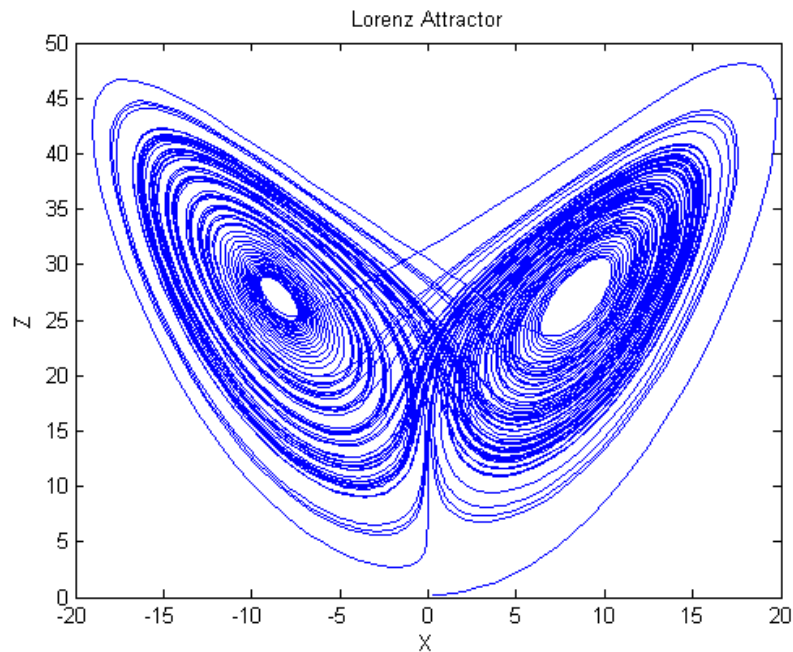


Figure 3.3.1: Lorenz system with Lorenz parameters $\sigma = 10, r = 28, b = 3/8$, and initial condition $[x(0) \ y(0) \ z(0)] = [0.3 \ 0.3 \ 0.3]$.

Till now, we have already known the basic knowledge of chaotic systems as well as several well studied examples. Further studies of the properties of both the discrete-time chaotic systems and continuous-time chaotic systems will be given in the Chapter 4. Due to the attractive features of chaotic signal, chaotic signal has been applied in many disciplines. In this thesis, we are concentrated on the application in the wireless communication and localization systems. Hence, in the following, we will introduce the existing applications of chaotic signal in wireless communication, radar and sonar systems.

3.4 APPLICATIONS OF CHAOS

From the definition of Chaos and the introduction of chaotic signals, we can summarize that chaotic signals are deterministic, aperiodic, and random-like signals derived from nonlinear dynamical systems, which offer a number of attractive features. First, its random-like behavior gives rise to the peaky autocorrelation and low cross-correlation function of chaotic signals, which further yields to an inherent wideband characteristic of chaotic signals. These properties are quite attractive to the current communication systems. Second, due to the sensitivity of initial conditions, a large number of chaotic signals could be generated easily. Further, the noise-like signal structure makes chaotic signals have a low probability of detection and intercept, which can be exploited by confidential communication systems. In addition, chaotic signals can be easily generated by simple circuits, which leads to low-complexity and low-cost products.

In the next chapter, further studies about the attractive properties will be presented in detail. In the following part of this section, it is shown that how these attractive features of chaotic signals are benefited by the in wireless communication and localization systems.

3.4.1 WIRELESS COMMUNICATION

Over the past decades, significant interest has been focused on exploiting the use of chaotic systems in wireless communication. Topics which have been explored include chaotic modulation for the transmission of analog and digital information and chaotic spreading sequences for multiuser access in spread spectrum systems.

A. Chaotic Modulation

Chaotic signals can be used to achieve the transmission of both analog and digital information. For transmitting an analog signal, chaotic masking and chaotic parameter modulation are proposed in [56–60]. For the side of chaotic digital modulation which is concerned with mapping digital information to analog chaotic waveforms, *Chaos Shift Keying (CSK)*, *Differential Chaos Shift Keying (DCSK)* and *Chaos On Off Keying (COOK)* have been proposed in the literature [61–63].

Chaotic Masking Modulation In chaotic masking modulation, a noise-like chaotic masking signal is added at the transmitter to the information bearing signal. The transmitted signal is $s(t) = m(t) + x(t)$, where $m(t)$ is the signal carrying the information added by the chaotic masking signal $x(t)$. Since this masking modulation hides the useful information $m(t)$ under

the noise-like chaotic signal $x(t)$, it is required that the amplitude of $m(t)$ should be much smaller than that of $x(t)$. At the receiver, the masking signal $x(t)$ is regenerated and subtracted from the received signal to recover the information signal $m(t)$ [64,65]. Chaotic masking modulation takes advantage of the random behavior of chaotic signals to enhance the security of communication. However, the regeneration of chaotic masking signal by the received signal, which is also known as synchronization process of chaotic signals, is the key point that the performance of chaotic masking modulation largely relies on.

Chaotic Parameter Modulation In chaotic parameter modulation, information signal is embedded in a parameter of chaotic systems [60]. By keeping this parameter in the chaotic regime, the output of chaotic system is sent for transmitting an information. For example, if the logistic map is chosen as the chaotic system, $x_{n+1} = ax_n(1 - x_n)$ in which $a \in [3.57, 4]$ is the chaotic regime for logistic map as introduced in 3.2. Instead of using the fixed parameter a , the value of a now varies in the chaotic regime and depends on the information signal. At the receiver, the information signal can be retrieved by estimating a from the received signal. Therefore, the process of estimating the chaotic parameter in noise effects the performance of chaotic parameter modulation. [60] shows that in the noise-free environment, the information signal is demodulated perfectly by the simple inverse function of modulation process. However, when channel noise exists, the effectiveness of this inversion approach decreases sharply.

Chaotic Shift Keying Chaotic shift keying (CFK) is a digital modulation scheme where chaotic signals generated by chaotic systems are used as the transmitting waveform corresponding to different symbols [66,67]. The chaotic systems may be the same dynamical system with different values of chaotic parameter or/and different initial condition, or completely different dynamical systems. The number of chaotic systems or initial conditions is equal to the number of different symbols.

The binary chaotic shift keying modulation, which is the simplest case of chaotic shift keying modulation, has been well studied in the past decades. In the binary chaotic shift keying, the binary data bits are modulated by transmitting the specific chaotic waveform corresponding to the “0” or “1” at a time. For instance, when data bit is “0” at the time t , the chaotic waveform $g_0(t)$ is transmitted. Otherwise, the other chaotic waveform $g_1(t)$ will be sent corresponding to the current data bit “1”. As mentioned above, these two chaotic waveforms can come from two different chaotic systems or the same system with different parameters. Then,

the transmitted signal $s(t)$ is equal to

$$s(t) = \begin{cases} g_o(t), & \text{symbol "0" transmitted} \\ g_i(t), & \text{symbol "1" transmitted} \end{cases} \quad (3.9)$$

If we choose $g_i(t)$ as the inverse copy of $g_o(t)$, i.e., $g_i(t) = -g_o(t)$, this kind of binary CSK is named as the **antipodal CSK**. Hence, the transmitted signal $s(t)$ can be expressed as

$$s(t) = \begin{cases} g_o(t), & \text{symbol "0" transmitted} \\ -g_o(t), & \text{symbol "1" transmitted} \end{cases} \quad (3.10)$$

At the receiver, both coherent and non-coherent receivers can be employed to demodulate the received signal. In a coherent correlation receiver, the sending data bits can be recovered by correlating the received signal with locally regenerated chaotic waveform $g_o(t)$ and $g_i(t)$. For the non-coherent receiver, the different bit energy for the two different data bits is required. Thus, the data bits can be obtained easily by comparing the receiver bit energy with a predefined threshold. The challenge lays in both coherent and non-coherent receivers is the noise sensitivity, particularly in the median or high noisy environment. In addition, accurate regeneration chaotic waveform $g_o(t)$ and $g_i(t)$ is also the problem for coherent receiver due to the high sensitivity of chaotic signal to initial condition.

Chaotic On-Off Keying Chaotic On-Off keying (COOK) works similar as chaotic shift keying, but instead of sending two different chaotic waveforms, chaotic on-off keying works like a on-off switch, the state is "on" or "off" is controlled by the transmitted data bit "1" or "0". When the state is "on", chaotic waveform is transmitted, otherwise, no signal is sent [67,68]. For example, if we define the transmitted signal $s(t)$ as following

$$s(t) = \begin{cases} 0, & \text{symbol "0" transmitted} \\ g_i(t), & \text{symbol "1" transmitted} \end{cases} \quad (3.11)$$

$g_i(t)$ is transmitted corresponding to the data bit "1". By contrast, the data bit "0" brings the silence of $s(t)$. Hence, the chaotic on-off keying provides a relatively high distance of bit energy for the two kind of data bits.

Chaotic on-off keying signal can be demodulated by both coherent and non-coherent receiver, which are similar as those for chaotic shift keying modulation. However, the perfect regeneration of transmitting waveform and sensitivity to noisy environment are also the problems to be faced for coherent and non-coherent receiver, respectively.

Differential Chaotic Shift Keying Differential Chaotic Shift Keying (DCSK) is a variant of chaotic shift keying [63,69]. The important feature of this scheme is that the transmitted chaotic waveform consists of the repeated segment of itself. With this property, in addition to a coherent correlation receiver, the simple differential coherent technique can be used for demodulation. According to differential Chaotic Shift Keying modulation, each transmitted chaotic waveform can be divided into two parts. The first part is the original chaotic signal, which serves as a reference signal. The second part serves as an information-bearing signal, depending on whether bit “0” or “1” is being transmitted. If “0” is to be transmitted, the information part is the inverted version of the reference part. If “1” is to be transmitted, the information part will be identical to the reference signal. Mathematically, symbols “0” and “1” can be represented by $s_0(t)$ and $s_1(t)$, respectively, which are shown as following,

$$s_0(t) = \begin{cases} g(t), & 0 \leq t \leq T_s/2 \\ -g(t - T_s/2), & t \leq T_s/2 \leq T_s \end{cases} \quad (3.12)$$

$$s_1(t) = \begin{cases} g(t), & 0 \leq t \leq T_s/2 \\ +g(t - T_s/2), & t \leq T_s/2 \leq T_s \end{cases} \quad (3.13)$$

where $g(t)$ and T_s are the chaotic waveform and bit duration, respectively.

At the receiver side, the received signal is correlated between the reference part and the information part, then, the data bit is recovered from the sign of correlation output. The differential correlation between information part and reference part makes the DCSK insensitive to channel distortion. The regeneration of chaotic waveform is also no longer required. However, this signal structure also doubles the transmitted power and halves the bit rate.

B. Chaotic CDMA

Instead of conventional narrowband communication systems, spread spectrum communication systems have played more and more important role in our daily life for its properties of suppressing interference, accommodating fading and providing a multiple access capability. Nowadays, with the explosive development of the third generation (3G) mobile systems, *Code division multiple access (CDMA) systems* may be the most well-known and impacted spread spectrum communication systems.

Direct-Sequence CDMA Direct-Sequence CDMA (DS-CDMA) system spreads a narrowband signal by multiplying it with the *spreading sequences*. Currently, the common used spreading sequences such as *Gold sequence*, *m-sequence* are *pseudo-random noise (PN)* sequences, which have relatively flat frequency spectrum, good autocorrelation and cross-correlation prop-

erties [70,71]. Due to the natural non-periodic and noise-like property, chaotic sequences is considered as an option of spreading sequences for DS-SSMA systems in the last decades. [72, 73] show that chaotic sequences have the similar even better autocorrelation, cross-correlation properties and *power spectral density* (PSD) when comparing with conventional PN sequences. [67,74–78] shows that chaotic sequences outperform classical PN sequences in many realistic environments and they are also proved to be the better choice when *multiple-access interference* (MAI) is the unique cause of error [79–83]. In addition, in conventional PN sequences generator, sequences are produced by visiting each state of the generator once in a determined manner. Since the number of state is finite, the number and length are restricted in the PN sequences. Oppositely, due to the high sensitivity of initial state, chaotic sequences theoretically have no such restriction on the length and number of sequences. Hence, the good correlation and infinite number of sequences make chaotic sequences be a new attractive class of DS-SSMA sequences. New accurate approaches for obtaining the bit error rate (BER) of chaos-based DS-SSMA systems are presented in the [84–86], which explores the dynamical properties of chaotic sequences. In addition, [87] proposes to use Gold sequences as the periodic pilot signal in the asynchronous chaos-based DS-SSMA systems to achieve good synchronization.

Frequency-Hopping CDMA In comparison with DS-SSMA, a major advantage of FH is that it can be implemented over a much wider frequency bandwidth, and bandwidth can be noncontinuous. Another advantage is that the requirement for power control is much less stringent in a multiuser system. These two advantages make FH-SSMA attractive for many applications. Several chaotic FH sequences have been proposed in the literature [88,89]. The analysis shows that chaotic FH sequences are harder to intercept and give a uniform spread over the entire frequency bandwidth. Meanwhile, the good Hamming correlation properties and ideal linear span of chaotic FH sequences also make them good candidate in multiple access applications [88]. In addition, the design and realization of a *field programmable gate arrays* (FPGA) based prototype for chaotic FH sequences generator has been realized in [89]. The BER performance evaluation of the chaos-based asynchronous FH-SSMA system suggests that the cost-effective and well-performing sequences generator has the potential to be incorporated into existing FH systems.

C. Chaotic UWB

Since the FCC allows the frequency band between 3.1–10.6 GHz available for unlicensed UWB devices, impulse radio UWB (IR-UWB) communication systems have become a great important point for researchers. IR-UWB systems employs ultra-short duration ($< 1\text{ns}$) pulses,

which also yield to ultra-wide bandwidth. UWB systems are particularly promising for short-range wireless communications as they potentially combine reduced complexity with low power consumption, low probability of intercept (LPI) and immunity to multipath fading.

The chaos-based communication technology offers a number of attractive features for UWB applications due to the inherent wideband, deterministic, nonperiodic, and random-like properties of chaotic signals [4]. In addition, chaotic waveforms can be easily generated by simple circuits and directly into required microwave band without the need for a local oscillator and a mixer, which is very suitable for the low-cost, low-complexity and low-power requirement applications [8]. In another way, instead of transmitting the chaotic waveform directly, employing chaotic sequences as the direct spreading sequences has been studied in [90]. When comparing with traditional PN sequences, chaos-based spreading results in a bit rate increase in synchronous UWB communication systems. More earlier, the *pseudo-chaotic time hopping* (PCTH), a modulation scheme for UWB impulse radio, was first proposed in [91]. PCTH exploits concepts from symbolic dynamics [92] to generate aperiodic time hopping sequences that, in contrast to the traditional fixed (periodic) time hopping sequences, depend on the input data. The PCTH scheme combines pseudo-chaotic encoding with multilevel pulse-position modulation. Multi-access PCTH (MA-PCTH) is an extension of PCTH, which assigns an unique pulse train to each user to distinguish different users [93]. PCTH modulation has the advantage of the noise-like spectrum, which is a desirable feature in terms of LPI and to reduce interference towards other users [91]. Almost at the same time, another chaotic modulation, named as the *chaotic pulse position modulation* (CPPM) is proposed for UWB communication system. CPPM generates a sequence of pulses where intervals between the pulses are determined by a chaotic law. Then, this pulse train with chaotic inter-pulse intervals is used as a carrier. Binary information is modulated on this carrier by pulse position modulation furthermore [94,95]. CPPM can improve the communication privacy and has a lower probability of intercept. Moreover, CPPM is not sensitive to the channel distortion and the negative effect of filtering.

3.4.2 RADAR AND SONAR

Besides wireless communication, a growing number of research interests has been emerged in the field of chaos-based radars and sonar [55,96–108]. The research topics include signal analysis and design, echo-signal processing, prototype system development and so on. These current advances reveal that the chaotic signals are suitable for radar and sonar application and may provide excellent processing and performance advantages.

In [96], chaotic waveform is first proposed to be used in the radar systems. Bauer in [96]

demonstrates that chaotic waveforms has a thumb tack ambiguity functions and points out that chaotic waveforms with different initial conditions are uncorrelated in the long term. In addition, the simple structure of chaos generator make it more attractive to radar systems. In [55], it is proved that many properties of Lorenz waveform including autocorrelation function, transmit power level are related to Lorenz parameters. And scaling the Lorenz parameters corresponds to an approximate time and amplitude scaling of Lorenz waveform and also corresponds to scaling the waveform bandwidth. In another words, these Lorenz waveforms can be generated with arbitrary time length and bandwidth. Based on these properties, a set of quasi-orthogonal chaotic waveforms based on Lorenz system are proposed for wideband and *multiple-input, multiple-output* (MIMO) radar applications in [55].

For the sonar side, chaotic pulse position modulation (CPPM) is proposed in [107] to improve the efficiency of sonar systems for ranging measurement in presence of noise and crosstalk. The main idea of CPPM is to generate a sequence of pulses in which the time interval between a pulse and subsequent one is controlled by a chaotic law. Both discrete-time and continuous-time chaotic signal can be used as the controller. [107] prefers to employing the continuous-time chaotic signal due to its entire simple analog circuitry without requiring any digital processor. At the receiver, the distance is estimated by correlating the echo pulses with transmitted pulses to obtain the transmitting time. [108] proposes another kind of CPPM for ultrasonic radar systems. A reference sinusoidal signal is added to a chaotic signal, and a whole signal is modulated by PPM method. After demodulating PPM, the sinusoidal signal is recovered from demodulated signal by subtracting the chaotic signal which is regenerated in the receiver side. Then, the distance is measured by the phase difference between recovered sinusoidal signal and reference sinusoidal signal. In this CPPM method, chaotic signal has the same use as the chaotic masking signal in chaotic masking modulation.

3.5 CONCLUSION

In this chapter, we firstly give a general introduction of chaos theory and dynamic systems. Then, a discrete-time chaotic system and a continuous-time chaotic system have been presented with several well-studied examples, respectively. After giving a brief summary of the special features of chaotic signals, the current application of chaotic systems in wireless communication, localization system have been presented. In the following chapter, we will give the further analysis of chaotic signals according to several interesting properties.

*"Look well into thyself, there is a source which will always
spring up if thou wilt always search there."*

Marcus Aurelius, Roman Emperor

4

Ranging-Related Properties of Some Chaotic Signals

In chapter 3, following an introduction of chaos theory and chaotic signals, current chaotic applications in many fields are presented. Due to its deterministic, aperiodic and random-like features, chaotic signals become more and more attractive in wireless communication and localization areas. In this chapter, we first introduce the three most important properties required for ranging signals, which are autocorrelation, cross-correlation and frequency spectrum property. Due to their significant effects on ranging performance, the three properties are often chosen as the criteria to evaluate the strengths and weakness of ranging signals. Then, the comparison between chaotic signals and classic ranging signals through all these three requirements are shown to illustrate that chaotic signals are an potential alternative to classic signals in UWB ranging system.

4.1 SPECTRUM PROPERTY

The first important property of ranging signal is the power spectrum density (PSD), which gives us a view of signals from the frequency domain. The power spectrum density is defined

as

$$\begin{aligned}\Phi_s(j\omega) &= S(j\omega)S^*(j\omega) \\ &= |S(j\omega)|^2\end{aligned}\tag{4.1}$$

where $S(j\omega)$ is the Fourier transform of transmitted signal $s(t)$. The power spectrum density can be related to the energy of $s(t)$ through Parseval's equation. In addition, the more interesting relation is that power spectrum density $\Phi_s(j\omega)$ and autocorrelation function are Fourier pairs.

Commonly, different ranging systems have different requirements in PSD according to the ranging signal they employ. For example, in UWB ranging systems, transmitted signals $s(t)$ should have an absolute $10dB$ bandwidth of at least $500MHz$ or a fractional $10dB$ bandwidth of larger than 20% [1]. And the PSD of UWB ranging signals should be below the power levels regularized by FCC to avoid the interference to other systems in the same frequency spectrum [22]. In addition, if the TOA or AOA ranging technique is employed, the effective bandwidth should also be taken into account when designing or choosing transmitted signals. Typically, larger frequency bandwidth gives rise to larger effective bandwidth, which yields to higher ranging accuracy. In this thesis, due to the main focus of TOA ranging technique, the frequency bandwidth is chosen as the most important criterion to evaluate the different ranging waveforms in the frequency domain.

For conventional pulses used in UWB ranging systems, such as raised cosine pulse, root raised cosine pulse and rectangular pulse, the frequency bandwidth B_p is inversely proportional to the first zero-cross duration of pulses t_p , as given by

$$B_p = \frac{1}{t_p}\tag{4.2}$$

Due to this inverse relation between B_p and t_p , the wideband systems, especially UWB system, must use extreme short pulses. For example, the pulse duration is in the order of a nanosecond in UWB system. Undoubtedly, how to generate such a short pulse precisely is a challenge to the transmitter.

In chaotic systems, continuous-time chaotic pulse/waveform is a fragment of the continuous-time chaotic signal whose duration T_c is longer than the quasi-period of chaotic oscillation t_c , i.e., $T_c \gg t_c$. The frequency bandwidth of chaotic pulse B_c is determined by the bandwidth of the original continuous-time chaotic signal generated by the chaotic source, but is independent of the pulse duration in a wide range of duration variation [109]. Chaotic source

generates a continuous-time chaotic signal with the a frequency bandwidth ΔF , then

$$\Delta F = F_u - F_l = \frac{1}{t_c} \quad (4.3)$$

where F_u and F_l are the upper and lower boundaries of the chaotic oscillation band, respectively. Based on the this definition, the bandwidth of chaotic pulse B_c is expressed as

$$B_c = \Delta F \neq \frac{1}{T_c} \quad (4.4)$$

Thus, theoretically, T_c can vary in the range of $T_c \approx \frac{1}{\Delta F}$ to $T_c \rightarrow \infty$, where the power spectrum density of chaotic pulse will be the same as that of original chaotic signals. In other word, the inverse relationship of bandwidth and pulse duration in classic pulses has no existence in the chaotic pulses, which makes the chaotic pulses essentially different from the conventional pulses. Instead of a short duration, an almost arbitrary pulse duration can be chosen for chaotic pulse in UWB ranging systems. Hence, the challenge for generating a short duration pulse is quite eased.

For showing the this property intuitively, PSD of Lorenz waveforms with different duration are given in the Fig.4.1.1. In this figure, Lorenz waveforms are generated with the same Lorenz parameters $\sigma = 30, r = 84, b = 8$, but in the different length $T_c = 31ns$ and $T_c = 127ns$. Since different initial conditions give rise to different Lorenz waveforms, the average power spectrum density over 100 realization is considered in the Fig.4.1.1. As shown in the Fig.4.1.1, although the length of two Lorenz waveforms are quite different, power spectrum density has almost no change. Consequently, the 10dB frequency bandwidth is also the same for two length of Lorenz waveforms. As discussed previously, chaotic waveforms is independent to time duration T_c for certain bandwidth B_c , which provides great convenient for choosing transmitting ranging waveforms.

Although chaotic pulses almost have no restriction in pulse duration, how to achieve the desired frequency bandwidth is the another question faced to chaotic pulses. For the classic pulses, frequency bandwidth can be adjusted easily by the variation of pulse parameters. For an instance, frequency bandwidth of raised cosine pulses can be controlled by the roll-off factor. Raised cosine pulses with different roll-off factor have different frequency bandwidths. Thus, these kind of pulses can be applied easily to different systems as its frequency bandwidth could satisfied different application requirements. Since frequency bandwidth of chaotic pulse is only determined by the chaotic source, how could we make chaotic waveforms satisfying certain frequency bandwidth? Could we change the parameters of chaotic source to

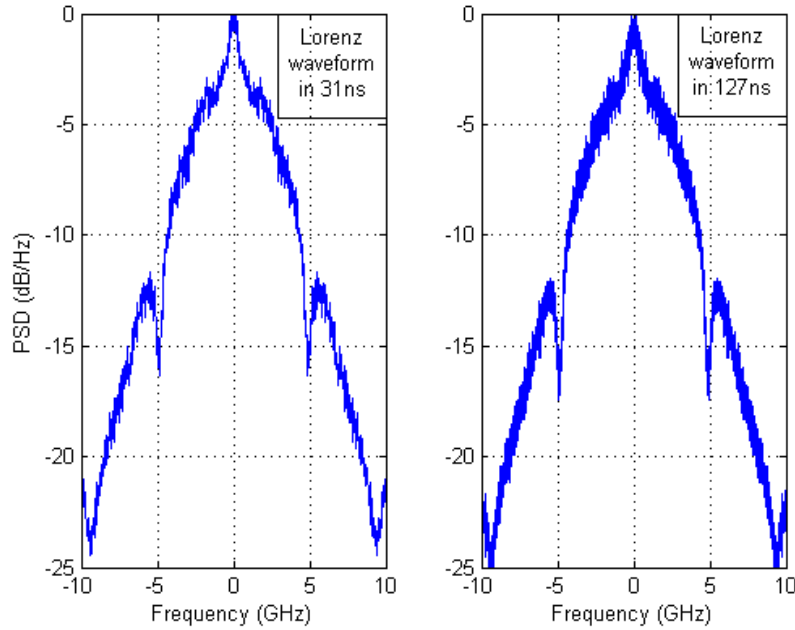


Figure 4.1.1: Power spectrum density of Lorenz waveforms with the same Lorenz parameters in the length $T_c = 31ns$ and $T_c = 127ns$.

obtain the chaotic pulses with different frequency bandwidth? In [55,106], Willsey has found that for Lorenz system, a slightly modification of Lorenz system gets rise to the exact time-scaling waveform. Consequently, frequency bandwidth is also scaled due to the time-domain and frequency-domain relationship. Furthermore, Willsey points out that scaling the system parameters can correspond to an approximate time and amplitude scaling of Lorenz waveforms and also corresponds to scaling the frequency bandwidth of Lorenz waveform.

As mentioned in Chapter 3, Lorenz system is expressed as Eq.(3.5). In order for the Lorenz system to give rise to chaotic dynamics, the Lorenz parameters σ , r and b must satisfy Eq.(3.6), Eq.(3.7) and Eq.(3.8). To simplify the representation of the Lorenz equations, we use the vector v and the vector $f(v)$ to denote the x, y, z state variables and Lorenz equations.

$$v = \begin{pmatrix} x \\ y \\ z \end{pmatrix} \quad (4.5)$$

$$f(v) = \begin{pmatrix} \sigma(y - x) \\ rx - y - xz \\ xy - bz \end{pmatrix} \quad (4.6)$$

With this notation, Lorenz system can be rewritten as

$$\dot{v} = f(v) \quad (4.7)$$

In [55,106], for identical initial condition, the exact time-scaling of Lorenz system is expressed as

$$\begin{aligned} \dot{v}_1 &= af(v) \\ v_1(t) &= v(at) \end{aligned} \quad (4.8)$$

where $a \geq 0$. Since the time-domain relationship implies a frequency-domain relationship between $v(t)$ and $v_1(t)$, the time-scaling by a factor a results in a frequency scaling by $\frac{1}{a}$. Hence, the bandwidth of $v_1(t)$ is a times the bandwidth of $v(t)$.

The PSD of Lorenz system with parameters $\sigma = 6$, $r = 36$, $b = 3$ is shown in the left side of Fig.4.1.2. The 10dB frequency bandwidth is almost 1.3GHz, but when we scale the Lorenz systems with $a = 3$ whose PSD is illustrated as the right side of Fig.4.1.2, frequency bandwidth grows to 3.9GHz which is 3 times the bandwidth of the left side. Hence, by exact time-scaling, Lorenz system could generate Lorenz waveforms with arbitrary bandwidth.

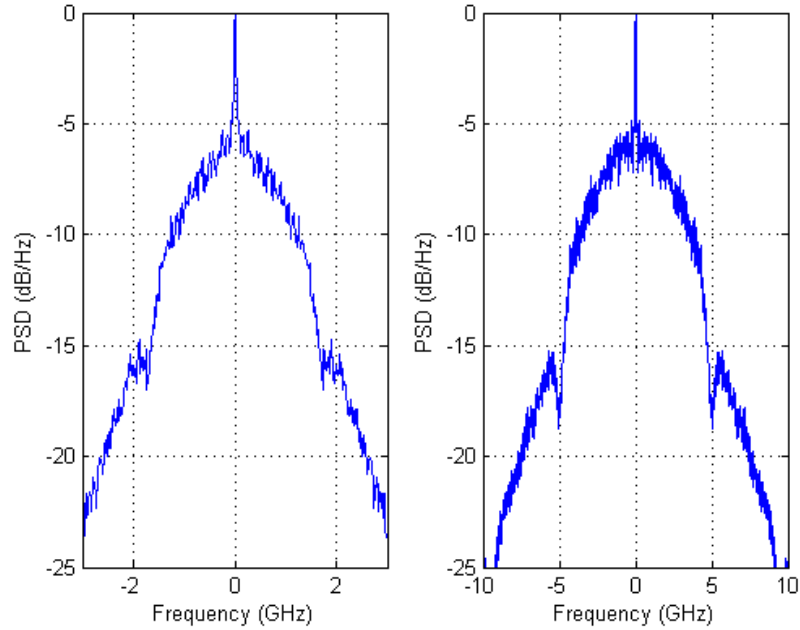


Figure 4.1.2: Power spectrum density of the exact time scaling Lorenz waveforms in the length $T_c = 31ns$.

The exact time scaling needs to scale the whole Lorenz equation by a factor a . The following method can achieve an approximate time-scaling by only changing the Lorenz parameters. It is shown in [55,106] that if we choose

$$\{\hat{\sigma}, \hat{r}, \hat{b}\} = \{a\sigma, ar, ab\} \quad (4.9)$$

with

$$\{\hat{x}(0), \hat{y}(0), \hat{z}(0)\} = \{ax(0), ay(0), az(0)\} \quad (4.10)$$

and the constraints

$$\begin{aligned} r &\geq 360 \\ a &\in [0.4, \infty] \end{aligned} \quad (4.11)$$

we can obtain

$$\hat{v}(t) \approx av(at) \quad (4.12)$$

This time domain relationship in Eq.(4.12) also implies a frequency domain relationship between the Fourier transform of $\hat{v}(t)$ and $v(t)$. A time scaling by a results in a frequency scaling by $\frac{1}{a}$. Consequently, the frequency bandwidth of $\hat{v}(t)$ increases by the factor of a regarding that of $v(t)$. All these changes are only caused by scaling a times the 3 parameters and initial condition. This interesting result gives us the idea that the bandwidth of Lorenz waveform can be adjusted only by scaling the 3 parameters and initial condition, which gives the Lorenz waveforms a great opportunity to be applied in ranging or communication systems.

4.2 AUTOCORRELATION PROPERTY

In this section, another important ranging related property is introduced detailedly, which is the autocorrelation property of ranging waveforms. The definitions of autocorrelation function are given at first, followed by the analysis of autocorrelation function in both DS-UWB and TH-UWB ranging systems. Finally, the detailed analysis of the autocorrelation property of chaotic signals is shown with the comparison to the current ranging signals.

4.2.1 AUTOCORRELATION FUNCTION

Autocorrelation describes the correlation of a signal with itself. Informally, it is the similarity between observations, which is a function of the time between them. Time here, may be an integer number for a discrete-time signal or a real number for a continuous-time signal. Mathematically, we can define the autocorrelation function, $R_s(\tau)$ in Eq.(4.13) for continuous-time

signal and $R_s(n)$ Eq.(4.14) for discrete-time signal, respectively, where "*" denotes a convolution and "*" denotes the complex conjugate.

$$\begin{aligned} R_s(t) &= s(t) * s^*(-t) \\ &= \int_{-\infty}^{+\infty} s(\tau)s^*(\tau - t)d\tau \end{aligned} \quad (4.13)$$

$$\begin{aligned} R_s(n) &= s(n) * s^*(-n) \\ &= \sum_{\tau=-\infty}^{+\infty} s(\tau)s^*(\tau - n) \end{aligned} \quad (4.14)$$

For comparing intuitively, the *normalized autocorrelation function* is introduced, which is formed by the autocorrelation function normalized by its maximum value. In the following part of this thesis, autocorrelation means the normalized autocorrelation function without particular indication. A typical autocorrelation function is shown in the Fig. 4.2.1, which illustrates that autocorrelation function consists of a high main-lobe as well as many small side-lobes.

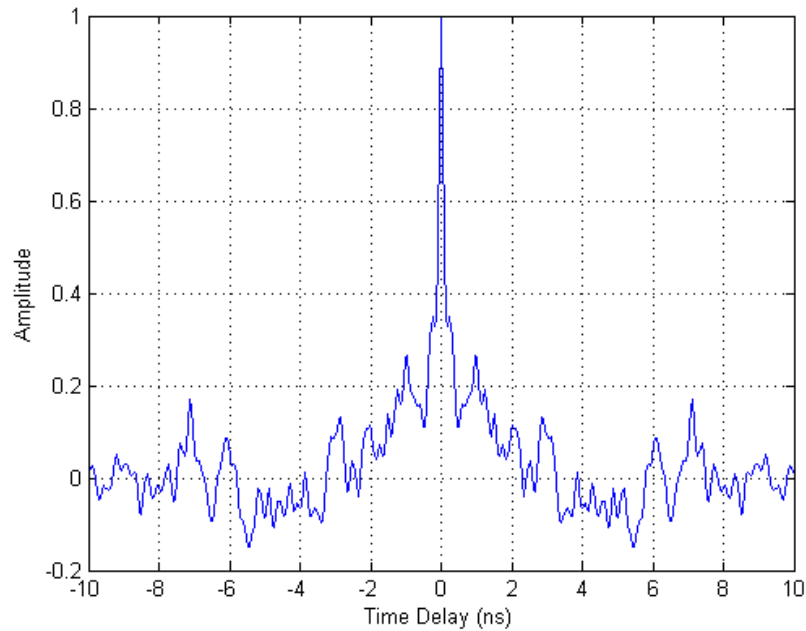


Figure 4.2.1: Autocorrelation function of a typical ranging waveform.

Why should we consider the autocorrelation property of transmitted signals in the ranging systems? In traditional ranging processing, in receiver side, the baseband received signal

$r(t)$ is matched filtered with the local template which is a replica of the baseband signal $s(t)$, corresponding to the transmitted signal. The matched filter operation can be expressed as

$$R_{MF}(t) = r(t) * s^*(-t) \quad (4.15)$$

It is obvious that the matched filter operation essentially is a correlation function. If a zero-noise single path environment is considered, which is the ideal channel condition, received signal can be rewritten as $r(t) = as(t - \tau_1)$ where a is a channel coefficient and τ_1 is a time delay. Then the output of matched filter $R_{MF}(t)$ is

$$\begin{aligned} R_{MF}(t) &= r(t) * s^*(-t) \\ &= \int_{-\infty}^{+\infty} as(\tau - \tau_1)s^*(\tau - t)d\tau \\ &= R_s(t - \tau_1) \end{aligned} \quad (4.16)$$

Obviously, $R_{MF}(t)$ is a time delayed and amplitude scaled version of autocorrelation function $R_s(t)$ where the time delay is related to the distance to the ranging target. If we consider a more complex but also more realistic condition, the noisy multipath environment, the received signal from a cluster of multipath is approximated by a collection of that in the ideal case with different time delay plus the additive noise. Hence, the output of matched filter signal in multipath channel, described by $R_{MF}(t)$, is a linear superposition of autocorrelation function $R_s(t)$ pulse noise. Consequently, features of autocorrelation, such as the main-lobe width and the side-lobe level, are extremely important in the ranging systems.

The main-lobe of $R_s(t)$, centered around $t = 0$, is the maximum value of the autocorrelation function. The width of the main-lobe is desired to be as narrow as possible, since a narrow main-lobe leads to a better capability of resolving multipath. The variation in the main-lobe width was observed to be due to a difference in bandwidth, which can be intuitively explained by the autocorrelation function and the power spectrum density being Fourier transform pairs.

In addition to a main-lobe width, $R_s(t)$ also has many smaller side-lobes. Ideally, the autocorrelation function should have side-lobes as low as possible, since large, peaky side-lobes result in false ranging estimation, particularly in the severe multipath or SNR environment. The amplitude of side-lobes can be evaluated directly from the autocorrelation function.

In the ranging systems, ranging signals are always transmitted continuously and/or periodically. In this case, $s(t)$ in Eq.(4.13) should be written as

$$s(t) = \sum_{m=0}^{+\infty} s_{sym}(t - mT_s) \quad (4.17)$$

where m is the number of symbols, $s_{sym}(t)$ is the transmitted signal per symbol with symbol duration T_s . Since that, the autocorrelation function $R_s(t)$ turns to the *cyclic autocorrelation function* $R_s^c(t)$, which is given as

$$\begin{aligned} R_s^c(t) &= s(t) * s^*(-t) \\ &= \int_{-\infty}^{+\infty} s(\tau) s^*(\tau - t)_{T_s} d\tau \end{aligned} \quad (4.18)$$

where $(\cdot)_{T_s}$ denotes to take modulo T_s . The modular operation is involved due to the consideration of the effect from the neighboring signal. In the following part of this thesis, autocorrelation means the non-cyclic autocorrelation unless particularly indicated. And cyclic autocorrelation denotes the autocorrelation of periodical transmitted signals.

4.2.2 AUTOCORRELATION FUNCTION OF DIRECT SPREADING SEQUENCES

In direct-sequences UWB (DS-UWB) ranging systems, each user is distinguished by a unique binary spreading sequence assigned by system. Thus, the transmitted signal of each user is formed by a waveform multiplied by the direct spreading sequences as shown in Eq.(4.19).

$$s_k(t) = \sum_{n=0}^{N-1} c_k(n) p(t - nT_p) \quad (4.19)$$

where $c_k(n) \in \{\pm 1\}$ is the spreading sequence of the k th user, N is the length of spreading sequences, $p(t)$ is the transmitting pulse with duration T_p . If we further define the $t = iT_p + \mu$, where $0 \leq i < N$ is a integer number and $0 \leq \mu < T_p$. Then, the autocorrelation function of $s_k(t)$ with substitution of Eq.(4.19) can be extended into

$$\begin{aligned} R_{s_k}(t) &= \int_{-\infty}^{+\infty} s_k(\tau) s_k^*(\tau - t) d\tau \\ &= \int_{-\infty}^{+\infty} \sum_{n=0}^{N-1} c_k(n) p(\tau - nT_p) \sum_{m=0}^{N-1} c_k(m+i) p^*(\tau - nT_p - \mu) d\tau \\ &= \sum_{n=0}^{N-1} c_k(n) c_k(n+i) \int_{-\infty}^{+\infty} p(\tau - nT_p) p^*(\tau - \mu - nT_p) d\tau \\ &= R_{c_k}(i) R_p(\mu) \end{aligned} \quad (4.20)$$

where $R_{s_k}(t)$, the autocorrelation function of $s_k(t)$, is $R_{c_k}(i)$, the autocorrelation function of spreading sequence $c_k(n)$ multiplied by the autocorrelation function of transmitting waveform $R_p(\mu)$. If $p(t)$ has been known and the energy of $p(t)$ is normalized, $R_{c_k}(i)$ is in the dominant

position of $R_{s_k}(t)$ which means the autocorrelation of transmitted signal $s_k(t)$ mainly depends on the autocorrelation of the spreading sequences $c_k(n)$.

If the periodical transmitted signal is considered, it can be rewritten from Eq.(4.19) to

$$s_k(t) = \sum_{m=0}^{+\infty} \sum_{n=0}^{N-1} c_k(n) p(t - nT_p - mT_s) \quad (4.21)$$

where m is also the number of symbols, $T_s = NT_p$ is the symbol duration, k is also the number of users. The cyclic autocorrelation function of $s_k(t)$ above is given as

$$\begin{aligned} R_{s_k}^c(t) &= \int_{-\infty}^{+\infty} s_k(\tau) s_k^*(\tau - t)_{T_s} d\tau \\ &= \sum_{n=0}^{N-1} c_k(n) c_k(n+i)_N \int_{-\infty}^{+\infty} p(\tau - nT_p) p^*(\tau - \mu - nT_p)_{T_p} d\tau \\ &= R_{c_k}^c(i) R_p^c(\mu) \end{aligned} \quad (4.22)$$

where $(\cdot)_N$ and $(\cdot)_{T_p}$ denotes to take modulo N and T_p , respectively. Similar to $R_{s_k}(t)$, $R_{s_k}^c(t)$ consists of two parts, the $R_{c_k}^c(i)$ and $R_p^c(\mu)$, which are the cyclic autocorrelation function of spreading sequence $c_k(n)$ and pulse $p(t)$, respectively. It is obvious that $R_{s_k}^c(t)$ is mainly determined by the $R_{c_k}^c(i)$ when $p(t)$ is fixed.

4.2.3 AUTOCORRELATION FUNCTION OF TIME HOPPING SEQUENCES

In time hopping UWB (TH-UWB) ranging system, time hopping sequences instead of direct spreading sequences are assigned to each user for accommodating the multiuser condition. Time hopping sequences are a set of integer numbers, allocated for each user to position each pulse over a large time frame T_f for the purpose of channelizing the pulse train. The transmitted signal $s_k(t)$ of TH-UWB system can be expressed as

$$s_k(t) = \sum_{n=0}^{N-1} p(t - c_k(n)T_c - nT_f) \quad (4.23)$$

where T_f is a frame duration which is segmented into equally spaced intervals called "chips" of duration T_c . N_h represents the number of chips per frame. $p(t)$ is the transmitting pulse with duration $T_p \leq T_c$. $c_k(n) \in \{0, 1, \dots, N_h - 1\}$ is the time hopping sequence of the k th user, which shows the pulse is located in the $c_k(n)$ th chip in the n th frame. And the other $N_h - 1$ chips are silent chips without sending signals. N is the length of time hopping sequences. As similar as the Eq.(4.20), the autocorrelation function of $s_k(t)$ of TH-UWB system can be extended as

following equations if we also define $t = iT_c + \mu$, which $0 \leq i < NN_h$ is a integer number and $0 \leq \mu < T_c$. And i can be split into $i = aN_h + b$ furthermore, where a, b are also integer numbers.

$$\begin{aligned}
 R_{s_k}(t) &= \int_{-\infty}^{+\infty} s_k(\tau) s_k^*(\tau - t) d\tau \\
 &= \int_{-\infty}^{+\infty} \sum_{n=0}^{N-1} p(\tau - c_k(n)T_c - nT_f) \sum_{n=0}^{N-1} p^*(\tau - c_k(n)T_c - nT_f - iT_c - \mu) d\tau \\
 &= \sum_{n=0}^{N-1} h(nN_h + c_k(n) + b, nN_h + c_k(n + a)) R_p(\mu) \\
 &\quad + \sum_{n=0}^{N-1} h(nN_h + c_k(n) + b, (n + 1)N_h + c_k(n + a + 1)) R_p(\mu)
 \end{aligned} \tag{4.24}$$

where

$$h(t, v) = \begin{cases} 0, & t \neq v \\ 1, & t = v \end{cases} \tag{4.25}$$

Note that Eq.(4.24) consists of two disjoint terms, the first summation corresponding to the case when $c_k(n) + b < N_h$, and the second summation corresponding to the case when $c_k(n) + b \geq N_h$. In Eq.(4.24), in addition to $R_p(\mu)$, we find that there is the other part $\sum_{n=0}^{N-1} h(t, v)$ where t and v denote the complicate parts in the Eq.(4.24). This function is actually defined as the autocorrelation function of the time hopping sequences, which is referred to as *Hamming correlation* H_{c_k} .

$$H_{c_k} = \sum_{n=0}^{N-1} h(t, v) \tag{4.26}$$

As its counterpart R_{c_k} in direct spreading systems, H_{c_k} is also in the dominant part of $R_{s_k}(t)$ for the fixed $p(t)$. Hence, as in DS-UWB system, the autocorrelation of TH-UWB signal is also determined by the autocorrelation of the time hopping sequences.

If the signal transmitted periodically, the cyclic hamming correlation should be considered, which is defined as

$$H_{c_k}^c = \sum_{n=0}^{N-1} h(t_N, v_N) \tag{4.27}$$

where $(\cdot)_N$ also means to take modulo N . And if the following periodical signal is sent

$$s_k(t) = \sum_{m=0}^{+\infty} \sum_{n=0}^{N-1} p(t - c_k(n)T_c - nT_f - mT_s) \tag{4.28}$$

the cyclic correlation of $s_k(t)$ is expressed as

$$\begin{aligned}
 R_{s_k}^c(t) &= \int_{-\infty}^{+\infty} s_k(\tau) s_k^*(\tau - t) d\tau \\
 &= \sum_{n=0}^{N-1} h(nN_h + c_k(n) + b, nN_h + c_k((n + a)_N)) R_p(\mu) \\
 &\quad + \sum_{n=0}^{N-1} h(nN_h + c_k(n) + b, (n + 1)N_h + c_k((n + a + 1)_N)) R_p(\mu)
 \end{aligned} \tag{4.29}$$

Note that in $R_{s_k}^c(t)$, $R_p(\mu)$ is still kept as the non-cyclic autocorrelation function of $p(t)$. Since only one pulse is transmitted per frame, although the $s_k(t)$ is transmitted periodically, pulse $p(t)$ is still seen as burst transmission.

4.2.4 ANALYSIS OF AUTOCORRELATION FUNCTION OF CHAOTIC SIGNALS

From the analysis we have done, we can find that the autocorrelation function of transmitted signal affects ranging systems importantly. Hence, new pulses or spreading sequences with good autocorrelation property are expected for ranging systems. In this section, we introduce chaotic signals as the new source of pulses and spreading sequences.

Following the generation of chaotic pulses and chaotic spreading sequences, the comparison of chaotic signals with their classic counterparts will be given consequently. The comparison consists two items, the autocorrelation function and the cyclic autocorrelation function since the consideration of periodic transmitted signals. As introduced previously, two features of autocorrelation function which are quite important to ranging systems are the main-lobe width and the side-lobes level. Since the main-lobe width is closed related to the power spectrum density, decreasing the main-lobe width of the autocorrelation function corresponds to the increase of bandwidth, which have discussed in Section 4.1. The reminder of this section focuses on the other metric of autocorrelation function, the side-lobe level.

A. AUTOCORRELATION FUNCTION OF CONTINUOUS CHAOTIC PULSE

We first consider the autocorrelation property of continuous-time chaotic pulse. The Lorenz system in Eq.(3.5) is chosen as a representative of continuous-time chaotic systems. The Lorenz pulse $s_c(t)$ is defined as a normalized x-state-variables with duration T_s . Due to the sensitivity of initial condition, K different initial conditions generates K different Lorenz pulses with the same Lorenz systems which are denoted as $s_{c,k}(t)$, respectively.

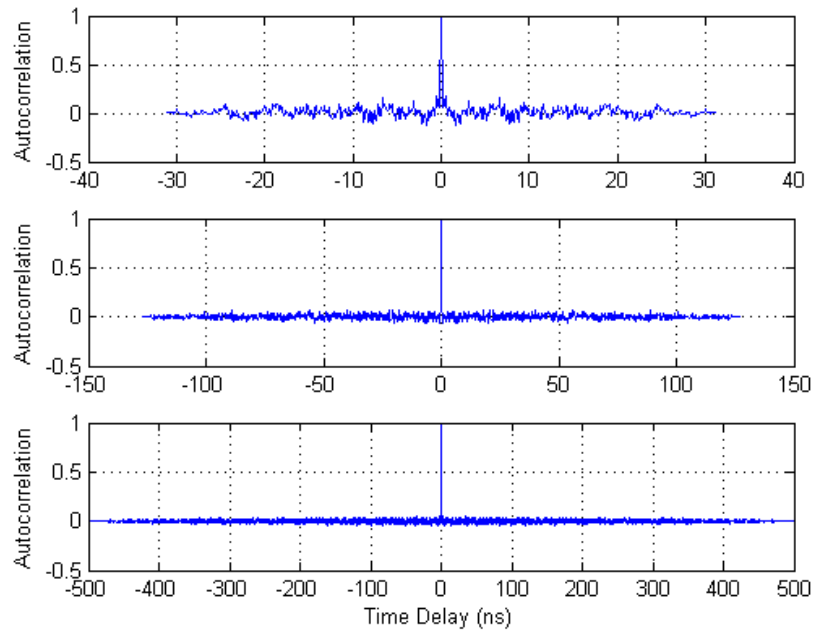


Figure 4.2.2: Autocorrelation function of Lorenz pluses with length $T_s = 31ns$, $T_s = 127ns$ and $T_s = 500ns$.

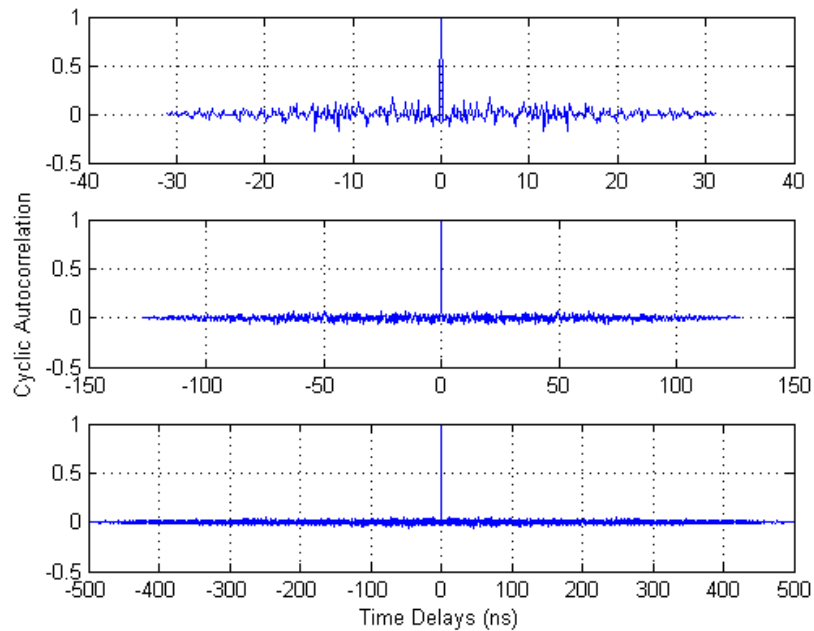


Figure 4.2.3: Cyclic Autocorrelation function of Lorenz pulses with length $T_s = 31ns$, $T_s = 127ns$ and $T_s = 500ns$.

In the Fig. 4.2.2, autocorrelation function of Lorenz pulses with 3 different durations $T_s = 31ns$, $T_s = 127ns$ and $T_s = 500ns$ are illustrated. These Lorenz pulses are generated by the same Lorenz system with parameters $\sigma = 30$, $r = 84$, $b = 8$. As shown in the Fig. 4.2.2, Lorenz waveforms have an obvious main-lobe with quite narrow width. In addition, the side-lobe values are also quite small and decrease with the increase of the T_s . The same properties can be also found in the cyclic autocorrelation of these Lorenz waveforms, which are shown in the Fig. 4.2.3.

In the DS-UWB or TH-UWB ranging systems, pulses such as raised cosine pulses are not transmitted directly but after being modulated by the spreading sequences as shown in Eq. (4.19) or Eq.(4.23). As analyzed previously, the autocorrelation function of transmitted signal $s(t)$ in DS-UWB and TH-UWB ranging systems are dominated by the autocorrelation of spreading sequences when pulse is fixed. Since the spreading sequences have quite good autocorrelation function, this procedure enhances the autocorrelation property of $s(t)$ in both narrowing the main-lobe width and decreasing side-lobes level aspects. Oppositely, chaotic pulses can be transmitted directly without other processing due to its inherent wideband and good autocorrelation property. Hence, the comparison is processed between chaotic pulse and classic pulses modulated by spreading sequences.

In the comparison, pulses with direct spreading sequences are chosen to compare with Lorenz pulses. Gold sequences $G_k(n)$ are used as direct spreading sequences for their good autocorrelation function and comparative large number of sequences. Although m-sequences have better autocorrelation property, the available number of sequences is quite small. For example, in the length of $N = 31$, there are only 6 m-sequences but 33 Gold sequences instead. In addition, since a preferred pair of m-sequences exists in each set of Gold sequences, if the selected chaotic pulses outperform pulses with all the Gold sequences, they can also perform better than the pulses modulated by m-sequences. After the choose of Gold sequences, raised cosine pulse $p(t)$ is selected as the representative of classic pulses. In order to avoid the affect of frequency bandwidth, raised cosine pulse has the roll-off parameter $\beta = 0.6$ and $t_p = 0.16$ in the duration $T_p = 1ns$. As shown in the fig.4.2.4, it has the same 10dB bandwidth as that of Lorenz pulse. According to the Eq.(4.19), the competitor of Lorenz pulse $s_{c,k}(t)$ is expressed as

$$s_{r,k}(t) = \sum_{n=0}^{N-1} G_k(n)p(t - nT_p) \quad (4.30)$$

Firstly, we compare $s_{c,k}(t)$ and $s_{r,k}(t)$ in short duration $T_s = 31ns$, which corresponds to using the Gold sequences of length $N = 31$ for the latter pulse. Due to the sensitivity of initial condition, a considerable number of Lorenz pulses with $T_s = 31ns$ can be generated. In order

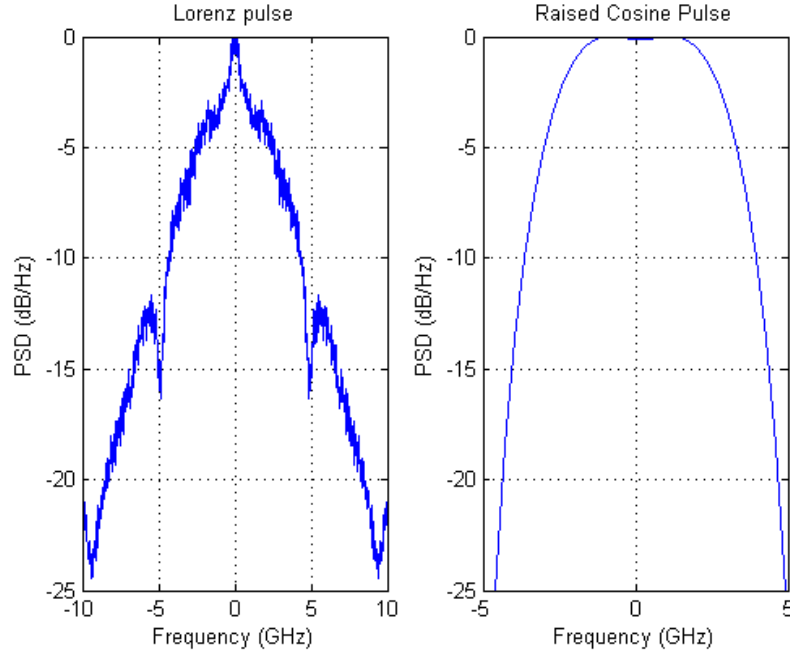


Figure 4.2.4: The frequency bandwidth of Lorenz pulse and Raised cosine pulse.

to select Lorenz pulses from such a large pool, the criterion $\varphi_{G,N}$ is introduced. $\varphi_{G,N}$ is the peak absolute side-lobe value of autocorrelation of all the Gold sequences in length N , which is defined as

$$\rho_k = \max(|R_{G_k}(\tau)|) \quad \tau \neq 0, \quad k = 1, 2, \dots, N+2 \quad (4.31)$$

and

$$\varphi_{G,N} = \max(\rho_k) \quad k = 1, 2, \dots, N+2. \quad (4.32)$$

where $R_{G_k}(\tau)$ is the autocorrelation function of Gold sequence in length N . ρ_k actually is the maximum side-lobe value of the k th Gold sequence in the set of Gold sequences of length N . As already known, the autocorrelation function of $s_{r,k}(t)$ is mainly determined by the autocorrelation function of $G_k(n)$. Hence, the use of criterion $\varphi_{G,N}$ ensures that selected Lorenz pulses have no worse autocorrelation property than Gold sequences.

As shown in Fig.4.2.5, side-lobe values of normalized autocorrelation function of 200 selected Lorenz pulse of length $T_s = 31$ are bounded in $(-0.2, +0.2)$. However, the absolute peaky value of that of raised cosine pulse with Gold sequences is more than 0.4. In addition, the number of Lorenz pulses in Fig.4.2.5 is 200 which is almost 6 times than that of classic pulse due to its initial condition sensitivity.

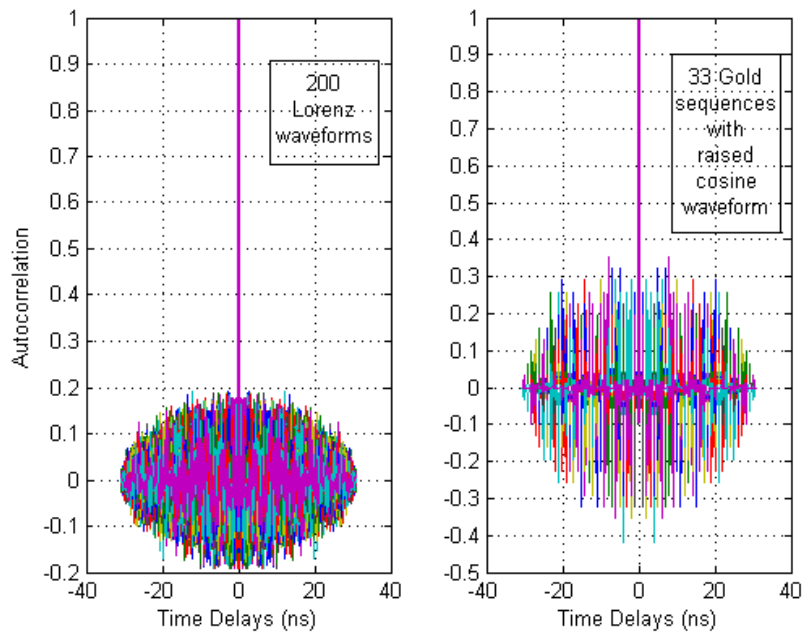


Figure 4.2.5: Autocorrelation function of selected Lorenz pulse and raised cosine pulse with Gold sequences in $T_s = 31ns$.

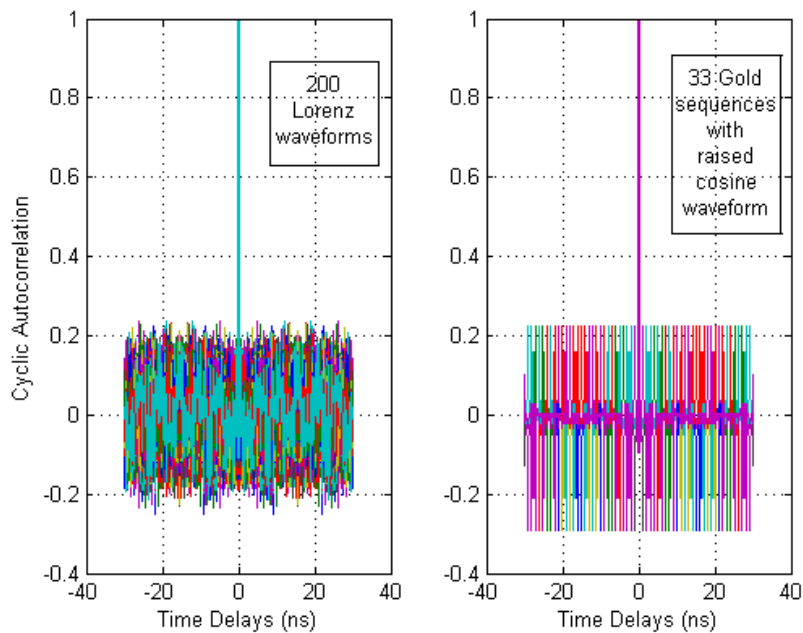


Figure 4.2.6: Cyclic autocorrelation function of selected Lorenz pulse and raised cosine pulse with Gold sequences in $T_s = 31ns$.

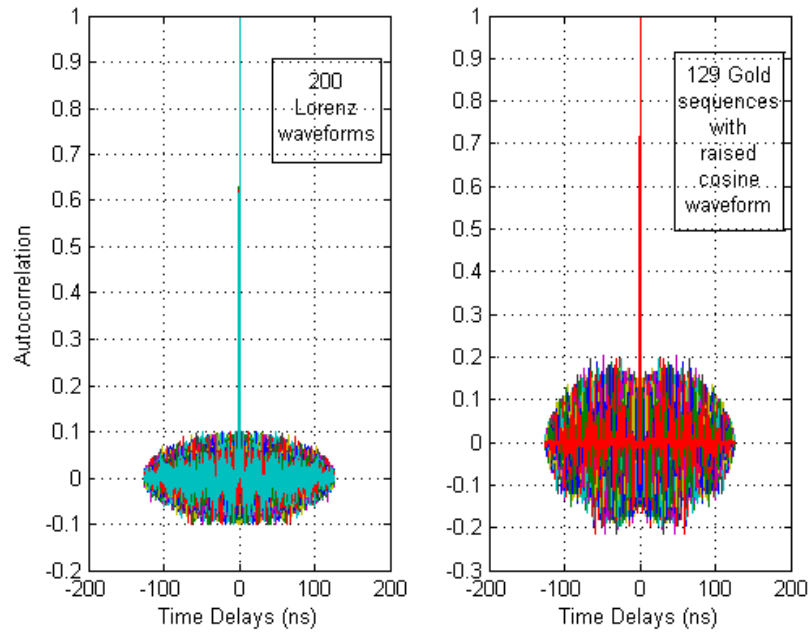


Figure 4.2.7: Autocorrelation function of selected Lorenz pulse and raised cosine pulse with Gold sequences in $T_s = 127ns$.

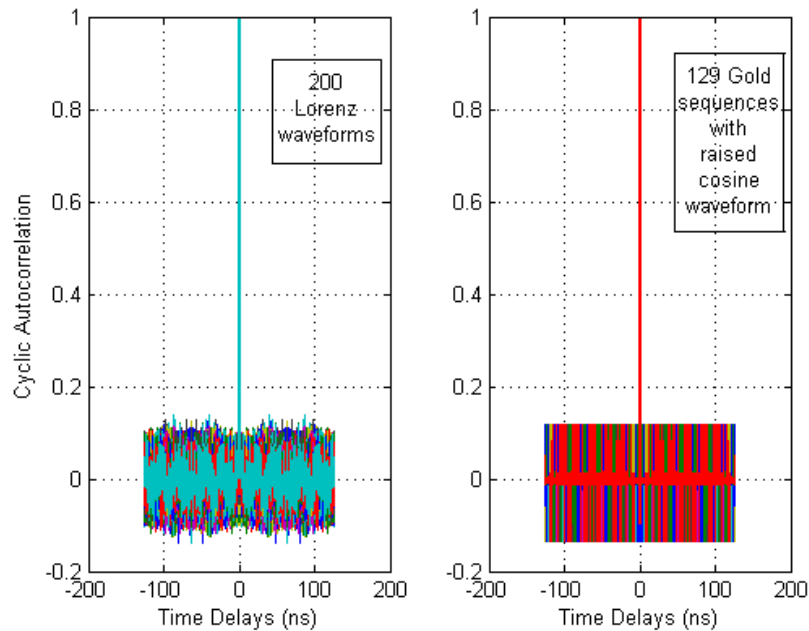


Figure 4.2.8: Cyclic autocorrelation function of selected Lorenz pulse and raised cosine pulse with Gold sequences in $T_s = 127ns$.

After illustrating the autocorrelation function, the comparison of cyclic autocorrelation function of these two waveforms is shown in Fig.4.2.6. Here, the criterion $\varphi_{G,N}^c$ is employed, which is defined as

$$\rho_k^c = \max(|R_{G_k}^c(\tau)|) \quad \tau \neq 0, \quad k = 1, 2, \dots, N+2 \quad (4.33)$$

and

$$\varphi_{G,N}^c = \max(\rho_k^c) \quad k = 1, 2, \dots, N+2. \quad (4.34)$$

where $R_{G_k}^c(\tau)$ is the cyclic autocorrelation function of Gold sequence in length N . $\varphi_{G,N}^c$ represents the peak absolute side-lobe value of cyclic autocorrelation of all the Gold sequences in length N . The 200 selected Lorenz waveforms with lower side-lobe value are shown in the left side of Fig.4.2.6 compared with the raised cosine waveform in the right side. Hence, for the both view of autocorrelation and cyclic autocorrelation function, a large number of Lorenz pulses with better autocorrelation can be easily selected, which gives the system an opportunity to support a large number of users in multiuser environment.

In the case of short duration $T_s = 31ns$, there is a large number of Lorenz pulses with better autocorrelation property. If we increase the duration, how is the performance of Lorenz pulses? Then we increase the duration to $T_s = 127ns$. The comparison of autocorrelation and cyclic autocorrelation function are shown in the Fig.4.2.7 and Fig.4.2.8, respectively. The criteria $\varphi_{G,N}$ and $\varphi_{G,N}^c$ are also employed with $N = 127$. As in $T_s = 31ns$, 200 selected Lorenz pulses are shown with better performance than their counterpart in both autocorrelation and cyclic autocorrelation. In the Fig.4.2.7, we can find that the absolute side-lobe values of Lorenz pulses are no more than 0.1. By contrast, their counterpart performs even larger than 0.2. However, the difference of two waveforms in cyclic autocorrelation become smaller.

B. AUTOCORRELATION FUNCTION OF CHAOTIC BINARY SEQUENCES

Before comparing the autocorrelation function of chaotic spreading sequences and conventional sequences, we first introduce the generation of chaotic direct spreading sequences. Here we only consider the binary spreading sequences. Although there are many chaotic maps that can be chosen as generators, *Chebyshev* map, *Tent* map are chosen in this thesis for its comparatively low complexity. Chebyshev map has been introduced in the Chapter. 3 with the definition

$$x(n+1) = 1 - 2x(n)^2 \quad (4.35)$$

where the initial condition $x(0)$ can be varied within $x_0 \in (-1, 1)$, the value of $x(n)$ is also mapped within $(-1, 1)$. For the Tent map, according to the bifurcation diagram in the Fig.3.2.6, the chaotic parameter μ is chosen to be 1.8 in order to generate the chaos dynamic. Then, the

Tent map can be given as

$$x(n+1) = \begin{cases} 1.8x(n) & \text{if } x(n) < 0.5 \\ 1.8(1-x(n)) & \text{otherwise.} \end{cases} \quad (4.36)$$

where the initial condition $x(0)$ should satisfy $x(0) \in (0, 1)$, then $x(n)$ is mapped in the same range $(0, 1)$. With these two very simple maps, we can generate chaotic sequences $x_k(n)$ with k different initial conditions which are chosen differently and independently.

Since the sequences generated by both Chebyshev map and Tent map are the real-valued, quantization function is required to map the real-valued sequences into binary sequences. As the range of values are different for these two maps, quantization function for Chebyshev map and Tent map are also different which are expressed as $Q_{C,DS}$ and $Q_{T,DS}$, respectively.

$$x'(n) = Q_{C,DS}(x(n)) = \begin{cases} 1 & \text{if } x(n) > 0 \\ -1 & \text{otherwise} \end{cases} \quad (4.37)$$

$$x'(n) = Q_{T,DS}(x(n)) = \begin{cases} 1 & \text{if } x(n) > 0.5 \\ -1 & \text{otherwise} \end{cases} \quad (4.38)$$

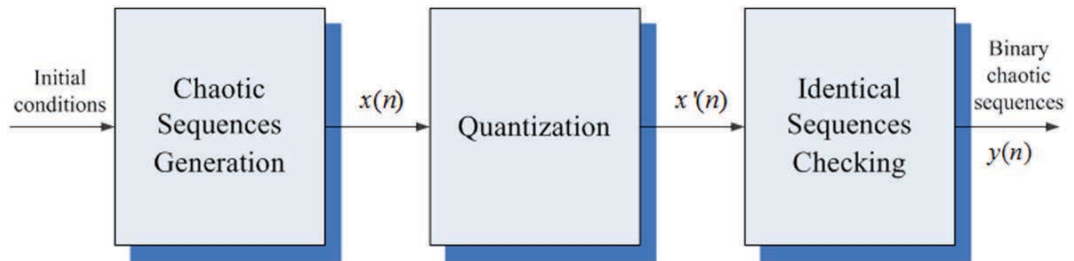


Figure 4.2.9: The procedure of the generation of Binary chaotic sequences.

After quantization, the original chaotic sequences $x(n)$ are mapped into binary chaotic sequences $x'(n)$. Although the initial conditions of $x(n)$ are different, some identical sequences may exist in $x'(n)$ due to the quantization processing. In order to avoid this situation, the last step of binary chaotic sequences generation is to check all the sequences to be different. The Fig.4.2.9 summarizes the generation of chaotic binary sequences as follows.

After passing the whole procedure above, we have already obtained a large number of chaotic binary sequences $y(n)$. In order to evaluate the autocorrelation function of $y(n)$, we also choose Gold sequences as the representatives of conventional direct spreading sequences to compare with as well as the criteria $\varphi_{G,N}$ and $\varphi_{G,N}^c$. The binary chaotic sequences whose autocorrelation or cyclic autocorrelation satisfies the criteria are selected finally.

Fig.4.2.10 and Fig.4.2.11 illustrate the autocorrelation and cyclic autocorrelation function of selected Chebyshev binary sequences and Gold sequences in the length $N = 31$, respectively. As shown in Fig.4.2.10, the selected Chebyshev binary sequences have the same even a litter better side-lobe level as that of Gold sequences, but with much more number of sequences. There are 200 Chebyshev binary sequences rather than only 33 Gold sequences with length 31. In the Fig.4.2.11, it is shown that the same situation has also been found in cyclic autocorrelation function. 200 selected Chebyshev binary sequences have the same autocorrelation function as Gold sequences.

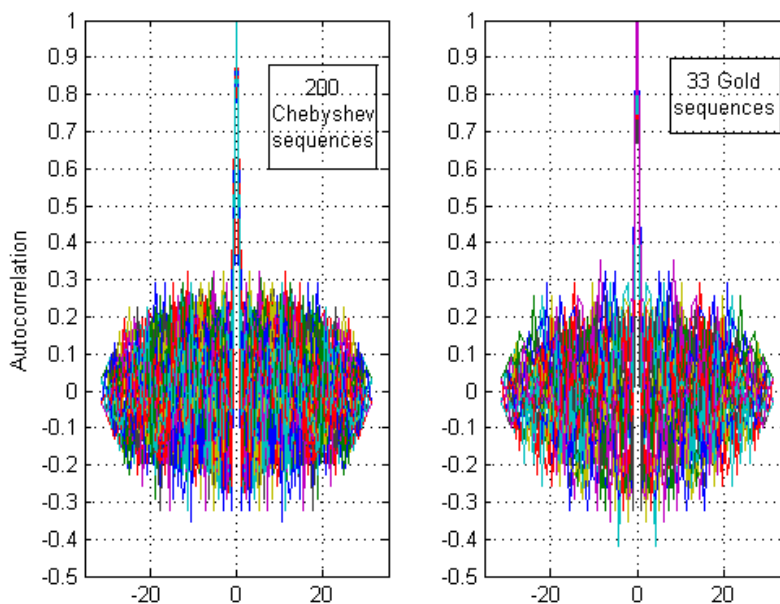


Figure 4.2.10: Autocorrelation function of selected Chebyshev sequences and Gold sequences with length $N = 31$.

Except the Chebyshev binary sequences, the autocorrelation and cyclic autocorrelation function of Tent binary sequences and Gold sequences are also illustrated in Fig.4.2.12 and Fig.4.2.13, respectively. As shown in the Fig.4.2.12 and Fig.4.2.13, a large number of Tent binary sequences also have the same performance as that of Gold sequences in the length 31. From the examples of Chebyshev and Tent binary sequences, we can find that in the aspect of autocorrelation function, the limitation of number of users in Gold sequences does not exist in the chaotic sequences any more, which can increase the system capability of multiuser greatly. However, this advantage of number of users is also smaller with the increase of length

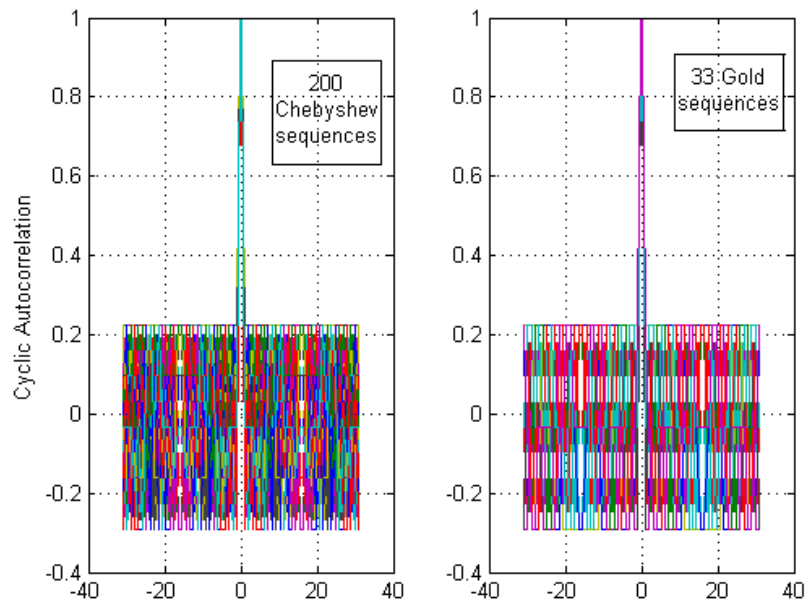


Figure 4.2.11: Cyclic autocorrelation function of selected Chebyshev sequences and Gold sequences with length $N = 31$.

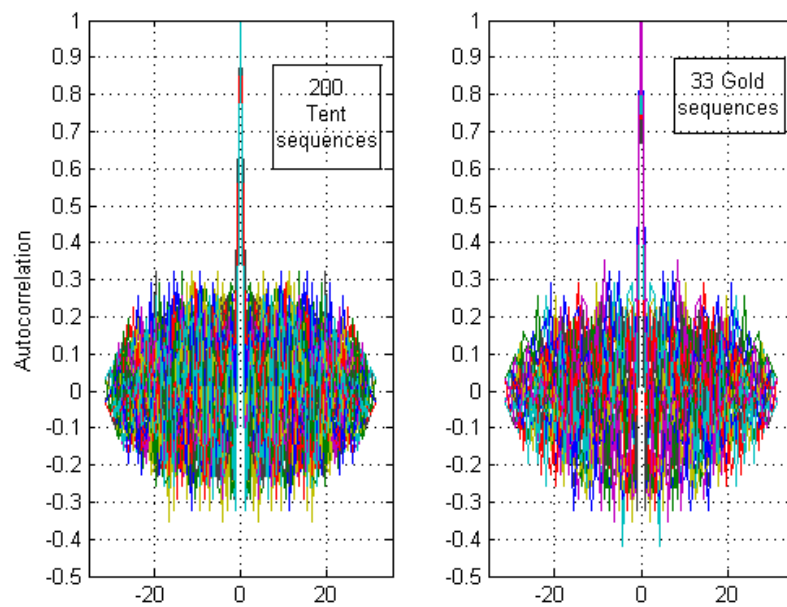


Figure 4.2.12: Autocorrelation function of selected Tent sequences and Gold sequences with length $N = 31$.

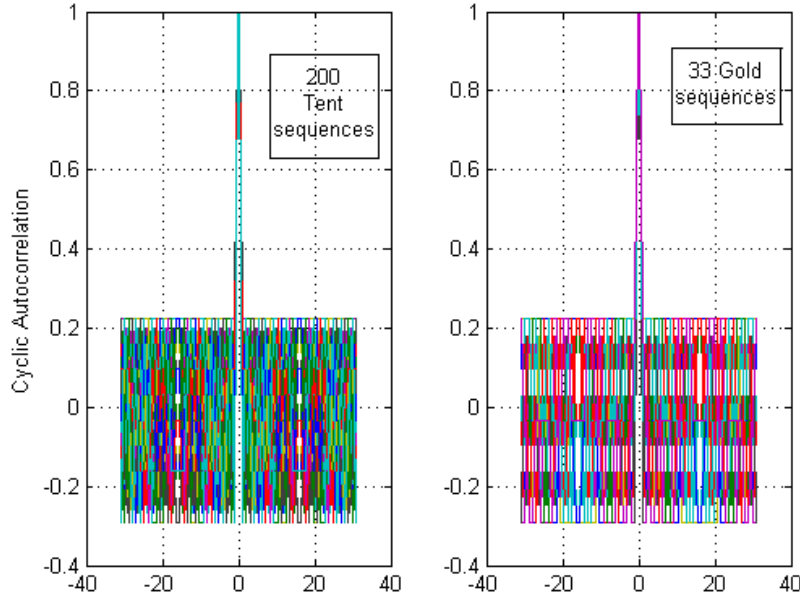


Figure 4.2.13: Cyclic autocorrelation function of selected Tent sequences and Gold sequences with length $N = 31$.

N . When N increases to 127, it is difficult to find 129 different chaotic sequences with the same performance as Gold sequences.

C. AUTOCORRELATION FUNCTION OF CHAOTIC MULTI-VALUED SEQUENCES

What's already discussed shows that the chaotic binary sequences can be used as substitutes for the classic direct spreading sequences. Considering another kind of spreading sequences, the time hopping sequences, can the chaotic sequences also be used as their alternatives? Before answering this question, the generation of chaotic time hopping sequences is presented firstly. Chebyshev map and Tent map are also employed, which have been given in Eq.(4.35) and Eq.(4.36). Unlike binary direct spreading sequences, time hopping sequences are multi-valued sequences as shown in the Eq.(4.23). Thus, the quantization function of time hopping sequences is different from that of binary chaotic sequences. The quantization functions of Chebyshev map and Tent map for time hopping sequences are expressed as $Q_{C,TH}$ and $Q_{T,TH}$, respectively.

$$x'(n) = Q_{C,TH}(x(n)) = \left\lfloor x(n) * \frac{N_h}{2} + \frac{N_h}{2} \right\rfloor \quad (4.39)$$

$$x'(n) = Q_{T,TH}(x(n)) = \lfloor x(n) * N_h \rfloor \quad (4.40)$$

where N_h is also the number of chips per frame. After quantization, the real-valued chaotic sequences turn to the integer multi-valued time hopping sequences. In the following, the checking procedure is also needed to eliminate the identical sequences. Consequently, we obtain a larger number of chaotic time hopping sequences $z(n)$. The procedure of generating the chaotic time hopping sequences can also be summarized in the Fig.4.2.9, but with different quantization function.

As mentioned before, the autocorrelation function of time hopping sequences referred to as Hamming autocorrelation is different from that of direct spreading sequences, which is shown as Eq.(4.25). It actually calculates the hits of a time hopping sequence with delayed itself, the value of which represents the hits of the corresponding delay. By convention, we also choose one of the classic time hopping sequences as the contrast of chaotic time hopping sequences. Quadratic congruence code (QCC) has been chosen for its relatively better autocorrelation property than other most common time hopping codes such as Linear congruence code (LCC), cubic congruence code (CCC), hyperbolic congruence code (HCC) and so on [110,111].

In the following comparison, N_h is chosen to be 13 due to the signals structure of TH-UWB system and the prime requirement of N_h . In addition, φ_{Q,N_h} and φ_{Q,N_h}^c corresponding to peak absolute side-lobe value of QCC autocorrelation and cyclic autocorrelation are chosen as the criteria for selecting chaotic time hopping sequences.

$$\rho_k = \max(|R_{Q_k}(\tau)|) \quad \tau \neq 0, \quad k = 1, 2, \dots, N_h - 1 \quad (4.41)$$

and

$$\varphi_{Q,N_h} = \max(\rho_k) \quad k = 1, 2, \dots, N_h - 1 \quad (4.42)$$

where $R_{Q_k}(\tau)$ is the hamming autocorrelation function of QCC sequence with N_h . For the side of φ_{Q,N_h}^c ,

$$\rho_k^c = \max(|R_{Q_k}^c(\tau)|) \quad \tau \neq 0, \quad k = 1, 2, \dots, N_h - 1 \quad (4.43)$$

and

$$\varphi_{Q,N_h}^c = \max(\rho_k^c) \quad k = 1, 2, \dots, N_h - 1 \quad (4.44)$$

where $R_{Q_k}^c(\tau)$ is the cyclic Hamming autocorrelation function of QCC sequence with N_h .

From the Fig.4.2.14, we can find 200 selected Chebyshev time hopping sequences have the

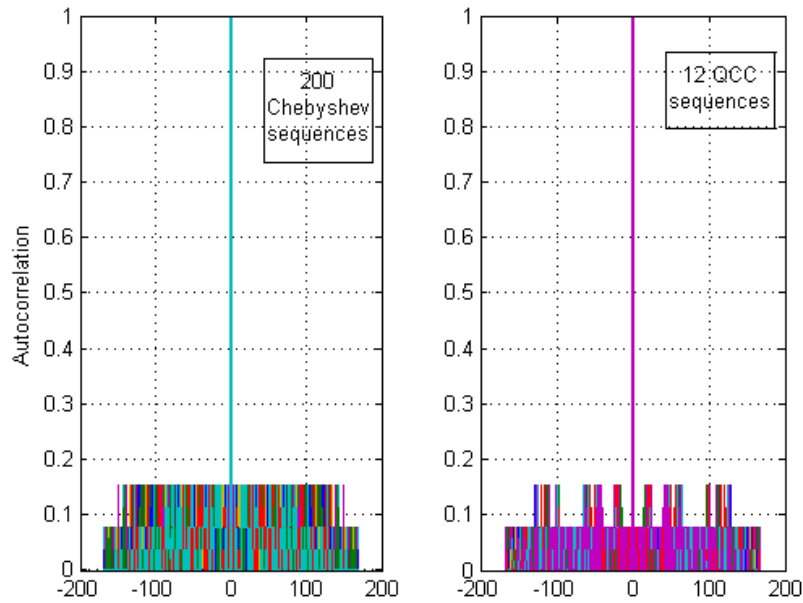


Figure 4.2.14: Autocorrelation function of selected Chebyshev sequences and QCC sequences with $N_h = 13$.

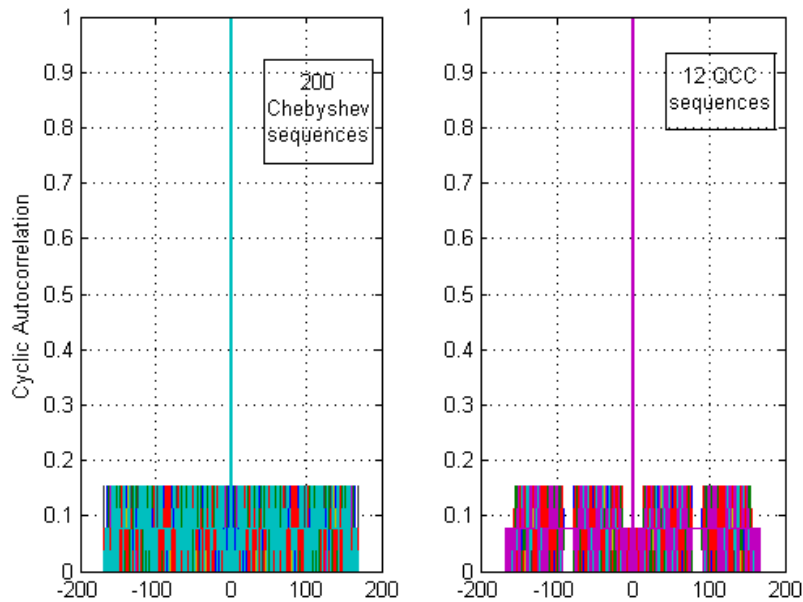


Figure 4.2.15: Cyclic autocorrelation function of selected Chebyshev sequences and QCC sequences with $N_h = 13$.

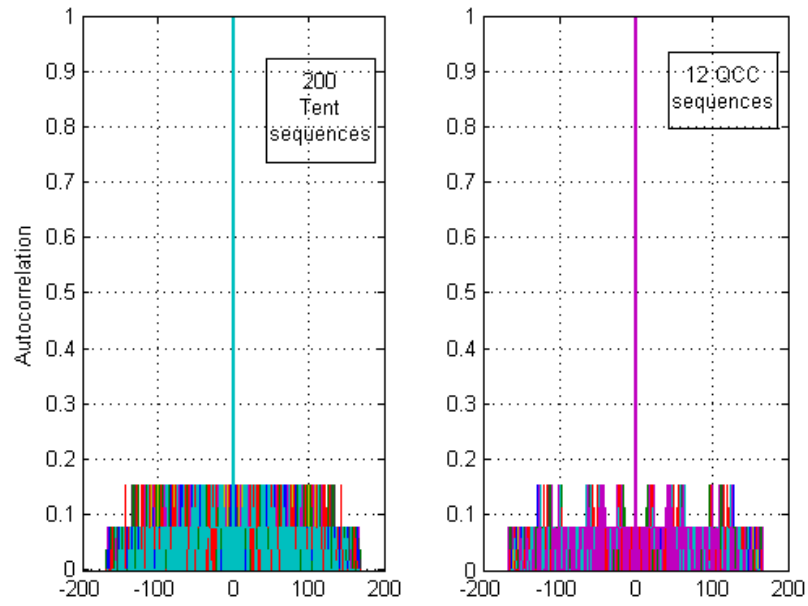


Figure 4.2.16: Autocorrelation function of selected Tent sequences and QCC sequences with $N_h = 13$.

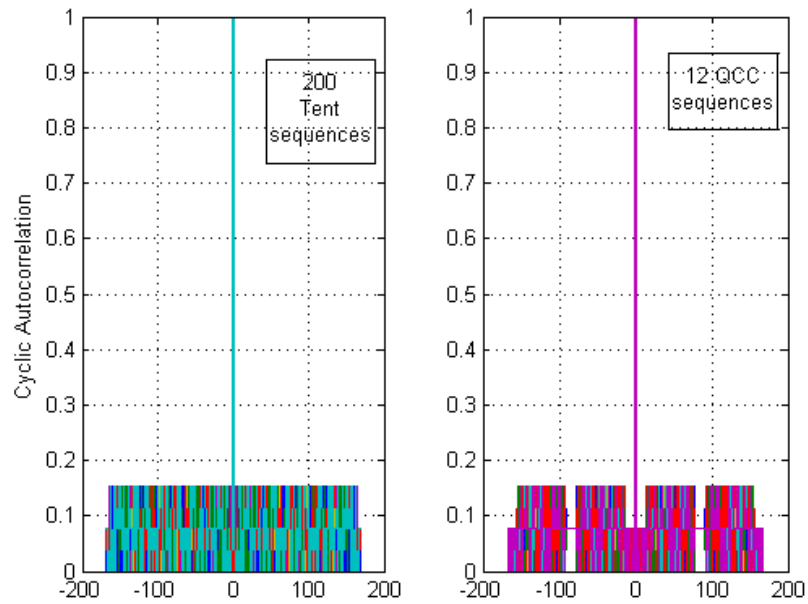


Figure 4.2.17: Cyclic autocorrelation function of selected Tent sequences and QCC sequences with $N_h = 13$.

same autocorrelation property as QCC sequences, which is 18 times of the number of QCC sequences. The same situation is also shown in the Fig.4.2.15 which illustrates the cyclic autocorrelation of two kinds of time hopping sequences. Hence, no matter comparing non-cyclic or cyclic autocorrelation function, Chebyshev time hopping sequences have a overwhelming number of sequences than QCC when considering the criterion φ_{Q,N_h} and φ_{Q,N_h}^c . This conclusion can be extended to the Tent time hopping sequences as well. As shown in the Fig.4.2.16 and Fig.4.2.17, the selected Tent time hopping sequences achieve the same performance but with much more number of sequences than QCC. Consequently, as in the direct spreading code, the chaotic time hopping sequences can be considered to replace the classic time hopping sequences for their capability to support much more users.

4.3 CROSS-CORRELATION PROPERTY

Following the autocorrelation function, another important ranging related property is cross-correlation property of ranging signals. The definitions of cross-correlation function and the analysis of cross-correlation function in both DS-UWB and TH-UWB ranging systems are introduced consecutively. Then, the detailed analysis of the cross-correlation property of chaotic signals is shown with the comparison to the current ranging signals.

4.3.1 CROSS-CORRELATION FUNCTION

In multiuser wireless communication or localization systems, received signal $r(t)$ consists of not only the desired user's signal but also the signals from many other interfered users. In the simplest case, the zero-noise single path channel,

$$r(t) = \sum_{k=1}^K a_k s_k(t - \tau_k) \quad (4.45)$$

where $s_k(t)$ denotes the transmitted signal of the k th user, a_k and τ_k are the channel coefficient and time delay of the k th user, respectively. The first user is assumed to be the user of interest. If the matched filter is still employed as the receiver or received filter, the output of matched

filter is

$$\begin{aligned}
R_{MF}(t) &= r(t) * s_1(-t) \\
&= \int_{-\infty}^{+\infty} \sum_{k=1}^K a_k s_k(\tau - \tau_k) s_1^*(\tau - t) d\tau \\
&= \sum_{k=1}^K a_k \int_{-\infty}^{+\infty} s_k(\tau - \tau_k) s_1^*(\tau - t) d\tau \\
&= a_1 R_{s_1}(t - \tau_1) + \sum_{k=2}^K a_k \int_{-\infty}^{+\infty} s_k(\tau - \tau_k) s_1^*(\tau - t) d\tau
\end{aligned} \tag{4.46}$$

where R_{s_1} is the autocorrelation of desired signal $s_1(t)$, the second term represents the correlation between the desired signal $s_1(t)$ and other interfered users' signal $s_k(t)$. Hence, we can find that in the multiuser environment, the output of matched filter not only depends on the autocorrelation function of $s_1(t)$, but also includes the correlation between $s_1(t)$ and other $s_k(t)$. This kind of correlation is referred to as the *cross-correlation function*.

Cross-correlation is defined as

$$\begin{aligned}
C_{sv}(t) &= s(t) * v^*(-t) \\
&= \int_{-\infty}^{+\infty} s(\tau) v^*(\tau - t) d\tau
\end{aligned} \tag{4.47}$$

where $s(t)$ and $v(t)$ are different signals. If autocorrelation describes the correlation of a signal with itself, the cross-correlation shows us the similarity of two different signals as a function of the time difference. The lower the magnitude is, the more uncorrelated $s(t)$ and $v(t)$ are. With the definition of cross-correlation function, the Eq. (4.46) can be rewritten as

$$\begin{aligned}
R_{MF}(t) &= a_1 R_{s_1}(t - \tau_1) + \sum_{k=2}^K a_k \int_{-\infty}^{+\infty} s_k(\tau - \tau_k) s_1^*(\tau - t) d\tau \\
&= a_1 R_{s_1}(t - \tau_1) + \sum_{k=2}^K a_k C_{s_1, s_k}(t - \tau_k)
\end{aligned} \tag{4.48}$$

Obviously, $C_{s_1, s_k}(t - \tau_k)$ appears an interference of $R_{s_1}(t - \tau_1)$. Fig.4.3.1 shows the cross-correlation of a typical ranging waveform. Unlike autocorrelation function, there is no peaky main lobe. However, a high peaky side-lobes of autocorrelation added by a high valued cross-correlation may lead to a large probability of false estimation. In order to avoid this interference from other users, a set of orthogonal or quasi-orthogonal waveforms are considered. Orthogonal or quasi-orthogonal set is a set where each waveform is orthogonal or quasi-orthogonal

with every other waveform in the same set. In this thesis, orthogonal or quasi-orthogonal waveforms mean that the cross-correlation between any of two distinct waveforms must be zero or "small".

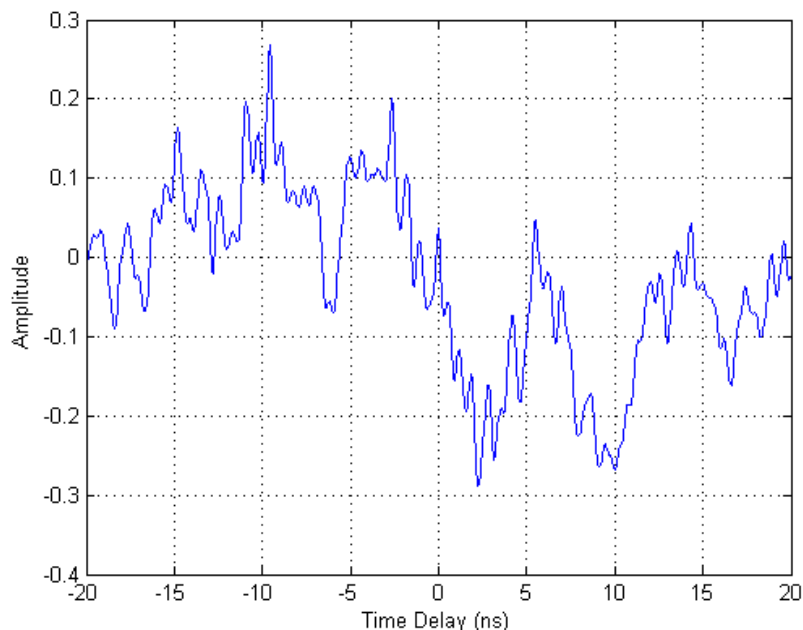


Figure 4.3.1: Cross-correlation function of typical ranging waveform.

For evaluating and comparing the cross-correlation function of different sets of waveform, a *normalized cross-correlation function* is defined as

$$C_{sv}^n(t) = C_{sv}(t)/R_s(o) \quad (4.49)$$

or $C_{sv}^n(t) = C_{sv}(t)/R_v(o)$

where $R_s(o)$ or $R_v(o)$ is the maximum value of autocorrelation function of $s(t)$ or $v(t)$, respectively. Since the transmitted signals always have the normalized energy, the two equations above are equivalent actually. The peak absolute value of normalized cross-correlation function denotes how large interference it can cause, consequently, it is chosen as the metric to evaluate the orthogonality or quasi-orthogonality. Since in the following, we only consider the normalized cross-correlation function, $C_{sv}(t)$ is used to denote it for simplicity.

If the ranging signals $s(t)$ and $v(t)$ are transmitted periodically as shown in Eq.(4.17), the

normalized cyclic cross-correlation function should be considered, which is expressed as

$$\begin{aligned} C_{sv}^c(t) &= s(t) * v^*(-t)/R_s(o) \\ &= \int_{-\infty}^{+\infty} s(\tau)v^*(\tau - t)_{T_s}d\tau \end{aligned} \quad (4.50)$$

where T_s is the duration of $s(t)$ and $v(t)$, $(\cdot)_{T_s}$ also denotes to take modulo T_s .

4.3.2 CROSS-CORRELATION FUNCTION OF DIRECT SPREADING SEQUENCES

In DS-UWB ranging system, as shown in Eq. (4.19), different users are distinguished by their own unique direct spreading sequences. Hence, the cross-correlation of different users' signals can be expressed as

$$\begin{aligned} C_{s_k s_m}(t) &= s_k(t) * s_m^*(-t)/R_s(o) \\ &= \int_{-\infty}^{+\infty} \sum_{n=0}^{N-1} c_k(n)p(\tau - nT_p) \sum_{m=0}^{N-1} c_m(n+i)p^*(\tau - \mu - nT_p)/R_s(o)d\tau \\ &= \sum_{n=0}^{N-1} c_k(n)c_m(n+i) \int_{-\infty}^{+\infty} p(\tau - nT_p)p^*(\tau - \mu - nT_p)/R_s(o)d\tau \\ &= C_{c_k}(i)R_p(\mu)/R_s(o) \end{aligned} \quad (4.51)$$

where $C_{c_k}(i)$ is the cross-correlation of spreading sequences, $t = iT_p + \mu$, which $0 \leq i < N$ is a integer number and $0 \leq \mu < T_p$. $R_p(\mu)$ here is still the autocorrelation of $p(t)$ since pulse $p(t)$ is same for all the users. As similar to Eq.(4.20), the cross-correlation function $C_{s_k s_m}(t)$ mainly depends on $C_{c_k}(i)$. The same result can also be obtained in the case of cyclic cross-correlation function, which is given as

$$C_{s_k s_m}^c(t) = C_{c_k}^c(i)R_p^c(\mu)/R_s^c(o) \quad (4.52)$$

where $C_{c_k}^c(i) = \sum_{n=0}^{N-1} c_k(n)c_m(n+i)_N$ is the cyclic cross-correlation of sequences $c_k(n)$.

4.3.3 CROSS-CORRELATION FUNCTION OF TIME HOPPING SEQUENCES

In TH-UWB ranging system, with the same derivation, we can also find that the cross-correlation and cyclic cross-correlation function of different waveforms are also dominated by that of time

hopping sequence, which are shown as following,

$$\begin{aligned}
 C_{s_k s_m}(t) &= \sum_{n=0}^{N-1} h(nN_h + c_k(n) + b, nN_h + c_m(n + a)) R_p(\mu) \\
 &+ \sum_{n=0}^{N-1} h(nN_h + c_k(n) + b, (n + 1)N_h + c_m(n + a + 1)) R_p(\mu)
 \end{aligned} \tag{4.53}$$

and

$$\begin{aligned}
 C_{s_k s_m}^c(t) &= \sum_{n=0}^{N-1} h(nN_h + c_k(n) + b, nN_h + c_m((n + a)_N)) R_p^c(\mu) \\
 &+ \sum_{n=0}^{N-1} h(nN_h + c_k(n) + b, (n + 1)N_h + c_m((n + a + 1)_N)) R_p^c(\mu)
 \end{aligned} \tag{4.54}$$

where $h(t, v)$ and $h((t)_N, (v)_N)$ has been defined in Eq.(4.25) and Eq.(4.27), respectively.

The above analysis shows that cross-correlation property of transmitted waveforms is also a key point in the multiuser ranging systems, which describes the interference coming from the other users. In direct spreading system or time hopping system, the cross-correlation property of transmitted signals can be simplified to the corresponding property of the spreading sequences. The absolute peak value of normalized cross-correlation is chosen as the metric to evaluate different sets of waveforms or spreading sequences. The lower absolute peak value is, the smaller the interference will be. In the following, we will give the comparison between chaotic signals and traditional signals based on this metric, including continuous pulses, direct spreading sequences and time hopping sequences.

4.3.4 ANALYSIS OF CROSS-CORRELATION FUNCTION OF CHAOTIC SIGNALS

A. CROSS-CORRELATION FUNCTION OF CONTINUOUS CHAOTIC PULSE

As the discussion of autocorrelation property, we firstly focus on the cross-correlation property of chaotic pulses. Lorenz waveforms are still the representative as chaotic waveforms. Note that Lorenz pulses here are selected firstly by the autocorrelation property with the criterion $\varphi_{G,N}$ or $\varphi_{G,N}^c$. The competitor of chaotic pulse is the raised cosine waveform modulated by the Gold sequences $G_k(n)$ as shown in the Eq.(4.21).

Fig.4.3.2 and Fig.4.3.3 illustrate the cross-correlation and cyclic cross-correlation function of selected Lorenz pulses compared raised cosine pulses in the length $T_s = 31ns$. Lorenz

waveforms are selected by the criterion $\psi_{G,N}$ and $\psi_{G,N}^c$, respectively.

$$\eta_k = \max(|C_{G_k}(\tau)|) \quad k = 1, 2, \dots, C_N^2 \quad (4.55)$$

and

$$\psi_{G,N} = \max(\eta_k) \quad k = 1, 2, \dots, C_N^2 \quad (4.56)$$

where $C_{G_k}(\tau)$ is the cross-correlation function of $G_k(n)$, C_N^2 denotes the combination operator. And

$$\eta_k^c = \max(|C_{G_k}^c(\tau)|) \quad k = 1, 2, \dots, C_N^2 \quad (4.57)$$

and

$$\psi_{G,N}^c = \max(\eta_k^c) \quad k = 1, 2, \dots, C_N^2 \quad (4.58)$$

where $C_{G_k}^c(\tau)$ is the cyclic cross-correlation function of $G_k(n)$. $\psi_{G,N}$ and $\psi_{G,N}^c$ denote the peak absolute value of cross-correlation and cyclic cross-correlation function of Gold sequences in length N . In the left side of Fig.4.3.2, we can find that there is a set of 40 Lorenz pulses whose normalized cross-correlation are bounded to $(-0.3, +0.3)$. By contrast, in the right side, a set of 33 classic raised cosine waveforms' cross-correlation are over the above boundary, the peak absolute value is even over 0.4. Hence, these 40 Lorenz pulses not only have a good autocorrelation, but also have a better cross-correlation property. What's more important is the larger number of sequences. The same conclusion can be also found in the Fig.4.3.3, which demonstrated the cyclic cross-correlation function of selected Lorenz waveforms.

After discussing cross-correlation property with $T_s = 31ns$, the Fig.4.3.4 shows the cross-correlation of two kind of waveforms in length of $T_s = 127ns$. As shown in the Fig.4.3.4, there is a set of 150 Lorenz pulses with the same cross-correlation property as the classic waveforms. The number of Lorenz pulses still the greatest advantage compared to classic waveforms. However, this advantage is not kept in the cyclic cross-correlation function. When the duration grows to 127ns, it is hard to find more than 129 different Lorenz pulses with the same cross-correlation property as that of classic waveforms. Under this condition, we slightly release the criterion from $\psi_{G,127} = 17/127$ to $\psi_{G,127} = 19/127$. Then, a set of 150 Lorenz waveforms can be selected with cross-correlation property shown in the Fig.4.3.5.

Conclusively, we can find that with the short duration, the Lorenz pulses can provide the same non-cyclic/ cyclic cross-correlation function as the classic waveforms. What's greater is the number of waveforms which is much more than that of classic waveforms. For the longer

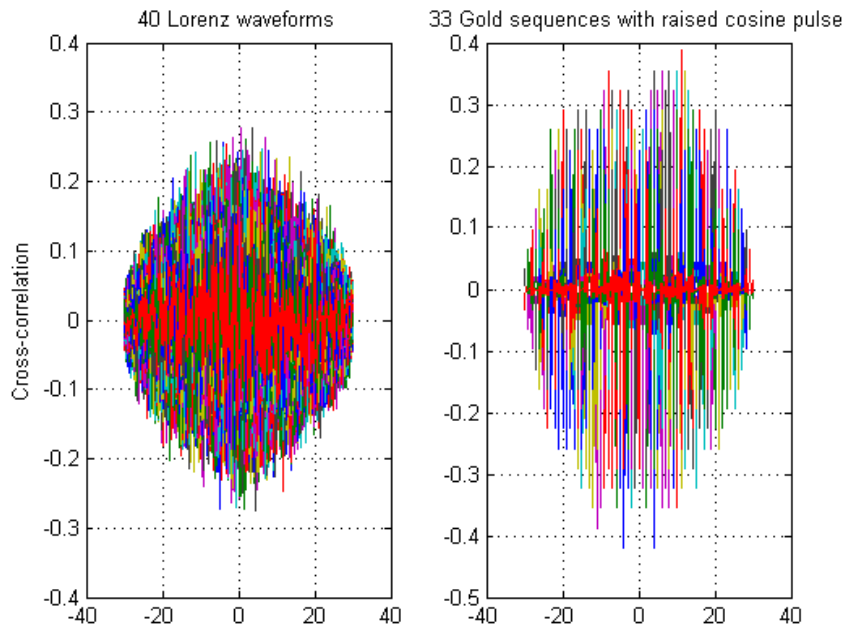


Figure 4.3.2: Cross-correlation function of selected Lorenz pulses and raised cosine pulse with Gold sequences in $T_s = 31ns$.

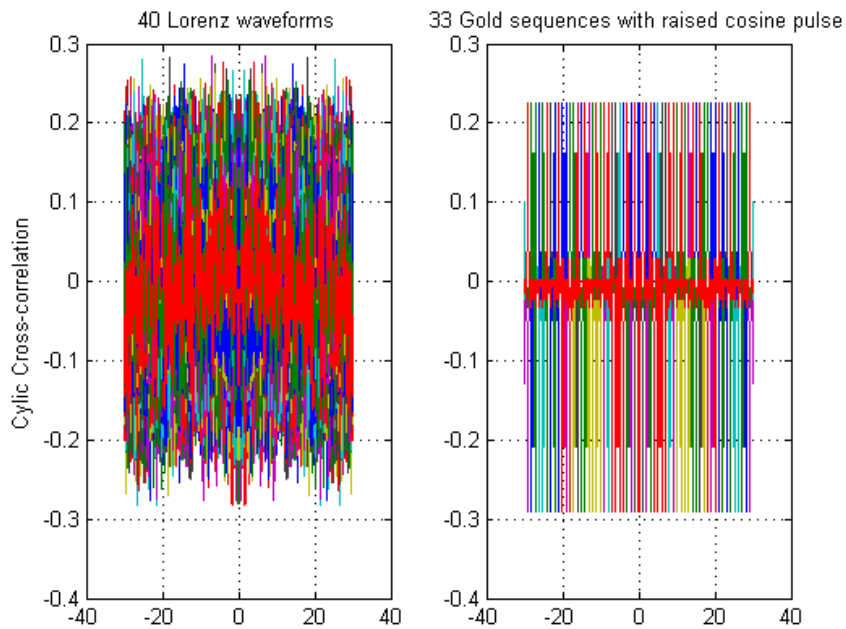


Figure 4.3.3: Cyclic cross-correlation function of selected Lorenz pulses and raised cosine pulse with Gold sequences in $T_s = 31ns$.

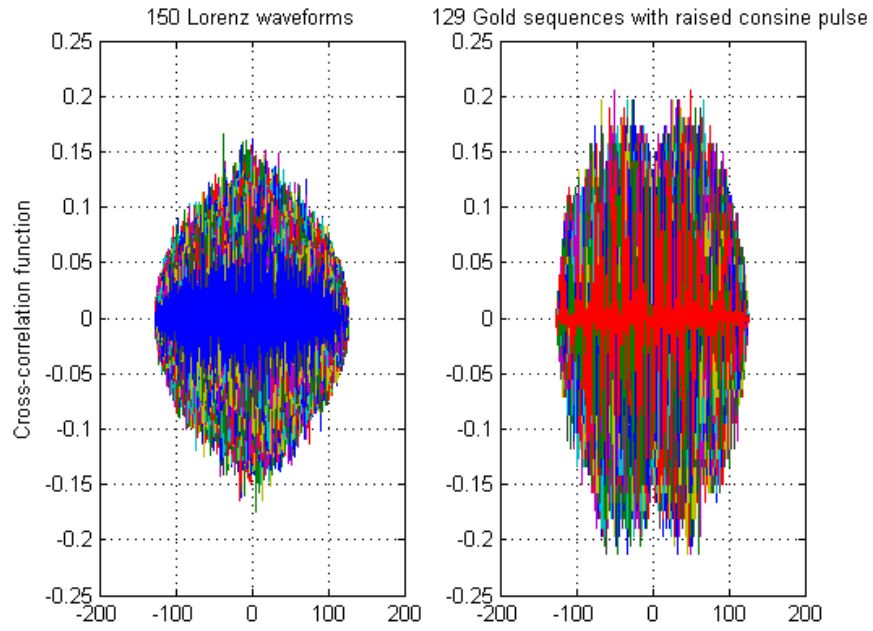


Figure 4.3.4: Cross-correlation function of selected Lorenz pulses and raised cosine pulse with Gold sequences in $T_s = 127ns$.

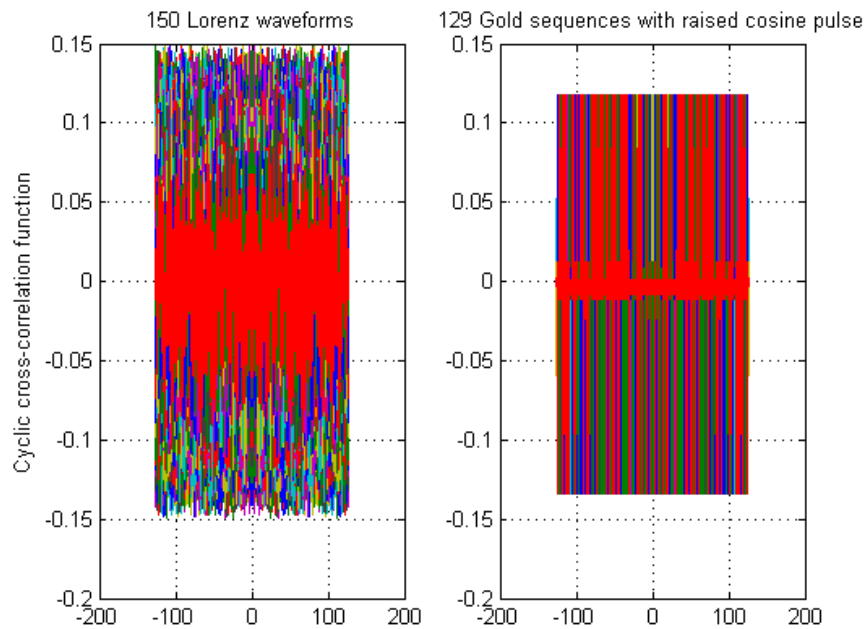


Figure 4.3.5: Cyclic cross-correlation function of selected Lorenz pulses and raised cosine pulse with Gold sequences in $T_s = 127ns$.

duration $T_s = 127ns$, although the non-cyclic cross-correlation of Lorenz waveforms keeps this advantage, the cyclic cross-correlation property does not have it any more. But if we loose the criterion mildly, a large number of Lorenz waveforms can be found as shown in the Fig.4.3.5. Hence, long duration Loren waveforms can be applied in some situation with less requirement of cross-correlation.

B. CROSS-CORRELATION FUNCTION OF CHAOTIC BINARY SEQUENCES

In the side of direct spreading sequences, both Chebyshev binary sequences and Tent binary sequences are also considered. And Gold sequences are still taken as the competitor. All the candidate binary chaotic sequences have already passed the autocorrelation selection with $\varphi_{G,N}$. However, among them, it is hard to find more than $N + 2$ chaotic sequences with the same cross-correlation property as Gold sequences. In this case, we also need to loose the criterion a little. Hence, the constraint of cross-correlation from $\psi_{G,31} = 13/31$ for length 31 to $\psi_{G,31} = 15/31$. Fig.4.3.6 and Fig.4.3.7 show the cross-correlation function of Chebyshev and Tent binary sequences compared with Gold sequences in the length $N = 31$, respectively. As shown in figures, a set of 40 Chebyshev or Tent sequences is found which satisfies the loose criterion. Although their peak absolute value are a little more than that of Gold sequences, the larger number of sequences is their advantage. As explained before, these sets of sequences may be suitable for the situation considering more on the number of users than the loss of cross-correlation. But for cyclic cross-correlation, even with the loose criterion $\psi_G = 15/31$, there are no more than 33 different chaotic sequences can be found from the candidates.

C. CROSS-CORRELATION FUNCTION OF CHAOTIC MULTI-VALUED SEQUENCES

For the time hopping sequences, the QCC sequences compare with the chaotic time hopping sequences with $N_h = 13$. Chebyshev and Tent time hopping sequences are also selected firstly by the autocorrelation property. The criterion ψ_{Q,N_h} and ψ_{Q,N_h}^c are employed to selected the qualified chaotic time hopping sequences.

$$\eta_k = \max(|C_{Q_k}(\tau)|) \quad k = 1, 2, \dots, C_{(N_h-1)}^2 \quad (4.59)$$

and

$$\psi_{Q,N_h} = \max(\eta_k) \quad k = 1, 2, \dots, C_{(N_h-1)}^2 \quad (4.60)$$

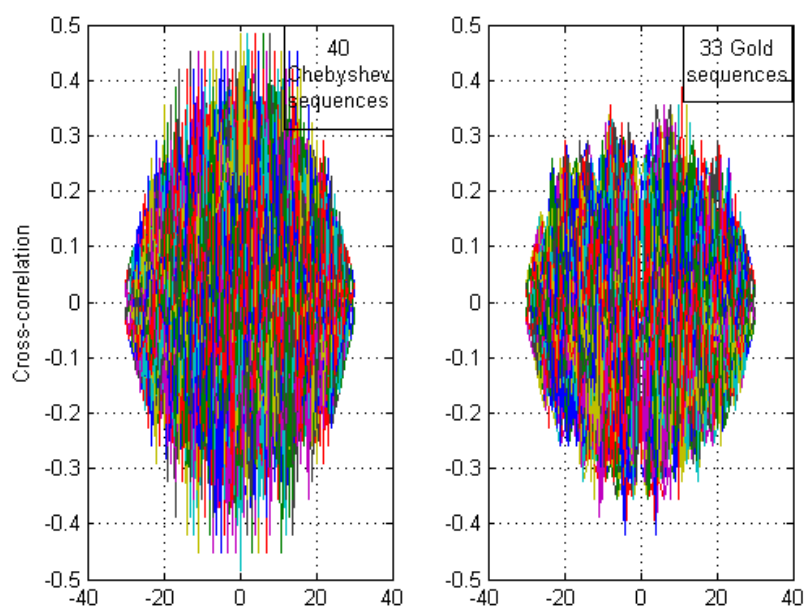


Figure 4.3.6: Cross-correlation function of selected Chebyshev sequences and Gold sequences with $N = 31$.

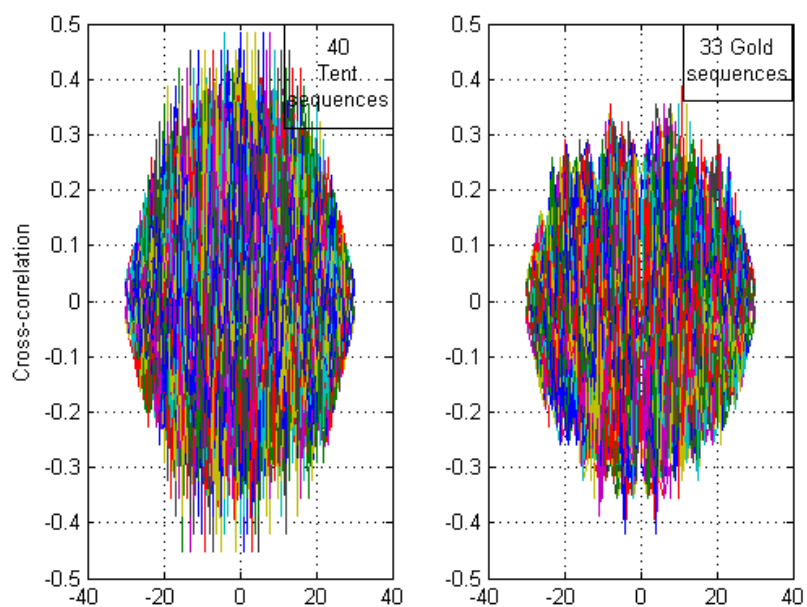


Figure 4.3.7: Cross-correlation function of selected Tent sequences and Gold sequences with $N = 31$.

where $C_{Q_k}(\tau)$ is the cross-correlation function of QCC sequence with N_h . For the side of ψ_{Q,N_h}^c ,

$$\eta_k^c = \max(|R_{Q_k}^c(\tau)|) \quad k = 1, 2, \dots, C_{(N_h-1)}^2 \quad (4.61)$$

and

$$\psi_{Q,N_h}^c = \max(\eta_k^c) \quad k = 1, 2, \dots, C_{(N_h-1)}^2 \quad (4.62)$$

where $R_{Q_k}^c(\tau)$ is the cyclic autocorrelation function of QCC sequence with N_h .

Since for chaotic time hopping sequence, it is also very difficult to find more than $N_h - 1$ sequences with the same cross-correlation property as Gold sequences, the criterion $\psi_{Q,13}$ is also loosed from $4/13$ to $6/13$. With $\psi_{Q,13} = 6/13$, a set of 20 Chebyshev time hopping sequences is found whose cross-correlation function is shown in the Fig.4.3.8. Although the peak absolute value of cross-correlation is larger than that of QCC sequences, the number of sequence is almost twice that of QCC. In addition, unlike the chaotic binary sequences, a set of 20 Chebyshev time hopping sequences can be found whose cyclic cross-correlation function also satisfies the $\psi_{Q,13} = 6/13$, which is shown in the Fig.4.3.9. If we consider the Tent time hopping sequence, the same conclusion is also found, which are shown in the Fig.4.3.10 and in the Fig.4.3.11, respectively.

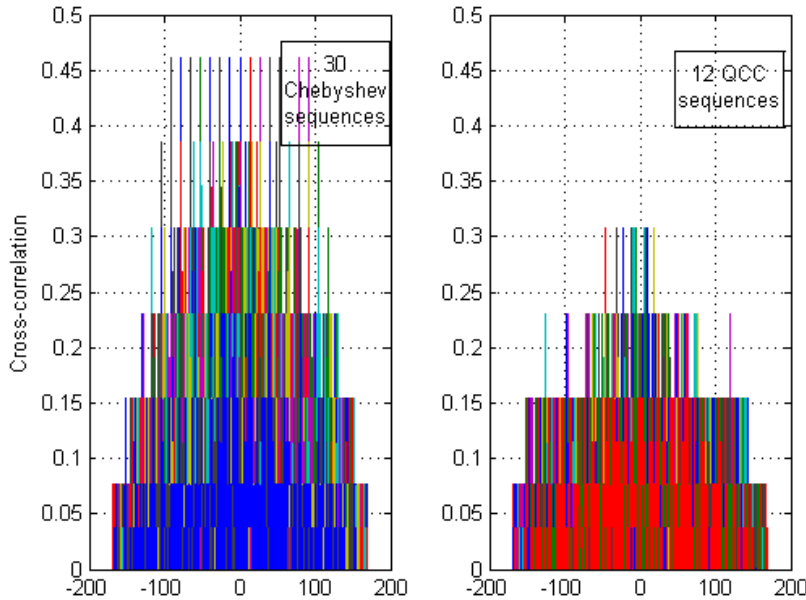


Figure 4.3.8: Cross-correlation function of selected Chebyshev sequences and QCC sequences with $N_h = 13$.

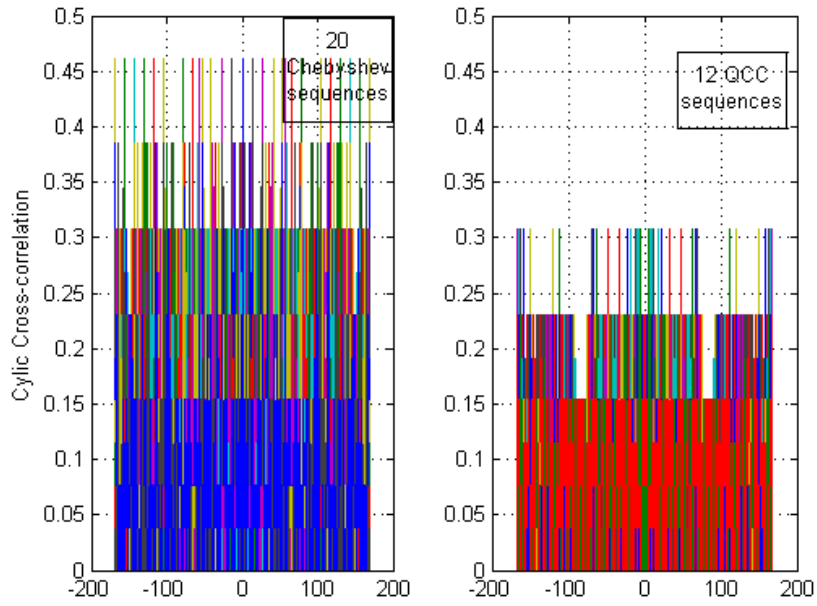


Figure 4.3.9: Cyclic cross-correlation function of selected Chebyshev sequences and QCC sequences with $N_h = 13$.

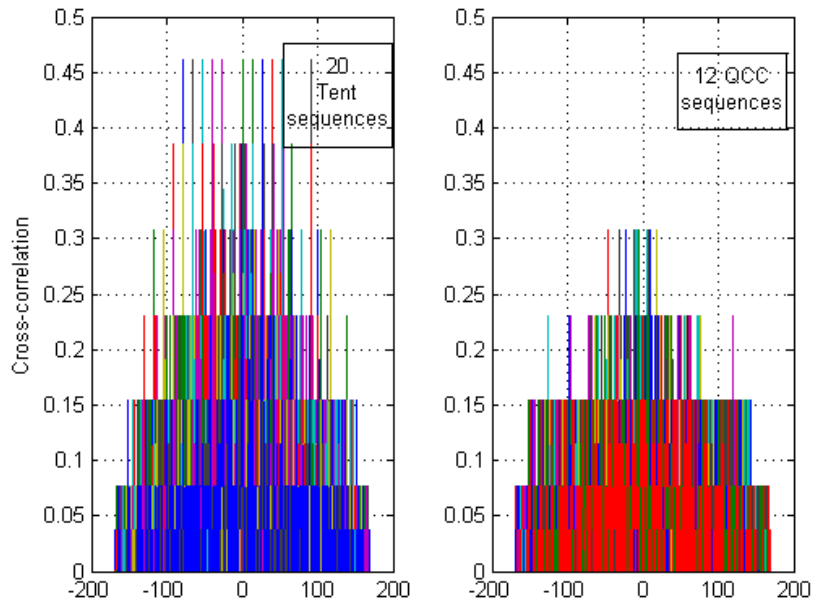


Figure 4.3.10: Cross-correlation function of selected Tent sequences and QCC sequences with $N_h = 13$.

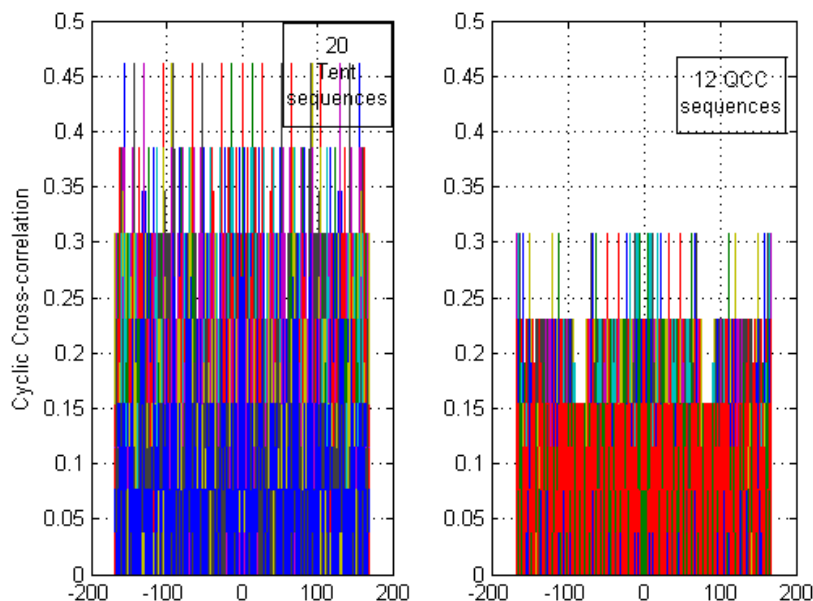


Figure 4.3.11: Cyclic cross-correlation function of selected Tent sequences and QCC sequences with $N_h = 13$.

4.4 CONCLUSION

In this Chapter, three ranging related properties are discussed, including frequency spectrum, non-cyclic/cyclic autocorrelation, non-cyclic/cyclic cross-correlation properties. These three properties are presented in the three sections. In each section, following the introduction of the affect of this property in ranging systems, the characters of conventional signals and chaotic signals are given and analyzed. Finally, in each section the analysis and comparison of chaotic signals and their classic counterparts are given. Conclusively, in the frequency spectrum property, no limitation of time duration of chaotic signals brings a great convenient for wideband and UWB systems. And the exact and approximate time-scaling method for Lorenz system can be used to generate the Lorenz waveforms in arbitrary bandwidth. In the autocorrelation property, selected chaotic signals not only achieve the same performance as classic signals, but also have the overwhelming advantage in number of signals. In the following cross-correlation property, this advantage is still kept in certain conditions.

"Less is more."

Robert Browning, Poet

5

Multiuser TOA Estimators

In the ranging environment, the existence of multiuser is a common application condition. Under this condition, ranging signals from multiuser may interfere with each other, which may degrade the ranging accuracy significantly. A common way to mitigate multiuser interference (MUI) effect is to assign different time slots, frequency bandwidth or spreading sequences to different users, which make users' signals orthogonal in time, frequency or code domain. However, the existence of dense multipath may deteriorate these orthogonality then give rise to the MUI. Although various algorithms have been proposed to mitigate MUI effect, current algorithms are only efficient when system is light-loaded even with power control mechanism. Hence, how to enhance the ranging performance under the heavy MUI environment is an important problem to be solved.

In this chapter, we present two new multiuser TOA estimators, the decoupled multiuser ranging (DEMR) algorithm and simplified large samples maximum likelihood (SLSML) algorithm for UWB ranging system. DEMR algorithm is inspired by the decoupled multiuser acquisition (DEMA) algorithm which is proposed for synchronization problem in CDMA system. DEMR algorithm extends DEMA algorithm into UWB ranging system and reduces the requirement of sampling rate and computational complexity significantly. Considering the requirements of DEMR algorithm, a simplified large samples maximum likelihood (SLSML) algorithm is introduced in the following, which required less prior information than DEMR

algorithm. Following the introduction of each algorithm, the analytical analysis and computational complexity will also be given. Finally, the performance comparison with existing algorithms through various channel condition are proposed in this chapter.

5.1 DECOUPLED MULTIUSER RANGING ALGORITHM

With the increasing requirement of highly accurate position information, UWB systems are considered as the most potential candidate for ranging system. As introduced in Chapter 2, TOA approach is most suitable for UWB ranging systems due to its wide to ultra wide bandwidth.

In multiuser environment, UWB ranging systems assign an unique spreading sequence to each user. However, the imperfect orthogonality of spreading sequences and the existence of dense multipath which spoils the orthogonality further result in MUI. This problem is worsened when the number of users is large or the interferers are sufficiently powerful, which is known as the *near-far* problem.

Although various algorithms have been proposed to mitigate the effect of MUI, existing algorithms are efficient with a small number of users. In the case of heavy or fully loaded system, especially with the near-far effect, these existing algorithms cannot achieve acceptable ranging performance. Hence, for the current ranging systems, an important problem needed to be solved is how to enhance the ranging performance in the presence of heavy MUI and near-far problem. And the computational complexity should be as low as possible due to the application requirement.

5.1.1 INTRODUCTION OF DECOUPLED MULTIUSER ACQUISITION ALGORITHM

[112] introduced an interesting synchronization algorithm for DS-CDMA system, which is referred to as decoupled multiuser acquisition (DEMA) algorithm. DEMA algorithm is an MF-based asymptotic Maximum Likelihood (ML) algorithm, it not only allows the system to be fully loaded, but is also quite near-far resistant even with fully-loaded system. Due to the similarity of ranging and synchronization, we try to develop DEMA algorithm from synchronization problem to ranging problem.

As a multiuser synchronization algorithm, DEMA algorithm requires the knowledge of the spreading sequences and the transmitted data bits for all the users. This requirement may be quite restrictive for communication systems, but it is not too difficult for ranging systems. This information can be stored in advance in each node as the prior information. For ranging system, data bits is considered as a kind of sequences referred to as data sequences if there is no need for transmitting data bits.

As a result of using such information, DEMA algorithm is extremely near-far resistant and allow a system to be fully loaded with little performance degradation. The DEMA algorithm is derived by taking all users into account so that the structure of received signal can be fully exploited. With the assumption that the transmitted data bits are independently and identically distributed (i.i.d), DEMA algorithm is a decoupled algorithm which obtains the time estimates for all the users simultaneously and efficiently. Although DEMA algorithm achieves quite impressive performance, DEMA algorithm requires not only high sampling rate, but the computational complexity is also quite high especially in multipath environment due to a search over a multi-dimensional parameter space.

5.1.2 DECOUPLED MULTIUSER ACQUISITION ALGORITHM IN UWB RANGING SYSTEMS

Although DEMA is proposed for DS-CDMA systems, it can be extended directly into DS-UWB and TH-UWB systems, which is presented detailedly in this section. In addition, DEMA algorithm is introduced from AWGN channel in [112] to multipath channel since it is widely considered in indoor ranging systems.

The system firstly under investigation is an K -user DS-UWB system using binary phase-shift keying (BPSK) modulation. The transmitted signal by the k th user is formed as

$$s_k(t) = \sqrt{P_k} \sum_{m=0}^{M-1} d_k(m) \sum_{n=0}^{N-1} u_k(n) p(t - nT_f - mT_d) \quad (5.1)$$

where P_k is the k th user's transmitted power, M is number of data bits considered for TOA estimation, $d_k(m) \in \{\pm 1\}$ is the m th transmitted bit, $u_k(n) \in \{\pm 1\}$ is the direct spreading sequence with length N of user k . $p(t)$ is the pulse shape with pulse duration T_p , T_c is chip duration $T_c \geq T_p$. $T_f = N_c T_c$ is the frame duration, where N_c is the number of chips in one frame. $T_d = NT_f$ is data bit interval. From the structure of $s_k(t)$, we can find that there is only one pulse transmitted per frame, which locates in the first chip of each frame. In other words, other chips except the first chip are all silent chip transmitting no pulse. Hence, the pulse repetition time is equal to T_f which is much longer than its duration T_p . We adopt an alternative spreading sequences $g_k(i) \in \{\pm 1, 0\}$ to illustrate this long repetition time property of DS-UWB signals. $g_k(i)$ is generated by adding $N_c - 1$ "0" between each element of the spreading sequence $u_k(n)$. Then, $s_k(t)$ can be rewritten as

$$s_k(t) = \sqrt{P_k} \sum_{m=0}^{M-1} d_k(m) \sum_{i=0}^{NN_c-1} g_k(i) p(t - iT_c - mT_d) \quad (5.2)$$

with

$$g_k(i) = \begin{cases} u_k(i/N_c) & \text{if } i \bmod N_c = 0 \\ 0 & \text{otherwise.} \end{cases} \quad (5.3)$$

When the transmitted signals are passed through the multipath channel described in IEEE 802.15.4a channel model [40], the received signal can be expressed as

$$r(t) = \sum_{k=1}^K \sum_{q=1}^{L_k} \alpha_{k,q} s_k(t - \tau_{k,q}) + n(t) \quad (5.4)$$

where $\alpha_{k,q}$ and $\tau_{k,q}$ denote the complex channel coefficient and time delays of the q th multipath component of the k th user respectively. L_k is the number of multipath for the k th user. $\tau_{k,1}$ is the parameter of interest in TOA estimation. $n(t)$ is the additive white Gaussian noise with zero mean and double sided power spectral density of $N_o/2$. For simplicity, we only consider the reception of M bits, and assume the first user is user of interest. Therefore,

$$r(t) = \sum_{k=1}^K \sum_{q=1}^{L_k} \sqrt{P_k} \alpha_{k,q} \sum_{m=0}^{M-1} d_k(m) \sum_{i=0}^{NN_c-1} g_k(i) p(t - iT_c - mT_d - \tau_{k,q}) + n(t) \quad (5.5)$$

Since UWB ranging systems are designed for short range localization, it is mild to assume $\tau(k, q)$ to be bounded into a bit interval T_d with proper selection of T_c and N .

The receiver front-end consists of a filter matched to the transmitted pulse $p(t)$ with sample interval $t_s = T_c/V$, where the integer $V > 0$ is called the oversampling factor. After frond-end filtering, the received sequences $r(l)$ is

$$r(l) = \sum_{k=1}^K \sum_{q=1}^{L_k} \int_{-\infty}^{+\infty} \alpha_{k,q} s_k(t - \tau_{k,q}) p(t - l \frac{T_c}{V}) dt + n(l) \quad (5.6)$$

$$l = 0, 1, 2, \dots, MNN_cV - 1$$

$n(l)$ denotes the zero-mean white Gaussian noise with variances σ_n^2 . The received vector of the m th bit interval $\mathbf{r}(m)$ is defined as

$$\mathbf{r}(m) = [r(mNN_cV + 1), r(mNN_cV + 2), \dots, r(mNN_cV + NN_cV)]^T \quad (5.7)$$

where $(\cdot)^T$ denotes the transpose, and $\mathbf{n}(m)$ is similarly formed by $n(l)$. We also define that

$$\mathbf{c}_k = [c_k(0), c_k(1), \dots, c_k(NN_cV - 1)]^T \quad (5.8)$$

which

$$c_k(l) = \int_{-\infty}^{+\infty} \sum_{i=0}^{NN_c-1} g_k(i) p(t - iT_c) p(t - l\frac{T_c}{V}) dt \quad (5.9)$$

For the time delay $\tau_{k,q}$, we let

$$\tau_{k,q} = (p_{k,q} + \mu_{k,q})t_s \quad (5.10)$$

where $p_{k,q}$ is an integer within $\{0, 1, \dots, NN_cV - 1\}$ and $0 \leq \mu_{k,q} < 1$.

In the m th bit interval, due to the time delay $\tau_{k,q}$, the received signal actually includes $\mathbf{a}_k^1(\tau_{k,q})$, the end part of $(m - 1)$ th bit; and $\mathbf{a}_k^2(\tau_{k,q})$, the beginning part of m th bit.

$$\mathbf{a}_k^1(\tau_{k,q}) = [(1 - \mu_{k,q})\mathbf{P}_1(p_{k,q}) + \mu_{k,q}\mathbf{P}_1(p_{k,q} + 1)]\mathbf{c}_k \quad (5.11)$$

$$\mathbf{a}_k^2(\tau_{k,q}) = [(1 - \mu_{k,q})\mathbf{P}_2(p_{k,q}) + \mu_{k,q}\mathbf{P}_2(p_{k,q} + 1)]\mathbf{c}_k \quad (5.12)$$

where $\mathbf{P}_1(p)$ and $\mathbf{P}_2(p)$ denote the $NN_cV \times NN_cV$ shifting matrices

$$\mathbf{P}_1(p) = \begin{bmatrix} 0 & \mathbf{I}_p \\ 0 & 0 \end{bmatrix} \quad \mathbf{P}_2(p) = \begin{bmatrix} 0 & 0 \\ \mathbf{I}_{NN_cV-p} & 0 \end{bmatrix} \quad (5.13)$$

and \mathbf{I}_p is $p \times p$ identity matrix. Then the received vector $\mathbf{r}(m)$ can be rewritten as

$$\mathbf{r}(m) = \sum_{k=1}^K \sum_{q=1}^{L_k} \beta_{k,q} \mathbf{A}_k(\tau_{k,q}) \mathbf{z}_k(m) + \mathbf{n}(m) \quad (5.14)$$

$$m = 0, 1, \dots, M - 1$$

where

$$\beta_{k,q} = a_{k,q} \sqrt{P_k} \quad (5.15)$$

$$\mathbf{A}_k(\tau_{k,q}) = [\mathbf{a}_k^1(\tau_{k,q}) \quad \mathbf{a}_k^2(\tau_{k,q})] \quad (5.16)$$

and

$$\mathbf{z}_k(m) = [d_k(m - 1) \quad d_k(m)]^T. \quad (5.17)$$

Note that when $m = 0$, $d_k(-1)$ is unknown. We can choose $d_k(-1) = 0$ which has little effect on the estimation. To facilitate our derivation, we rewrite $\mathbf{r}(m)$ as

$$\mathbf{r}(m) = \mathbf{B}\mathbf{s}(m) + \mathbf{n}(m) \quad (5.18)$$

where

$$\mathbf{B} = \left[\sum_{q=1}^{L_1} \beta_{1,q} \mathbf{A}_1(\tau_{1,q}) \sum_{q=1}^{L_2} \beta_{2,q} \mathbf{A}_2(\tau_{2,q}) \dots \sum_{q=1}^{L_K} \beta_{K,q} \mathbf{A}_K(\tau_{K,q}) \right] \quad (5.19)$$

and

$$\mathbf{s}(m) = [\mathbf{z}_1^T(m) \mathbf{z}_2^T(m) \dots \mathbf{z}_K^T(m)]^T. \quad (5.20)$$

Here, we assume that spreading sequences and data bits for all the users are known. If we let

$$\mathbf{R}_{\mathbf{ss}}(M) = \frac{1}{M} \sum_{m=0}^{M-1} \mathbf{s}(m) \mathbf{s}^T(m) \quad (5.21)$$

and assume data bits for all users are i.i.d, hence, $\mathbf{R}_{\mathbf{ss}}(M) = \mathbf{I}_{2K}$, when $M \rightarrow +\infty$ [112].

Finally, we also assume that $\mathbf{s}(m)$ and $\mathbf{n}(m)$ are uncorrelated, i.e,

$$\lim_{M \rightarrow \infty} \frac{1}{M} \sum_{m=0}^{M-1} \mathbf{s}(m) \mathbf{n}^H(m) = \mathbf{o}. \quad (5.22)$$

with probability 1

where $(\cdot)^H$ denotes the Hermitian transpose.

The TOA estimation problem now turns to estimate $\{\tau_{k,1}\}_{k=1}^{K=K}$, or equivalently $\{p_{k,1}, \mu_{k,1}\}_{k=1}^{k=K}$ from the received signal $\{\mathbf{r}(m)\}_{m=1}^{m=M}$. With the received signal $\mathbf{r}(m)$, the Maximum Likelihood (ML) estimation is equivalent to

$$\begin{aligned} \{\{\hat{\beta}_{k,q}, \hat{\tau}_{k,q}\}_{q=1}^{L_k}\}_{k=1}^K = \arg \min_{\{\{\beta_{k,q}, \tau_{k,q}\}_{q=1}^{L_k}\}_{k=1}^K} \operatorname{tr} \left\{ \frac{1}{M} \sum_{m=0}^{M-1} [\mathbf{r}(m) - \mathbf{B}(\beta_{k,q}, \tau_{k,q}) \mathbf{s}(m)] \right. \\ \left. [\mathbf{r}(m) - \mathbf{B}(\beta_{k,q}, \tau_{k,q}) \mathbf{s}(m)]^H \right\} \end{aligned} \quad (5.23)$$

where $\operatorname{tr}\{\cdot\}$ is trace operator. Let

$$\mathbf{R}_{\mathbf{sr}}(M) = \frac{1}{M} \sum_{m=0}^{M-1} \mathbf{s}(m) \mathbf{r}^H(m) \quad (5.24)$$

$\mathbf{R}_{\mathbf{rr}}(M)$ is similarly defined from $\{\mathbf{r}(m)\}_{m=1}^{m=M}$ and $\mathbf{R}_{\mathbf{ss}}(M)$ is from $\{\mathbf{s}(m)\}_{m=1}^{m=M}$. According to [112], minimizing (5.23) with respect to \mathbf{B} gives

$$\hat{\mathbf{B}} = \mathbf{R}_{\mathbf{sr}}^H(M) \mathbf{R}_{\mathbf{ss}}^{-1}(M) \quad (5.25)$$

where we have assumed that $\mathbf{R}_{\text{ss}}^{-1}(M)$ exists. With the definition of $\hat{\mathbf{B}}$, the rear-range of cost function (5.23) can be rewritten as

$$\begin{aligned} & \text{tr}\left\{\frac{1}{M}\sum_{m=0}^{M-1}[\mathbf{r}(m) - \mathbf{B}(\beta_{k,q}, \tau_{k,q})\mathbf{s}(m)][\mathbf{r}(m) - \mathbf{B}(\beta_{k,q}, \tau_{k,q})\mathbf{s}(m)]^H\right\} \\ &= \text{tr}\{\mathbf{R}_{\text{rr}}(M) - \hat{\mathbf{B}}\mathbf{R}_{\text{ss}}(M)\hat{\mathbf{B}}^H\} + \text{tr}\{(\mathbf{B} - \hat{\mathbf{B}})\mathbf{R}_{\text{ss}}(M)(\mathbf{B} - \hat{\mathbf{B}})^H\} \end{aligned} \quad (5.26)$$

Since the first term of (5.26) is independent of \mathbf{B} , minimizing the (5.26) is simplified to

$$\{\{\hat{\beta}_{k,q}, \hat{\tau}_{k,q}\}_{q=1}^{L_k}\}_{k=1}^K = \arg \min_{\{\{\beta_{k,q}, \tau_{k,q}\}_{q=1}^{L_k}\}_{k=1}^K} \text{tr}\{(\mathbf{B} - \hat{\mathbf{B}})\mathbf{R}_{\text{ss}}(M)(\mathbf{B} - \hat{\mathbf{B}})^H\} \quad (5.27)$$

The exact ML estimation of all the unknown time delays and amplitudes $\{\{\hat{\beta}_{k,q}, \hat{\tau}_{k,q}\}_{q=1}^{L_k}\}_{k=1}^K$ are obtained by minimizing the new cost function (5.27), which in general requires a search over a $3\sum_{k=1}^K L_k$ -dimensional parameter space (note that $\beta_{k,q}$ is complex-valued). Hence, the computational complexity is almost prohibitive. In the following, we will show that DEMA algorithm for DS-UWB system can be computationally efficient.

Note that $\mathbf{R}_{\text{ss}}(M)$ is a $(1/\sqrt{M})$ -consistent estimate of \mathbf{R}_{ss} . Similarly, due to the assumption that the data bits and the noise samples are independent of each other, $\hat{\mathbf{B}}$ is also a $(1/\sqrt{M})$ -consistent estimate of \mathbf{B} . Hence, the solution of (5.27) is asymptotically equivalent to

$$\{\{\hat{\beta}_{k,q}, \hat{\tau}_{k,q}\}_{q=1}^{L_k}\}_{k=1}^K = \arg \min_{\{\{\beta_{k,q}, \tau_{k,q}\}_{q=1}^{L_k}\}_{k=1}^K} \text{tr}\{\mathbf{R}_{\text{ss}}(\mathbf{B} - \hat{\mathbf{B}})^H(\mathbf{B} - \hat{\mathbf{B}})\} \quad (5.28)$$

where with the criterion of the identity $\text{tr}\{\mathbf{A}\mathbf{B}\} = \text{tr}\{\mathbf{B}\mathbf{A}\}$ for any matrices \mathbf{A} and \mathbf{B} of compatible dimensions. Let

$$\hat{\mathbf{B}} = [\hat{\mathbf{B}}_1 \hat{\mathbf{B}}_2 \dots \hat{\mathbf{B}}_K], \quad (5.29)$$

Since the $\mathbf{R}_{\text{ss}} = \mathbf{I}_{2K}$, (5.28) is decoupled into a series of K minimization problems

$$\begin{aligned} \{\{\hat{\beta}_{k,q}\}_{q=1}^{L_k}, \{\hat{\tau}_{k,q}\}_{q=1}^{L_k}\} &= \arg \min_{\{\{\beta_{k,q}\}_{q=1}^{L_k}, \{\tau_{k,q}\}_{q=1}^{L_k}\}} \left\| \sum_{q=1}^{L_k} \beta_{k,q} \mathbf{A}_k(\tau_{k,q}) - \hat{\mathbf{B}}_k \right\|_F^2 \\ & k = 1, 2, \dots, K \end{aligned} \quad (5.30)$$

where $\|\cdot\|_F$ is Frobenius norm [112].

We first consider the simplest condition, the AWGN channel, i.e., the $L_k = 1$ for all the K

users, the cost function is simplified to

$$\begin{aligned} \{\hat{\beta}_k, \hat{\tau}_k\} &= \arg \min_{\beta_k, \tau_k} \|\beta_k \mathbf{A}_k(\tau_k) - \hat{\mathbf{B}}_k\|_F^2 \\ k &= 1, 2, \dots, K \end{aligned} \quad (5.31)$$

We define

$$\mathbf{a}_k(\tau_k) = \text{vec}[\mathbf{A}_k(\tau_k)] \quad (5.32)$$

$$\hat{\mathbf{b}}_k = \text{vec}[\hat{\mathbf{B}}_k] \quad (5.33)$$

where $\text{vec}[\cdot]$ denotes stacking the columns of a matrix on top of one another. Then, minimizing the cost function in (5.30) with respect to τ_k and β_k yields

$$\hat{\tau}_k = \arg \max_{\{\tau_k\}} \frac{|\mathbf{a}_k^T(\tau_k) \hat{\mathbf{b}}_k|^2}{\mathbf{a}_k^T(\tau_k) \mathbf{a}_k(\tau_k)} \quad (5.34)$$

$$\hat{\beta}_k = \frac{\mathbf{a}_k^T(\hat{\tau}_k) \hat{\mathbf{b}}_k}{\mathbf{a}_k^T(\hat{\tau}_k) \mathbf{a}_k(\hat{\tau}_k)} \quad (5.35)$$

The TOA and amplitude are estimated as $\hat{\tau}_k$ and $|\hat{\beta}_k|$, respectively. In [112], since the rectangular pulse is employed in the DS-CDMA system, the maximization of (5.34) is simple to perform. For each p_k , $\hat{\mu}_k$ can be conveniently found by rooting a second-order polynomial. However, when band limited pulse such as raised cosine pulse is employed, second-order polynomial rooting cannot be used. Hence, some nonlinear optimization routine have to be used to estimate τ_k .

When we consider the more complex but more practical environment, the multipath channel conditions, the cost function (5.30) can not be simplified anymore. Since DEMA algorithm can decouple different users but not different paths, although the search over a $3 \sum_{k=1}^K L_k$ -dimensional parameter space have been reduce as a series of K different $3L_k$ -dimensional search problems, the computational complexity is still too high to be used in the multipath channel condition.

From the above analysis, we can find that the DEMA algorithm can be extended to DS-UWB ranging system smoothly, its multiuser decoupling property is also maintained in ranging systems. However, the band limited pulses employed in DS-UWB ranging systems requires the nonlinear optimization algorithm in addition. Moreover, the dense multipath channel condition make the computational complexity of DEMA algorithm quite high. The last problem when using DEMA algorithm in DS-UWB ranging problem is the high sampling rate.

As the matched filter is the receiver front-end, the sampling rate should achieve Nyquist rate at least. The requirement of Nyquist sampling rate or higher is impractical to UWB systems due to its large bandwidth. If we cannot solve these problem successfully, although DEMA algorithm can support large number of users and is near-far resistant, its implementation is still problematic.

Based on this point, we present our decoupled multiuser ranging (DEMR) algorithm, which not only keeps the attractive features of DEMA algorithm, but also works with low computational complexity and low sampling rate and have no modification when transmitted pulse is different.

5.1.3 DECOUPLED MULTIUSER RANGING ALGORITHM

The transmitted and received signal of DEMR algorithm is the same as DEMA algorithm, which are shown in the Eq.(5.2) and Eq.(5.5). In DEMR algorithm, we assume that

$$\tau_{k,q} = p_{k,q} T_c \quad (5.36)$$

where $p_{k,q}$ is an integer within $\{0, 1, \dots, NN_c - 1\}$. Compare with (5.10), time delay is approximated to be integer multiples of chip duration T_c not containing the fractional part in the scaling of T_c . Since in UWB system, T_c is in the order of nano-second, it is a mild approximation for ranging accuracy. Then, TOA estimation of all the K users is equivalent to estimating $p_{k,1}$.

The approximation of $\tau_{k,q}$ is the first difference between DEMA and DEMR. The second is the frond-end filter of the receiver. In DEMA algorithm, matched filter (MF) is chosen as the received filter for its high accuracy. On another hand, the sampling rate is required to be Nyquist rate or higher which is a challenge for UWB system due to its extremely large bandwidth. In this case, we adopt an integrate-and-dump filter (IDF) with integration time T_c instead of MF as the receiver front-end. As seen in the Fig.5.1.1, if raised cosine pulse is the transmitted pulse, the output of MF has a peaky, narrow main lobe, which decreased sharply when time differences increases. If the sampling rate is higher enough, it is certain that a sample is located closed to the peak value which brings the accurate time delay estimation. Consequently, the accurate ranging performance is achieved. By contrast, if the sampling rate is not at least as high as Nyquist rate, the performance of time delay estimation degrades dramatically due to no sample being close enough to the peak value. In the side of IDF, although the highest value is smaller than the peak value of MF output, the output of IDF achieves a floor when the time within $[-0.4T_c, 0.4T_c]$. This phenomenon is a drawback when sampling rate is Nyquist rate or higher. Since the range of ambiguity is quite wide, you cannot find the ex-

act time delay. However, if a lower sampling rate is employed and the precision of time delay estimation is only needed in the order of T_c , IDF is much suitable than MF. Due to the existence of the floor from $[-0.4T_c, 0.4T_c]$ in the output of IDF, no matter where the samples are located, the output values are almost the same. Although in the area $[-0.5T_c, -0.4T_c]$ and $[0.4T_c, 0.5T_c]$, the output goes down to half of the floor gradually, it still quite higher than the samples out of the duration $[-0.5T_c, 0.5T_c]$ whose values are close to 0.

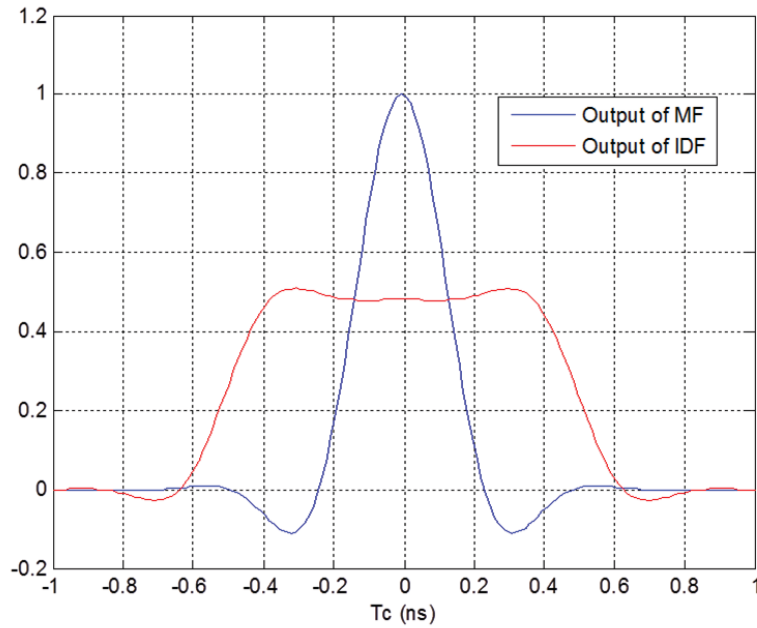


Figure 5.1.1: The output of matched filter (MF) and integrate-and-dump filter (IDF) of raised cosine pulse

With the IDF as the front-end with integral time T_c , the received sequence is no longer (5.6) but is expressed as

$$r(l) = \sum_{k=1}^K \sum_{q=1}^{L_k} \frac{1}{T_c} \int_{(l-1)T_c}^{lT_c} a_{k,q} s_k(t - \tau_{k,q}) dt + n(l) \quad (5.37)$$

$$l = 1, 2, \dots, NN_c$$

$n(l)$ also denotes the zero-mean white Gaussian noise with variances σ_n^2 . And the $\mathbf{r}(m)$ in (5.7) turns to

$$\mathbf{r}(m) = [r(mNN_c + 1), r(mNN_c + 2), \dots, r(mNN_c + NN_c)]^T \quad (5.38)$$

where the length of $\mathbf{r}(m)$ is shortened to NN_c not NN_cV anymore. Consequently, \mathbf{c}_k is redefined as

$$\mathbf{c}_k = [c_k(1), c_k(2), \dots, c_k(NN_c)]^T \quad (5.39)$$

where

$$c(l) = \frac{1}{T_c} \int_{(l-1)T_c}^{lT_c} \sum_{i=0}^{NN_c-1} g_k(i) p(t - iT_c) dt \quad (5.40)$$

Since the approximation of $\tau_{k,q}$, the $\mathbf{a}_k^1(\tau_{k,q})$ in Eq.(5.11) and $\mathbf{a}_k^2(\tau_{k,q})$ Eq.(5.12) can be rewritten as

$$\mathbf{a}_k^1(\tau_{k,q}) = \mathbf{P}_1(p_{k,q}) \mathbf{c}_k \quad (5.41)$$

$$\mathbf{a}_k^2(\tau_{k,q}) = \mathbf{P}_2(p_{k,q}) \mathbf{c}_k \quad (5.42)$$

where $\mathbf{P}_1(p)$ and $\mathbf{P}_2(p)$ denote the $NN_c \times NN_c$ shifting matrices

$$\mathbf{P}_1(p) = \begin{bmatrix} \circ & \mathbf{I}_p \\ \circ & \circ \end{bmatrix} \quad \mathbf{P}_2(p) = \begin{bmatrix} \circ & \circ \\ \mathbf{I}_{NN_c-p} & \circ \end{bmatrix} \quad (5.43)$$

and \mathbf{I}_p is also the $p \times p$ identity matrix.

With the above modification of each element of $\mathbf{r}(m)$, $\mathbf{r}(m)$ can be also expressed as

$$\mathbf{r}(m) = \mathbf{B}\mathbf{s}(m) + \mathbf{n}(m) \quad (5.44)$$

where $\mathbf{B}(m)$ and $\mathbf{s}(m)$ have the same definition as (5.19) and (5.20). We also assume that we know the data bits and spreading sequences of all the users. And the $\mathbf{s}(m)$ and $\mathbf{n}(m)$ are uncorrelated as shown in (5.22).

If we still consider the Maximum Likelihood estimation, the ML estimation can be also simplified from (5.23) to (5.30) due to the same conditions and assumptions. As the DEMA algorithm, if we also consider the AWGN firstly, the cost function for all the K user is expressed as

$$\{\hat{\beta}_k, \hat{\tau}_k\} = \arg \min_{\beta_k, \tau_k} \|\beta_k \mathbf{A}_k(\tau_k) - \hat{\mathbf{B}}_k\|_F^2 \quad (5.45)$$

$$k = 1, 2, \dots, K$$

and the time delay estimation can be obtained by

$$\hat{\tau}_k = \arg \max_{\{\tau_k\}} \frac{|\mathbf{a}_k^T(\tau_k) \hat{\mathbf{b}}_k|^2}{\mathbf{a}_k^T(\tau_k) \mathbf{a}_k(\tau_k)} \quad (5.46)$$

and the amplitude is

$$\hat{\beta}_k = \frac{\mathbf{a}_k^T(\hat{\tau}_k)\hat{\mathbf{b}}_k}{\mathbf{a}_k^T(\hat{\tau}_k)\mathbf{a}_k(\hat{\tau}_k)} \quad (5.47)$$

which is the same as those in the DEMA algorithm. However, using the integer approximation of time delay $\tau_{k,q}$, the estimation of fractional part is not needed any more.

In the multipath channel, as analysis before, DEMA algorithm become impractical due to a series of K different $3L_k$ -dimensional search problems. But due to the integer approximation of $\tau_{k,q}$ and DS-UWB signal structure, DEMR algorithm simplifies the K different $3L_k$ -dimensional search problem into the K different L_k maximums in one dimensional search problem.

Since we define

$$\mathbf{a}_k(\tau_{k,q}) = \text{vec}[\mathbf{A}_k(\tau_{k,q})] \quad (5.48)$$

$$\hat{\mathbf{b}}_k = \text{vec}[\hat{\mathbf{B}}_k] \quad (5.49)$$

With the substitution of $\mathbf{a}_k^1(\tau_{k,q})$ in Eq.(5.41) and $\mathbf{a}_k^2(\tau_{k,q})$ in Eq.(5.41), $\mathbf{a}_k(\tau_{k,q})$ can be rewritten as

$$\mathbf{a}_k(\tau_{k,q}) = \begin{bmatrix} \mathbf{P}_1(p_{k,q})\mathbf{c}_k \\ \mathbf{P}_2(p_{k,q})\mathbf{c}_k \end{bmatrix} \quad (5.50)$$

Since the $\tau_{k,q} = p_{k,q}T_c$, we can find that $\mathbf{a}_k(\tau_{k,q})$ is a cyclic shift of $\mathbf{a}_k(0)$ which is named as the stacked code and is given as

$$\mathbf{a}_k(0) = \begin{bmatrix} \mathbf{P}_1(0)\mathbf{c}_k \\ \mathbf{P}_2(0)\mathbf{c}_k \end{bmatrix} \quad (5.51)$$

Since $\mathbf{P}_1(0)$ is an all-zero matrix, the $\mathbf{P}_1(0)\mathbf{c}_k$ is an all-zero vector with the same length as \mathbf{c}_k . And $\mathbf{P}_2(0)$ is a identity matrix. Thus, $\mathbf{a}_k(0)$ consists of \mathbf{c}_k following a all-zero vector in the same length as \mathbf{c}_k . As g_k is formed by inserted $N_c - 1$ "o" between each element in $u_k(n)$, \mathbf{c}_k , furthermore $\mathbf{a}_k(0)$ also has this "o" inserted property. Consequently, both non-cyclic and cyclic autocorrelation function of $\mathbf{a}_k(0)$ also be "o" inserted into each element. On the other hand, the autocorrelation function of $\mathbf{a}_k(0)$ is a sparse function which has a non-zero value in every N_c values. When considering the practical meaning of autocorrelation function, the $\mathbf{a}_k(0)$ is uncorrelated with itself with the delays whose corresponding value of autocorrelation function is zero.

In multipath environment, since both desired signal $\mathbf{a}_k(\tau_{k,1})$ and interference signal $\mathbf{a}_k(\tau_{k,q})$ are cyclic shifts of $\mathbf{a}_k(0)$, the multipath interference can be described as the side-lobe of auto-

correlation function of $\mathbf{a}_k(\tau_{k,1})$ which is the same as that of $\mathbf{a}_k(\mathbf{o})$. If multipath delays $\tau_{k,q}$ correspond to the zero valued points in the autocorrelation function, $\mathbf{a}_k(\tau_{k,q})$ is considered to be uncorrelated with $\mathbf{a}_k(\tau_{k,1})$, which mitigates the interference of multipath.

Moreover, with the multipath delay spread $\max(\tau_{k,q})$, there is only $\lfloor \max(\tau_{k,q})/N_c \rfloor$ possible delay corresponding to non-zero value. Hence, if the multipath delay spread is much smaller than $NN_c T_c$, so $\max(\tau_{k,q}) \ll NN_c T_c$, the number of delay corresponding to non-zero value is quite small. In this case, we can ignore $\mathbf{a}_k^T(\tau_{k,s})\mathbf{a}_k(\tau_{k,r})$, which is equal to assuming $\mathbf{a}_k^T(\tau_{k,s})\mathbf{a}_k(\tau_{k,r}) = \mathbf{o}$ when $s \neq r, s, r \in \{1, 2, \dots, L_k\}$. With the ignorance of the side-lobe value of autocorrelation function of $\mathbf{a}_k(\mathbf{o})$, $\mathbf{a}_k(\mathbf{o})$ has a white noise like autocorrelation function which means $\mathbf{a}_k(\mathbf{o})$ only correlates with itself without any time difference.

Since $s(t)$ is transmitted continuously and periodically, the cyclic-autocorrelation function should be considered. However, the existence of all-zero vector in stacked code $\mathbf{a}_k(\mathbf{o})$ turns the cyclic-autocorrelation to the non-cyclic autocorrelation function actually. Hence, in DEMR algorithm, the non-cyclic autocorrelation function is much more important.

With the white noise like autocorrelation function of $\mathbf{a}_k(\mathbf{o})$, minimizing the cost function of Eq.(5.30) is not impractical anymore. The cost function of Eq.(5.30) with respect to $\tau_{k,q}$ and $\beta_{k,q}$ yields

$$\{\hat{\tau}_{k,q}\}_{q=1}^{L_k} = \arg \max_{\{\tau_{k,q}\}_{q=1}^{L_k}} \sum_{q=1}^{L_k} \frac{|\mathbf{a}_k^T(\tau_{k,q})\hat{\mathbf{b}}_k|^2}{\mathbf{a}_k^T(\tau_{k,q})\mathbf{a}_k(\tau_{k,q})} \quad (5.52)$$

$$\{\hat{\beta}_{k,q}\}_{q=1}^{L_k} = \frac{\mathbf{a}_k^T(\{\hat{\tau}_{k,q}\}_{q=1}^{L_k})\hat{\mathbf{b}}_k}{\mathbf{a}_k^T(\{\hat{\tau}_{k,q}\}_{q=1}^{L_k})\mathbf{a}_k(\{\hat{\tau}_{k,q}\}_{q=1}^{L_k})} \quad (5.53)$$

Since $\mathbf{a}_k^T(\tau_{k,q})\mathbf{a}_k(\tau_{k,q}) = \mathbf{a}_k^T(\mathbf{o})\mathbf{a}_k(\mathbf{o})$ and $|\mathbf{a}_k^T(\tau_{k,q})\hat{\mathbf{b}}_k|^2$ is non-negative, the L_k -dimensional search problem in Eq.(5.52) can be simplified to L_k independent maximum search in one dimensional with the constraint $\hat{\tau}_{k,s} \neq \hat{\tau}_{k,r}, s, r \in \{1, 2, \dots, L_k\}$.

The maximum of Eq.(5.52) is easy to perform, we first rewrite Eq.(5.52) as

$$\{\hat{\tau}_{k,q}\}_{q=1}^{L_k} = \arg \max_{\{\tau_{k,q}\}_{q=1}^{L_k}} \frac{\sum_{q=1}^{L_k} |\mathbf{a}_k^T(\tau_{k,q})\hat{\mathbf{b}}_k|^2}{\mathbf{a}_k^T(\mathbf{o})\mathbf{a}_k(\mathbf{o})} \quad (5.54)$$

and let

$$W(\tau_{k,q}) = \frac{|\mathbf{a}_k^T(\tau_{k,q})\hat{\mathbf{b}}_k|^2}{\mathbf{a}_k^T(\mathbf{o})\mathbf{a}_k(\mathbf{o})} \quad (5.55)$$

$\{\hat{\tau}_{k,q}\}_{q=1}^{L_k}$ which correspond to the L_k -largest values of $W(\tau_{k,q})$ are the estimations of time delays. The earliest time delay among $\{\hat{\tau}_{k,q}\}_{q=1}^{L_k}$ is the TOA estimation of the user k .

In the real environment, since the exact number of multipath components L_k is unknown,

we need to use some estimation strategies to detect the TOA. X-max criterion proposed in [32] is based on the selection of the earliest $\hat{\tau}_{k,q}$ as the TOA estimation of user k among $\{\hat{\tau}_{k,q}\}_{q=1}^X$ which corresponds to the X largest values of $W(\tau_{k,q})$. Simple threshold criterion in [16] is based on comparing the values of $W(\tau_{k,q})$ to a threshold, the first threshold crossing event is taken as the TOA estimation of the user k . Recently, a new approach based on information theoretic criterion is proposed in [113] [114], this new blind estimation has no requirement of channel information or predefined threshold. In this thesis, we employ the X-max criterion to detect the first path due to its comparative low complexity.

Note that DEMA and DEMR algorithm cannot perform a TOA estimate until $M \geq 2K$ for the existence of $\mathbf{R}_{ss}^{-1}(M)$ [112].

Compared with DEMA algorithm, DEMR algorithm employs an IDF as the front-end to reduce the sampling rate from at least Nyquist rate to chip rate and simplifies the receiver structure. The fractional part of time delay is removed furthermore due to the integer approximation of time delays, which also reduce the complexity of receiver since the nonlinear optimization procedure is not needed anymore. The integral approximation of time delay also brings another simplification in multipath channel. In multipath channel, DEMA algorithm has quite high computational complexity. Oppositely, DEMR algorithm is extended into multipath smoothly due to the long repetition time of UWB pulse and integer approximation of time delay. Searching over a multi-dimensional parameter space problem is simplified to a set of one-dimensional (1-D) problems, which has almost the same complexity as in AWGN channel condition. Although reducing complexity considerably, we show that DEMR estimator is quite near-far resistant and can obtain noticeable performance in fully-loaded system in the dense multipath channel in the following numerical evaluation section.

On the above, the simplification of computational complexity is only analyzed qualitatively. Here, a quantitative analysis is given to show the improvement intuitively. In [112], DEMA algorithm only analyzes the computational complexity with rectangular pulse in the AWGN channel condition, which is $O(K^3 + K^2M + K^2NN_cV + KMNN_cV + K(NN_c)^2V^2)$. With band limited pulse such as raised cosine pulse, additional nonlinear optimization procedure is needed to estimate the fractional part of time delay of τ_k with the scaling of t_s . If we use a simple nonlinear optimization algorithm which firstly divides t_s into L parts evenly, then calculate the cost function Eq.(5.34) with the each possible p_k , finally chose p_k and $\mu_k = l/L$ where $l \in 1, 2, \dots, L$ corresponding to the largest value of cost function Eq.(5.34). Hence, the complexity raises to $O(K^3 + K^2M + K^2NN_cV + KMNN_cV + K(NN_c)^2V^2L)$ in this case. Here, we only discuss the simplest nonlinear optimization algorithm. If other complex algorithm is used, the computational complexity will increase further. For our DEMR algorithm, the computational complexity is only $O(K^3 + K^2M + K^2NN_c + KMNN_c + K(NN_c)^2)$ for all kinds

of pulses due to no need of oversampling and fractional part estimation.

In the multipath channel condition, according to Eq.(5.30), a series of K different $3L_k$ -dimensional search problems is needed to obtain the estimation $\tau_{k,q}$ and $\beta_{k,q}$. We assume that the number of possible values of both real part and imaginary part of $\beta_{k,q}$ is X and the number of possible values of $\tau_{k,q}$ is Y . Hence, the computational complexity increases dramatically to $O(K^3 + K^2M + K^2NN_cV + KMNN_cV + \sum_{k=1}^{k=K} X^{2L_k} \frac{Y!}{(Y-L_k)!L_k!})$. However, for DEMR algorithm, the computational complexity is still $O(K^3 + K^2M + K^2NN_c + KMNN_c + K(NN_c)^2)$ for dense multipath channel since the 3 differences from DEMA algorithm: 1) the use of IDF results no need for oversampling; 2) the integral approximation of time delay makes the fractional part estimation not needed; 3) the long repetition time of pulse and the integral approximation of time delay lead to a reasonable white noise like assumption of spreading code.

From the quantitative analysis, our DEMR algorithm can indeed reduce the complexity substantially, especially in the dense multipath channel condition. Besides the TOA estimation, DEMR algorithm can also derive the amplitude estimation $\hat{\beta}_{k,q}$ in Eq.(5.53) for $\beta_{k,q}$.

The above analysis shows that DEMR algorithm can decoupled multiuser and multipath in DS-UWB ranging systems. In the following we show that DEMR algorithm is also efficient in TH-UWB systems.

The transmitted signals of the k th user in TH-UWB systems with time hopping sequences as spreading sequence can be expressed as

$$s_k(t) = \sqrt{P_k} \sum_{m=0}^{M-1} d_k(m) \sum_{n=0}^{N-1} p(t - u_k(n)T_c - nT_f - mT_b) \quad (5.56)$$

where $u_k(n)$ here is time hopping code distributed in $\{1, 2, \dots, N_h\}$, $N_h \leq N_c$. Other parameters have the same meaning as those in Eq.(5.1). In DS-UWB systems, pulses are always transmitted in the first chip in each frame. Unlike DS-UWB system, time hopping sequences in TH-UWB system determine in which position or chip the pulse is located. Hence, the generation of alternative sequences $g_k(i)$ is different. In TH-UWB system, $g_k(i)$ is within $\{1, 0\}$, where $i \in \{1, 2, \dots, NN_c\}$. If no pulse is sent, $g_k(i) = 0$, otherwise, $g_k(i) = 1$. Hence, transmitted signal $s_k(t)$ is rewritten as

$$s_k(t) = \sqrt{P_k} \sum_{m=0}^{M-1} d_k(m) \sum_{i=0}^{NN_c-1} g_k(i) p(t - iT_c - mT_d) \quad (5.57)$$

The use of $g_k(i)$ allow us to express the transmitted signal $s_k(t)$ in the same format as that in DS-UWB system. In addition, due to the use of $g_k(i)$, the Hamming correlation of TH sequences $u_k(n)$ is equivalent to the common correlation of DS sequences $g_k(i)$. And the value

of correlation function of $g_k(i)$ represents the number of hits. Hence, DEMR algorithm can be simply extended to TH-UWB system.

5.2 SIMPLIFIED LARGER SAMPLING MAXIMUM LIKELIHOOD ALGORITHM

In the last section, DEMR algorithm is introduced as an efficient multiuser ranging algorithm. DEMR algorithm reaches the chip-level ranging accuracy with relatively low complexity. Although DEMR is robust against MUI, the requirement of all the users' data bits and spreading code makes it impractical under some practical condition.

In this section, we present a simplified large sample maximum likelihood (SLSML) algorithm. The LSML algorithm is proposed for solving the multiuser synchronization problem in the DS-CDMA system in AWGN channel [115]. The LSML algorithm is an MF-based algorithm which is also quite against near-far effect even the system is fully loaded. However, the need of high sampling rate is not eased and [115] has not known clearly how to extend it to the multipath channel. Motivated by DEMR algorithm, the SLSML algorithm adopted the IDF with chip integration time rather than MF with Nyquist sampling rate as the receiver front-end to achieve a chip-level ranging. In addition, with the property of a long repetition time of pulse, the SLSML estimator is not only extended to the dense multipath channel, but also is simplified considerably. The multi-dimensional parameter space search problem is also simplified to a one-dimensional problem. Although decreasing the sampling rate and complexity considerably, the SLSML estimator is still quite near-far resistant and efficient in fully loaded system in both AWGN and multipath channel. Comparing with DEMR estimator, the SLSML algorithm reaches almost the same performance only relying on the data bits and spreading sequence of desired user though only time delay and amplitude of desired user are estimated.

In SLSML algorithm, received signal is the same as that in DEMR algorithm in Eq.(5.5). We also assume that the time delay is approximated as the integer multiples of T_c Eq.(5.36). The first user is the user of interest. If the IDF is still employed as the frond-end filter, then, the received sequences can be expressed also as in Eq.(5.37). The received vector $\mathbf{r}(m)$ now is expressed as

$$\begin{aligned}\mathbf{r}(m) &= \sum_{q=1}^{L_1} \beta_{1,q} \mathbf{A}_1(\tau_{1,q}) \mathbf{z}_1(m) + \mathbf{e}(m) \\ &= \mathbf{B}(\beta_{1,q}, \tau_{1,q}) \mathbf{z}_1(m) + \mathbf{e}(m).\end{aligned}\tag{5.58}$$

with

$$\mathbf{B}(\beta_{1,q}, \tau_{1,q}) = \sum_{q=1}^{L_1} \beta_{1,q} \mathbf{A}_1(\tau_{1,q}) \quad (5.59)$$

Here, \mathbf{B} only contains the time delays and amplitude information of the first user but not all the users. The noise and MUI are all included into an unstructured term $\mathbf{e}(m)$. The LSML algorithm is derived by modeling $\mathbf{e}(m)$ as a circularly symmetric complex Gaussian noise with zero-mean and unknown covariance matrix \mathbf{Q} that satisfies

$$E[\mathbf{e}(m_i)\mathbf{e}^H(m_j)] = \mathbf{Q}\delta_{i,j} \quad (5.60)$$

where $\delta_{i,j}$ denotes the Kronecker delta [115]. We assume that the spreading sequence and the data bits of the user of interest is known to both the transmitter and receiver.

Considering the received vector above, the Maximum Likelihood estimation criterion gives:

$$\{\hat{\beta}_{1,q}, \hat{\tau}_{1,q}\}_{q=1}^{L_1} = \arg \max_{\{\beta_{1,q}, \tau_{1,q}\}_{q=1}^{L_1}} \{-\ln|\mathbf{Q}| - \text{tr}\{\mathbf{Q}^{-1} \frac{1}{M} \sum_{m=0}^{M-1} [\mathbf{r}(m) - \mathbf{B}(\beta_{1,q}, \tau_{1,q})\mathbf{z}_1(m)] [\mathbf{r}(m) - \mathbf{B}(\beta_{1,q}, \tau_{1,q})\mathbf{z}_1(m)]^H\}\} \quad (5.61)$$

where $|\cdot|$ denotes the determinant of a matrix. According to [115], Eq.(5.61) is maximized by

$$\hat{\mathbf{Q}} = \sum_{m=0}^{M-1} [\mathbf{r}(m) - \hat{\mathbf{B}}(\beta_{1,q}, \tau_{1,q})\mathbf{z}_1(m)][\mathbf{r}(m) - \hat{\mathbf{B}}(\beta_{1,q}, \tau_{1,q})\mathbf{z}_1(m)]^H \quad (5.62)$$

and $\hat{\mathbf{B}}$ may be obtained by minimizing the following cost function

$$\mathbf{F} = \left| \sum_{m=0}^{M-1} [\mathbf{r}(m) - \mathbf{B}(\beta_{1,q}, \tau_{1,q})\mathbf{z}_1(m)][\mathbf{r}(m) - \mathbf{B}(\beta_{1,q}, \tau_{1,q})\mathbf{z}_1(m)]^H \right| \quad (5.63)$$

Minimizing the cost function \mathbf{F} gives an unstructured estimation $\hat{\mathbf{B}}$ of \mathbf{B} [115]

$$\hat{\mathbf{B}} = \mathbf{R}_{\mathbf{z}_1\mathbf{r}}^H \mathbf{R}_{\mathbf{z}_1\mathbf{z}_1}^{-1} \quad (5.64)$$

where

$$\mathbf{R}_{\mathbf{z}_1\mathbf{r}} = \frac{1}{M} \sum_{m=0}^{M-1} \mathbf{z}_1(m)\mathbf{r}^H(m), \quad (5.65)$$

and

$$\mathbf{R}_{\mathbf{z}_1} = \frac{1}{M} \sum_{m=0}^{M-1} \mathbf{z}_1(m) \mathbf{z}_1^H(m), \quad (5.66)$$

By substituting Eq.(5.64) into Eq.(5.62), $\hat{\mathbf{Q}}$ is rewritten as

$$\hat{\mathbf{Q}} = \mathbf{R}_{\mathbf{r}} - \mathbf{R}_{\mathbf{z}_1}^H \mathbf{R}_{\mathbf{z}_1}^{-1} \mathbf{R}_{\mathbf{z}_1} \quad (5.67)$$

where

$$\mathbf{R}_{\mathbf{r}} = \frac{1}{M} \sum_{m=0}^{M-1} \mathbf{r}(m) \mathbf{r}^H(m). \quad (5.68)$$

In [115], It has been shown that minimizing (F) is asymptotically (for large M) equivalent to minimizing

$$\mathbf{F}_2 = \text{tr}[\mathbf{R}_{\mathbf{z}_1} (\mathbf{B} - \hat{\mathbf{B}})^H \hat{\mathbf{Q}}^{-1} (\mathbf{B} - \hat{\mathbf{B}})] \quad (5.69)$$

Since $d_k(m)$ is an independently and identically distributed in $\{\pm 1\}$, $\mathbf{R}_{\mathbf{z}_1}$ is a diagonal matrix with equal diagonal elements. Then, maximizing cost function Eq.(5.61), corresponding to minimizing \mathbf{F}_2 , is equivalent to minimizing

$$\{\hat{\beta}_{1,q}, \hat{\tau}_{1,q}\}_{q=1}^{L_1} = \arg \min_{\{\beta_{1,q}, \tau_{1,q}\}_{q=1}^{L_1}} \text{tr}\{[\mathbf{B}(\beta_{1,q}, \tau_{1,q}) - \hat{\mathbf{B}}]^H \hat{\mathbf{Q}}^{-1} [\mathbf{B}(\beta_{1,q}, \tau_{1,q}) - \hat{\mathbf{B}}]\}. \quad (5.70)$$

if substituting Eq.(5.59) into Eq.(5.70), Eq.(5.70) is rewritten as

$$\{\hat{\beta}_{1,q}, \hat{\tau}_{1,q}\}_{q=1}^{L_1} = \arg \min_{\{\beta_{1,q}\}_{q=1}^{L_1}, \{\tau_{1,q}\}_{q=1}^{L_1}} \left\| \sum_{q=1}^{L_1} \beta_{1,q} \mathbf{Q}^{-1/2} \mathbf{A}_1(\tau_{1,q}) - \mathbf{Q}^{-1/2} \hat{\mathbf{B}} \right\|_F^2 \quad (5.71)$$

where $\|\cdot\|_F$ is the Frobenius norm. By minimizing the above function, we can obtain the estimation $\{\hat{\beta}_{1,q}, \hat{\tau}_{1,q}\}_{q=1}^{L_1}$ of $\{\beta_{1,q}, \tau_{1,q}\}_{q=1}^{L_1}$.

In AWGN channel, $L_1 = 1$, we can get

$$\hat{\tau}_1 = \arg \max_{\tau_1} \frac{|\mathbf{a}_1^T(\tau_1) \mathbf{b}|^2}{\mathbf{a}_1^T(\tau_1) \mathbf{a}_1(\tau_1)}, \quad (5.72)$$

$$\hat{\beta}_1 = \frac{\mathbf{a}_1^T(\tau_1) \mathbf{b}}{\mathbf{a}_1^T(\tau_1) \mathbf{a}_1(\tau_1)}. \quad (5.73)$$

in which

$$\mathbf{a}_1(\tau_1) = \text{vec}[\hat{\mathbf{Q}}^{-1/2} \mathbf{A}_1(\tau_1)] \quad (5.74)$$

$$\mathbf{b} = \text{vec}[\hat{\mathbf{Q}}^{-1/2} \hat{\mathbf{B}}] \quad (5.75)$$

where $\text{vec}[\cdot]$ also represents stacking the columns of a matrix on top of one another.

In the multipath channel, Eq.(5.71) requires the $3L_1$ -dimensional search over parameter space to get the time delay and amplitude estimation. But due to a long repetition time of a UWB pulse and the integer delay approximation, the SLSML algorithm simplifies the $3L_1$ -dimensional search problem into the L_1 maximums search problems in one dimension as in DEMR algorithm.

If we let

$$\mathbf{a}_1(\tau_{1,q}) = \text{vec}[\hat{\mathbf{Q}}^{-1/2} \mathbf{A}_1(\tau_{1,q})] \quad (5.76)$$

and rewrite the $\mathbf{a}_1(\tau_{1,q})$ as

$$\mathbf{a}_1(\tau_{1,q}) = \begin{bmatrix} \hat{\mathbf{Q}}^{-1/2} \mathbf{P}_1(p_{1,q}) \mathbf{c}_1 \\ \hat{\mathbf{Q}}^{-1/2} \mathbf{P}_2(p_{1,q}) \mathbf{c}_1 \end{bmatrix}, \quad (5.77)$$

then, we can find that $\mathbf{a}_1(\tau_{1,q})$ can be seen as a set of codes corresponding to different $\tau_{1,q}$, which is also referred to as the stacked code due to the way of generation. In DEMR algorithm the stacked codes $\mathbf{a}_k(\tau_{k,q})$ are the cyclic shift of $\mathbf{a}_k(o)$, but in SLSML algorithm, this cyclic shift relationship is not existed because of the presence of $\hat{\mathbf{Q}}^{-1/2}$. Since the "o" inserted property of u_i , \mathbf{c}_1 and the stacked code $\mathbf{a}_1(\tau_{1,q})$ also has this "o" inserted correlation property, which mean the autocorrelation and cross-correlation function of the $\mathbf{a}_1(\tau_{1,q})$ are also inserted $N_c - 1$ "o" between each non-zero elements. Since in DEMR algorithm, $\mathbf{a}_k(\tau_{k,q})$ are the cyclic shift of $\mathbf{a}_k(o)$, the interference of other paths corresponding to the side lobe of autocorrelation function of $\mathbf{a}_k(\tau_{k,q})$. However, in SLSML algorithm, this relationship is not existed. The interference of other paths should be considered as the cross-correlation function of the set of code $\mathbf{a}_1(\tau_{1,q})$ since $\mathbf{a}_1(\tau_{1,q})$ is different according to different $\tau_{1,q}$.

If we also assume that the multipath delay spread is much smaller than $NN_c T_c$ and we also ignore $\mathbf{a}_1^T(\tau_{1,s}) \mathbf{a}_1(\tau_{1,r})$, which is equivalent to assuming $\mathbf{a}_1^T(\tau_{1,s}) \mathbf{a}_1(\tau_{1,r}) = o$ when $s \neq r$, $s, r \in \{1, 2, \dots, L_1\}$. In this way, $\mathbf{a}_1(\tau_{1,q})$ also has a white noise correlation property.

With this white noise like correlation property, minimizing the cost function Eq.(5.71) is

equivalent to

$$\{\hat{\tau}_{1,q}\}_{q=1}^{L_1} = \arg \max_{\{\tau_{k,q}\}_{q=1}^{L_1}} \sum_{q=1}^{L_1} \frac{|\mathbf{a}_1^T(\tau_{1,q})\tilde{\mathbf{b}}_1|^2}{\mathbf{a}_1^T(\tau_{1,q})\mathbf{a}_1(\tau_{1,q})} \quad (5.78)$$

$$\{\hat{\beta}_{1,q}\}_{q=1}^{L_1} = \frac{\mathbf{a}_1^T(\{\hat{\tau}_{1,q}\}_{q=1}^{L_1})\tilde{\mathbf{b}}_1}{\mathbf{a}_1^T(\{\hat{\tau}_{1,q}\}_{q=1}^{L_1})\mathbf{a}_1(\{\hat{\tau}_{1,q}\}_{q=1}^{L_1})} \quad (5.79)$$

Since $|\mathbf{a}_1^T(\tau_{1,q})\tilde{\mathbf{b}}_1|^2$ and $\mathbf{a}_1^T(\tau_{1,q})\mathbf{a}_1(\tau_{1,q})$ are non-negative, $\{\hat{\tau}_{1,q}\}_{q=1}^{L_1}$ is obtained by the L_1 independent maximums search in one dimensional rather than the $3L_1$ -dimensional search problem, with the constraint $\hat{\tau}_{1,s} \neq \hat{\tau}_{1,r}$, $s, r \in \{1, 2, \dots, L_1\}$. To obtain the TOA estimation, we firstly let

$$W(\tau_{1,q}) = \frac{|\mathbf{a}_1^T(\tau_{1,q})\tilde{\mathbf{b}}_1|^2}{\mathbf{a}_1^T(\tau_{1,q})\mathbf{a}_1(\tau_{1,q})} \quad (5.80)$$

$\{\hat{\tau}_{1,q}\}_{q=1}^{L_1}$ corresponding to the L_1 -largest values of $R(\tau_{1,q})$ are the time delays estimation. The earliest among $\{\hat{\tau}_{1,q}\}_{q=1}^{L_1}$ is the first path delay, then the TOA estimation of user one. Consequently, the estimation $\hat{\beta}_{1,1}$ of $\beta_{1,1}$ can be obtained.

As in DEMR algorithm, the X-max criterion is chosen to detect the TOA due to its relatively low complexity when the exact number of L_1 is not known. And the SLSML algorithm requires $M \geq NN_c$ since $\mathbf{R}_{\mathbf{r}\mathbf{r}}$ must be full rank in order to form \mathbf{Q}^{-1} [115].

SLSML algorithm simplified the LSML algorithm by using IDF instead of MF as the received filter and approximating the time delay as the integer multiples of chip duration T_c . As a result, the sampling rate and fractional delay estimation part are not required anymore. Moreover, this approximation also leads to a considerable reduction of computational complexity in multipath channel. Although SLSML is more simplified than LSML algorithm, SLSML algorithm is also quite near-far resistant and allows the ranging system to be fully-loaded. Comparing with DEMR algorithm, SLSML algorithm only requires the data bits and spreading sequence of desired users not all the users' as in DEMR algorithm. However, SLSML algorithm can only estimate the time delay and amplitude of the user of interest not all the K users simultaneously as in DEMR algorithm.

The complexity of SLSML algorithm is also analyzed. In the AWGN channel with single user, LSML algorithm leads to the computational complexity of $O((NN_c)^3V^3 + M(NN_c)^2V^2)$ with rectangular pulse [115]. With band limited pulse, for example raised cosine pulse, the computational complexity becomes $O((NN_c)^3V^3 + M(NN_c)^2V^2 + (NN_c)^3V^3L)$ where L is also the possible number of values of fractional part of time delay μ_k . A K -user time delay estimation with LSML algorithm requires the complexity as $O(K(NN_c)^3V^3 + KM(NN_c)^2V^2)$ and $O(K(NN_c)^3V^3 + KM(NN_c)^2V^2 + K(NN_c)^3V^3L)$ for rectangular pulse and band-limited

pulse, respectively. By contrast, SLSML algorithm only needs $O(K(NN_c)^3 + KM(NN_c)^2)$ complexity for all kinds of pulse due to the use of IDF and time delay approximation in AWGN channel. In multipath channel, since the use of simplification, the computational complexity for SLSML algorithm maintains $O(K(NN_c)^3 + KM(NN_c)^2)$. Hence, SLSML simplifies the LSML algorithm substantially in both AWGN channel and multipath channel, which make the SLSML algorithm more practical.

Like DEMR algorithm, SLSML algorithm can also be extended into TH-UWB ranging system in the same way which we have introduced in the last section.

5.3 NUMERICAL EVALUATION

DEMR and SLSML algorithms are proposed and analyzed in the previous two sections. Due to the integer approximation of time delay and long repetition time of UWB pulse, DEMR and SLSML algorithm reduce the computational complexity considerably even in multipath channel. In this section, the ranging performance of these two algorithms in AWGN channel and dense multipath channel will be given.

Before we give the detailed performance of our proposed algorithms, the theoretical bound is presented firstly to give us a clear expectation how accurate precision can be achieved theoretically. Estimation error bounds play a fundamental role since they serve as a baseline for assessing the performance of a specific algorithm by providing the performance limitation of any estimator in terms of the mean square error (MSE) or root mean square error (RMSE).

5.3.1 THEORETICAL BOUND

Conventionally, non-linear estimation problems such as TOA estimation are analyzed based on the Cramer-Rao inequality in order to obtain bounds on the attainable MSE. Its use is justified by invoking an asymptotic theorem asserting that the ML estimators approaches the Cramer-Rao Lower Bound (CRLB) arbitrarily closely for sufficiently long observation times or for high signal-to-noise ratios (SNR) [16]. In addition, it is well-known that non-linear estimation suffers from the ambiguity effect, which is not accounted for by the CRLB [13]. For example, the correlator output as a typical ML estimator presents adjacent peaks with approximately equal height which arouses ambiguity. The reliable identification of the first peak requires either exceedingly long observation time or very large SNR. Therefore, in many practical situation, the performance of ML or any other estimation algorithm may be drastically inferior to that predicted by the CRLB.

In theoretical analysis, if we consider the received signal $r(t)$ as

$$r(t) = \sqrt{E_p}p(t - \tau) + n(t) \quad (5.81)$$

where E_p represents the average received energy, $n(t)$ is additive white Gaussian noise with zero mean and two-sided power spectral density $N_o/2$, τ is the TOA needed to be estimated. Under this model, TOA estimation is a classical nonlinear parameter estimation problem. With the MF receiver, the received signal is first processed by a filter matched to the pulse $p(t)$ (or, equivalently, by a correlator with template $p(t)$). TOA estimate is given by the time instant corresponding to the maximum absolute peak at the output of the MF over the observation interval. This yields a ML estimate, which is known to asymptotically achieve the CRLB.

It is well-known from the estimation theory that the MSE of any unbiased estimate $\hat{\tau}$ of τ is bounded by the CRLB [13], as following

$$\mathbf{Var}(\varepsilon^2) = \mathbf{E}(\hat{\tau} - \tau)^2 \geq \mathbf{CRLB} \quad (5.82)$$

where $\varepsilon = \hat{\tau} - \tau$ is the estimation error and $\mathbf{E}\{\cdot\}$ denotes the statistical expectation. In the ideal case of AWGN channel, CRLB reduces to the well-known expression

$$\mathbf{CRLB} = \frac{N_o/2}{(2\pi)^2 E_p \beta^2} = \frac{1}{8\pi^2 \beta^2 \text{SNR}} \quad (5.83)$$

where $\text{SNR} = E_p/N_o$, and the parameter β^2 represents the second moment of the spectrum $P(f)$ of $p(t)$, that is given in Eq.(2.4).

Note that the CRLB decreases with both SNR and the constant β^2 which depends on the shape of pulse. This reveals that signals with high power and wide transmission bandwidth are beneficial for ranging.

5.3.2 PERFORMANCE OF DEMR ALGORITHM

A. PERFORMANCE OF DEMR ALGORITHM IN DS-UWB RANGING SYSTEMS

We first consider the DS-UWB ranging systems. In the transmitter side, each user is assigned a Gold sequence of length $N = 31$. In the following, TOA of the first user is evaluated with transmitted power $P_1 = 1$ with no loss of generality. All interfering users are given a random received power with a log-normal distribution with a mean d dB above the desired signal and a standard deviation of 10dB. That is $P_k = 10^{\varepsilon_k/10}$, where $\varepsilon_k \sim N(d, 100)$. The near-far ratio is defined as the ratio of the mean of the random powers of the interfering users to that of the

desired user. Hence, the near-far ratio is d in decibels. SNR is defined to be E_b/N_o , where E_b is energy per bit for the first user. The pulse $p(t)$ is raised cosine pulse with roll-off factor $\beta = 0.6$, pulse and chip duration are set equal to 1ns, i.e., $T_c = T_p = 1ns$, and $N_c = 16$. Time delays of channel are uniformly distributed over $[0, 100ns)$, which are the real-valued delays including the fractional part.

Simulations are carried out on both AWGN channel and multipath channel. For the multipath channel, IEEE 802.15.4a channel mode 1 (CM1) which is a typical dense multipath channel for UWB systems is chosen. In CM1 channel, X is chosen to be 3, which is 1 in AWGN channel for the X -max criterion. The results below are based on 500 Monte-Carlo trials. In each trial, different user passes through different CM1 channel realization. Performance is presented by root mean square error (RMSE) of TOA estimation.

Fig.5.3.1 depicts the ranging performance of MF-based DEMA and IDF-based DEMR algorithms with the single user in AWGN channel. Since we transmit the band-limited pulse, the nonlinear optimization is employed to estimate fractional delay in DEMA estimator. We choose the simplest optimization described in the Chapter 5.1.3. In addition, CRLB is also presented. Note that due to the different definition of SNR, there is a $10\log_{10}(N) \approx 15$ dB shift of CRLB compared to that obtaining from eq.(5.81). As shown in the Fig.5.3.1, although MF-based DEMA estimator can reach CRLB with over-Nyquist sampling rate, it performs much worse than IDF-based DEMR estimator at the chip sampling rate. In the medium and high SNR region, the IDF-based DEMR estimator exhibits a floor equal to $T_c/\sqrt{12} \approx 0.2887ns$ which is the quantization floor since we have estimated the integer part of TOA $p_{k,q}$ but ignored the fractional part. Though chip sampling rate limits the accuracy of IDF-based DEMR estimator to $T_c/\sqrt{12}$, its low sampling rate and complexity make it be more practical than MF-based DEMA estimator.

In Fig.5.3.2 and Fig.5.3.3, we compare the ranging performance of DEMR algorithm with DEMA algorithm and the other estimator, namely Nonlinear filter estimator. Nonlinear filter estimator in [29] proposed as a low complexity TOA estimator working at sub-Nyquist sampling rate. It performs nonlinear filtering on the received signal energy to mitigate MUI for ED-based estimator. In our simulation, Nonlinear filter estimator works in chip sampling rate. [29] proposed 2 different nonlinear filters, we employ minimum filter in our simulation since it outperforms the median filter in the presence of severe MUI. Nonlinear filter estimator for DS-UWB system needs a extra burst modulation. In burst modulation, a symbol interval is equal to two data bit duration, each half of symbol interval is called *burst*. $s_k(t)$ is transmitted either in the first or the second half in a pseudorandom pattern depending on the data bit. In Fig.2, DEMA estimator is implemented at both chip-rate sampling and Nyquist sampling rate

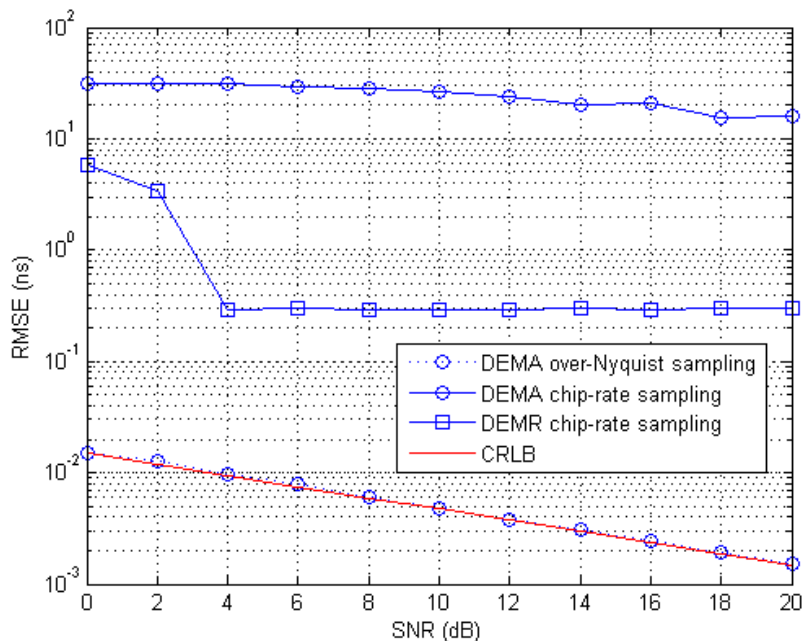


Figure 5.3.1: RMSE of DEMR algorithm in DS-UWB system as a function of SNR in an AWGN channel with $T_a = 100ns$.

which is equal to 8 times the chip sampling rate in our simulation.

RMSE as the function of near-far ratio in AWGN channel with $k = 10$ users ($k = 2$ users for Nonlinear filter estimator) is shown in Fig.5.3.2. We can find that DEMA algorithm obtains a very precise TOA estimation with Nyquist sampling rate, RMSE of which approaches to $0.0380ns$. However, performance degrades sharply to about $13ns$ in the case of chip sampling rate even with smallest near-far ratio. This severe degradation is due to the use of MF-based estimator at sub-Nyquist sampling rate. By contrast, DEMR algorithm reaches noticeable ranging performance in the low chip sampling rate and almost is not influenced by near-far ratio. RMSE of DEMR estimator approaches to $0.2887ns$ which is the theoretical optimal value. As shown in this figure, Nonlinear filter estimator which also works at chip sampling rate has no robustness to near-far ratio. When near-far ratio is up to $10dB$, RMSE soars to $25ns$ even with only 2 users.

In Fig.5.3.3, we show RMSE of DEMA and DEMR algorithm as the function of the number of users in AWGN channel with $10dB$ near-far ratio. We can find that RMSE of DEMR algorithm is around $0.2887ns$ when K increases from 1 to 31, which means DEMR algorithm can achieve almost exact integer part estimation of TOA even with full-loaded system. DEMA

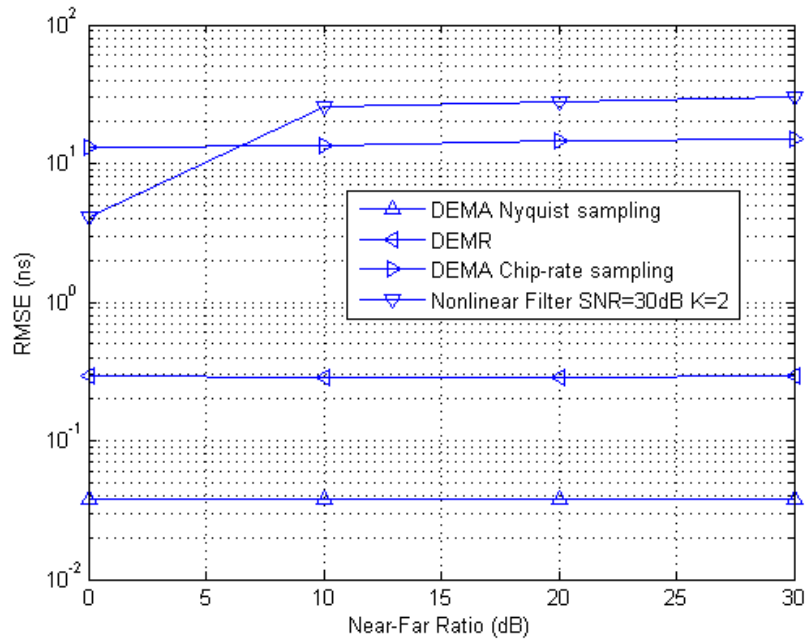


Figure 5.3.2: RMSE versus near-far ratio for different estimators with $M = 100$, $N = 31$, $SNR = 20dB$, $K = 10$ in DS-UWB system in AWGN channel .

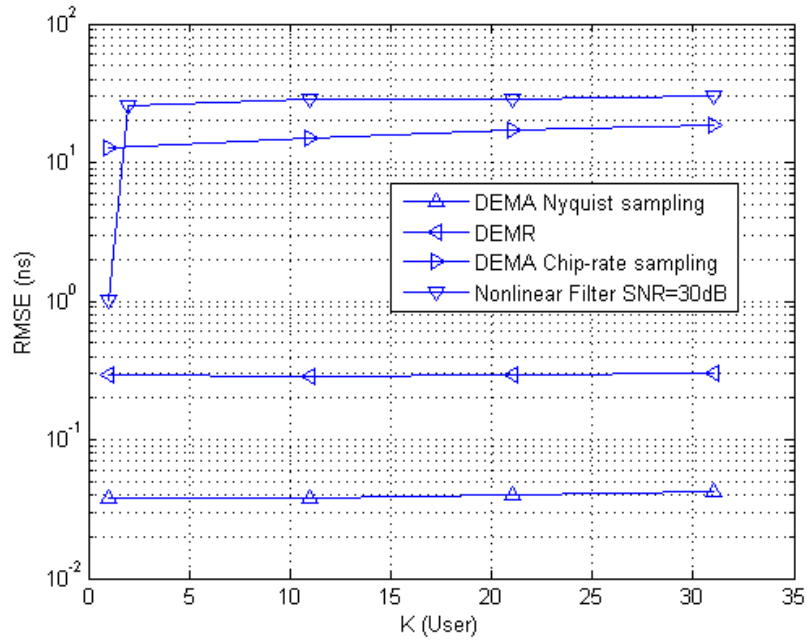


Figure 5.3.3: RMSE versus K for different estimators with $M = 100$, $N = 31$, $SNR = 20dB$ and near-far ratio is 10 dB DS-UWB system in AWGN channel.

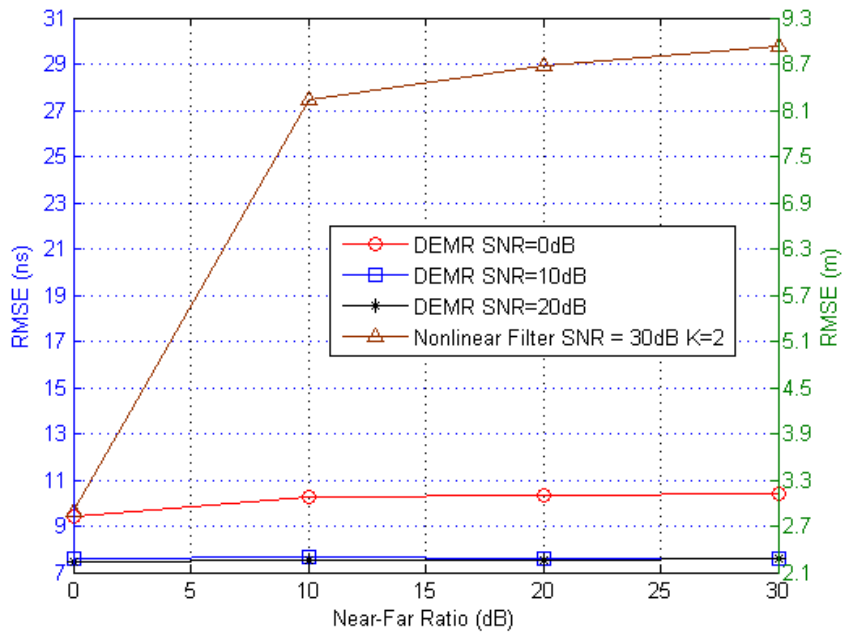


Figure 5.3.4: RMSE versus near-far ratio for different SNR values with $M = 100$, $N = 31$, and $K = 10$ in DS-UWB system CM1 channel.

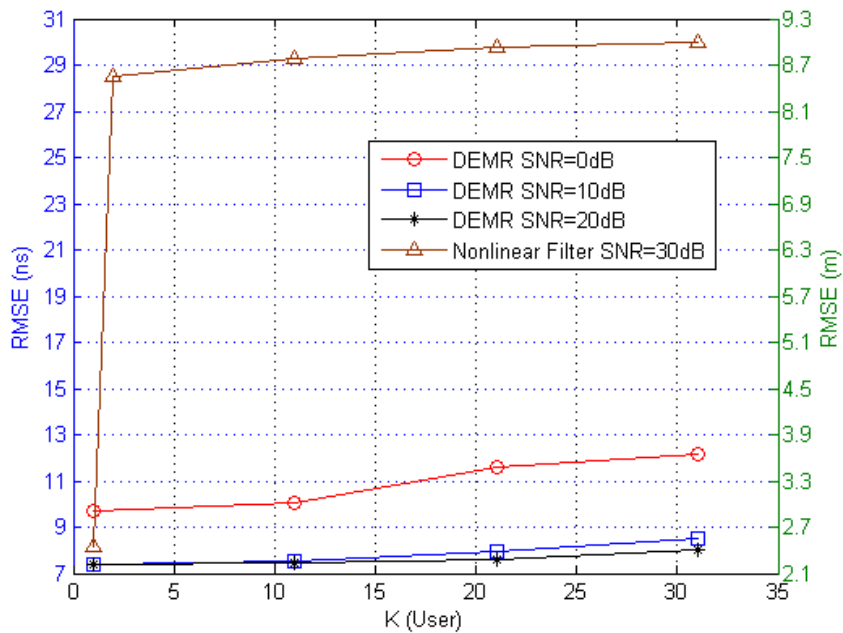


Figure 5.3.5: RMSE versus K for different SNR values with $M = 100$, $N = 31$, and near-far ratio is 10 dB in DS-UWB system CM1 channel.

algorithm in Nyquist sampling rate can also obtain very precious TOA estimation. But in the case of chip-rate sampling, the ranging performance deteriorates to $13ns$ even with only one user. For Nonlinear filter, RMSE increases from about $1ns$ to $25ns$ when K varies from 1 to 2 since Nonlinear filter is not efficient with $10dB$ near-far ratio as shown in Fig.5.3.2.

Since we are more interested in the algorithm with low complexity and low sampling rate and the computational complexity of DEMA algorithm in dense multipath channel is quite high as analyzed before, DEMR algorithm and Nonlinear filter estimator are considered in the simulation in multipath channel. In Fig. 5.3.4, we investigate RMSE of DEMR and Nonlinear filter estimator with respect to near-far ratios for different SNR in CM1 channel. For DEMR algorithm, RMSE increases no more than $1ns$ when near-far ratio grows from $0dB$ to $30dB$ for all the SNR. However, as in AWGN channel, Nonlinear filter cannot resist to near-far ratio even with $SNR = 30dB$. The simulation results show that in the dense multipath channel, near-far problem appears to have little effect on the proposed estimator.

Fig.5.3.5 shows RMSE of DEMR and Nonlinear filter estimator as a function of the number of users K for different SNR in CM1 channel. For DEMR algorithm, RMSE increases within $3ns$ approximately as K varies from 1 to 31 even with severe noise. Especially, for the two higher SNR, the differences are less than $1ns$. This performance is opposed to the significant degradation of Nonlinear filter estimator as K increases. It is shown that the DEMR estimator has capability to support larger number of users with little performance degradation.

B. PERFORMANCE OF DEMR ALGORITHM IN TH-UWB RANGING SYSTEMS

In the TH-UWB system, the simulation conditions are a litter different from that of DS-UWB systems. Each user is assigned a quadratic congruence code (QCC) with $N_h = 13$. Hence, the length of this quadratic congruence code is also $N = 13$. As in the case of DS-UWB system, the first user is the user of interest with transmitted power $P_1 = 1$. The other users are interfering users with a random received power which follows as a log-normal $P_k = 10^{\varepsilon_k/10}$, where $\varepsilon_k \sim N(d, 100)$. The parameter d here also represents the near-far ratio. SNR is defined to be E_b/N_o where $E_b = NE_p$, E_p is the energy of pulse. We still choose the raised cosine pulse with roll-off factor $\beta = 0.6$ as transmitted pulse $p(t)$, pulse and chip duration are equal to $1ns$, i.e., $T_c = T_p = 1ns$. Time delays of channel are uniformly distributed over $[0, T_a)$, $T_a = 100ns$. Note that in the following simulations, time delays are the real-valued delays including the fractional part.

As in DS-UWB systems, simulations are also carried out on both AWGN channel and CM1 channel for evaluating the ranging performance. For X-max criterion, $X = 1$ is used for AWGN channel and $X = 3$ is for CM1 channel. The following results are based on 500 realizations.

Fig.5.3.6 compares DEMA algorithm at both over-Nyquist sampling rate and chip sampling rate and DEMR algorithm with the theoretical bound CRLB in the AWGN channel with only one user. First, due to $SNR = E_b/N_o$, there is about $10\log_{10}(N) \approx 11$ dB shift of CRLB compared with that in eq(5.81). In TH-UWB system, DEMA algorithm with over-Nyquist sampling rate also reaches the CRLB even $SNR = 0dB$. However, the performance decreases dramatically to $13ns$ approximately even with $SNR = 20dB$ with chip-rate sampling. By contrast, DEMR performs quite well with this low sampling rate. When $SNR \geq 4dB$, the ranging performance reaches a floor equal to $T_c/\sqrt{12} \approx 0.2887ns$, which is caused by ignoring the fractional part of time delays. But on another word, reaching this quantization floor presents that DEMR algorithm obtains the exact TOA estimation in chip-level accuracy in the TH-UWB ranging systems.

In the Fig.5.3.7, DEMR algorithm is performed in AWGN channel with respect to near-far ratio with $SNR = 20dB$ and $K = 10$. Note that, since the number of users in TH-UWB systems is limited to $N_h - 1$, $K = 10$ users in the TH system with $N_h = 13$ is quite heavy, almost fully-loaded. As shown in Fig.5.3.7, the performance of DEMR algorithm in TH-UWB system is insensitive to near-far ratio. And the RMSE approaches to the theoretical bound $0.2887ns$. In addition, DEMA algorithm in both Nyquist sampling rate and Chip sampling rate is also evaluated. As already known in DS-UWB systems, DEMA algorithm in Nyquist sampling rate achieves very accurate ranging performance about $0.0360ns$, but when sampling rate increases to chip rate, the ranging performance deteriorates dramatically to over $13ns$. The nonlinear filter with $SNR = 30dB$, $K = 2$ is also shown. When using nonlinear filter in TH-UWB system, the T_a should be no greater than N_h . Therefore, T_a in nonlinear filter is no longer $100ns$ but only $10ns$. However, even with much smaller delay spread and number of users, higher SNR, the RMSE of nonlinear filter is over $5ns$. Through the comparison in Fig.5.3.7, we find that DEMR is quite against near-far effect and achieves an accurate ranging performance even with low sampling rate.

After talking about the influence of near-far effect, the RMSE with respect to the number of users is also given in the Fig.5.3.8. In the case of $SNR = 20dB$, $10dB$ near-far ratio, DEMA algorithm and DEMR algorithm are not impacted by the increase of the number of users K . DEMA algorithm with Nyquist sampling rate and DEMR algorithm approach their optimum values, respectively. DEMA algorithm with sub-Nyquist sampling rate performs over $10ns$ due to using sub-Nyquist sampling rate in MF based receiver. Nonlinear filter with $SNR = 30dB$,

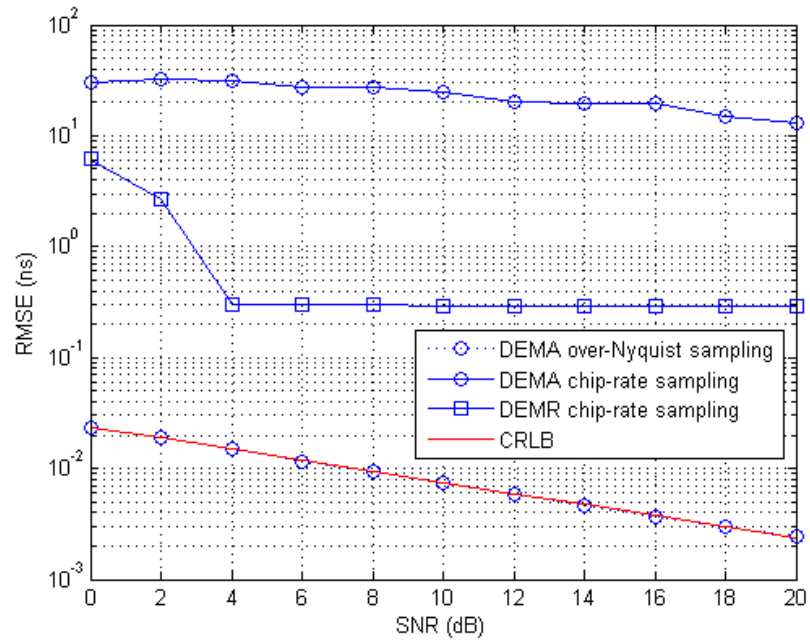


Figure 5.3.6: RMSE of DEMR algorithm in TH-UWB system as a function of SNR in an AWGN channel with $T_a = 100ns$.

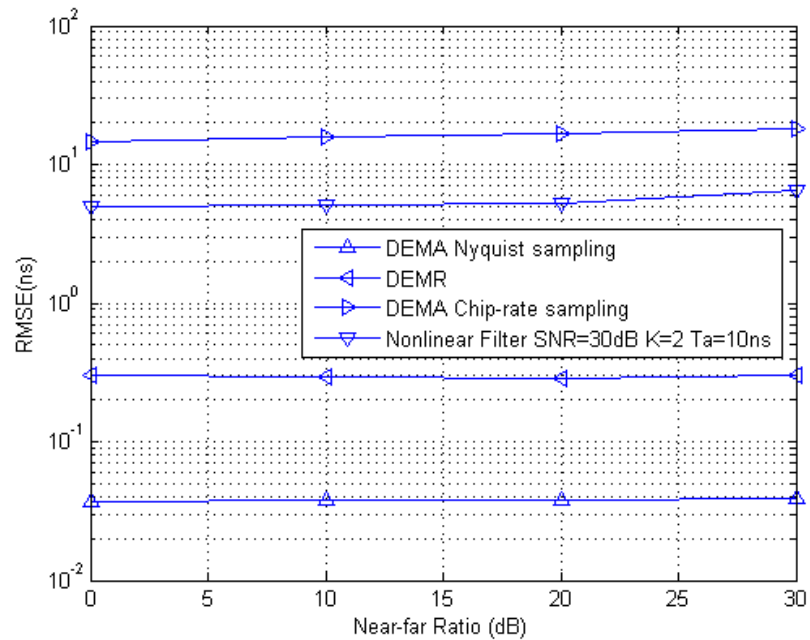


Figure 5.3.7: RMSE versus near-far ratio for different estimators with $M = 100$, $N_h = 13$, $SNR = 20dB$, $K = 10$ in TH-UWB system in AWGN channel.

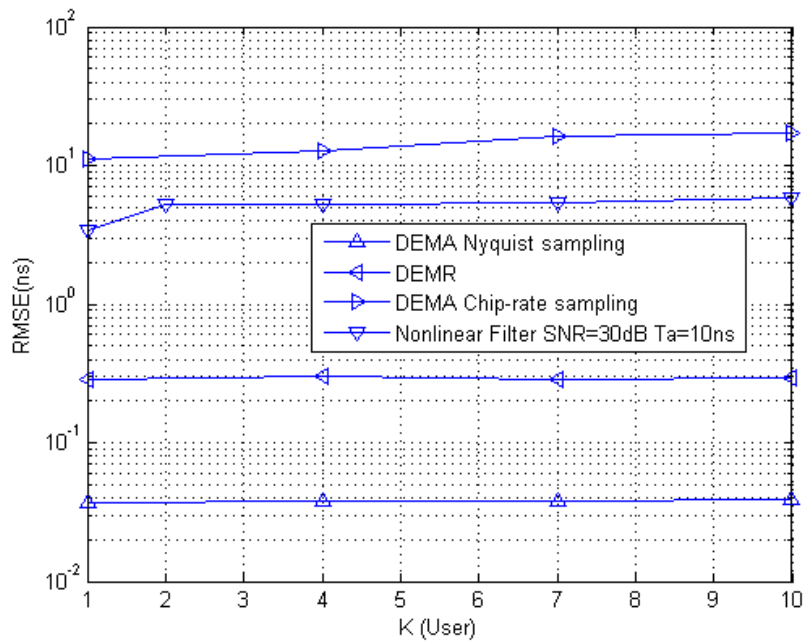


Figure 5.3.8: RMSE versus K for different estimators with $M = 100$, $N - h = 13$, $SNR = 20dB$ and near-far ratio is 10 dB in TH-UWB system in AWGN channel.

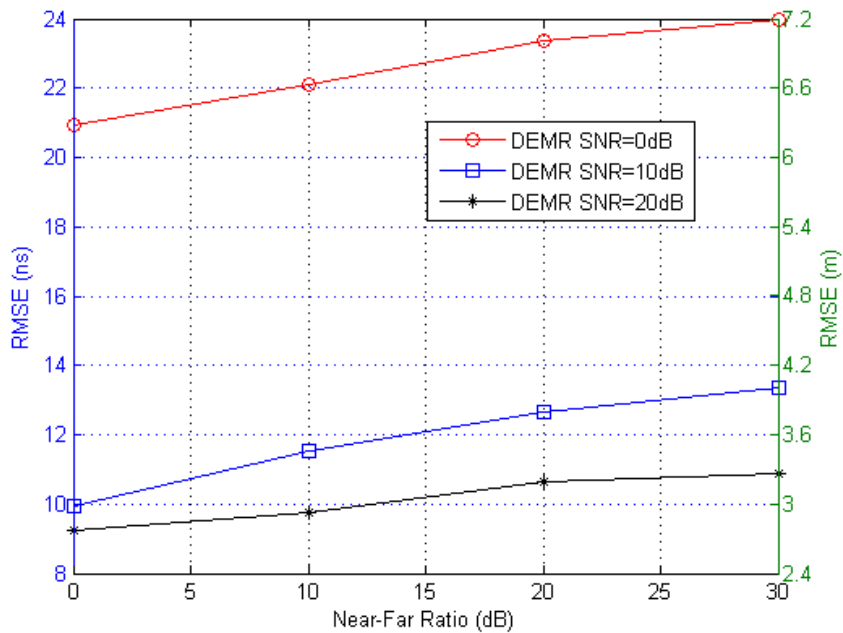


Figure 5.3.9: RMSE versus near-far ratio for different SNR values with $M = 100$, $N_h = 13$, and $K = 10$ in TH-UWB system in CM1 channel.

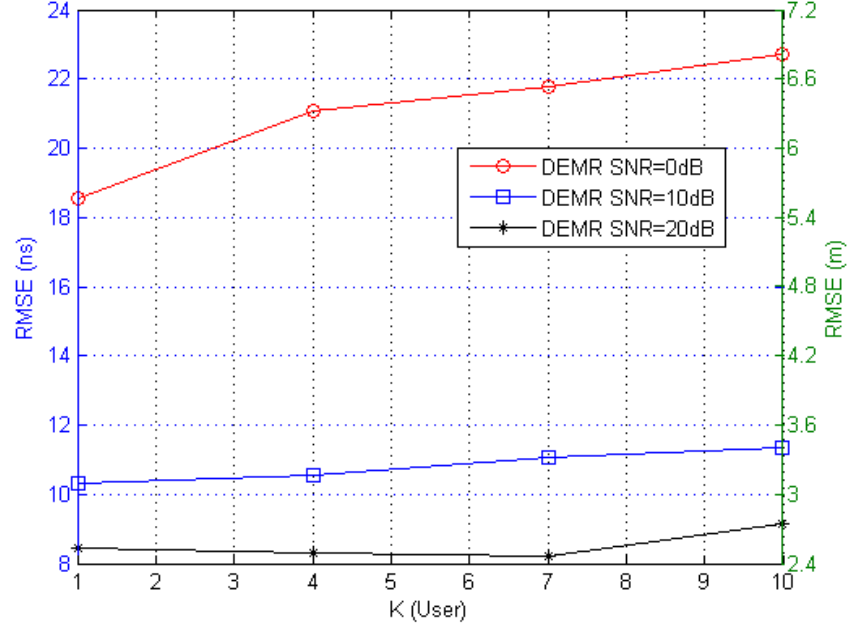


Figure 5.3.10: RMSE versus K for different SNR values with $M = 100$, $N_h = 13$, and near-far ratio is 10 dB in TH-UWB system in CM1 channel.

$T_a = 10ns$ is still sensitive to the increase of K . When K is greater than 2, the RMSE is over $5ns$.

Fig.5.3.9 and Fig.5.3.10 show the DEMR algorithm for TH-UWB system in the CM1 channel condition. The maximum allowed time delays of Nonlinear filter is only $13ns$, which is much smaller than the simulation range $100ns$, and Nonlinear filter in the AWGN channel is sensitive to the increase of the number of users and near-far effect. For this reason we will not consider it in the CM1 channel. In Fig.5.3.9, RMSE is given as the function of near-far ratio with different SNR values. When SNR increasing from $0dB$ to $20dB$, the ranging performance reduces from above $20ns$ to no more than $11ns$. For $SNR = 20dB$, the RMSE grows only $1ns$ when the near-far ratio varies from $0dB$ to $30dB$.

Comparing with DEMR algorithm in DS-UWB system shown in Fig.5.3.4, we can find that DEMR algorithm in TH-UWB system performs a little worse than in DS-UWB system and the difference increases with the decrease of SNR values. For instance, when $SNR = 20dB$, $d = 0dB$, RMSE of DS-UWB is about $7.7ns$ and is $9.7ns$ in TH-UWB system, the difference is $2ns$ approximately. But in the case of $SNR = 0dB$, $d = 0dB$, the difference becomes to about $11ns$. The reason why this happens is concluded as 2 points. First and most importantly, DS-UWB has the "o" inserted signal structure due to using alternative sequences u_k to model the long repetition time of pulse. Therefore, the number of non-zero values of autocorrela-

tion side-lobe value within T_a is only the integral part of T_a/N_c , which is 6 in our simulation. However, in TH-UWB system, there is no such "o" inserted property due to different signal structure. The non-zero side-lobe value occupies the dominant position. Hence, in dense multipath channel with severe noise interference, DEMR algorithm in DS-UWB system outperforms TH-UWB system. Second, in DS-UWB system, up to 33 users can be supported theoretically when $N = 31$. 10 users is about $1/3$ loading. But in TH-UWB systems with $N_h = 13$, 10 users is $5/6$ loading. With such heavy loading, although DEMR approaches the theoretical bound in AWGN channel, the interference brought by the dense multipath channel results in the decrease of ranging performance.

In Fig.5.3.10, RMSE with respect to the number of users K is presented also with different SNR values. We can find that RMSE increases no more than $3ns$ when K changes from 1 to 10 for all the SNR values. Especially, for two higher SNR, the difference is below $2ns$. However, the performance of DEMR algorithm in TH-UWB system is also worse than in DS-UWB system for the reasons analyzed above. Hence, we have the conclusion that although DEMR algorithm is proposed for DS-UWB systems, it can be employed in the TH-UWB system as well. In TH-UWB ranging systems, DEMR algorithm is also resistant to the near-far effect and can support almost fully-loaded users though the ranging performance is a little decrease compared with that in DS-UWB systems due to its signal structure.

5.3.3 PERFORMANCE OF SLSML ALGORITHM

A. PERFORMANCE OF SLSML ALGORITHM IN DS-UWB RANGING SYSTEMS

After discussing the DEMR algorithm, the performance of SLSML algorithm in DS-UWB is given with the same simulation condition as that in DEMR algorithm except for $M = 600$ since the requirement of the number of bits is different from that in DEMR algorithm. And the range of TOA is determined to be $T_a = 30ns$. The comparison between SLSML algorithm and DEMR algorithm is also given to show their own advantages and disadvantages.

Fig.5.3.11 is first given to illustrate that the IDF-based SLSML algorithm can achieve the quantization floor $T_c/\sqrt{(12)} \approx 0.2887ns$ when SNR is greater than $2dB$. Although LSML algorithm with over-Nyquist sampling rate approaches the CRLB, the quite high sampling rate and computational complexity make it impractical in real application environment. Hence, the sub-Nyquist sampling rate and low complexity receiver structure make SLSML algorithm more attractive than the MF based counterpart though estimation precision is also limited to $T_c/\sqrt{12}$.

In the following simulations, SLSML algorithm is compared with DEMR algorithm and

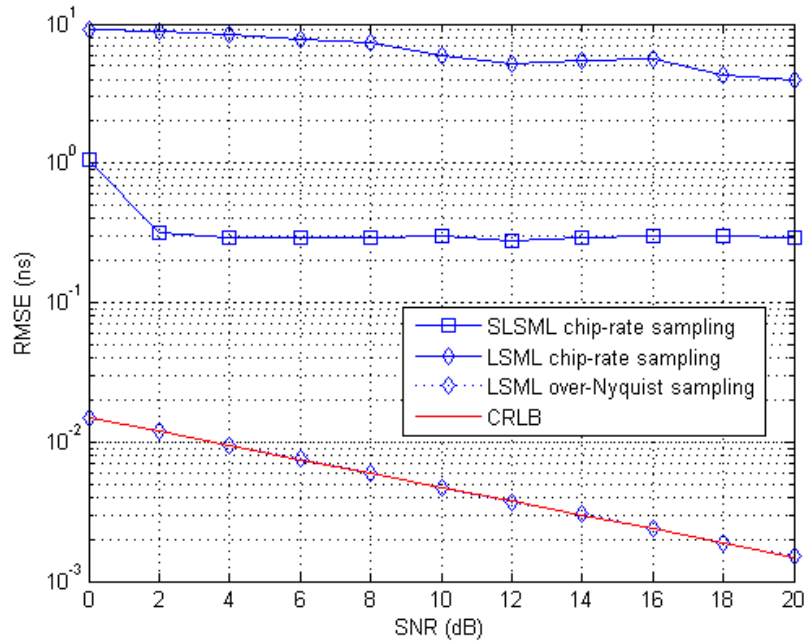


Figure 5.3.11: RMSE of SLSML algorithm as a function of SNR in an AWGN channel with $T_a = 30ns$.

Nonlinear filter estimator. Fig.5.3.12 and Fig.5.3.13 depict RMSE as the function of the near-far ratio and the number of users in AWGN channel, respectively. As shown in Fig.5.3.12 and Fig.5.3.13, the SLSML and DEMR algorithm are not affected by the near-far ratio and the number of users. The two algorithms approach the quantization floor with both $SNR = 10dB$ and $SNR = 20dB$. Although DEMR estimator uses more prior information, it achieves the same ranging performance as SLSML estimator in AWGN channel, which is constrained by the sampling rate. By contrast, Nonlinear filter has no resistance to near-far ratio or the increase of K . When the near-far ratio is equal to $10dB$, RMSE deteriorates over $8ns$ with the $SNR = 30dB$ and 2 users in Fig.5.3.12. In Fig.5.3.13, when $K = 2$, RMSE roars to $8ns$ since Nonlinear filter can not perform properly when the near-far ratio is greater than $10dB$. The performance of LSML algorithm is no longer shown since the similar comparison have been done in the DEMR algorithm whose conclusion can be also extended to LSML algorithm.

In Fig.5.3.14 and Fig.5.3.15, we investigate the ranging performance of the SLSML estimator, DEMR estimator and Nonlinear filter in CM1 channel. RMSE evaluated as a function of the near-far ratio with different SNR is shown in Fig.5.3.14. For the SLSML estimator, RMSE with $30dB$ near-far ratio decreases no more than $0.8ns$ compared with $0dB$ near-far ratio in all

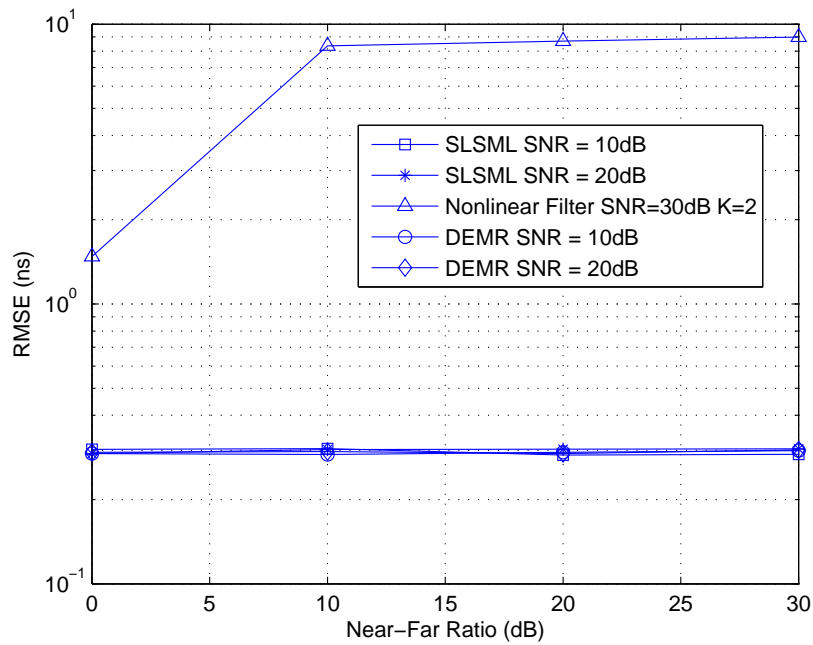


Figure 5.3.12: RMSE versus near-far ratio for different SNR values with $M = 600$, $N = 31$, and $K = 10$ in DS-UWB system in AWGN channel.

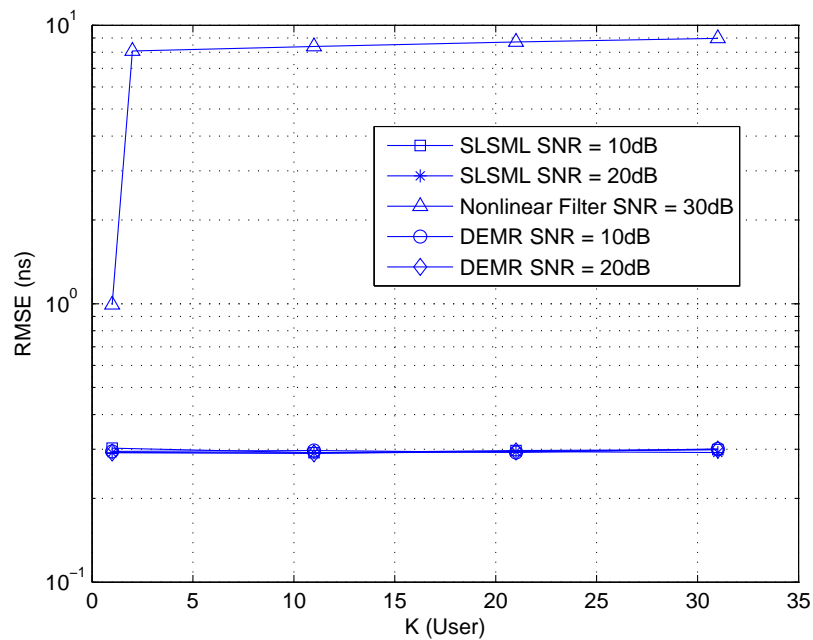


Figure 5.3.13: RMSE versus K for different SNR values with $M = 600$, $N = 31$, and near-far ratio is 10 dB in DS-UWB system in AWGN channel.

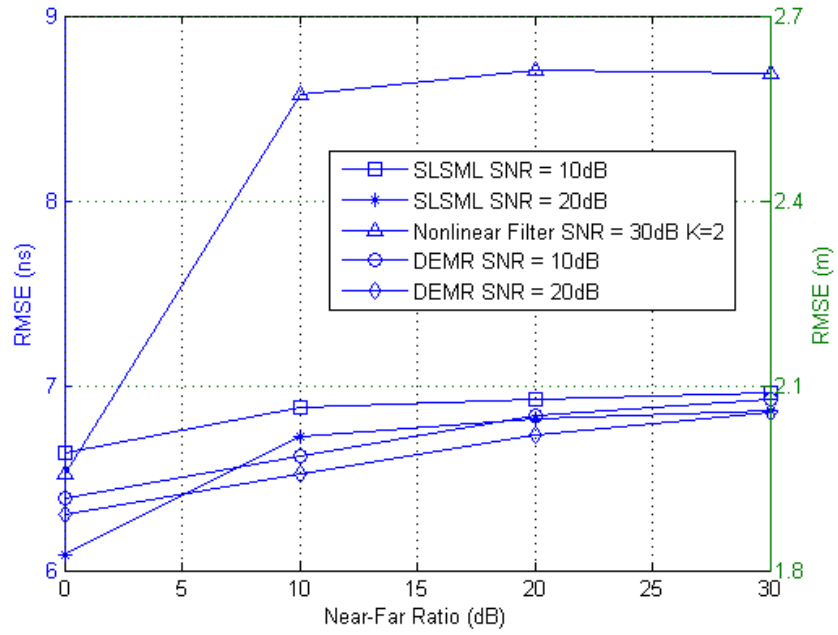


Figure 5.3.14: RMSE versus near-far ratio for different SNR values with $M = 600$, $N = 31$, and $K = 10$ in DS-UWB system in CM1 channel.

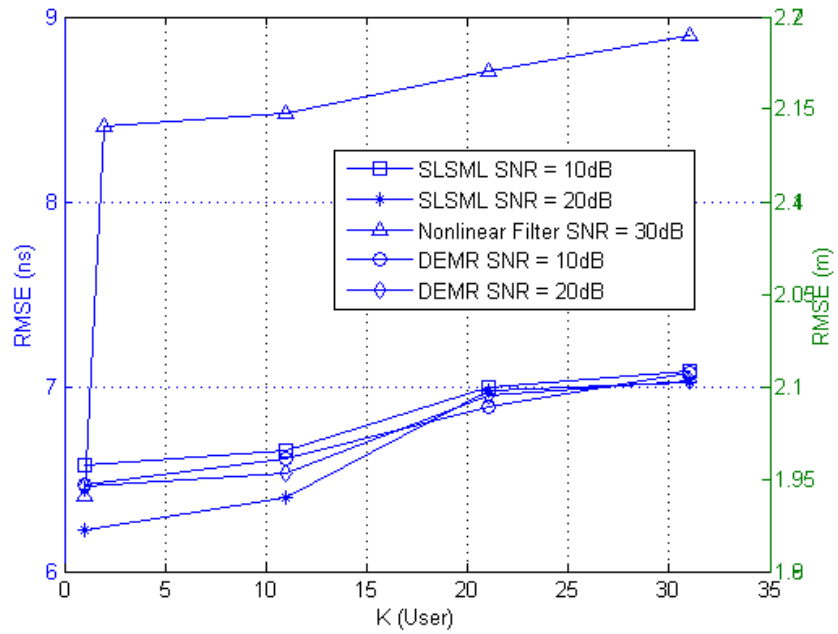


Figure 5.3.15: RMSE versus K for different SNR values with $M = 600$, $N = 31$, and near-far ratio is 10 dB in DS-UWB system in CM1 channel.

the SNR. Hence, it is shown that the proposed estimator has the capability to be the near-far resistant in the multipath channel. By taking the advantage of more prior information, DEMR algorithm performs slightly better than SLSML algorithm. But the difference becomes quite small with the increasing of MUI since the first path detecting error is in the dominated position in the heavy MUI region. However, as in AWGN channel, Nonlinear filter has no robustness to the near-far ratio even with $SNR = 30dB$.

Fig.5.3.15 shows RMSE of the SLSML estimator, DEMR estimator and Nonlinear filter with respect to the number of users with different SNR in CM₁ channel. In both SLSML estimator and DEMR estimator, RMSE grows no more than $1ns$ when K increases from 1 to 31 even with the lower SNR, which is opposed to the sharp decrease of that of Nonlinear filter when K varies. As found in the AWGN channel, the less requirement of prior information has almost no influence on SLSML algorithm when comparing with DEMR algorithm. It is illustrated that the SLSML estimator is little effected by the increase of K even only with the prior information of the user of interest.

B. PERFORMANCE OF SLSML ALGORITHM IN TH-UWB RANGING SYSTEMS

In the following, SLSML algorithm is simulated in the TH-UWB ranging system. The simulation parameters are the same as those in DEMR algorithm. Except time delays of channel is $T_a = 30ns$ and $M = 200$ due to the requirement of SLSML algorithm.

As usual, the performance of SLSML algorithm is first compared with CRLB in AWGN channel with only one user. In addition, LSML algorithm is also shown with both over-Nyquist sampling rate and chip sampling rate. LSML algorithm with over-Nyquist sampling rate reaches the CRLB but decreases sharply when with chip sampling rate since LSML algorithm is based on the matched filter. SLSML algorithm with IDF as the front-end outperforms its counterpart in chip sampling rate. The floor of SLSML algorithm is also the quantization floor which is reached when $SNR \geq 8dB$.

Fig.5.3.17 and Fig.5.3.18 show the SLSML algorithm performance in the AWGN channel with two SNR values as the function of near-far ratio and number of users, respectively. The DEMR algorithm and nonlinear filter are also shown for comparison. In both figures, we notice that SLSML algorithm and DEMR algorithm approach the quantization floor in the case of $SNR = 20dB$ no matter how server near-far ratio is or how large the K is . However, for $SNR = 10dB$, SLSML algorithm does not reach the quantization floor as DEMR algorithm

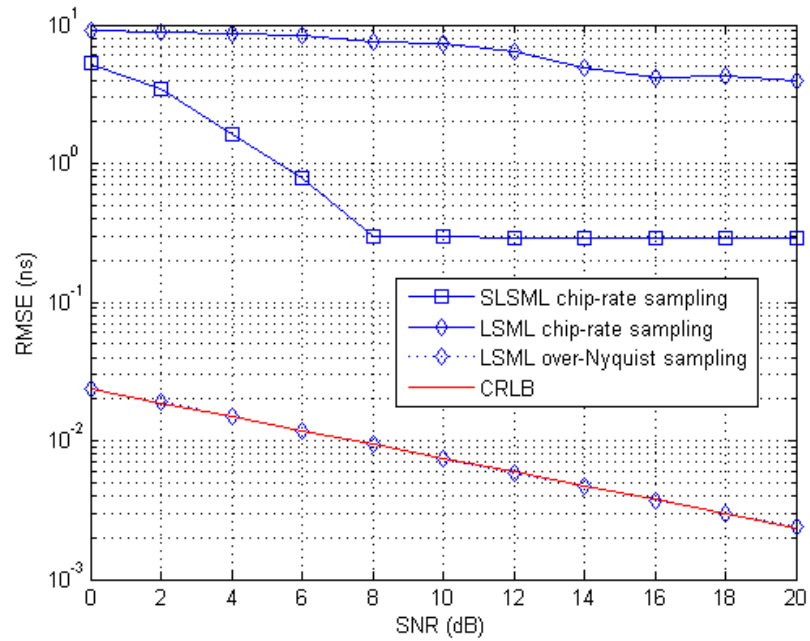


Figure 5.3.16: RMSE of DEMR algorithm in TH-UWB system as a function of SNR in an AWGN channel with $T_a = 30ns$.

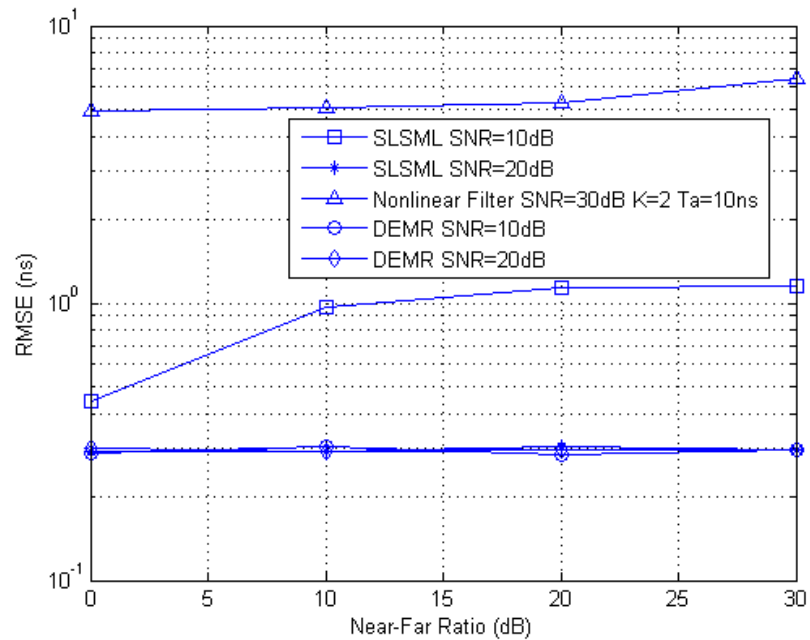


Figure 5.3.17: RMSE versus near-far ratio for different estimators with $M = 200$, $N_h = 13$, $K = 10$ in TH-UWB system in AWGN channel.

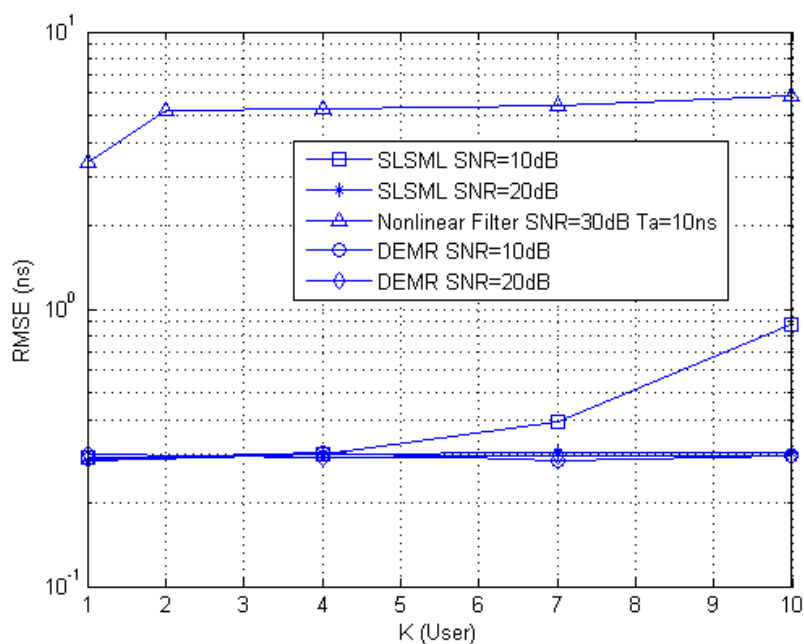


Figure 5.3.18: RMSE versus K for different estimators with $M = 200$, $N - h = 13$, near-far ratio is 10 dB in TH-UWB system in AWGN channel.

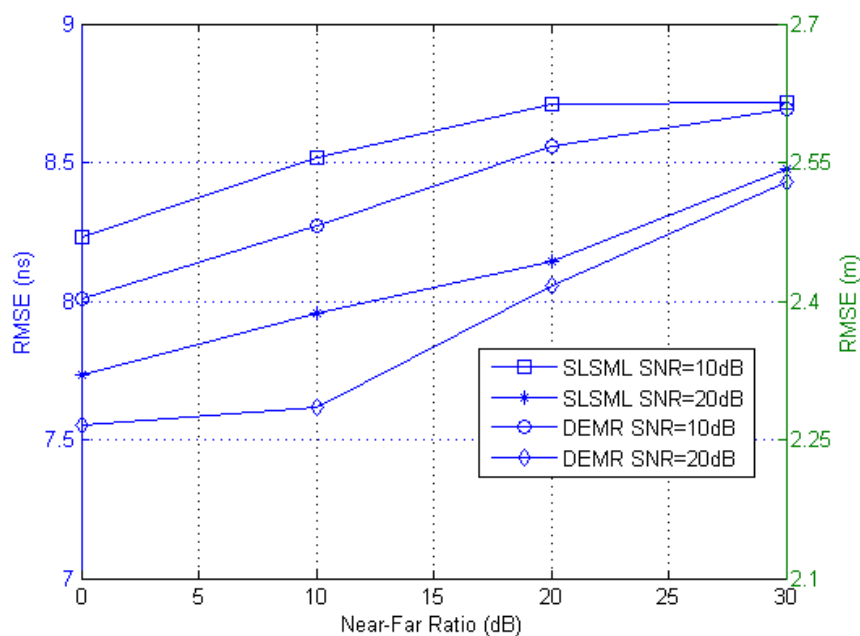


Figure 5.3.19: RMSE versus near-far ratio for different SNR values with $M = 200$, $N_h = 13$, and $K = 10$ in TH-UWB system in CM1 channel.

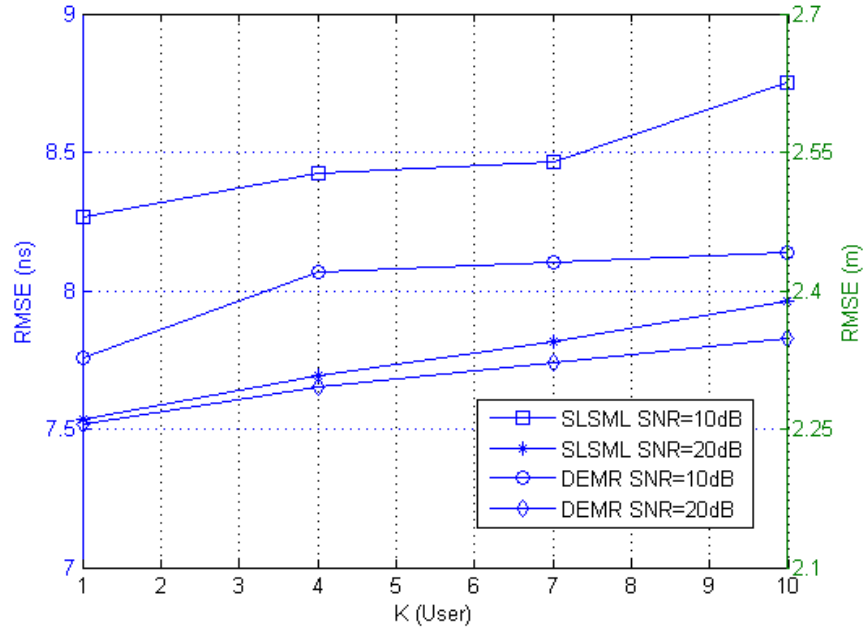


Figure 5.3.20: RMSE versus K for different SNR values with $M = 200$, $N_h = 13$, and near-far ratio is 10 dB in TH-UWB system in CM1 channel.

due to the less known prior information. Compared with SLSML algorithm in the DS-UWB system, the reason why it can not reach the floor is the side-lobe of autocorrelation function caused interference. As discussed previously, since no "o" inserted property in TH-UWB system, side lobes of autocorrelation function plus noise results the deterioration of ranging performance. This problem will be worsen in the case of multipath channel which is given in the following part. By contrast, nonlinear filter have no advantage when compared with both SLSML algorithm or DEMR algorithm even with higher SNR, smaller T_a or smaller K in Fig.5.3.17.

Fig.5.3.19 and Fig.5.3.20 compares the SLSML algorithm with DEMR algorithm as a function of near-far ratio and number of users in CM1 channel with different SNR values, respectively. First of all, we can find that the near-far ration and the increase of number of users have almost no effect on SLSML algorithm. The increase of RMSE caused by these interference is no more than $1ns$. And from these two figures, although DEMR algorithm outperforms SLSML algorithm, the difference between the two algorithm is no more than $1ns$ for all the SNR, which means the lost brought by less prior information of SLSML algorithm is acceptable. Furthermore, if compared with SLSML algorithm in DS-UWB system, the performance in TH-UWB actually decreases due to the different signal structure as mentioned previously.

5.4 CONCLUSION

In this Chapter, DEMR and SLSML algorithms are introduced as the low complexity multiuser TOA estimation algorithms. Due to the use of IDF instead of MF as received filter, DEMR and SLSML algorithms only need the chip sampling rate instead of Nyquist sampling rate. With the integer approximation of time delay and long repetition time of pulse in UWB ranging system, DEMR and SLSML algorithms are simplified furthermore in the dense multipath channel condition. Therefore, DEMR and SLSML algorithms have almost the same computational complexity for both AWGN and multipath channel. Although reducing complexity considerably, DEMR and SLSML algorithm are still quite near-far resistant and can obtain noticeable performance in fully-loaded system in the dense multipath channel which have been shown in the section of performance. Finally, DEMR and SLSML algorithm are also extended into TH-UWB systems.

"Our aspirations are our possibilities."

Robert Browning, Poet

6

Chaos-Based Multiuser TOA Estimator

In the Chapter 5, we propose two low complexity TOA estimation algorithms, referred to as DEMR and SLSML algorithm. DEMR and SLSML algorithm are quite against near-far effect and allow ranging systems to be fully-loaded. However, the use of classic Gold sequences limits the number of users and the further improvement of ranging accuracy. In Chapter 4, we present that the chaotic sequences and waveforms can be used as good alternatives to the classic sequences and waveforms. As analyzed in Chapter 5, the performance of DEMR algorithm depends on the non-cyclic autocorrelation function of spreading sequences, therefore, which can be chosen as the criterion to select sequences. In the side of SLSML algorithm, the ranging performance is determined by not only the spreading sequence but also by covariance matrix of MUI and noise which can not be unknown in prior. As a result, there is not a specific criterion can be used as the criterion to select the chaotic sequences. Hence, in this chapter, we will present the chaotic based DEMR algorithm in which chaotic waveforms and chaotic spreading sequences are used instead of their classic counterparts. In the first section, the use of chaotic binary sequences in DEMR algorithm is introduced, followed by the use of multi-valued chaotic sequences in DEMR algorithm in TH-UWB systems. Finally, the continuous chaotic waveforms are considered and employed in the DEMR algorithm. We can find that chaotic based DEMR algorithm can support not only more users than the system based on classic sequences and waveforms, but is also quite near-far resistant and achieves noticeable

ranging accuracy even in over-loaded system.

6.1 CHAOTIC BINARY CODE BASED DEMR ALGORITHM

In Chapter 5, we can find that TOA and amplitude estimation in DEMR algorithm are simplified to Eq.(5.52) and Eq.(5.53) that are repeated here for convenience.

$$\{\hat{\tau}_{k,q}\}_{q=1}^{L_k} = \arg \max_{\{\tau_{k,q}\}_{q=1}^{L_k}} \sum_{q=1}^{L_k} \frac{|\mathbf{a}_k^T(\tau_{k,q})\hat{\mathbf{b}}_k|^2}{\mathbf{a}_k^T(\tau_{k,q})\mathbf{a}_k(\tau_{k,q})} \quad (6.1)$$

$$\{\hat{\beta}_{k,q}\}_{q=1}^{L_k} = \frac{\mathbf{a}_k^T(\{\hat{\tau}_{k,q}\}_{q=1}^{L_k})\hat{\mathbf{b}}_k}{\mathbf{a}_k^T(\{\hat{\tau}_{k,q}\}_{q=1}^{L_k})\mathbf{a}_k(\{\hat{\tau}_{k,q}\}_{q=1}^{L_k})} \quad (6.2)$$

As shown in the Chapter 5, $\mathbf{a}_k(\tau_{k,q})$ is a cyclic shift of stacked code $\mathbf{a}_k(\circ)$ due to the integer delay approximation $\tau_{k,q} = p_{k,q}T_c$. Therefore, the time delay estimation $\tau_{k,q}$ of each user depends primarily on the cyclic autocorrelation property of the stacked code $\mathbf{a}_k(\circ)$. Consequently, the number of users which can be supported by ranging system depends on the number of stacked codes $\mathbf{a}_k(\circ)$.

In Eq.(5.51), we can find that the stacked code $\mathbf{a}_k(\circ)$ consists of a sequence \mathbf{c}_k and an all-zero vector of the same length stacked above. Since \mathbf{c}_k is formed by a sequence g_k as shown in Eq.5.40, the cyclic autocorrelation property of stacked code $\mathbf{a}_k(\circ)$ is actually the non-cyclic autocorrelation property of g_k . In addition, g_k is formed by inserted $N_c - 1$ "o" between each element in the spreading sequence $u_k(n)$, hence, the non-zero value of non-cyclic autocorrelation property of g_k is determined by the non-cyclic autocorrelation function of $u_k(n)$. Therefore, we can conclude that the ranging performance of the DEMR algorithm actually depends on the non-cyclic autocorrelation property of spreading sequences $u_k(n)$. On the other word, increasing the number of users that the ranging systems can support or improving the ranging performance further would be achieved by choosing another kind of spreading sequences with better non-cyclic autocorrelation function.

Since the ranging performance of DEMR algorithm mainly depends on the non-cyclic autocorrelation property of $u_k(n)$, in order to enhance the ranging performance of DEMR algorithm, we introduce a set of binary chaotic sequences with good non-cyclic autocorrelation function to replace the Gold sequences. Moreover, unlike the Gold sequences which has finite number of sequences for a certain length, an ideally large number of chaotic sequences with good correlation property can be generated depending on the different initial conditions.

6.1.1 CHAOTIC BINARY SEQUENCE GENERATION AND SELECTION

The generation of binary chaotic sequences follows the same procedure introduced in the Fig.4.2.9. Since in this section, we focus on the binary chaotic sequence, the Chebyshev map and Tent map are chosen as the chaotic sequences generator, whose mathematical expressions are given in the Eq.(4.35) and Eq.(4.36), respectively. For each of the K users, we can generate chaotic sequences $x_k(n)$ with different and independent initial condition $x_k(0)$. After passing through a quantization function $Q_{C,DS}$ in Eq.(4.37) for Chebyshev map and $Q_{T,DS}$ in Eq.(4.38) for Tent map, a set of binary chaotic spreading sequences $x'(n)$ is obtained. Although the initial conditions of $x(n)$ are different, there may be some identical sequences in $x'(n)$ due to the quantization processing. In order to avoid this situation, the last step of binary chaotic sequences generation is to check all the sequences to be different. After the whole procedure of binary chaotic sequences generation, we have already obtained a large number of chaotic binary sequences $y(n)$.

In the section 4.2.4, we compare the non-cyclic autocorrelation function of chaotic binary sequences with Gold sequence using the criterion $\varphi_{G,N}$, which is the maximum peak absolute side lobe value of autocorrelation of all the Gold sequences in length N . The criterion $\varphi_{G,N}$ ensures that all the selected chaotic binary sequences have no higher side lobe value than $\varphi_{G,N}$. However, if we want to achieve a better ranging performance corresponding to better non-cyclic autocorrelation function, we must choose another criterion. Here, we introduce a new criterion $\rho_{G,N}$ which is the minimum peak absolute side lobe value of autocorrelation of all the Gold sequences in length N .

Let $R_{G_k}(\tau)$ be the non-cyclic autocorrelation function of Gold sequence G_k of length N , $k = 1, 2, \dots, N+2$. The maximum absolute value of the side lobe of non-cyclic autocorrelation function ρ_k is defined as

$$\rho_k = \max_{\tau \neq 0} (|R_{G_k}(\tau)|) \quad k = 1, 2, \dots, N+2 \quad (6.3)$$

and

$$\varphi_{G,N} = \max_{1 \leq k \leq N+2} (\rho_k) \quad (6.4)$$

but

$$\rho_{G,N} = \min_{1 \leq k \leq N+2} (\rho_k) \quad (6.5)$$

Compared with $\varphi_{G,N}$ which ensure the selected sequences have no higher side lobe value than the worst case of Gold sequences, $\rho_{G,N}$ is much more strict. With this criterion, all the selected binary chaotic sequences have lower side lobe values than any Gold sequences in the same

length. Hence, we can say that these selected binary chaotic sequences have better non-cyclic autocorrelation property than Gold sequences in the same length.

The selection procedure is operated as follows:

- Non-cyclic autocorrelation function is first calculated for each sequence in a large pool of binary Chebyshev or Tent candidate sequences.
- Group the sequences whose maximum absolute value of autocorrelation sidelobe ρ_k is lower than $\rho_{G,N}$, k is the number of sequences.
- Above coarsely chosen sequences are sorted by increasing ρ_k .
- Select the first K binary chaotic sequences as the selected chaotic binary spreading sequences, where K is number of users that the ranging systems need to support.

6.1.2 NUMERICAL EVALUATION

The simulations have also been carried out on the IEEE 802.15.4a CM1 channel to evaluate the performance of chaos-based DEMR algorithm. Performance is evaluated by RMSE of TOA estimation as well.

Each user is assigned a spreading sequence of length $N = 31$ for both chaotic sequences and Gold sequence. TOA of the first user is evaluated. When using Gold sequences as spreading codes, sequence with autocorrelation parameter $\rho_{G,31}$ is assigned to user 1. With no loss of generality, transmitted power of user 1 $P_1 = 1$. All interfering users are given a random received power with a log-normal distribution with a mean d dB above the desired signal and a standard deviation equal to 10dB. That is $P_k = 10^{\varepsilon_k/10}$, where $\varepsilon_k \sim N(d, 100)$. The near-far ratio is defined as the ratio of the mean of the random powers of the interfering users to that of the power of user 1. Hence, the near-far ratio is d in dB. SNR is defined to be E_b/N_o , where E_b is the energy per bit for the first user. The pulse $p(t)$ is a raised cosine pulse with roll-off factor $\beta = 0.6$, pulse and chip duration are set equal to 1ns, i.e., $T_c = T_p = 1ns$, N_c is taken equal to 16. Time delays of the first path of all the users are uniformly distributed over $[0, 100ns)$, which are the real-valued actual delays including a fractional part. In the CM1 channel, X is chosen to be 3. The results below are based on 500 Monte-Carlo trials.

We compare the ranging performance of chaos-based DEMR estimator with Gold-based DEMR estimator and the Nonlinear filter estimator. In Fig.6.1.1, we show the RMSE performance as the function of the Near-Far ratio for different SNR in the CM1 channel. As shown

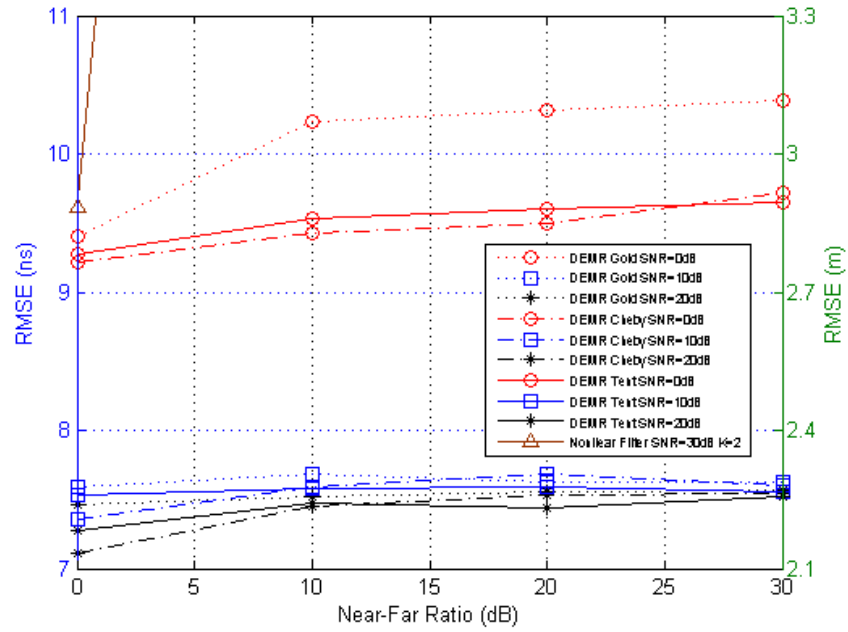


Figure 6.1.1: RMSE versus near-far ratio for different SNR values with $M = 100$, $N = 31$, and $K = 10$ in CM1 channel.

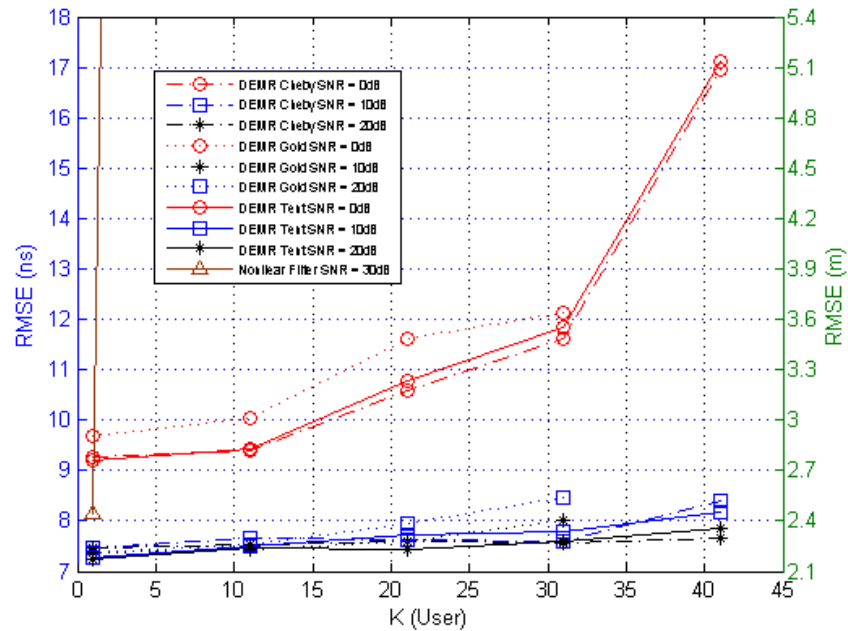


Figure 6.1.2: RMSE versus K for different SNR values with $M = 100$, $N = 31$, and near-far ratio is 10 dB in CM1 channel.

in Fig.6.1.1, Nonlinear filter estimator has no robustness to near-far ratio. By contrast, near-far problem appears to have little effect on chaos-based DEMR estimator. Comparing with Gold-based DEMR, the use of selected chaotic sequences enhances the ranging performance further.

In Fig.6.1.2, two sets of 41 selected chaotic sequences of length 31 are generated by Chebyshev map and Tent map, respectively. We assign these two sets of the chaotic sequences to $K = 41$ users and compare the RMSE of chaos-based DEMR with that of Gold-based DEMR and Nonlinear filter as the function of K . In chaos-based DEMR algorithm, since the selected chaotic sequences have lower autocorrelation sidelobe than that of Gold sequences, ranging performances are improved for all SNR. For the two higher SNR, RMSE of chaotic sequences with 41 users is still lower than that of Gold sequences with 31 users. For Nonlinear filter, RMSE soars to $25ns$ when K varies from 1 to 2. It is shown that DEMR estimator with selected binary chaotic sequences increases the system capacity and improves the ranging accuracy.

Hence, we can find that the use of chaotic binary sequences in DEMR algorithm enlarges the system capacity as well as improves the ranging performance.

6.2 CHAOTIC MULTI-VALUED CODE BASED DEMR ALGORITHM

In the Chapter 5, we have extended the DEMR algorithm into TH-UWB ranging system. In the TH-UWB ranging system, DEMR algorithm keeps the properties of near-far effect resistance and no sensitivity of number of users. As in DS-UWB ranging systems, the ranging performance of DEMR algorithm in TH-UWB systems also mainly depends on the non-cyclic autocorrelation property of the spreading sequence. Therefore, the key point of improving the ranging performance and increasing system capacity is turned to select a set of spreading sequences with better non-cyclic autocorrelation function. In the following part of this section, we introduce the chaos-based time hopping sequences as an alternative to the conventional QCC sequences. Firstly, we present how to generate a set of chaotic time hopping sequences. Then, the selection criteria are given. Finally, the comparison of ranging performance between chaotic time hopping sequences and QCC sequences are presented.

6.2.1 CHAOTIC TIME HOPPING SEQUENCE GENERATION AND SELECTION

The generation of chaotic time hopping sequences follows the same procedure as generating the chaotic binary sequences in Fig.4.2.9. The only difference exists in the quantization part since time hopping sequences are multi-valued sequence. After generating a larger number of chaotic sequences $x(n)$ by Chebyshev map or Tent map in Eq.(4.35) and Eq.(4.36), $x(n)$ are passed through the quantization function $Q_{C,TH}$ in Eq.(4.39) for Chebyshev map and $Q_{T,TH}$

for Tent map in Eq.(4.40). The output of quantization function is the multi-valued time hopping sequences. In order to ensure no existence of identical sequences, the identical checking part is added after quantization. After passing through all these three parts, we finally obtain the chaotic time hopping sequences.

When selecting the chaotic binary sequences, the criterion $\rho_{G,N}$ is employed in order to ensure all the selected binary chaotic sequences have lower side-lobe values than any Gold sequences in the same length. For time hopping sequences, the criterion ρ_{Q,N_h} is defined as

$$\rho_k = \max(|R_{Q_k}(\tau)|) \quad \tau \neq 0, \quad k = 1, 2, \dots, N_h - 1 \quad (6.6)$$

and

$$\rho_{Q,N_h} = \min(\rho_k) \quad k = 1, 2, \dots, N_h - 1 \quad (6.7)$$

where $R_{Q_k}(\tau)$ is the Hamming autocorrelation function of QCC sequence in N_h . In the domain of time hopping sequences, unfortunately, only this criterion is not enough to select the proper chaotic time hopping sequences. If we take the QCC with $N_h = 13$ as example, the $\varphi_{Q,13}$ in Eq.(4.42) is equal to $\rho_{Q,13}$ as $2/13$, which is shown in the Fig.4.2.14. It is shown that every QCC sequence with length $N_h = 13$ has the same peak side-lobe value $2/13$. The Chebyshev time hopping sequences and Tent time hopping sequences have been found in the Chapter 4 are the sequences whose maximum peak side lobe value is not greater than $\varphi_{Q,13}$. However, among all these sequences, there is no chaotic sequence whose maximum peak side lobe value is smaller than $\rho_{Q,13}$.

In order to find a set of chaotic time hopping sequences with good autocorrelation function, we introduce the other criterion *hit percentage*. Although the maximum side lobe value in the autocorrelation function gives the information about the sequences property, a more realistic approach would be analysis about the probability distribution of the side lobe values. Under the condition that the peak side lobe values are equal, the percentage of this peak value become quite important. Since the higher side lobe has a large probability to give rise to false detection in the multipath channel, its percentage should be as low as possible. Based on this consideration, the hit percentage is employed as the second criterion after filtering by the first criterion ρ_{Q,N_h} . Here, we define ζ_k as the percentage of the ρ_{Q,N_h} in the autocorrelation function of each QCC sequence with certain N_h . Then, ζ_{Q,N_h} is the maximum value of all the ζ_k . Hence, we get the second criterion ζ_{Q,N_h} .

The selection is processed as follows: 1. Non-cyclic Hamming autocorrelation function is calculated for each sequence in a large pool of binary Chebyshev or Tent candidate sequences. 2. Sequences are selected by the criterion ρ_{Q,N_h} whose the maximum absolute value of autocorrelation sidelobe is lower than ρ_{Q,N_h} . If sequences satisfied ρ_{Q,N_h} are existed, we sort these

sequence by increasing ρ_k as the selected chaotic time hopping sequences. Otherwise, we loose the criterion from lower than ρ_{Q,N_h} to not higher than ρ_{Q,N_h} as the first step of selection. 3. These firstly selected sequences are passed through the second criterion ζ_{Q,N_h} in order to control the probability of peak side lobe value ρ_{Q,N_h} . Finally, the rest sequences are grouped by the increasing of hit percentage ζ_k . The first K chaotic time hopping sequences are chosen as the selected chaotic time hopping sequences $y_k(n)$, where K is the number of users.

6.2.2 NUMERICAL EVALUATION

Each user is assigned a time hopping sequences with $N_h = 13$ for both QCC sequence and selected chaotic sequences. The length of all these time hopping sequences is also $N = 13$. The first user is the user of interest with the transmitted power $P_1 = 1$. The other users are interfering user with a random received power which follows as a log-normal $P_k = 10^{\varepsilon_k/10}$, where $\varepsilon_k \sim N(d, 100)$. The parameter d here also represents the near-far ratio. SNR is defined to be E_b/N_o where $E_b = NE_p$, E_p is the energy per bit. We still choose the raised cosine pulse with roll-off factor $\beta = 0.6$ as transmitted pulse $p(t)$, pulse and chip duration are equal to $1ns$, i.e., $T_c = T_p = 1ns$. Time delays of channel are uniformly distributed over $[0, T_a)$, $T_a = 100ns$. Note that in following simulations time delays are the real-valued delays including the fractional part. Simulations are also carried out on both AWGN channel and CM1 channel for evaluating the ranging performance. For X-max criterion, $X = 3$ is for CM1 channel. The following results are based on based on 500 realization and is evaluated by RMSE as well.

Fig.6.2.1 illustrates the ranging performance of DEMR algorithm with chaotic time hopping sequences as the function of near-far ratio with $K = 10$ uses and different SNR values in CM1 channel. In addition, the performance of DEMR algorithm with QCC sequences is also shown for comparison. For the side of chaotic sequences, both selected Chebyshev and Tent chaotic time hopping sequences are considered. As shown in the Fig.6.2.1, selected chaotic time hopping sequences achieve the similar ranging performance as QCC sequences. With $K = 10$ users, the RMSE of DEMR algorithm with all the three sequences increases no more than $4ns$ when near-far ratio grows from $0dB$ to $30dB$. In the case of SNR= $20dB$, this difference is less than $2ns$. Hence, we can have the conclusion that selected chaotic time hopping sequences have the same ranging performance as classic QCC sequences when employed by DEMR algorithm. Although DEMR algorithm in TH system is not such near-far resistance as in DS system due to the difference of signal structure as analyzed previously, the decrease of ranging performance is also acceptable, especially under the condition of high SNR values.

In the Fig.6.2.2, the RMSE performance with respect to the number of user K is given with

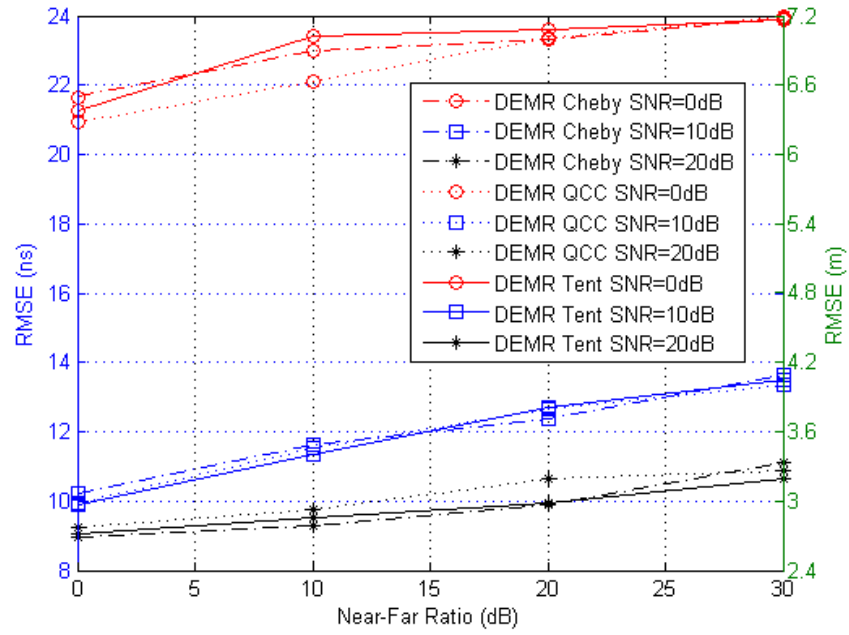


Figure 6.2.1: RMSE versus near-far ratio for different SNR values with $M = 100$, $N_h = 13$, and $K = 10$ in CM1 channel.

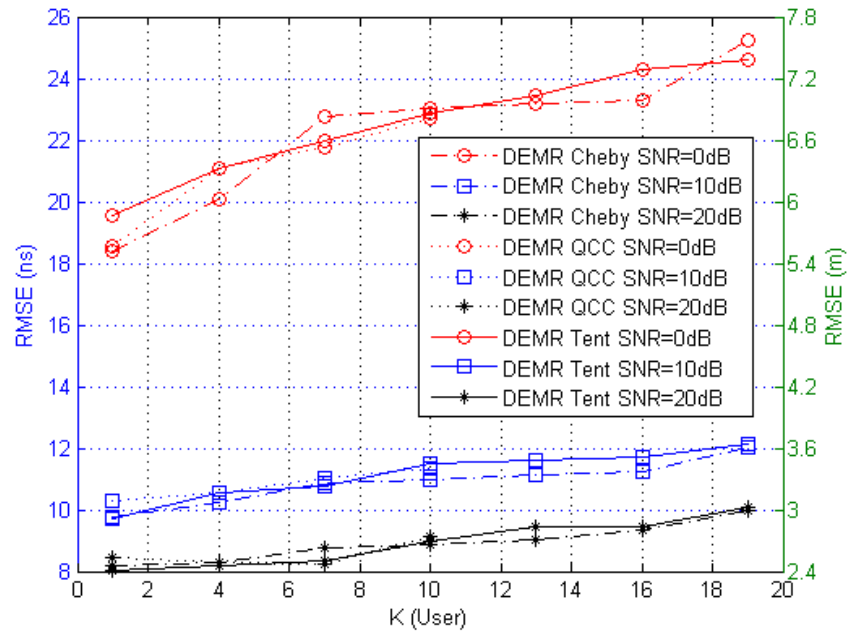


Figure 6.2.2: RMSE versus K for different SNR values with $M = 100$, $N_h = 13$, and near-far ratio is 10 dB in CM1 channel.

10dB near-far ratio and difference SNR in the CM1 channel. Two sets of 19 selected chaotic time hopping sequences with $N_h = 13$ are assigned to $K = 19$ users, which are based on Chebyshev map and Tent map, respectively. By contrast, the maximum number of user supported by QCC sequences is only 12, which is also shown in the Fig.6.2.2. In the Fig.6.2.2, we find that the chaotic time hopping sequences and QCC sequences get rise to the same ranging performance when the number of users $K < 12$. The RMSE grows only about $1ns$ with the two higher SNR values. When k is larger than the 12, QCC sequences with $N_h = 13$ have no capability to support it. However, selected chaotic sequence is beyond this limitation and enlarges the system capacity to $K = 19$ users. Although the number of users $K = 19$, the RMSE performance only increases no more than $2ns$ compared with $K = 1$. Hence, it is shown that the use of selected chaotic time hopping sequences instead of classic sequences not only has no degradation of performance but also enlarges the system capacity at least $7/12 = 58\%$.

In TH-UWB systems, chaotic time hopping sequences can be employed as an alternative of classic time hopping sequences due to achieving the same performance as that with QCC sequences. In addition, a larger number of chaotic time hopping sequences has the possibility to support much more users in the ranging systems than conventional time hopping sequences.

6.3 CHAOTIC WAVEFORM BASED DEMR ALGORITHM

In the Chapter 5, DEMR algorithm for DS-UWB ranging systems is introduced to obtain a chip-level ranging accuracy with relatively low complexity even in the dense multipath channel. In DEMR algorithm, transmitted signals are formed by pulses modulated by spreading sequences which include DS sequences and TH sequences. After sequences modulated, transmitted signals have a much better good correlation properties. On the other word, the use of spreading code brings the orthogonality to the transmitted signals of each user in multiuser systems. It is a common way in multiuser communication and ranging systems.

In the Chapter 4, we have shown that Lorenz waveforms have very good even better autocorrelation and cross-correlation property compared with classic transmitted signal. This inherent good correlation property inspires us that Lorenz waveforms could be a good alternative to classic transmitted signals. In addition, Lorenz waveforms are easily generated by simple circuits whose bandwidth can be arbitrary and has no relationship with time duration. All these properties make Lorenz waveforms quite suitable to ranging systems. No requirement of sequences modulation gives rise to simple receiver structure furthermore. Hence, in this following, we introduce the Lorenz waveforms based DEMA algorithm and DEMR algorithm.

The transmitted signal the k th user of UWB systems with Lorenz waveforms is expressed as

$$s_k(t) = \sqrt{P_k} \sum_{m=0}^{M-1} d_k Lz_k(t - mT_d) \quad (6.8)$$

where P_k is the k th user's transmitted power, M is number of data bits considered for TOA estimation, $d_k(m) \in \{\pm 1\}$ is the m th transmitted bit, $Lz_k(t)$ is the Lorenz waveform with duration $T_L \leq T_d$ for the k th user. If transmitted signals pass through the channel model given by IEEE 802.15.4a channel model [40], received signals are written as

$$r(t) = \sum_{k=1}^K \sum_{q=1}^{L_k} a_{k,q} s_k(t - \tau_{k,q}) + n(t) \quad (6.9)$$

All the parameters have the same meaning as that in Eq.(5.5).

In stead of a matched filter, the receiver front-end only consists of a sampler with interval $t_s = T_d/V$, where the integer $V > 0$ is called the oversampling factor. Then, the received sequences $r(l)$ is

$$r(l) = \sum_{k=1}^K \sum_{q=1}^{L_k} a_{k,q} s_k(lt_s - \tau_{k,q}) + n(l) \quad (6.10)$$

$$l = 1, 2, \dots, MV$$

$n(l)$ denotes the zero-mean white Gaussian noise with variances σ_n^2 . Consequently, the received vector of the m th bit interval $\mathbf{r}(m)$ is written as

$$\mathbf{r}(m) = [r(mV + 1), r(mV + 2), \dots, r(mV + V)]^T \quad (6.11)$$

In DEMR algorithm, we approximates time delays $\tau_{k,q}$ as the integer multiples of chip duration T_c due to the ambiguity of IDF. In the chaotic waveform based DEMR algorithm, we approximate the time delays $\tau_{k,q}$ to

$$\tau_{k,q} = p_{k,q} t_s \quad (6.12)$$

where $p_{k,q}$ is an integer within $\{0, 1, \dots, V - 1\}$. Hence, time delay $\tau_{k,q}$ is approximated as the

integer multiples of sampling interval t_s . The received vector $\mathbf{r}(m)$ is expressed as

$$\mathbf{r}(m) = \sum_{k=1}^K \sum_{q=1}^{L_k} \beta_{k,q} \mathbf{A}_k(\tau_{k,q}) \mathbf{z}_k(m) + \mathbf{n}(m) \quad (6.13)$$

$$m = 0, 1, \dots, M-1$$

where

$$\beta_{k,q} = \alpha_{k,q} \sqrt{P_k} \quad (6.14)$$

$$\mathbf{A}_k(\tau_{k,q}) = [\mathbf{a}_k^1(\tau_{k,q}) \quad \mathbf{a}_k^2(\tau_{k,q})] \quad (6.15)$$

and

$$\mathbf{z}_k(m) = [d_k(m-1) \quad d_k(m)]^T. \quad (6.16)$$

Note that the $\mathbf{a}_k^1(\tau_{k,q})$ and $\mathbf{a}_k^2(\tau_{k,q})$ here are different from Eq.(5.41) and Eq.(5.42) in DEMR algorithm.

$$\mathbf{a}_k^1(\tau_{k,q}) = \mathbf{P}_1(p_{k,q}) \mathbf{Lz}_k \quad (6.17)$$

$$\mathbf{a}_k^2(\tau_{k,q}) = \mathbf{P}_2(p_{k,q}) \mathbf{Lz}_k \quad (6.18)$$

where

$$\mathbf{Lz}_k = [Lz_k(1), Lz_k(2), \dots, Lz_k(V)] \quad (6.19)$$

and

$$Lz_k(l) = Lz_k(t = lt_s) \quad (6.20)$$

$\mathbf{P}_1(p)$ and $\mathbf{P}_2(p)$ denote the $V \times V$ shifting matrices as expressed in Eq.(5.43) in DEMR algorithm. Since when $m = 0$, $d_k(-1)$ is unknown, $d_k(-1) = 0$ is chosen which has little effect on the estimation.

We rewrite the $\mathbf{r}(m)$ further as

$$\mathbf{r}(m) = \mathbf{B}\mathbf{s}(m) + \mathbf{n}(m) \quad (6.21)$$

where

$$\mathbf{B} = \left[\sum_{q=1}^{L_1} \beta_{1,q} \mathbf{A}_1(\tau_{1,q}) \quad \sum_{q=1}^{L_2} \beta_{2,q} \mathbf{A}_2(\tau_{2,q}) \quad \dots \quad \sum_{q=1}^{L_K} \beta_{K,q} \mathbf{A}_K(\tau_{K,q}) \right] \quad (6.22)$$

and

$$\mathbf{s}(m) = [\mathbf{z}_1^T(m) \mathbf{z}_2^T(m) \dots \mathbf{z}_K^T(m)]^T \quad (6.23)$$

We also assume that data bits and waveforms for all the users are known. Hence, this problem become the same problem solved by DEMR algorithm.

By using DEMR algorithm, we firstly obtain the estimation $\hat{\mathbf{B}}$ of \mathbf{B} as follows

$$\hat{\mathbf{B}} = \mathbf{R}_{\text{sr}}^H(M) \mathbf{R}_{\text{ss}}^{-1}(M) \quad (6.24)$$

and

$$\hat{\mathbf{B}} = [\hat{\mathbf{B}}_1 \hat{\mathbf{B}}_2 \dots \hat{\mathbf{B}}_K], \quad (6.25)$$

Hence, different users have been decoupled. If we also introduce

$$\hat{\mathbf{b}}_k = \text{vec}[\hat{\mathbf{B}}_k] \quad k = 1, 2, \dots, K \quad (6.26)$$

we can find that $\hat{\mathbf{b}}_k$ of the k th user represents the sum of \mathbf{Lz}_k delayed by $\tau_{k,q}$. Since each user's transmitted waveform is known at the receiver side. Theoretically, $\tau_{k,q}$ can be estimated by correlating $\hat{\mathbf{b}}_k$ with local template \mathbf{Lz}_k .

In the AWGN channel, as shown in Chapter 5, time delay τ_k can be easily estimated as

$$\hat{\tau}_k = \arg \max_{\{\tau_k\}} \frac{|\mathbf{a}_k^T(\tau_k) \hat{\mathbf{b}}_k|^2}{\mathbf{a}_k^T(\tau_k) \mathbf{a}_k(\tau_k)} \quad (6.27)$$

and amplitude estimation is

$$\hat{\beta}_k = \frac{\mathbf{a}_k^T(\hat{\tau}_k) \hat{\mathbf{b}}_k}{\mathbf{a}_k^T(\hat{\tau}_k) \mathbf{a}_k(\hat{\tau}_k)} \quad (6.28)$$

where $\mathbf{a}_k(\tau_k)$ is defined the same as Eq.(5.48). As the classic pulse based DEMR algorithm, we can also find that the autocorrelation property of transmitted waveform $Lz_k(t)$ dominants the ranging performance, consequently, and the amplitude estimation.

In the more complex case, the dense multipath channel condition, DEMR algorithm in Chapter 5 estimates the time delay $\tau_{k,q}$ by approximating the autocorrelation function of stack code $\mathbf{a}_k(o)$ to the white noise like autocorrelation. Here, in the Lorenz based DEMR algorithm, if we ignore the side-lobe value of autocorrelation function of $Lz_k(t)$, the time delay $\tau_{k,q}$ and amplitude $\beta_{k,q}$ can be estimated as

$$\{\hat{\tau}_{k,q}\}_{q=1}^{L_k} = \arg \max_{\{\tau_{k,q}\}_{q=1}^{L_k}} \sum_{q=1}^{L_k} \frac{|\mathbf{a}_k^T(\tau_{k,q}) \hat{\mathbf{b}}_k|^2}{\mathbf{a}_k^T(\tau_{k,q}) \mathbf{a}_k(\tau_{k,q})} \quad (6.29)$$

$$\{\hat{\beta}_{k,q}\}_{q=1}^{L_k} = \frac{\mathbf{a}_k^T(\{\hat{\tau}_{k,q}\}_{q=1}^{L_k})\hat{\mathbf{b}}_k}{\mathbf{a}_k^T(\{\hat{\tau}_{k,q}\}_{q=1}^{L_k})\mathbf{a}_k(\{\hat{\tau}_{k,q}\}_{q=1}^{L_k})} \quad (6.30)$$

Since the $\mathbf{a}_k^T(\tau_{k,q})\mathbf{a}_k(\tau_{k,q}) = \mathbf{a}_k^T(\mathbf{o})\mathbf{a}_k(\mathbf{o})$ and $|\mathbf{a}_k^T(\tau_{k,q})\hat{\mathbf{b}}_k|^2$ is non-negative, the L_k -dimensional search problem in Eq.(6.29) can be simplified to L_k independent maximum search in one dimensional with the constraint $\hat{\tau}_{k,s} \neq \hat{\tau}_{k,r}, s, r \in \{1, 2, \dots, L_k\}$. The following processing is the same as that in the DEMR algorithm, we first rewrite Eq.(6.29) as

$$\{\hat{\tau}_{k,q}\}_{q=1}^{L_k} = \arg \max_{\{\tau_{k,q}\}_{q=1}^{L_k}} \frac{\sum_{q=1}^{L_k} |\mathbf{a}_k^T(\tau_{k,q})\hat{\mathbf{b}}_k|^2}{\mathbf{a}_k^T(\mathbf{o})\mathbf{a}_k(\mathbf{o})} \quad (6.31)$$

and let

$$W(\tau_{k,q}) = \frac{|\mathbf{a}_k^T(\tau_{k,q})\hat{\mathbf{b}}_k|^2}{\mathbf{a}_k^T(\mathbf{o})\mathbf{a}_k(\mathbf{o})} \quad (6.32)$$

$\{\hat{\tau}_{k,q}\}_{q=1}^{L_k}$ which correspond to the L_k -largest values of $W(\tau_{k,q})$ are the estimations of time delays. The earliest time delay among $\{\hat{\tau}_{k,q}\}_{q=1}^{L_k}$ is the TOA estimation of the user k . Since the number of paths is usually unknown for the receiver side, the X-max criterion is also employed in the real application environment.

In order to simplify the estimation, we ignore the side lobe value of $Lz_k(t)$'s autocorrelation function in the above discussion. It's a mild assumption when the side lobe value is much smaller compared with the peak value. Otherwise, the ranging performance will be effected. In the following numerical evaluation part, we will see this effect intuitively with simulation results.

As the approximation that $\tau_{k,q} = p_{k,q}t_s$, the precision of chaotic waveform based DEMR is determined by t_s , the sampling interval. It's easy to find that the higher sampling rate gives rise to more accurate ranging performance, but the complexity also become higher with the increase of V . By contrast, a low sampling rate corresponding to a low complexity estimation leads to a low precision ranging performance. According to the method for calculating the complexity of DEMR algorithm, the complexity of chaotic based DEMR algorithm is $O(K^3 + K^2M + K^2V + KMV + KV^2)$ for both AWGN channel and multipath channel condition.

When estimating TOA in multipath channel, in order to simplify the estimation, we ignore the side lobe value of $Lz_k(t)$'s autocorrelation function. It's a mild assumption when the side lobe value is much smaller compared with the peak value. Otherwise, the ranging performance will be effected. In the following numerical evaluation part, we will see this effect intuitively with simulation results.

6.3.1 SELECTION OF CHAOTIC WAVEFORM

In this section, what we study is the continuous chaotic waveform which is transmitted continuously without long pause. Hence, although this system also satisfies the definition of UWB system, it is not the impulse radio UWB which is characterized by transmitting very short duration pulse in low duty cycle.

Faced to this difference, the following two criteria are determined as the selection conditions. Since Lorenz waveforms are the continuous waveforms, their counterparts are the conventional waveforms which consists of pulses modulated by the spreading sequences. As shown in Chapter 4, the $\varphi_{G,N}$ can be employed as the first criterion to ensure the autocorrelation function of Lorenz waveforms, where N is chosen according to the length of Lorenz waveform T_L and classic pulse duration T_p , $T_L = NT_p$. The shorter T_p is, the longer N is which yields to the smaller $\varphi_{G,N}$.

As we analyzed in the Chapter 5, in IR-UWB systems, although DEMR algorithm can decouple different users efficiently, the MUI cannot be eliminated completely when M is far from infinity since it is a asymptotic algorithm. Due to the long pulse repetition time which is modeled mathematically as those inserting "o" between each elements of sequence, we can ignore the MUI and only focus on the autocorrelation property. But in the continuous UWB systems, Lorenz waveforms transmit continuously. Hence, there is nonexistence long silent time between waveforms. However, this important property is no longer existed in the continuous UWB system. Therefore, the cross-correlation property must be taken into account. Hence, the second criterion we propose is the $\psi_{G,N}$ to make sure the selected Lorenz waveforms with good cross-correlation property.

All the Lorenz waveforms passed through the first test $\varphi_{G,N}$ will go through the second criterion $\psi_{G,N}$. Finally, the Lorenz waveforms passing through all the two criteria are sorted in ascending order of peak absolute value of autocorrelation function. The first K Lorenz waveform are selected as our candidate chaotic waveforms. From the Fig.4.2.7 and Fig.4.3.4, we can find that it exists not only a large number of Lorenz waveforms satisfying the above two criteria, these selected Lorenz waveforms outperform their counterpart greatly, which give us an opportunity to enhance the ranging performance further.

6.3.2 NUMERICAL EVALUATION

The simulations have also been carried out on the AWGN channel and IEEE 802.15.4a CM1 channel to evaluate the performance of chaotic waveform based DEMR algorithm. Performance is evaluated by RMSE of TOA estimation as well.

Each user is assigned a selected Lorenz waveform of length $T_L = 127ns$. The parameter of

Lorenz waveform is set to be $\sigma = 30, r = 84, b = 8$. TOA of the first user is evaluated. On the purpose of comparison, two kinds of the conventional waveforms are also presented. In the first case, the transmitted signals is defined as Eq.(5.2), where $p(t)$ is also the raised cosine pulses with duration $T_p = 1ns$ and $g_k(i)$ is the Gold sequences with length $N = 127$. If $N_c = 1$ and $T_c = T_p = 1ns, T_d = NN_cT_c = 127ns$ is equal to T_L . The second case, it also transmits the raised cosine waveforms modulated by the Gold sequence as shown in Eq.(5.2), but $N = 31$ and N_c is set to be 4. Hence, $T_d = NN_cT_c = 124ns$. For the latter two raised cosine pulse based signal, roll-off factor is $\beta = 0.6$ and $t_p = 0.16$. As shown in the Fig.4.2.4, the -10dB frequency bandwidth for all these three kinds of signal are the same. The sampling frequency is 8GHz, which is the Nyquist rate of both Lorenz waveform and raised cosine waveform. The other definitions are totally same as the previous simulations parameters, including power, SNR and near-far effect. Time delays of the first path of all the users are uniformly distributed over $[0, 30ns)$, which are the real-valued actual delays including a fractional part. In the CM1 channel, X is chosen to be 3. The results below are based on 500 Monte-Carlo trials.

Fig.6.3.1 and Fig.6.3.2 illustrate the RMSE performance as the function of near-far ratio and number of users in AWGN channel, respectively. The DEMR algorithm with raised cosine pulse and Gold sequence in $N = 127$ and in $N = 31$ are also taken for comparison. In Fig.6.3.1, we can find that all the three systems achieve a accuracy precision about 0.0360ns and keep stable no matter that the near-far ratio varies from 0dB to 30dB and SNR changes from 0dB to 10dB. Hence, although we use the Lorenz waveform to replace the classic waveforms, the property of resistance of near-far effect has not changed.

In the Fig.6.3.2, the ranging performance is shown with the increase of the number of users K . As introduced in Chapter 4, Lorenz waveform has no constraint of K due to its sensitivity to initial conditions. By contrast, system using Gold sequence has the maximum number of users $K = N + 2$.

In the Fig.6.3.2, K increases from 1 to 41 with two different SNR values. When $K = 41$, it is already beyond the capacity of system with Gold sequences $N = 31$, therefore, only Lorenz waveforms and pulses with Gold sequences $N = 127$ perform in this point. When $SNR = 10dB$, all the three systems reach precious ranging performance about 0.0360ns even when $K = 41$. When $SNR = 0dB$, there are some different performance. Firstly, system with Gold sequences $N = 31$ still keeps its accuracy precision when K varies from 1 to 31. However, Lorenz based system can not maintain such precision when K is greater than 31. The deteriorate performance also occurs in system with Gold sequences $N = 127$ when K is greater than

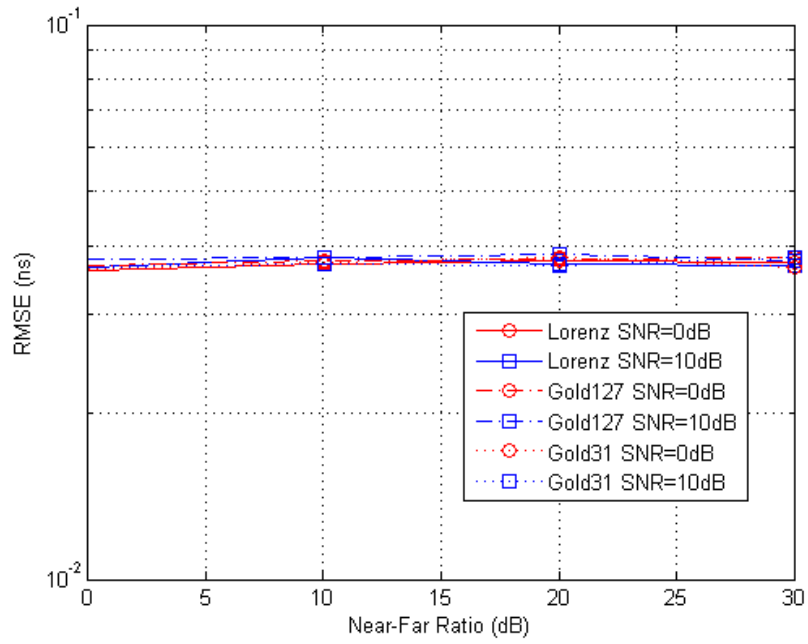


Figure 6.3.1: RMSE versus near-far ratio for different SNR values with $M = 100$, $T_s = 127ns$, and $K = 10$ in AWGN channel.

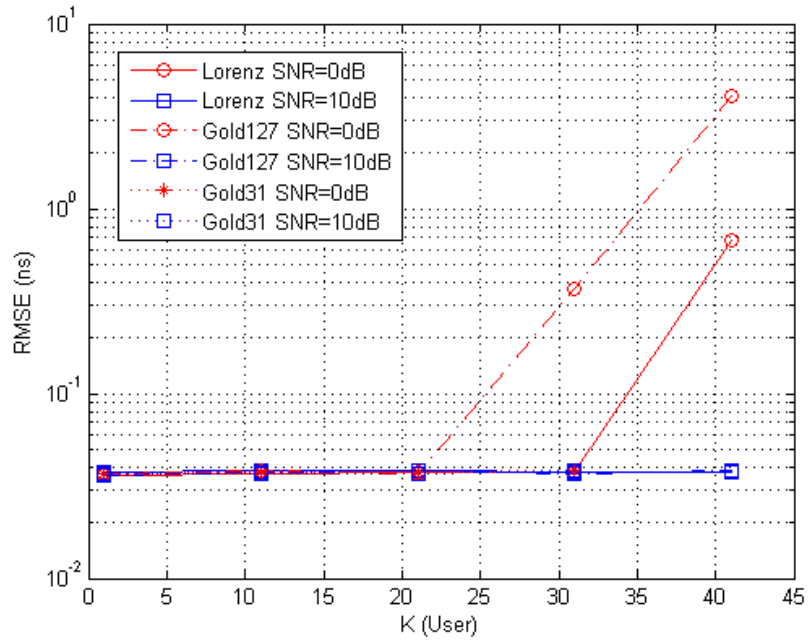


Figure 6.3.2: RMSE versus K for different SNR values with $M = 100$, $T_s = 127ns$, and near-far ratio is 10 dB in AWGN channel.

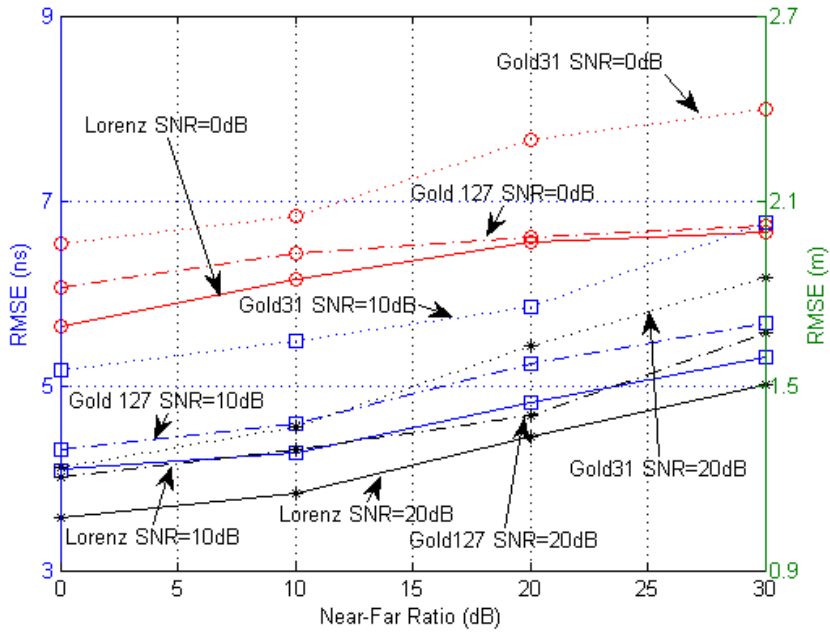


Figure 6.3.3: RMSE versus near-far ratio for different SNR values with $M = 100$, $T_s = 127ns$, and $K = 10$ in CM1 channel.

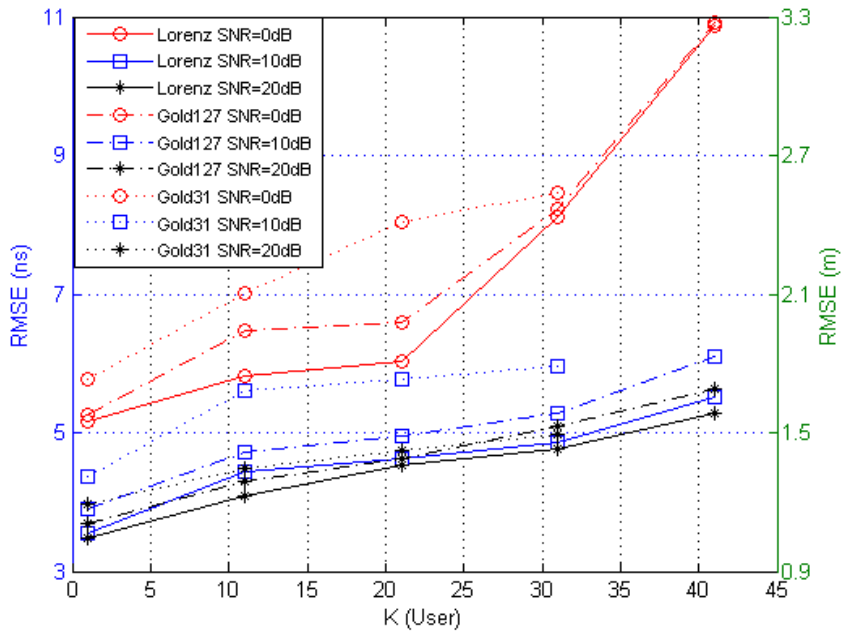


Figure 6.3.4: RMSE versus K for different SNR values with $M = 100$, $T_s = 127ns$, and near-far ratio is 10 dB in CM1 channel.

21. Although selected Lorenz waveforms and system with Gold sequences $N = 127$ has lower autocorrelation and cross-correlation side lobe value than that of Gold sequence $N = 31$, the "o" inserted model of impulse radio UWB system has the better resistance of multiuser interference. Since the selected Lorenz waveforms have lower side-lobe values in both autocorrelation and cross-correlation function than system with Gold sequences $N = 127$, they perform much better than its counterpart when $K = 41$. Hence, we can find that comparing with short Gold sequences based system, the use of Lorenz waveforms and long Gold sequences increases the system capacity. Selected Lorenz waveforms outperform long Gold sequences due to its low side lobe value of correlation functions.

After discussing the ranging performance in AWGN channel, Fig.6.3.3 show us the RMSE performance as the function of near-far ratio in CM1 channel with difference SNR values. As shown in the Fig.6.3.3, the RMSE of Lorenz based system deteriorates no more than $2ns$ when near-far ratio increasing from $0dB$ to $30dB$ even with the severe condition $SNR = 0dB$. Moreover, the use of Lorenz waveform shows its advantage of improving the ranging performance comparing with classic waveform due to its better correlation properties.

The RMSE performance with respect to the number of users in CM1 channel is given in Fig.6.3.4. We can see that Lorenz based system also outperforms its two counterparts due to its better correlation property in all the SNR values. For the two higher SNR, RMSE of Lorenz based system with 41 users is still lower than that of Gold sequences with 31 users. It is shown that the use of Lorenz waveform not only increases the number of users but also enhances the ranging performance.

Finally, we can find that the using of continuous chaotic waveforms in UWB ranging systems gives rise to not only in transceiver simplification, but also in performance improvement and enhancement of systems capacity.

6.4 CONCLUSION

In this chapter, we propose to use chaotic signals in DEMR algorithm and compare it to classic ranging signals under the same frequency spectrum, energy and channel propagation conditions. Chaotic binary sequences and direct continuous waveforms are considered for DS-UWB ranging systems and multi-valued chaotic sequences are proposed for TH-UWB systems. Numerical evaluation results show that besides bringing the ranging performance improvement, the significant benefit is in the number of users that systems can be supported, which is higher than fully-loaded classic ranging systems.

7

Conclusion and Perspective

In this dissertation, our research focuses on improving the ranging precision under the severe MUI and dense multipath condition. For the sake of this objective, chaotic signals are introduced into short range localization field due to their attractive features.

The state of art has been introduced in two research branches: the current ranging technologies and systems in Chapter 2, and the introduction and existing applications of chaotic signals in Chapter 3. In Chapter 2, the common used ranging technologies that have been considered for indoor localization are presented at first. The principle of each ranging method has been explained followed by their drawbacks and benefits. Then, UWB ranging systems are introduced as the promising candidate for indoor localization problem, which is also the ranging system that our research is based on. Following the introduction of the history and regulation of UWB systems, the ranging approach, main error sources, current estimators of UWB ranging systems are presented detailedly. In Chapter 3, we first present a brief introduction of chaos theory and chaotic signals. Then, the application of chaotic signals in various fields is given with explanation of the advantages and disadvantages that the use of chaotic signals may bring.

Our research has been investigated in two steps. In the first step, two new multiuser TOA estimation algorithms named DEMR and SLSML algorithms have been proposed, which are quite near-far resistant and allow the ranging system to be fully-loaded. DEMR algorithm ob-

tains the chip-level TOA estimation with low complexity due to the employment of IDF filter rather than MF filter in the front-end of receiver. In the SLSML algorithm, the prior requirements are less restrictive than that of DEMR algorithm, thus it is more complex than DEMR algorithm but also works at low sampling rate due to the use of IDF filter. The presentation on this part of work can be found in the Chapter 5.

The second step of our research has been concentrated on the application of chaotic signals in ranging systems, particularly on our new proposed TOA algorithms. Ranging related properties of chaotic signals have been investigated in the Chapter 4, including the autocorrelation, cross-correlation and frequency spectrum properties of both continuous-time chaotic signals and discrete-time chaotic sequences. Lorenz waveforms are the representative of continuous-time chaotic signals, Chebyshev and Tent maps are chosen as the examples of discrete-time chaotic sequences. For the autocorrelation and cross-correlation properties, following the introduction of the generation of chaotic waveforms and sequences, chaotic signals are compared with their conventional counterparts. The numerical results show that selected chaotic waveforms and sequences can obtain the same even better correlation properties than that of conventional competitors. Moreover, the number of chaotic waveforms and sequences are quite larger than that of classic signal due to the sensitivity of initial conditions. In addition, the frequency spectrum of Lorenz waveforms are not only independent on the waveform duration, but also can be adjusted to certain bandwidth by varying the Lorenz parameters. Hence, we can find that chaotic signals can be considered as the alternative of conventional UWB ranging signals. Since in the Chapter 5, we find that the ranging performance of DEMR algorithm mainly depends on the autocorrelation property of ranging signals, we apply the selected chaotic signals with DEMR algorithm in the UWB ranging systems. Firstly, selected chaotic binary sequences are used to replace the Gold sequences. It is shown that using chaotic binary sequences in the DEMR algorithm increases the ranging accuracy as well as enlarges the capacity of ranging systems. The same situation can be also found when selected chaotic time hopping sequences replaces the QCC sequences. In addition, when Lorenz waveforms are employed as the ranging waveforms, except having the above advantages, the complexity can be simplified further.

As a PhD research work of a period of three years, our work is far from completed. Various challenging issues await exploration in the future research. There are several areas in this dissertation that can be extended, which are shown as following:

- *Joint TOA and AOA estimation:* As introduced in the Chapter 2, both AOA and TOA ranging approaches can benefit from the large bandwidth of UWB signals. TOA-based approaches are commonly chosen due to the requirement of antenna array in AOA based methods which increases the cost and complexity. However, for two-dimensional

positioning, three reference nodes are needed to determine one target node if TOA measuring is used. The number of reference nodes can be reduced to two if AOA instead of TOA is employed as the ranging technology. And just one reference node is sufficient if both TOA and AOA measurements are performed. Hence, AOA estimation or joint AOA and TOA estimation has their outstanding merits in the positioning processing. In addition, as shown in the Chapter 2, in AOA measurement, angle of arrival is estimated by the time difference in arrival time of each antenna elements. Hence, to some extent, AOA is also a time based ranging technology. Based on this knowledge, the DEMR and SLSML algorithms can be extended into the AOA estimation or joint TOA and AOA estimation to fill this gap. Additionally, as in the TOA estimation area, chaotic signals can be used in joint AOA and TOA estimation to enhance the positioning performance and system capacity.

- *Multiuser interference cancellation:* Although DEMR algorithm is not sensitive to the number of users in the medium and high SNR region, its performance degrades with the increase of number of users in the low SNR region as shown in the Chapter 5 and Chapter 6. In DEMR algorithm, the estimation of both time delays and amplitudes of each path can be obtained in each user, which provides an opportunity to enhance the ranging accuracy by the multiuser interference cancellation processing. All the signals from interfering user can be eliminated according to the estimation of time delays and amplitudes. Hence, the TOA estimation of desired user can be performed after MUI cancellation according to the last estimation. In this way, the MUI can be mitigate greatly, which may yield to better ranging performance in low SNR region.
- *First path detection:* In both DEMR and SLSML algorithms, the P -max criterion is used to detect the first path, which is chosen for its low complexity. Other complicated first path detection criteria may be interesting if the requirement of ranging performance is higher and is regardless of complexity.
- *Chaotic sequences and chaotic waveforms based DEMR algorithm:* In this thesis, we have developed the chaotic sequence based DEMR algorithm and chaotic waveforms based DEMR algorithm separately. While, in section 6.3, we find that in the chaotic waveform based DEMR algorithm, the binary identical independent distributed data bits are transmitted in order to decouple the different users at the receiver side, this inspires us to use the chaotic binary sequences here as the alternative of these data bits. The use of well designed chaotic sequences may give rise to the better multiuser decoupling as well as the reduction of the requirement of the number of bits (length of sequences).

- *Chaotic generators:* In this thesis, Chebyshev and Tent sequences are chosen as the representatives of discrete chaotic sequences for their simple generators. Without regards to complexity, other complex dynamic systems may be also interesting. In addition, the deep insight of the chaotic generators such as the analysis of probability density function may provide us an opportunity to generate chaotic sequences with better required properties. In other words, other continuous chaotic waveforms can be also introduced in our algorithms as the alternatives of Lorenz waveforms as long as they satisfy the system requirements.

References

- [1] S. Gezici, Zhi Tian, G. B. Giannakis, H. Kobayashi, A. F. Molisch, H. V. Poor, and Z. Sahinoglu, "Localization via ultra-wideband radios: a look at positioning aspects for future sensor networks," *IEEE Signal Process. Mag.*, vol. 22, no. 4, pp. 70–84, Jul. 2005.
- [2] Z. Sahinoglu, S. Gezici, and I. Guvenc, *Ultra-Wideband Positioning Systems: Theoretical Limits, Ranging Algorithms, and Protocols*, Cambridge, U.K.: Cambridge Univ. Press, 2008.
- [3] M. Flury, R. Merz, J.-Y. Le Boudec, and J. Zory, "Performance evaluation of an IEEE 802.15.4a physical layer with energy detection and multi-user interference," in *Proc. IEEE Int. Conf. Ultra-Wideband (ICUWB)*, Sept. 2007, pp. 663–668.
- [4] F. C. M. Lau and C. K. Tse, *Chaos-Based digital Communication Systems: Operating Principles, Analysis Methods, and Performances Evaluation*, Berlin Germany: Springer-Verlag, 2003.
- [5] G. Mazzini, G. Setti, and R. Rovatti, "Chaotic complex spreading sequences for asynchronous DS-CDMA. I. System modeling and results," *IEEE Trans. Circuits Syst. I: Fundam. Theory Appl.*, vol. 44, no. 10, pp. 937–947, Oct 1997.
- [6] A. P. Kurian, S. Puthusserypady, and Su Myat Htut, "Performance enhancement of DS/CDMA system using chaotic complex spreading sequence," *IEEE Trans. Wireless Commun.*, vol. 4, no. 3, pp. 984–989, May 2005.
- [7] G. Cimatti, R. Rovatti, and G. Setti, "Chaos-based spreading in DS-UWB sensor networks increases available bit rate," *IEEE Trans. Circuits Syst. I: Reg Papers*, vol. 54, no. 6, pp. 1327–1339, June 2007.
- [8] Chia-Chin Chong and Su Khiong Yong, "Uwb direct chaotic communication technology for low-rate wpan applications," *IEEE Trans. on Vehicular Technology*, vol. 57, no. 3, pp. 1527–1536, 2008.
- [9] A. J. Weiss, "Direct position determination of narrowband radio frequency transmitters," *IEEE Signal Processing Letters*, vol. 11, no. 5, pp. 513–516, 2004.
- [10] Yihong Qi, Hisashi Kobayashi, and H. Suda, "Analysis of wireless geolocation in a non-line-of-sight environment," *IEEE Transactions on Wireless Communications*, vol. 5, no. 3, pp. 672–681, 2006.

REFERENCES

- [11] R. Verdone, D. Dardari, G. Mazzini, and A. Conti, *Wireless Sensor and Actuator Networks: Technologies, Analysis and Design*, Amsterdam, The Netherlands: Elsevier, 2008.
- [12] T. S. Rappaport, *Wireless Communication*, Upper Saddle River, NJ: Prentice-Hall, 1996.
- [13] H. L. Van Trees, *Detection, Estimation and Modulation Theory*, New York Wiley, 1968.
- [14] S. Severi, Gianluigi Liva, M. Chiani, and D. Dardari, "A new low-complexity user tracking algorithm for wlan-based positioning systems," in *Mobile and Wireless Communications Summit, (IST)*, 2007, pp. 1–5.
- [15] A. Mallat, J. Louveaux, and L. Vandendorpe, "UWB based positioning in multipath channels: CRBs for AOA and for hybrid TOA-AOA based methods," in *IEEE International Conference on Communications, (ICC)*, 2007, pp. 5775–5780.
- [16] D. Dardari, A. Conti, U. Ferner, A. Giorgetti, and M. Z. Win, "Ranging with ultrawide bandwidth signals in multipath environments," *Proc. IEEE*, vol. 97, no. 2, pp. 404–426, Feb. 2009.
- [17] Joon-Yong Lee and R. A. Scholtz, "Ranging in a dense multipath environment using an UWB radio link," *IEEE J. Sel. Areas Commun.*, vol. 20, no. 9, pp. 1677–1683, Dec. 2002.
- [18] H. V. Poor, *An introduction to Signal Detection and Estimation*, New York: Springer-Verlag, 1994.
- [19] Li Cong and Weihua Zhuang, "Hybrid TDOA/AOA mobile user location for wide-band CDMA cellular systems," *IEEE Transactions on Wireless Communications*, vol. 1, no. 3, pp. 439–447, 2002.
- [20] A. Catovic and Z. Sahinoglu, "The Cramer-Rao bounds of hybrid TOA/RSS and TDOA/RSS location estimation schemes," *IEEE Communications Letters*, vol. 8, no. 10, pp. 626–628, 2004.
- [21] R. I. Reza, *Data fusion for improved TOA/TDOA position determination in wireless systems*, Ph.D. thesis, Virginia Tech., 2000.
- [22] Federal Communications Commission, "Revision of part 15 of the commission's rules regarding ultra-wideband transmission systems, first report and order," Feb. 2002.
- [23] Liuqing Yang and G. B. Giannakis, "Ultra-wideband communications: an idea whose time has come," *IEEE Signal Processing Magazine*, vol. 21, no. 6, pp. 26–54, 2004.
- [24] M. Z. Win, D. Dardari, A. F. Molisch, W. Wiesbeck, and Jinyun Zhang, "History and applications of uwb," *Proceedings of the IEEE*, vol. 97, no. 2, pp. 198–204, 2009.
- [25] "The commission of the european communities, commission decision of 21 february 2007 on allowing the use of the radio spectrum for equipment using ultra-wideband technology in a harmonised manner in the community. official journal of the european union," Feb. 2007.

-
- [26] R. Kohno, "Interpretation and future modification of Japanese regulation for UWB," *IEEE P802.15-06/261r0*, May 2006.
- [27] M. Z. Win and R. A. Scholtz, "Impulse radio: how it works," *IEEE Communications Letters*, vol. 2, no. 2, pp. 36–38, 1998.
- [28] "IEEE 802.15.4a WPAN low rate alternative PHY task group 4a (tg4a)," 2007.
- [29] Zafer Sahinoglu and Ismail Guvenc, "Multiuser interference mitigation in noncoherent UWB ranging via nonlinear filtering," *EURASIP J. Wireless Commun. Netw.*, vol. 2006, no. 1, pp. 1–10, 2006.
- [30] I. Guvenc, Z. Sahinoglu, and P. V. Orlik, "ToA estimation for IR-UWB systems with different transceiver types," *IEEE Transactions on Microwave Theory and Techniques*, vol. 54, no. 4, pp. 1876–1886, 2006.
- [31] L. Stoica, A. Rabbachin, and I. Oppermann, "A low-complexity noncoherent IR-UWB transceiver architecture with ToA estimation," *IEEE Transactions on Microwave Theory and Techniques*, vol. 54, no. 4, pp. 1637–1646, June 2006.
- [32] Chiara Falsi, Davide Dardari, Lorenzo Mucchi, and Moe Z Win, "Time of arrival estimation for UWB localizers in realistic environments," *EURASIP J. Appl. Signal Process.*, vol. 2006, no. 1, pp. 1–13, 2006.
- [33] I. Guvenc and Z. Sahinoglu, "Threshold-based TOA estimation for impulse radio UWB systems," in *Proc. IEEE Int. Conf. Ultra-Wideband (ICUWB)*, Sept. 2005, pp. 420–425.
- [34] I. Guvenc and Z. Sahinoglu, "Threshold-based TOA estimation for impulse radio UWB systems," in *IEEE International Conference on Ultra-Wideband*, 2005, pp. 420–425.
- [35] R. Hoor and H. Tomlinson, "Delay-hopped transmitted-reference RF communications," in *IEEE Conference on Ultra Wideband Systems and Technologies, Digest of Papers.*, 2002, pp. 265–269.
- [36] Liuqing Yang and G. B. Giannakis, "Timing ultra-wideband signals with dirty templates," *IEEE Trans. Commun.*, vol. 53, no. 11, pp. 1952–1963, Nov. 2005.
- [37] E. Ekrem, M. Koca, and H. Delic, "Iterative synchronization of multiuser ultra-wideband signals," *IEEE Trans. Wireless Commun.*, vol. 9, no. 10, pp. 3040–3051, Oct. 2010.
- [38] D. Dardari, Chia-Chin Chong, and M. Z. Win, "Threshold-based time-of-arrival estimators in UWB dense multipath channels," *IEEE Trans. Commun.*, vol. 56, no. 8, pp. 1366–1378, Aug. 2008.
- [39] D. Dardari, A. Giorgetti, and M. Z. Win, "Time-of-arrival estimation of UWB signals in the presence of narrowband and wideband interference," in *Proc. IEEE Int. Conf. Ultra-Wideband (ICUWB)*, Sept. 2007, pp. 71–76.

REFERENCES

- [40] A. F. Molisch, Kannan Balakrishnan, Chia-Chin Chong, and Andrew Emami, Shahriar Fort, "IEEE 802.15.4a channel model final report," Tech. Rep., IEEE 802.15-04-0662-02-004a, 2005.
- [41] Christopher M. Danforth, "Chaos in an atmosphere hanging on a wall," *Mathematics of Planet Earth*, vol. Retrieved 4, April. 2013.
- [42] Jules Henri Poincare, "Sur le problem des trois corps et les equations de la dynamique. divergence des series de m. lindstedt," *Acta Mathematica*, pp. 1–270, 1890.
- [43] Florin Diacu and Philip Hølems, *Celestial Encounters: The Origins of Chaos and Stability*, Princeton University Press, 1996.
- [44] Edward N. Lorenz, "Deterministic non-periodic flow," *Journal of the atmospheric sciences*, vol. 20, pp. 130–141, 1963.
- [45] J. M. Ottino, F. j. Muzzio, M. Tjahjadi, J. G. Franjioe, S. C. Jana, and H. A. Kusch, "Chaos, symmetry and self-similarity: Exploiting order and disorder in mixing process," *Science*, vol. 257, pp. 754–760, 1992.
- [46] Ljupco Kocarev, "Chaos-based cryptography: A brief overview," *IEEE Communication Magazine*, vol. 1, pp. 6–21, 2001.
- [47] P. Bergamo, P. D'Arco, A. De Santis, and L. Kocarev, "Security of public key cryptosystems based on chebyshev polynomials," *IEEE Trans. on circuit and system I: Regular Paper*, vol. 52, no. 7, pp. 1382–1393, 2005.
- [48] Tao Yang, C.W. Wu, and L.O. Chua, "Cryptography based on chaotic systems," *IEEE Trans. on Circuits and Systems I: Fundamental Theory and Applications*, vol. 44, no. 5, pp. 469–472, 1997.
- [49] A. Garfinkel, M. L. Spano, W. L. Ditto, and J. Weiss, "Controlling cardiac chaos," *Science*, vol. 257, pp. 1230–1235, 1992.
- [50] S. J. Schiff, K. Jerger, D. H. Duong, T. Chang, M. L. Spano, and W. L. Ditto, "Controlling chaos in the brain," *Nature*, vol. 370, pp. 615–620, 1994.
- [51] Celso Grebogi and James A. Yorke, *The impact of chaos on science and society*, United National University Press, 1997.
- [52] Stephen H. Kellert, *In the Wake of Chaos: Unpredictable Order in Dynamical Systems*, University of Chicago Press, 1993.
- [53] Kathleen T. Alligood, Tim D. Sauer, and James A. Yorke, *Chaos: An Introduction to Dynamical System*, Springer, 2001.
- [54] Robert M. May, "Simple mathematical models with very complicated dynamics," *Nature*, vol. 261, pp. 459–467, 1976.

- [55] M. S. Willsey, K. M. Cuomo, and A. V. Oppenheim, "Selecting the Lorenz parameters for wideband radar waveform generation," *International Journal of Bifurcation and Chaos*, 2010.
- [56] J. M. H. Elmirghani and R. A. Cryan, "Communication using chaotic masking," in *IEE Colloquium on Exploiting Chaos in Signal Processing*, 1994, pp. 12/1–12/6.
- [57] J. M. H. Elmirghani and R. A. Cryan, "New chaotic based communication technique with multiuser provision," *IEEE Electronics Letters*, vol. 30, no. 15, pp. 1206–1207, 1994.
- [58] K. Murali, H. Leung, and Haiyang Yu, "Design of noncoherent receiver for analog spread-spectrum communication based on chaotic masking," *IEEE Trans. on Circuits and Systems I: Fundamental Theory and Applications*, vol. 50, no. 3, pp. 432–441, 2003.
- [59] Nan Xie and H. Leung, "An analog multi-user spread spectrum technique for wireless home automation," *IEEE Trans. on Consumer Electronics*, vol. 48, no. 4, pp. 1016–1025, 2002.
- [60] H. Leung and J. Lam, "Design of demodulator for the chaotic modulation communication system," *IEEE Trans. on Circuits and Systems I: Fundamental Theory and Applications*, vol. 44, no. 3, pp. 262–267, 1997.
- [61] Chuan Lian Koh and T. Ushio, "Digital communication method based on m-synchronized chaotic systems," *IEEE Trans. on Circuits and Systems I: Fundamental Theory and Applications*, vol. 44, no. 5, pp. 383–390, 1997.
- [62] G. Kolumban, "Theoretical noise performance of correlator-based chaotic communications schemes," *IEEE Trans. on Circuits and Systems I: Fundamental Theory and Applications*, vol. 47, no. 12, pp. 1692–1701, 2000.
- [63] G. Kolumban, M. P. Kennedy, Z. Jako, and G. Kis, "Chaotic communications with correlator receivers: theory and performance limits," *Proceedings of the IEEE*, vol. 90, no. 5, pp. 711–732, 2002.
- [64] K. M. Cuomo, A. V. Oppenheim, and Steven H. Strogatz, "Synchronization of lorenz-based chaotic circuits with applications to communications," *IEEE Trans. on Circuits and Systems II: Analog and Digital Signal Processing*, vol. 40, no. 10, pp. 626–633, 1993.
- [65] K. M. Cuomo and A. V. Oppenheim, "Circuits implementation of synchronized chaos with applications to communications," *Physics Rev. Letter*, vol. 71, pp. 65–68, 1993.
- [66] H. Dedieu, M. P. Kennedy, and Martin Hasler, "Chaos shift keying: modulation and demodulation of a chaotic carrier using self-synchronizing chua's circuits," *IEEE Trans. on Circuits and Systems II: Analog and Digital Signal Processing*, vol. 40, no. 10, pp. 634–642, 1993.
- [67] M. P. Kennedy, R. Rovatti, and G. Setti, *Chaotic Electronics in Telecommunication*, CRC Press, 2000.

REFERENCES

- [68] G. Kolumban, M. P. Kennedy, and G. Kis, "Performance improvement of chaotic communication systems," in *Proceeding European Conference on Circuit Theory and Design*, Sept. 1997, pp. 284–289.
- [69] G. Kolumban, B. Vizvari, W. Schwarz, and A. Abel, "Differential chaos shift keying: a robust coding for chaotic communication," in *Proceeding International Specialist Workshop on Nonlinear Dynamics of Electronics Systems*, June 1996, p. 81.
- [70] R. L. Pickholtz, L. B. Milstein, and D. L. Schilling, "Spread spectrum for mobile communications," *IEEE Trans. on Vehicular Technology*, vol. 40, no. 2, pp. 313–322, May 1991.
- [71] E. H. Dinan and B. Jabbari, "Spread codes for direct sequence CDMA and wideband CDMA cellular networks," *IEEE Communication Magazine*, pp. 48–54, June 1998.
- [72] G. Heidari-Bateni and C. D. McGillem, "Chaotic sequences for spread spectrum: an alternative to pn-sequences," in *Proceedings of IEEE International Conference on Selected Topics in Wireless Communications*, June 1992, pp. 437–440.
- [73] G. Heidari-Bateni and C. D. McGillem, "A chaotic direct-sequence spread-spectrum communication system," *IEEE Trans. on Communications*, vol. 42, no. 234, pp. 1524–1527, Apr. 1994.
- [74] G. Mazzini, G. Setti, and R. Rovatti, "Chaotic complex spreading sequences for asynchronous DS-CDMA. I. System modeling and results," *IEEE Trans. Circuits Syst. I: Fundam. Theory Appl.*, vol. 44, no. 10, pp. 937–947, Oct 1997.
- [75] R. Rovatti, G. Setti, and G. Mazzini, "Chaotic complex spreading sequences for asynchronous ds-cdma. part ii. some theoretical performance bounds," *IEEE Trans. on Circuits and Systems I: Fundamental Theory and Applications*, vol. 45, no. 4, pp. 496–506, Apr. 1998.
- [76] R. Rovatti, G. Mazzini, and G. Setti, "Interference bounds for DS-CDMA systems based on chaotic piecewise-affine markov maps," *IEEE Trans. on Circuits and Systems I: Fundamental Theory and Applications*, vol. 47, no. 6, pp. 885–896, June 2000.
- [77] G. Setti, G. Mazzini, and R. Rovatti, "Chaos-based spreading sequence optimization for DS-CDMA synchronization," *IEICE Trans. Fund.*, vol. E82-A, no. 9, pp. 1737–1746, 1999.
- [78] R. Rovatti, G. Mazzini, and G. Setti, "Enhanced rake receivers for chaos-based ds-cdma," *IEEE Trans. on Circuits and Systems I: Fundamental Theory and Applications*, vol. 48, no. 7, pp. 818–829, July 2001.
- [79] R. Rovatti and G. Mazzini, "Interference in DS-CDMA systems with exponentially vanishing autocorrelations: chaos-based spreading is optimal," *Electronics Letters*, vol. 34, no. 20, pp. 1911–1913, 1998.

- [80] G. Mazzini, R. Rovatti, and G. Setti, "Interference minimisation by autocorrelation shaping in asynchronous ds-cdma systems: chaos-based spreading is nearly optimal," *Electronics Letters*, vol. 35, no. 13, pp. 1054–1055, 1999.
- [81] T. Kohda and H. Fujisaki, "Variances of multiple access interference code average against data average," *Electronics Letters*, vol. 36, no. 20, pp. 1717–1719, 2000.
- [82] G. Setti, G. Mazzini, R. Rovatti, and S. Callegari, "Statistical modeling of discrete-time chaotic processes-basic finite-dimensional tools and applications," *Proceedings of the IEEE*, vol. 90, no. 5, pp. 662–690, 2002.
- [83] R. Rovatti, G. Mazzini, and G. Setti, "On the ultimate limits of chaos-based asynchronous ds-cdma-i: basic definitions and results," *IEEE Trans. on Circuits and Systems I: Regular Papers*, vol. 51, no. 7, pp. 1336–1347, 2004.
- [84] G. Kaddoum, P. Charge, and D. Roviras, "A generalized methodology for bit-error-rate prediction in correlation-based communication schemes using chaos," *IEEE Communications Letters*, vol. 13, no. 8, pp. 567–569, August 2009.
- [85] Georges Kaddoum, Martial Coulon, Daniel Roviras, and Pascal Chargé, "Theoretical performance for asynchronous multi-user chaos-based communication systems on fading channels," *Signal Processing*, vol. 90, no. 11, pp. 2923–2933, 2010.
- [86] Georges Kaddoum, Daniel Roviras, Pascal Charge, and Daniele Fournier-Prunaret, "Accurate bit error rate calculation for asynchronous chaos-based DS-CDMA over multipath channel," *EURASIP Journal on Advances in Signal Processing*, vol. 2009, no. 1, pp. 1–12, 2009.
- [87] Georges Kaddoum, Daniel Roviras, Pascal Chargé, and Danièle Fournier-Prunaret, "Robust synchronization for asynchronous multi-user chaos-based DS-CDMA," *Signal Processing*, vol. 89, no. 5, pp. 807–818, 2009.
- [88] Ling Cong and Sun Songgeng, "Chaotic frequency hopping sequences," *IEEE Trans. on Communications*, vol. 46, no. 11, pp. 1433–1437, 1998.
- [89] Ling Cong and Wu Xiaofu, "Design and realization of an fpga-based generator for chaotic frequency hopping sequences," *IEEE Trans. on Circuits and Systems I: Fundamental Theory and Applications*, vol. 48, no. 5, pp. 521–532, 2001.
- [90] G. Cimatti, R. Rovatti, and G. Setti, "Chaos-based spreading in ds-ubw sensor networks increases available bit rate," *EEE Trans. on Circuits and Systems I: Regular PapersI*, vol. 54, no. 6, pp. 1327–1339, 2007.
- [91] G. M. Maggio, N. Rulkov, and L. Reggiani, "Pseudo-chaotic time hopping for ubw impulse radio," *IEEE Trans. on Circuits and Systems I: Fundamental Theory and Applications*, vol. 48, no. 12, pp. 1424–1435, 2001.
- [92] D. Lind and B. Marcus, *An Introduction to Symbolic Dynamics and Coding*, Cambridge University Press, 1995.

REFERENCES

- [93] D. C. Laney, G. M. Maggio, F. Lehmann, and L. Larson, "Multiple access for uwb impulse radio with pseudochaotic time hopping," *IEEE Journal on Selected Areas in Communications*, vol. 20, no. 9, pp. 1692–1700, 2002.
- [94] Jr. Sushchik, M., N. Rulkov, L. Larson, L. Tsimring, H. Abarbanel, K. Yao, and A. Volkovskii, "Chaotic pulse position modulation: a robust method of communicating with chaos," *IEEE Communications Letters*, vol. 4, no. 4, pp. 128–130, 2000.
- [95] N. F. Rulkov, M. M. Sushchik, L. S. Tsimring, and A. R. Volkovskii, "Digital communication using chaotic-pulse-position modulation," *IEEE Trans. on Circuits and Systems I: Fundamental Theory and Applications*, vol. 48, no. 12, pp. 1436–1444, 2001.
- [96] A. Bauer, "Chaotic signals for cw-ranging systems. a baseband system model for distance and bearing estimation," in *Circuits and Systems, 1998. ISCAS '98. Proceedings of the 1998 IEEE International Symposium on*, 1998, vol. 3, pp. 275–278.
- [97] B. C. Flores, E. A. Solis, and G. Thomas, "Assessment of chaos-based fm signals for range-doppler imaging," *IEE Proceedings - Radar, Sonar and Navigation*, vol. 150, no. 4, pp. 313–322, 2003.
- [98] Fan-Yi Lin and Jia-Ming Liu, "Chaotic radar using nonlinear laser dynamics," *IEEE Journal of Quantum Electronics*, vol. 40, no. 6, pp. 815–820, 2004.
- [99] T. L. Carroll, "Chaotic system for self-synchronizing Doppler measurement," *Chaos*, vol. 15, pp. 1–5, 2005.
- [100] K.A. Lukin, "Millimeter wave noise radar applications: theory and experiment," in *Physics and Engineering of Millimeter and Sub-Millimeter Waves, 2001. The Fourth International Kharkov Symposium on*, 2001, vol. 1, pp. 68–73.
- [101] V. Venkatasubramanian and H. Leung, "A novel chaos-based high-resolution imaging technique and its application to through-the-wall imaging," *IEEE Signal Processing Letters*, vol. 12, no. 7, pp. 528–531, 2005.
- [102] Xin Wu, Weixian Liu, Lei Zhao, and J. S. Fu, "Chaotic phase code for radar pulse compression," in *Radar Conference, 2001. Proceedings of the 2001 IEEE*, 2001, pp. 279–283.
- [103] Wen Hu, Zhong Liu, and Chunbiao Li, "Synchronization-based scheme for calculating ambiguity functions of wideband chaotic signals," *IEEE Trans. on Aerospace and Electronic Systems*, vol. 44, no. 1, pp. 367–372, 2008.
- [104] V. Venkatasubramanian, H. Leung, and Xiaoxiang Liu, "Chaos uwb radar for through-the-wall imaging," *IEEE Trans. on Image Processing*, vol. 18, no. 6, pp. 1255–1265, 2009.
- [105] E. Gambi, F. Chiaraluce, and S. Spinsante, "Chaos-based radars for automotive applications: Theoretical issues and numerical simulation," *IEEE Trans. on Vehicular Technology*, vol. 57, no. 6, pp. 3858–3863, 2008.

-
- [106] M. S. Willsey, K. M. Cuomo, and A. V. Oppenheim, "Quasi-orthogonal wideband radar waveforms based on chaotic systems," *IEEE Trans. on Aerospace and Electronic Systems*, vol. 47, no. 3, pp. 1974–1984, 2011.
- [107] L. Fortuna, M. Frasca, and A. Rizzo, "Chaotic pulse position modulation to improve the efficiency of sonar sensors," *IEEE Trans. on Instrumentation and Measurement*, vol. 52, no. 6, pp. 1809–1814, 2003.
- [108] F. Alonge, M. Branciforte, and F. Motta, "A novel method of distance measurement based on pulse position modulation and synchronization of chaotic signals using ultrasonic radar systems," *IEEE Trans. on Instrumentation and Measurement*, vol. 58, no. 2, pp. 318–329, 2009.
- [109] A. S. Dmitriev, M. Hasler, A. I. Panas, and K. V. Zakharchenko, "Basic principles of direct chaotic communications," *Nonlinear Phenomena in Complex System*, vol. 4, no. 1, pp. 1–14, 2002.
- [110] I. Guvenc and H. Arslan, "Design and performance analysis of TH sequences for UWB-IR systems," in *IEEE Wireless Communications and Networking Conference, (WCNC)*, 2004, vol. 2, pp. 914–919.
- [111] Zhenyu Zhang, Fanxin Zeng, and Lijia Ge, "Correlation properties of time-hopping sequences for impulse radio," in *Pro. IEEE International Conference on Acoustics, Speech, and Signal Processing, (ICASSP)*, 2003, vol. 4, pp. IV–141–4.
- [112] Hongbin Li, Jian Li, and S. L. Miller, "Decoupled multiuser code-timing estimation for code-division multiple-access communication systems," *IEEE Trans. Commun.*, vol. 49, no. 8, pp. 1425–1436, Aug. 2001.
- [113] A. Giorgetti and M. Chiani, "A new approach to time-of-arrival estimation based on information theoretic criteria," in *Proc. IEEE Int. Conf. Ultra-Wideband (ICUWB)*, Sept. 2011, pp. 460–464.
- [114] A. Giorgetti and M. Chiani, "Time-of-arrival estimation based on information theoretic criteria," *IEEE Trans. Signal Process.*, 2013, doi: 10.1109/TSP.2013.2239643.
- [115] D. M. Zheng, Jian Li, and S. L. Miller, "An efficient code-timing estimator for DS-CDMA signals," *IEEE Trans. Signal Process.*, vol. 45, no. 1, pp. 82–89, Jan 1997.

REFERENCES

List of Publications

- Hang Ma, Pascal Acco, Marie-Laure Boucheret and Daniele Fournier-Prunaret, "Low complexity TOA Estimator for Multiuser DS-UWB system" in *10th Workshop on Positioning Navigation and Communication (WPNC)*, 20th-21th March, 2013.
- Hang Ma, Pascal Acco, Marie-Laure Boucheret and Daniele Fournier-Prunaret, "Multiuser Interference Mitigation in DS-UWB Ranging System" in *10th International Symposium on Wireless Communication Systems (ISWCS)*, 27th-30th August, 2013.
- Hang Ma, Pascal Acco, Marie-Laure Boucheret and Daniele Fournier-Prunaret, "Chaos-based TOA Estimator for DS-UWB Ranging Systems in Multiuser Environment" in *21st European Signal Processing Conference (EUSIPCO)*, 9th-13th September, 2013.

Résumé

Dans les décennies à venir, la connaissance d'informations très précises concernant la position d'un objet permettra de créer des applications révolutionnaires dans les domaines sociaux, médicaux, commerciaux et militaires. La technologie Ultra-Wideband (UWB) est considérée comme un bon candidat permettant de fournir des capacités de localisation précise grâce à la mesure de l'estimation du temps d'arrivée (TOA). Dans cette thèse, des algorithmes de mesure de distance dans le cas multi-utilisateurs pour des systèmes UWB sont étudiés afin d'atteindre une bonne précision pour une faible complexité, avec de la robustesse aux interférences multi-utilisateur et dans le cas d'un grand nombre d'utilisateurs.

Au cours de la dernière décennie, les signaux chaotiques ont reçu une attention significative en raison d'un certain nombre de caractéristiques intéressantes. Les signaux chaotiques sont des signaux non périodiques, déterministes ou considérés comme pseudo-aléatoires provenant de systèmes dynamiques non linéaires. Leur bonne autocorrélation et leurs faibles propriétés d'inter corrélation les rendent particulièrement résistants aux évanouissements par trajets multiples et capables d'atténuer les interférences multi-utilisateur (MUI). En raison de leur grande sensibilité aux conditions initiales, il est possible de générer un grand nombre de signaux chaotiques pour accroître la capacité globale du système.

Dans cette thèse, deux nouveaux algorithmes d'estimation de TOA sont proposés dans un cadre multi-utilisateur avec une faible complexité et une bonne robustesse. Le nombre d'utilisateurs pris en charge par ces deux algorithmes est beaucoup plus grand que dans le cas des estimateurs de TOA actuels. Cependant, l'utilisation de séquences d'étalement classique et d'impulsion limite l'amélioration des performances et la capacité du système. Afin d'apporter des améliorations, des signaux chaotiques sélectionnés sont utilisés comme séquences d'étalement ou impulsion dans les algorithmes proposés. Grâce à l'utilisation de signaux chaotiques, notre algorithme est non seulement amélioré, mais permet également l'utilisation d'un plus grand nombre d'utilisateurs par comparaison avec l'algorithme utilisant des signaux classiques.

La motivation de la thèse est de développer de nouveaux estimateurs TOA qui sont plus robustes de multiples graves et l'effet de MUI et à exploiter la propriété des systèmes chaotiques afin de renforcer la capacité de résistance des interférences et à agrandir la capacité du système de systèmes allant UWB. En travaillant sur une recherche inter-domaines, l'organisation de cette thèse est donnée comme suit:

Le chapitre 2 présente d'abord une brève introduction de technologies allant. Le principe de technologies allant communes sera expliquée avec leurs avantages et leurs inconvénients.

Après les technologies allant, la vue d'ensemble des systèmes allant UWB actuels sont introduits. Les principales sources d'erreur, le type typique des estimateurs, les algorithmes existants allant multi-utilisateurs et l'état de canal UWB sont exprimés consécutivement.

Dans le chapitre 3, la définition des systèmes chaotiques et leur génération sont expliqués au début de ce chapitre, suivie par l'introduction de deux signaux chaotiques différents, les signaux chaotiques en temps continu et signaux chaotiques à temps discret. La dernière partie de ce chapitre est consacrée à l'application de signaux chaotiques dans divers domaines tels que la communication sans fil, radar et sonar.

Les propriétés connexes allant de signaux chaotiques sont présentés dans le chapitre 4. Les principaux axes sont l'auto-corrélation, corrélation croisée et de spectre de fréquence propriétés des signaux chaotiques en temps continu et signaux chaotiques à temps discret. Cartes de Chebyshev et tente sont les exemples de signaux chaotiques à temps discret, et la forme d'onde Lorenz est choisi comme représentant de signaux chaotiques à temps continu. Par comparaison avec les séquences et les courbes de classe propagation, il est montré que les signaux chaotiques peuvent obtenir identique encore mieux autocorrélation et la propriété de corrélation croisée. De plus, le spectre de fréquence de forme d'onde Lorenz peut être facilement ajusté à la bande passante en changeant certains paramètres de Lorenz .

Après l'instauration de l'état de l'art des algorithmes allant UWB, deux nouveaux estimateurs multi de TOA sont proposées dans le chapitre 5, qui sont adaptés à l'environnement multi-utilisateur et laissez le système allant à entièrement chargée. Après avoir donné les détails des deux algorithmes, la complexité et les évaluations numériques sont présentés. Dans la partie de l'évaluation numérique, comparaison avec des algorithmes multi-utilisateurs actuels peuvent être abordés.

Dans le chapitre 6, afin d'améliorer la performance allant, les séquences et les formes d'ondes chaotiques sont choisis en fonction des besoins de l'estimateur de TOA proposé. Après l'introduction de critères de sélection, l'algorithme proposé avec des signaux chaotiques sont comparées à leurs homologues dans le cadre de l'évaluation numérique.

Dans la dernière partie, la conclusion et de la perspective de la thèse sont donnés.

CHAPITRE 2: TECHNOLOGIES ET SYSTÈME DE TÉLÉMÉTRIE

Heure d'arrivée (TOA)

En TOA estimation, la distance entre les nœuds peut être mesurée à partir du temps de propagation du signal, ou le temps de vol $\tau_f = d/c$, où d est la distance réelle entre deux nœuds et c est la vitesse de la lumière. Limites précises de TOA estimation peuvent également être quantifiés par la BCR, qui est donné dans la suite [18]

$$\sqrt{\text{Var}(\hat{\tau})} \geq \frac{1}{2\sqrt{2\pi}\sqrt{\text{SNR}\beta}} \quad (\text{R.1})$$

où $\hat{\tau}$ représente une estimation de TOA impartiale, SNR est le rapport signal-sur-bruit et β est également la bande passante effective de signal transmis. Il est observé que la précision de TOA estimation varie dans une relation inverse avec SNR et efficace de la bande passante β . Le SNR plus ou efficace de la bande passante β est, la plus précise l'estimation TOA seront.

Système de télémétrie Ultra-Wideband

Un signal UWB est caractérisé par sa très grande largeur de bande par rapport aux systèmes conventionnels à bande étroite. Selon la FCC, les signaux UWB sont caractérisés par une largeur de bande de 10 dB absolue d'au moins 500MHz, ou une largeur de bande de 10 dB fraction de plus grand que 20% [22]. Comme le montre la Fig.R.1 [1], la largeur de bande de 10 dB absolu est calculé comme la différence entre la fréquence supérieure f_H du $-10dB$ point d'émission et la fréquence inférieure f_L de la $-10dB$ point d'émission [1].

$$B = f_H - f_L \quad (R.2)$$

D'autre part, la largeur de bande fractionnaire est définie comme

$$B_{frac} = \frac{B}{f_c} \quad (R.3)$$

ou f_c est la fréquence centrale et est donnée par

$$f_c = \frac{f_H + f_L}{2} \quad (R.4)$$

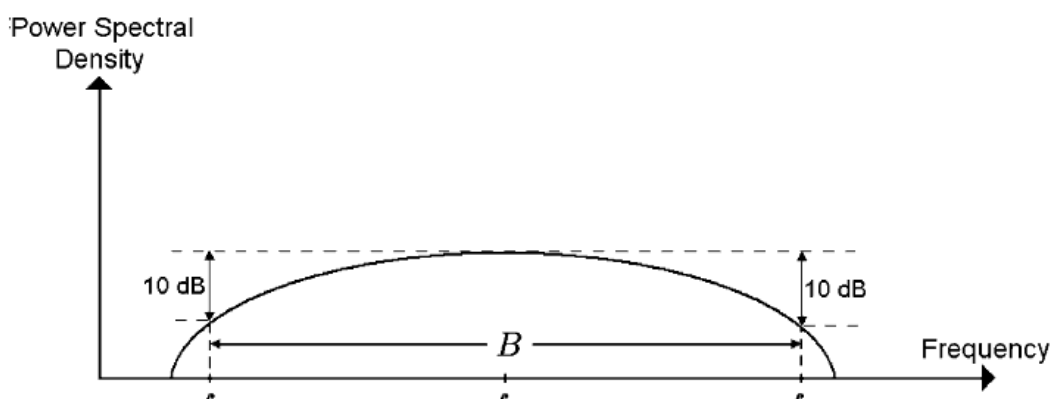


Figure R.1: La définition des signaux UWB

En raison de leur grande largeur de bande occupée, les systèmes UWB sont caractérisés par de très courtes impulsions d'une durée dans le domaine temporel. Comme la durée d'impulsion est généralement de l'ordre de la nanoseconde et est transmis dans un cycle de service faible, ce type de systèmes UWB est désigné comme la radio impulsion (IR) systèmes UWB [27]. En raison de l'utilisation d'impulsions de durée très courte et longue transmission de temps de répétition, des systèmes IR-UWB ont une possibilité d'avoir une faible consommation électrique et faible structure de la complexité de l'émetteur-récepteur, qui peut être utilisé pour la communication sans fil et les systèmes de télémétrie avec de telles exigences.

A. SOURCES D'ERREUR DANS TOA

Il y a un certain nombre de sources d'erreur qui peuvent dégrader sérieusement la précision de l'estimation de gamme. Avant d'entrer dans différents algorithmes allant, certaines de ces sources d'erreur seront examinées brièvement.

TRAJETS MULTIPLES INTERFÉRENCES Dans les systèmes basés sur l'estimation du temps, le retard de propagation du trajet direct est le paramètre souhaité. Dans les environnements pratiques, en particulier les environnements intérieurs, les signaux transmis arrivent généralement au niveau du récepteur par des chemins différents en raison des mécanismes de propagation complexes telles que la réflexion, la diffusion et la diffraction. Par conséquent, la façon de choisir la première voie d'arriver chez multiples dense est un défi pour les systèmes de télémétrie UWB.

MULTI-UTILISATEUR INTERFÉRENCES Interférence multi-utilisateurs (MUI) décrit l'interférence des autres utilisateurs (nœuds). Pour les systèmes allant, il est courant de travailler dans un environnement avec plusieurs utilisateurs, ici dans chaque récepteur, le signal reçu ne contient pas seulement le signal de l'utilisateur souhaité, mais aussi d'autres utilisateurs interférents. Comme représenté sur la Fig.R.2, le nœud A est le nœud cible, la distance de ce qui est sur le point d'être estimé par le nœud de référence. Si compte tenu de l'approche de la TOA à sens unique, Lorsque les signaux de nœud A arrivent au niveau du nœud de référence, ils ont été détériorées en raison de la présence d'interférer Node B et le nœud C. Dans ce cas, si ignorant MUI, la précision de la TOA basé envergure peut être significativement dégradée. Par conséquent, la façon d'atténuer le MUI est une autre question difficile pour les systèmes allant UWB.

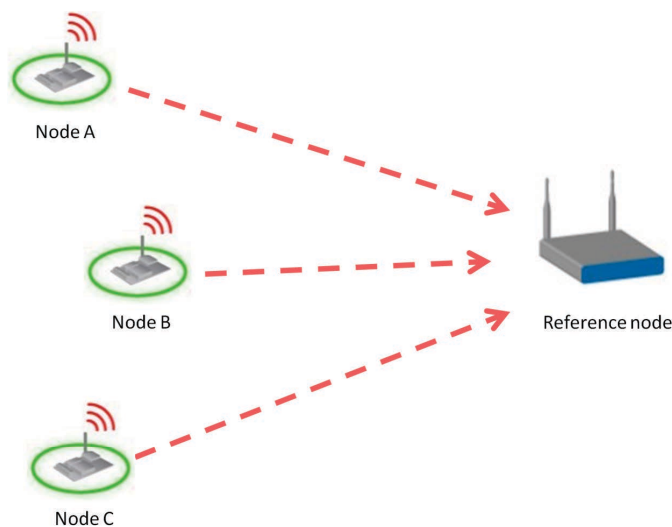


Figure R.2: The schematic diagram of multiuser interference.

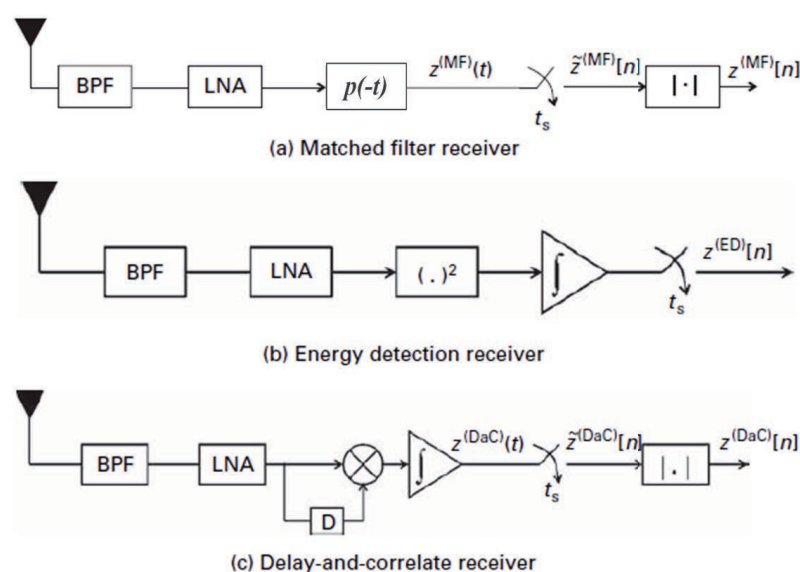


Figure R.3: Les différents régimes de l'estimateur de TOA.

B. TOA ESTIMATORS

Après l'introduction de la source de base de temps allant signal UWB et d'erreurs, les estimateurs de TOA actuelles et leur performance sont présentées dans cette section pour donner une connaissance approfondie des systèmes allant UWB. Divers estimateurs de TOA ont été proposés dans la littérature. En général, ils peuvent être classés en trois architectures de récepteurs communs, qui sont Filtre adapté (MF), la détection de l'énergie (ED), et le retard-et-corrélation (DAC) de récepteurs en fonction.

CHAPTRE 3: SYSTÈMES ET SIGNAUX CHAOTIQUES

Chaos est un comportement aperiodique dans un système déterministe qui présente dépendance sensible aux conditions initiales. Cette définition met en évidence trois caractéristiques distinguer contenues par les systèmes chaotiques,

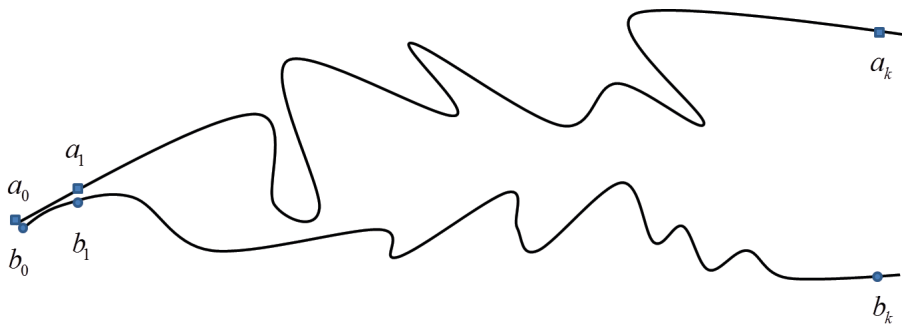


Figure R.4: Schéma de la sensibilité d'un système chaotique sous différents mais très proches des conditions initiales a_0 et B_0 .

1. Comportement apériodique implique système chaotique est erratique, pas simplement quasi-périodique avec un grand nombre de périodes.
2. Système déterministe signifie que le système chaotique n'a pas de variables aléatoires, le comportement apériodique découle de la dynamique non linéaire, mais pas de moteurs bruyants.
3. Dépendance sensible aux conditions initiales doit être la caractéristique la plus importante des systèmes chaotiques, qui est populairement appelé l'effet papillon. De petites différences dans les conditions initiales (telles que celles qui sont dues à des erreurs d'arrondi dans le calcul numérique) donnent des résultats très divergents de ces systèmes dynamiques, rendant prédiction à long terme impossible en général [52]. Fig. R.4 utilise un schéma pour montrer la sensibilité de la situation initiale dans les systèmes chaotiques, où a_0 et B_0 sont deux conditions initiales différentes avec une distance euclidienne très proche.

Système chaotique à temps discret

Tent équation

Tent équation avec le paramètre μ est la fonction réelle définie par

$$x_{n+1} = \mu \min(x_n, 1 - x_n) \tag{R.5}$$

où $x_0 \in [0, 1)$.

Chebyshev équation

Chebyshev équation est le deuxième ordre polynômes de Chebyshev exprimés en

$$x_{n+1} = 1 - 2x_n^2 \tag{R.6}$$

où $x_0 \in (-1, 1)$.

Système chaotique à temps continu

Un système chaotique en temps continu bien étudié est le système de Lorenz nommé d'après Edward Lorenz. Lorenz système est un système chaotique à trois dimensions défini par

$$\begin{aligned}\dot{x} &= \sigma(y - x) \\ \dot{y} &= rx - y - xz \\ \dot{z} &= xy - bz\end{aligned}\tag{R.7}$$

où σ , r et b sont considérés comme les paramètres de Lorenz et tous sont supérieurs à zéro. Si les contraintes suivantes sont remplies, système de Lorenz n'a pas d'état stable, et peut conduire à un comportement chaotique [55].

$$b > 0\tag{R.8}$$

$$\sigma > b + 1\tag{R.9}$$

$$r > \frac{\sigma(\sigma + b + 3)}{(\sigma - b - 1)}\tag{R.10}$$

CHAPTRE 4: PROPRIÉTÉS DE CERTAINS SIGNAUX CHAOTIQUES

Propriété de spectre

La première propriété importante du signal de mesure est la densité spectrale de puissance (PSD), ce qui nous donne un point de vue des signaux à partir du domaine de fréquence. La densité spectrale de puissance est défini comme

$$\begin{aligned}\Phi_s(j\omega) &= S(j\omega)S^*(j\omega) \\ &= |S(j\omega)|^2\end{aligned}\tag{R.11}$$

où $S(j\omega)$ est la transformée de Fourier du signal émis $s(t)$. La densité spectrale de puissance peut être reliée à l'énergie de la $s(t)$ par l'intermédiaire de l'équation de Parseval.

Dans les systèmes chaotiques, en temps continu chaotique forme d'onde est un fragment du signal chaotique en temps continu dont la durée T_c est plus longue que t_c la quasi-période d'oscillation chaotique, i.e., $T_c \gg t_c$. La largeur de bande de fréquence du pouls chaotique B_c est déterminée par la largeur de bande du signal chaotique continu en temps originale générée par la source chaotique, mais est indépendant de la durée de l'impulsion dans une large gamme de variation de la durée [109].

Pour montrer la cette propriété intuitive, PSD de Lorenz formes d'onde avec une durée différente sont donnés dans la Fig.R.5. Dans cette figure, les formes d'onde de Lorenz sont générés avec le même Lorenz paramètres $\sigma = 30$, $r = 84$, $b = 8$, mais dans la longueur différente $T_c = 31ns$ et $T_c = 127ns$. Depuis des conditions initiales différentes donnent lieu à différentes formes d'onde de Lorenz, la densité moyenne du spectre de puissance de plus de

100 réalisations est considérée comme la Fig.R.5. Comme représenté sur la Fig.R.5, bien que la longueur de deux formes d'onde de Lorenz sont très différentes, de la densité du spectre de puissance a presque pas de changement. Par conséquent, la largeur de bande de fréquence de 10 dB est également la même pour deux formes d'onde de longueur de Lorenz. Comme indiqué précédemment, les signaux chaotiques est indépendante de la durée de temps T_c pour certaine bande passante B_c , ce qui offre une grande pratique pour choisir la transmission des signaux allant.

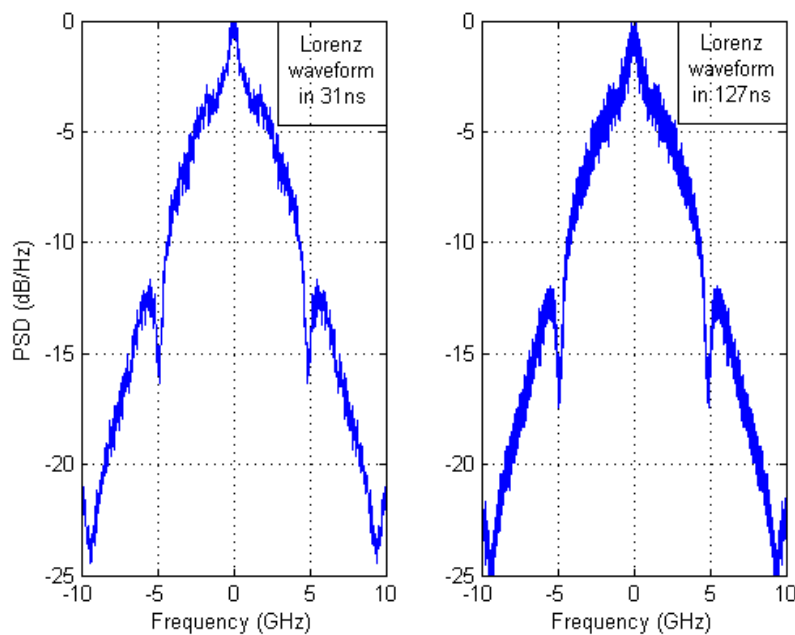


Figure R.5: Densité spectrale de puissance de Lorenz formes d'onde avec les mêmes paramètres de Lorenz dans la longueur $T_c = 31ns$ et $T_c = 127ns$.

Dans [55,106], Willsey a constaté que pour le système de Lorenz, un peu modification de système de Lorenz obtient lieu à l'exact moment-échelle forme d'onde. Par conséquent, la largeur de bande de fréquence est également mis à l'échelle en raison de la relation dans le domaine temporel et le domaine fréquentiel. En outre, Willsey rappelle que les paramètres de mise à l'échelle du système peut correspondre à un temps approximatif et mise à l'échelle d'amplitude des formes d'onde de Lorenz et correspond à l'extension de la largeur de bande de fréquence de forme d'onde aussi Lorenz.

Le PSD de système de Lorenz avec des paramètres $\sigma = 6, r = 36, b = 3$ est représentée dans la partie gauche de la Fig.R.6. La largeur de bande de fréquence de 10 dB est presque 1.3GHz, mais quand nous escaladons les systèmes de Lorenz avec $a = 3$ dont PSD est illustré comme le côté droit de la Fig.R.6, bande de fréquence pousse à 3.9GHz qui est 3 fois les largeur de bande du côté gauche. Ainsi, par heure exacte-échelle, système de Lorenz pourrait générer des signaux de Lorenz avec une bande passante arbitraire.

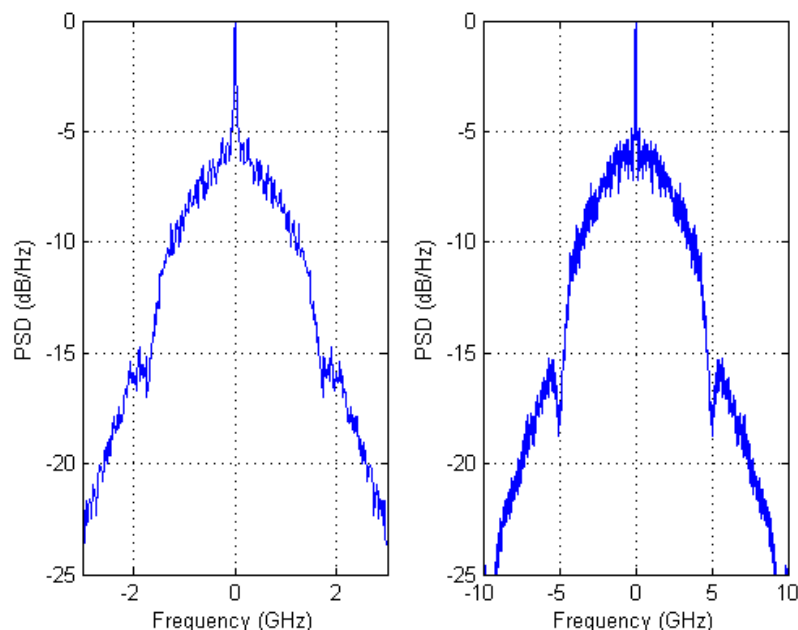


Figure R.6: Densité spectrale de puissance de l'heure exacte échelle des formes d'onde de Lorenz dans la longueur $T_c = 31ns$.

Propriété de autocorrélation

A. FONCTION AUTOCORRÉLATION DES IMPULSIONS CONTINU CHAOTIQUE

Nous considérons d'abord la propriété d'auto-corrélation de temps continu impulsion chaotique. Le système de Lorenz est choisi en tant que représentant des systèmes chaotiques à temps continu. L'impulsion Lorenz $s_c(t)$ est définie comme un état-normalisées x variables d'une durée T_s . En raison de la sensibilité de la situation initiale, K des conditions initiales différentes génère K différentes impulsions de Lorenz avec les mêmes systèmes de Lorenz qui sont désignés comme $s_{c,k}(t)$, respectivement.

En comparaison, avec les séquences d'étalement des impulsions directes sont choisis pour le comparer avec les impulsions de Lorenz. Séquences Gold $G_K(n)$ sont utilisés comme des séquences d'étalement directs pour leur bonne fonction d'autocorrélation et comparative grand nombre de séquences avec la longueur N . $p(t)$ est l'impulsion en cosinus surélevé avec la durée $T_p = 1ns$, facteur roll-off $\beta = 0.6$.

$$s_{r,k}(t) = \sum_{n=0}^{N-1} G_k(n)p(t - nT_p) \quad (\text{R.12})$$

Tout d'abord, nous comparons $s_{c,k}(t)$ et $s_{r,k}(t)$ dans la durée $T_s = 31ns$, ce qui correspond à l'utilisation des séquences Gold de longueur $N = 31$ pour cette dernière impulsion. En raison de la sensibilité de la situation initiale, un nombre considérable de Lorenz impulsions avec $T_s = 31ns$ peuvent être générés. Afin de sélectionner des impulsions de Lorenz d'une telle

grande piscine, le critère $\Phi_{G,N}$ est introduit. $\Phi_{G,N}$ est la valeur absolue des lobes latéraux pic d'autocorrélation de toutes les séquences Gold en longueur N , qui est défini comme

$$\rho_k = \max(|R_{G_k}(\tau)|) \quad \tau \neq 0, \quad k = 1, 2, \dots, N + 2 \quad (\text{R.13})$$

et

$$\varphi_{G,N} = \max(\rho_k) \quad k = 1, 2, \dots, N + 2. \quad (\text{R.14})$$

où $R_{G_k}(\tau)$ est la fonction d'autocorrélation de la séquence Gold de longueur N .

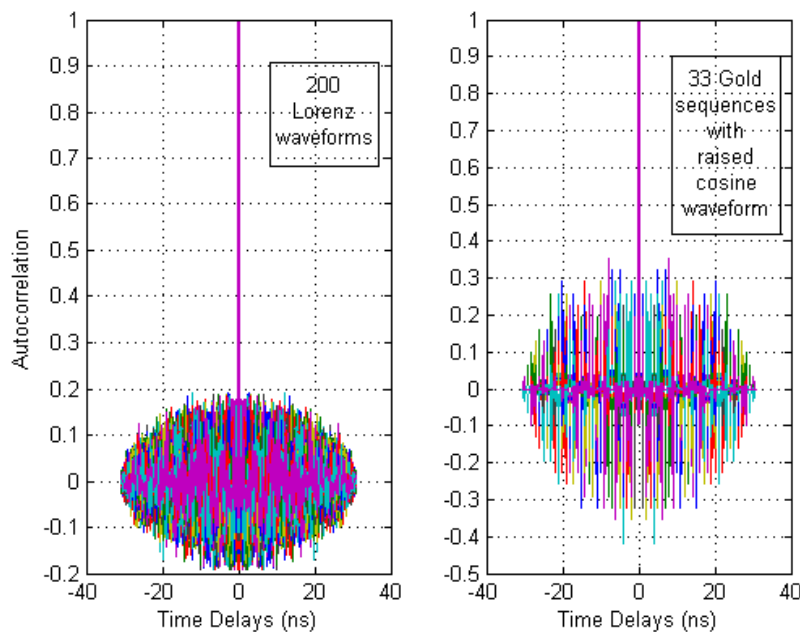


Figure R.7: Fonction d'autocorrélation de l'impulsion Lorenz sélectionné et élevé impulsion de cosinus avec des séquences Gold en $T_s = 31ns$.

Comme le montre la Fig.R.7, les valeurs des lobes latéraux de la fonction d'autocorrélation normalisée de 200 sélectionné impulsion Lorenz de longueur $T_s = 31$ sont bornées dans $(-0.2, 0.2)$. Cependant, la valeur absolue de peaky que des impulsions en cosinus surélevé avec des séquences d'or est supérieur à 0.4. En outre, le nombre d'impulsions de Lorenz dans la Fig.R.7 est 200, qui est presque six fois plus que celle de l'impulsion classique en raison de sa sensibilité à la condition initiale. Le même résultat peut également être trouvée dans la plus longue durée $T_s = 127$ comme le montre la Fig.R.8.

B. FONCTION AUTO-CORRÉLATION DES SÉQUENCES BINAIRES CHAOTIQUES

Nous présentons d'abord la génération de séquences d'étalement chaotiques directs. *Chebyshev* équation, *Tent* équation sont choisis dans cette thèse pour sa relativement faible complex-

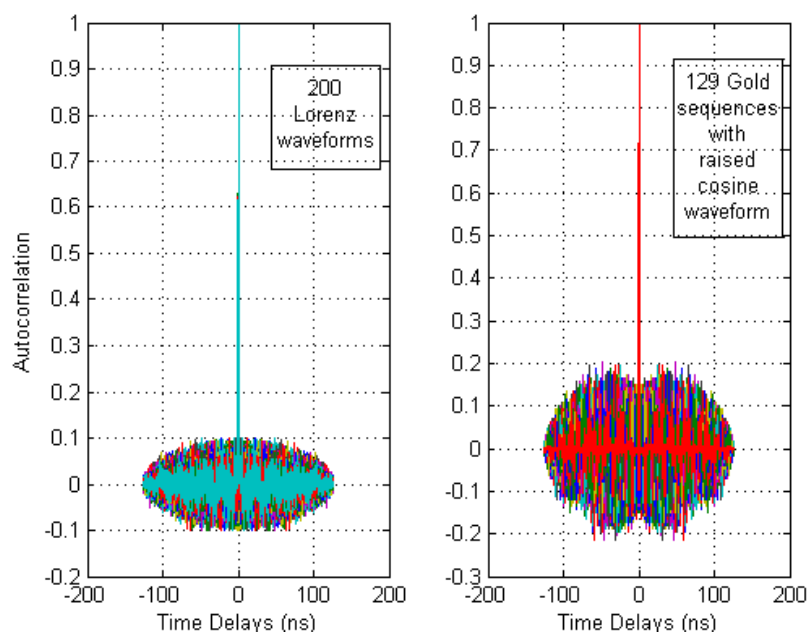


Figure R.8: Fonction d'autocorrélation de l'impulsion Lorenz sélectionné et élevé impulsion de cosinus avec des séquences Gold en $T_s = 127ns$.

ité, qui sont définis comme

$$x(n+1) = 1 - 2x(n)^2 \quad (\text{R.15})$$

et

$$x(n+1) = \begin{cases} 1.8x(n) & \text{if } x(n) < 0.5 \\ 1.8(1-x(n)) & \text{otherwise.} \end{cases} \quad (\text{R.16})$$

Depuis les séquences générées à la fois par équations de Chebyshev et Tent sont la fonction réelle, quantification est nécessaire pour cartographier les séquences de valeurs réelles en séquences binaires. Comme la plage de valeurs sont différentes pour ces deux équations, la fonction de quantification pour une équation de Chebyshev et Tent sont également différents, qui sont exprimés en tant que $Q_{C,DS}$ and $Q_{T,DS}$, respectivement.

$$x'(n) = Q_{C,DS}(x(n)) = \begin{cases} 1 & \text{if } x(n) > 0 \\ -1 & \text{otherwise} \end{cases} \quad (\text{R.17})$$

$$x'(n) = Q_{T,DS}(x(n)) = \begin{cases} 1 & \text{if } x(n) > 0.5 \\ -1 & \text{otherwise} \end{cases} \quad (\text{R.18})$$

Après quantification, les chaotiques originaux séquences $x(n)$ sont mappés en binaire chaotique séquences $x'(n)$. Bien que les conditions initiales de $x(n)$ sont différentes, certaines séquences identiques peuvent exister dans $x'(n)$ en raison du traitement de quantification. Afin d'éviter cette situation, la dernière étape du binaire chaotique génération des séquences est de vérifier toutes les séquences d'être différent. La Fig.R.9 résume la génération de séquences

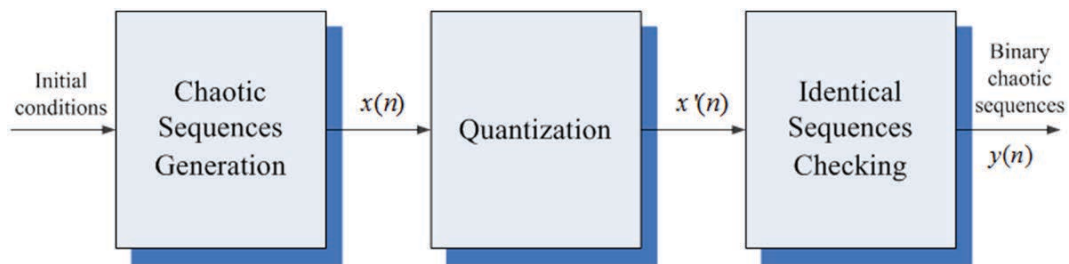


Figure R.9: The procedure of the generation of Binary chaotic sequences.

binaires chaotiques comme suit.

Après avoir passé l'ensemble de la procédure ci-dessus, nous avons obtenu un grand nombre de séquences binaires chaotique $y(n)$. Afin d'évaluer la fonction d'auto-corrélation de $y(n)$, nous choisissons également des séquences d'or que les représentants des séquences d'étalement directs classiques à comparer avec ainsi que les critères $\Phi_{G,N}$ et $\Phi_{G,N}^c$. Les séquences chaotiques binaires dont autocorrélation ou cycliques satisfait d'auto-corrélation des critères sont sélectionnés enfin.

Fig.R. 10 illustre l'autocorrélation de séquences binaires Chebyshev sélectionnés et séquences Gold dans la longueur $N = 31$, respectivement. Comme le montre la Fig.R.10, les séquences binaires de Chebyshev sélectionnés ont la même litière même un meilleur niveau des lobes latéraux de séquences que celui de Gold, mais avec beaucoup plus de nombre de séquences. Il ya 200 Chebyshev séquences binaires plutôt que seulement 33 séquences Gold de longueur 31.

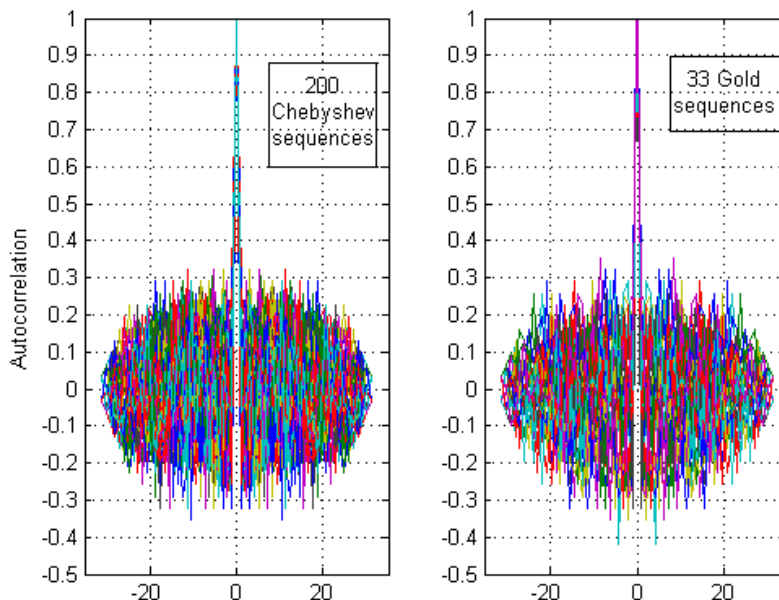


Figure R.10: Fonction d'autocorrélation des séquences de Chebyshev sélectionnés et séquences Gold avec la longueur $N = 31$.

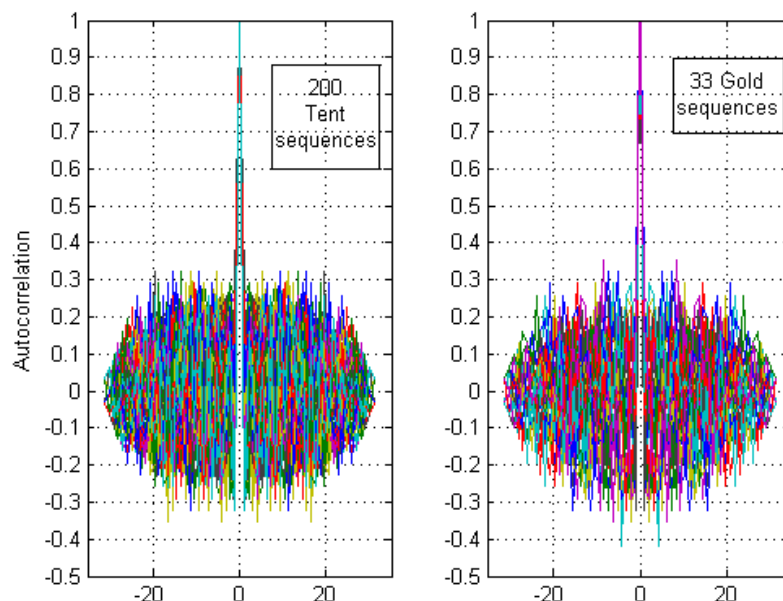


Figure R.11: Fonction d'autocorrélation des séquences de Tent sélectionnés et séquences Gold avec la longueur $N = 31$.

Sauf les séquences binaires Chebyshev, des séquences binaires de Tent ont également la même propriété d'auto-corrélation qui sont présentés comme la Fig.R.11. A partir des exemples de Chebyshev et des séquences binaires de tente, nous pouvons constater que dans l'aspect de la fonction d'auto-corrélation, la limitation de nombre d'utilisateurs dans les séquences d'or n'existe pas dans les séquences chaotiques plus, ce qui peut augmenter la capacité du système de multi grandement.

CHAPTRE 5: MULTI-UTILISATEUR TOA ESTIMATEURS

Le système d'une part à l'étude est un système K utilisateur DS-UWB utilisant binaire déplacement de phase modulation (BPSK). Le signal transmis par le k ième utilisateur est réalisée sous la forme

$$s_k(t) = \sqrt{P_k} \sum_{m=0}^{M-1} d_k(m) \sum_{n=0}^{N-1} u_k(n) p(t - nT_f - mT_d) \quad (\text{R.19})$$

où P_k est la puissance transmise de l'utilisateur k -ième, M est le nombre de bits de données considérées pour TOA estimation, $d_k(m) \in \{\pm 1\}$ est le m -ième bit transmis, $u_k(n) \in \{\pm 1\}$ est la séquence d'étalement direct avec longueur N de l'utilisateur k . $p(t)$ est la forme d'impulsion avec une durée d'impulsion T_p , T_c est la durée de la puce $T_c \geq T_p$. $T_f = N_c T_c$ est la durée de trame, où N_c est le nombre de jetons dans un cadre. $T_d = NT_f$ est l'intervalle de bits de données. Si nous adoptons une alternative séquences d'étalement $g_k(i) \in \{\pm 1, 0\}$, $s_k(t)$ peut

être réécrite comme

$$s_k(t) = \sqrt{P_k} \sum_{m=0}^{M-1} d_k(m) \sum_{i=0}^{NN_c-1} g_k(i) p(t - iT_c - mT_d) \quad (\text{R.20})$$

with

$$g_k(i) = \begin{cases} u_k(i/N_c) & \text{if } i \bmod N_c = 0 \\ 0 & \text{otherwise.} \end{cases} \quad (\text{R.21})$$

Lorsque les signaux transmis sont passés à travers le canal à trajets multiples est décrit dans le modèle de canal IEEE 802.15.4a [40], le signal reçu peut être exprimé sous la forme

$$r(t) = \sum_{k=1}^K \sum_{q=1}^{L_k} a_{k,q} s_k(t - \tau_{k,q}) + n(t) \quad (\text{R.22})$$

où $a_{k,q}$ et $\tau_{k,q}$ désignent les coefficients et temps de canal retards complexes de l' q -ième composante de trajets multiples de la k e utilisateur respectivement. L_k est le nombre de trajets multiples pour la k -ième utilisateur. $\tau_{k,1}$ est le paramètre d'intérêt dans TOA estimation. $n(t)$ est le bruit blanc gaussien additif avec zéro densité spectrale de puissance moyenne et double face de $N_o/2$. Par souci de simplicité, nous ne considérons que la réception de M bits, et supposons que le premier utilisateur est l'utilisateur d'intérêt. Par conséquent,

$$r(t) = \sum_{k=1}^K \sum_{q=1}^{L_k} \sqrt{P_k} a_{k,q} \sum_{m=0}^{M-1} d_k(m) \sum_{i=0}^{NN_c-1} g_k(i) p(t - iT_c - mT_d - \tau_{k,q}) + n(t) \quad (\text{R.23})$$

Nous supposons que

$$\tau_{k,q} = p_{k,q} T_c \quad (\text{R.24})$$

où $p_{k,q}$ est un entier dans $\{0, 1, \dots, NN_c - 1\}$. Temporisation est approchée à être des multiples entiers de la durée de puce T_c ne contenant pas la partie fractionnaire de la mise à l'échelle de T_c . Etant donné que dans le système UWB, T_c est de l'ordre de la nano-seconde, il s'agit d'un rapprochement doux pour allant de précision. Ensuite, TOA estimation de tous les utilisateurs K est équivalente à l'estimation de $p_{k,1}$.

Pour le récepteur, nous adoptons intégrer-and-dump filtre (IDF) avec temps d'intégration T_c comme le filtre de réception. Comme on le voit dans la Fig.R.12, si le pouls de cosinus est l'impulsion émise, la sortie de MF a un lobe principal étroit pointu, qui a fortement diminué lorsque les différences de temps augmente. Si le taux d'échantillonnage est suffisamment élevée, il est certain que l'échantillon est située à proximité de la valeur de crête qui amène le temps de retard précis estimation. Par conséquent, le rendement allant précis est obtenu. En revanche, si la fréquence d'échantillonnage n'est pas au moins aussi élevée que la fréquence de Nyquist, les performances de l'estimation de retard de temps se dégrade pas de façon importante en raison de l'échantillon étant suffisamment proche de la valeur de crête. Dans la partie de la FID, bien que la plus grande valeur est inférieure à la valeur de crête de sortie MF, la sortie de la FID atteint un plancher lorsque le temps dans $[-0.4T_c, 0.4T_c]$. Ce phénomène est un inconvenient quand le taux d'échantillonnage est le taux de Nyquist ou supérieur. Depuis la plage

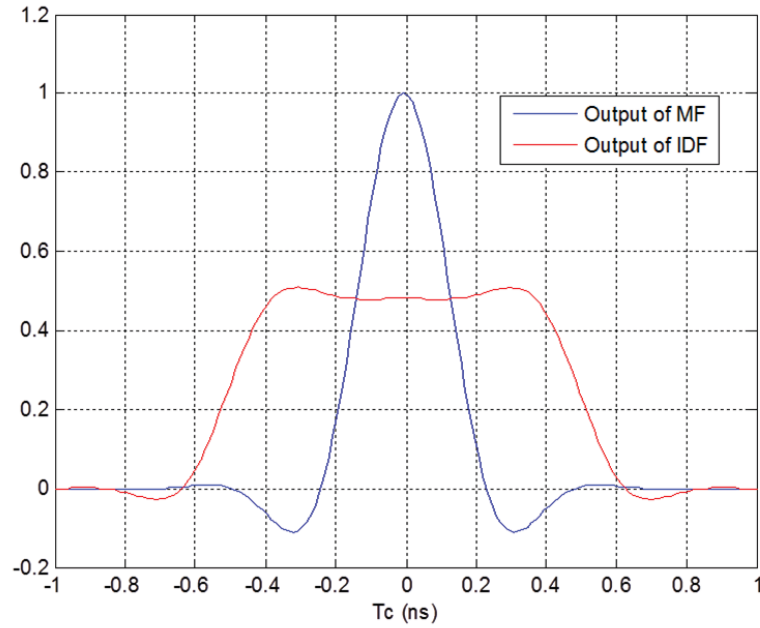


Figure R.12: La sortie du filtre adapté (MF) et intégrer-et-dump filtre (IDF) de l'impulsion de cosinus.

de l'ambiguïté est assez large, vous ne pouvez pas trouver le temps de retard exact. Toutefois, si un taux d'échantillonnage plus faible est utilisée et la précision de la temporisation estimation est seulement nécessaire de l'ordre de T_c , IDF est bien adapté à MF. En raison de l'existence de la parole à partir de $[-0.4T_c, 0.4T_c]$ dans la sortie de la IDF, peu importe où se trouvent les échantillons, les valeurs de sortie sont presque les mêmes. Bien que dans la zone $[-0.5T_c, -0.4T_c]$ et $[0.4T_c, 0.5T_c]$, la sortie passe à la moitié de la chaussée progressivement, il reste bien supérieure à celle des échantillons sur la durée $[-0.5T_c, 0.5T_c]$ dont les valeurs sont proches de 0.

Avec IDF comme le front-end avec intégrante T_c , la séquence reçue est exprimé en

$$r(l) = \sum_{k=1}^K \sum_{q=1}^{L_k} \frac{1}{T_c} \int_{(l-1)T_c}^{lT_c} a_{k,q} s_k(t - \tau_{k,q}) dt + n(l) \quad (\text{R.25})$$

$$l = 1, 2, \dots, NN_c$$

Si nous considérons l'estimation du maximum de vraisemblance et supposons que tous les bits de données et séquences d'étalement de tous les utilisateurs sont connus, on peut obtenir l'estimation de temps de retard d'estimation d'amplitude et en tant que

$$\{\hat{\tau}_{k,q}\}_{q=1}^{L_k} = \arg \max_{\{\tau_{k,q}\}_{q=1}^{L_k}} \frac{\sum_{q=1}^{L_k} |\mathbf{a}_k^T(\tau_{k,q}) \mathbf{b}_k|^2}{\mathbf{a}_k^T(\mathbf{o}) \mathbf{a}_k(\mathbf{o})} \quad (\text{R.26})$$

$$\{\hat{\beta}_{k,q}\}_{q=1}^{L_k} = \frac{\mathbf{a}_k^T(\{\hat{\tau}_{k,q}\}_{q=1}^{L_k})\hat{\mathbf{b}}_k}{\mathbf{a}_k^T(\{\hat{\tau}_{k,q}\}_{q=1}^{L_k})\mathbf{a}_k(\{\hat{\tau}_{k,q}\}_{q=1}^{L_k})} \quad (\text{R.27})$$

Dans la simulation, dans le côté de l'émetteur, chaque utilisateur se voit attribuer une séquence de Gold de longueur $N = 31$. Dans ce qui suit, TOA du premier utilisateur est évaluée avec la puissance transmise $P_1 = 1$, sans perte de généralité. Tous les utilisateurs interférents sont donnés une puissance reçue aléatoire avec une distribution log-normale avec une moyenne d dB au-dessus du signal désiré et un écart type de 10 dB. C'est $P_k = 10^{\varepsilon_k/10}$, où $\varepsilon_k \sim N(d, 100)$. Le rapport proche-lointain est défini comme le rapport entre la moyenne des puissances aléatoires des utilisateurs interférant à celle de l'utilisateur désiré. Ainsi, la radio proche-lointain est d en décibels. SNR est défini comme E_b/N_o , où E_b est énergie par bit pour le premier utilisateur. L'impulsion $p(t)$ est soulevée impulsion de cosinus avec roll-off facteur $\beta = 0.6$, impulsion et la durée de la puce sont égal à 1 ns, soit $T_c = T_p = 1\text{ns}$, et $N_c = 16$. Les retards de canal sont répartis uniformément sur $[0, 100\text{ns})$, qui sont les retards à valeurs réelles, y compris la partie fractionnaire.

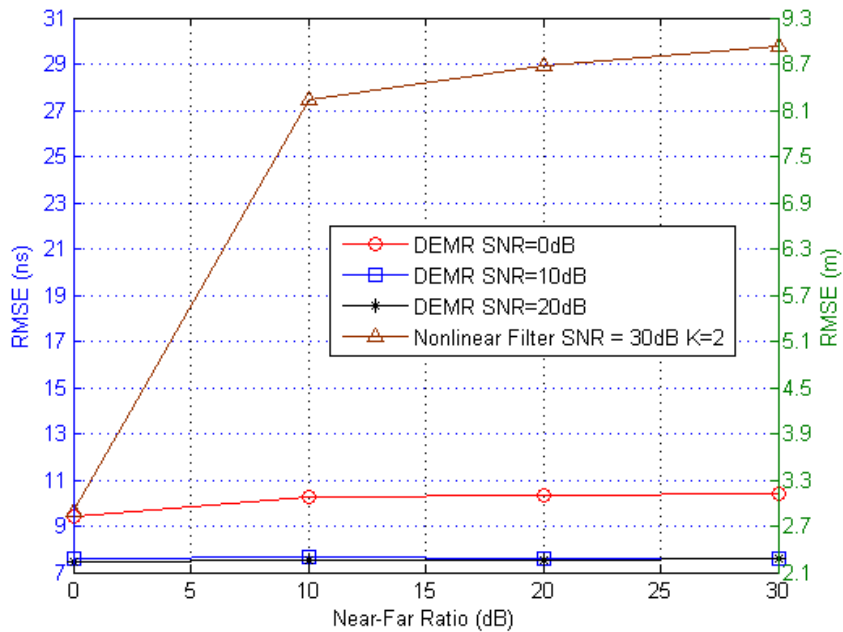


Figure R.13: RMSE en fonction du rapport proche-lointain pour différentes valeurs de SNR avec $M = 100$, $N = 31$, et $K = 10$ dans le canal CM1.

Dans la Fig.R.13, nous étudions RMSE de filtre estimateur DEMR et non linéaire par rapport à des ratios proches, loin de SNR différente dans le canal CM1. Pour algorithme de DEMR, RMSE augmente pas plus de 1ns lorsque le ratio proche-lointain pousse à partir de 0dB à 30dB pour toute la SNR. Les résultats des simulations montrent que dans le canal à trajets multiples dense, problème proche-lointain semble avoir peu d'effet sur l'estimateur proposé.

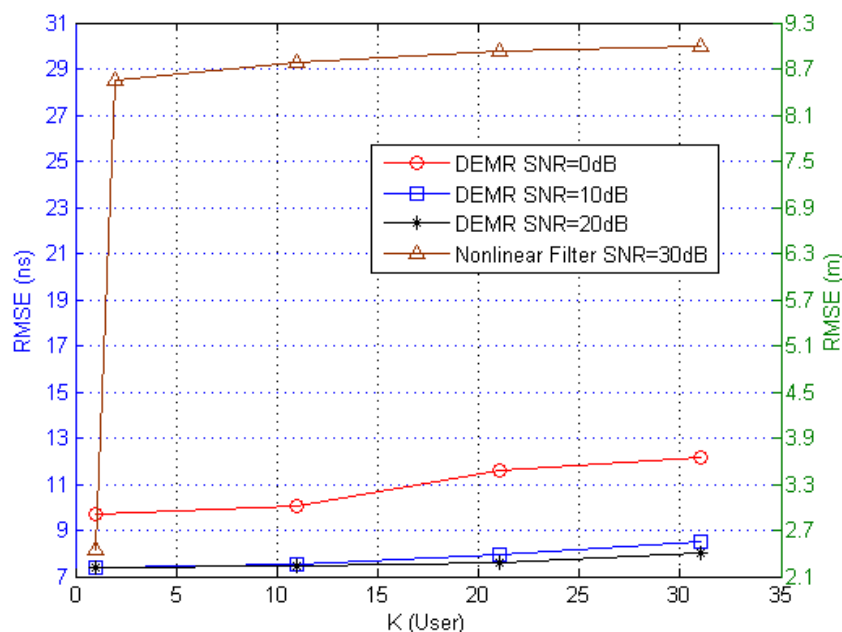


Figure R.14: RMSE en fonction du K pour différentes valeurs de SNR avec $M = 100$, $N = 31$, and near-far ratio is 10 dB dans le canal CM1.

Fig.R.14 montre RMSE de DEMR et estimateur de filtre non linéaire en fonction du nombre d'utilisateurs K pour SNR différente dans le canal CM1. Pour algorithme de DEMR, RMSE augmente dans 3ns environ que K varie de 1 à 31, même avec un bruit grave. Surtout, pour le SNR deux plus, les différences sont moins de 1 ns. Cette performance est opposée à la dégradation significative de l'estimateur de filtre non linéaire comme K augmente. Il est montré que l'estimateur de DEMR a la capacité de soutenir plus grand nombre d'utilisateurs avec peu de dégradation des performances.

CHAPTRE 6: ÉVALUATEUR DE TOA MULTI-UTILISATEUR BASÉE SUR LE CHAOS

Les performances allant de DEMR algorithme dépend principalement de la propriété d'auto-corrélation non-cyclique de $u_k(n)$, afin d'améliorer la performance allant de l'algorithme de DEMR, nous introduisons un ensemble de séquences chaotiques binaires avec une bonne fonction d'auto-corrélation non-cyclique pour remplacer les séquences Gold. En outre, contrairement aux séquences d'or qui a nombre fini de séquences pour une certaine durée, un nombre idéal grande de séquences chaotiques avec de bonnes propriétés de corrélation peut être généré en fonction des différentes conditions initiales.

Nous comparons les performances allant de l'estimateur de DEMR basé chaos-estimateur avec DEMR basé sur Gold et l'estimateur de filtre non-linéaire. Dans la Fig.R.15, nous montrons les performances de l'erreur quadratique moyenne en fonction du rapport Near-Far pour différents SNR dans le canal CM1. Comme le montre la Fig.R.15, filtre estimateur non linéaire

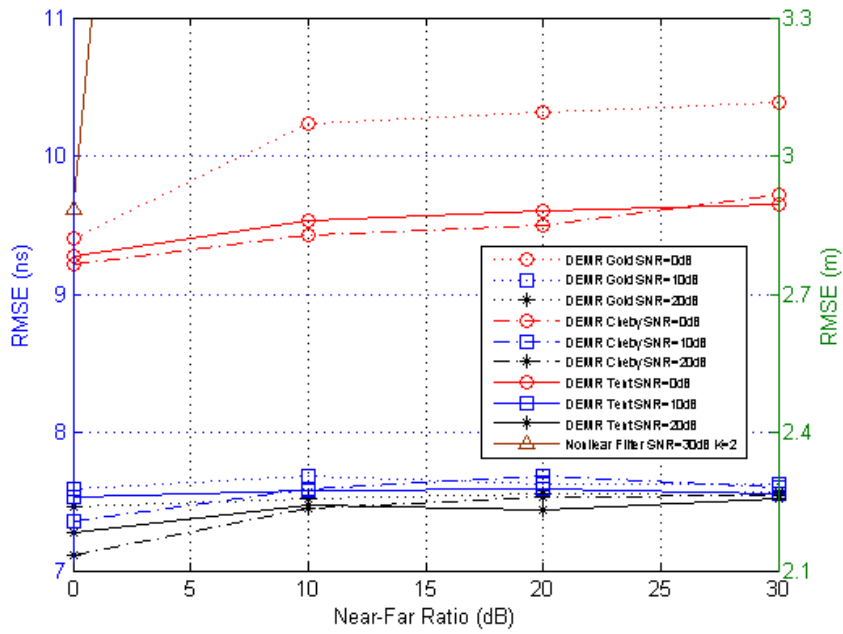


Figure R.15: RMSE en fonction du rapport proche-lointain pour différentes valeurs de SNR avec $M = 100$, $N = 31$, et $K = 10$ dans le canal CM1.

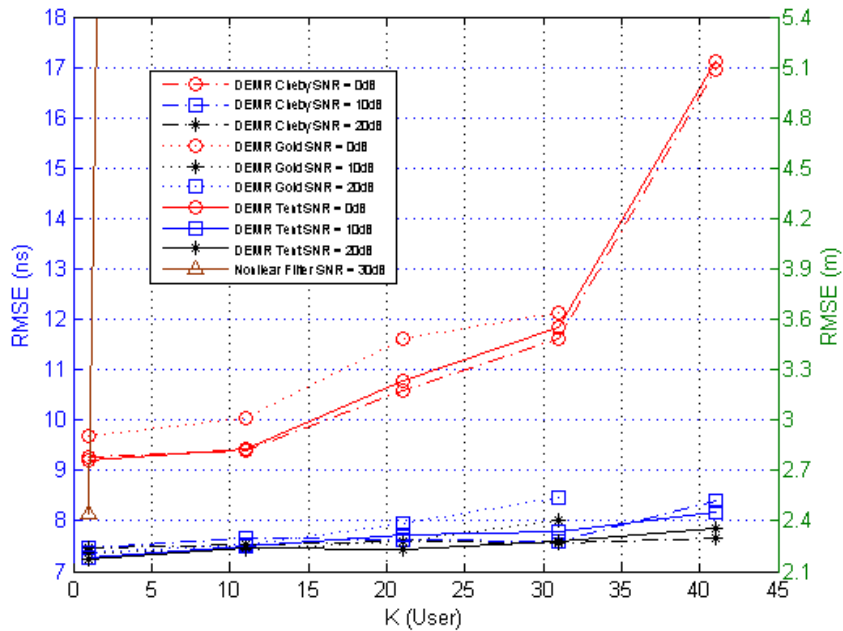


Figure R.16: RMSE en fonction du K pour différentes valeurs de SNR avec $M = 100$, $N = 31$, and near-far ratio is 10 dB dans le canal CM1.

n'a pas la robustesse ratio proche-lointain. En revanche, le problème proche-lointain semble avoir peu d'effet sur l'estimateur de DEMR basé chaos. En comparant avec DEMR à base Gold, l'utilisation de séquences chaotiques choisies améliore les performances allant plus loin. Dans la Fig.R. 16, deux ensembles de 41 sélectionnées séquences chaotiques de longueur 31 sont générés par la carte de Chebyshev et Tent, respectivement. Nous attribuons ces deux ensembles de séquences chaotiques à $K = 41$ utilisateurs et comparer l'erreur quadratique moyenne de DEMR basé chaos avec celle de DEMR base-or et filtre non linéaire comme la fonction de K . Dans l'algorithme de base DEMR chaos, puisque les séquences chaotiques sélectionnés ont moins lobes d'auto-corrélation que de séquences d'or, les performances sont améliorées allant pour tous SNR. Pour le SNR deux plus, RMSE de séquences chaotiques avec 41 utilisateurs est encore inférieur à celui des séquences Gold avec 31 utilisateurs. Ainsi, nous pouvons constater que l'utilisation de séquences binaires chaotiques dans l'algorithme de DEMR élargit la capacité du système tout en améliorant la performance allant.